Chairman:	Prof. Dr Marlies Van Bael
Promoter:	Prof. Dr Wouter Maes
Copromoters:	Prof. Dr Dirk Vanderzande
	Dr Laurence Lutsen, IMO-IMOMEC
Members of the jury:	Prof. Dr Tanja Junkers, UHasselt
	Prof. Dr Wanda Guedens, UHasselt
	Prof. Dr Rachel C. Evans, University of Cambridge
	Prof. Dr Sandra Van Vlierberghe, Ghent University

TABLE OF CONTENTS

Chapter 7: Summary and Outlook

Chapter 1

Context and Aim of the Thesis

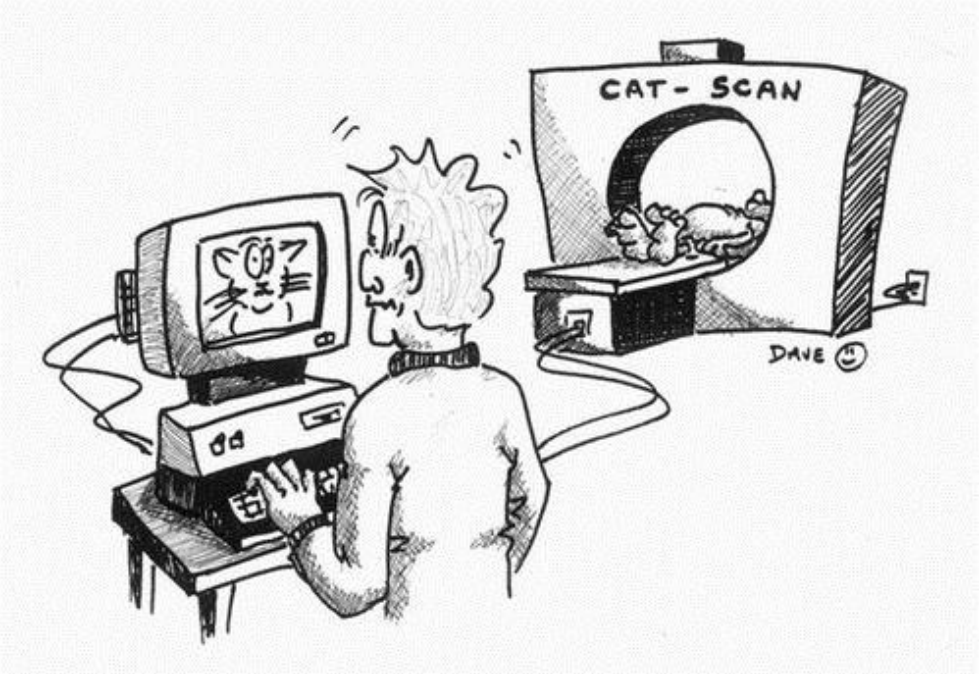

1.1 GENERAL OVERVIEW

Most polymeric materials are classified as insulators, e.g. the plastic protection layers around electrical wires, plastic bottles and rubber shoe soles. They are insulating due to the absence of free charge carriers that can move along the polymer backbone.[1] However, when Shirakawa, Heeger and MacDiarmid discovered conducting behaviour in iodine-doped *trans*-polyacetylene in 1977, a new application field opened up.[2] In the years to follow, different conjugated polymers (CPs) have been developed. A common feature of all those materials is that they are constructed of alternating single and multiple bonds along the polymer backbone. Due to the parallel orientation of p-orbitals, overlap occurs and delocalization of the π-electrons over the polymer backbone is possible. Furthermore, when multiple polymer chains aggregate, π-stacks can be formed, enabling intermolecular charge transport.[3] Nowadays, a wide range of conjugated polymers has been developed, all of them executing different chemical and electronic properties.[4] This wide variety in available materials makes the scope of applications very diverse, from organic field-effect transistors (OFETs) to organic photovoltaics (OPVs), solid-state lasers, light-emitting diodes (LEDs), sensors, imaging probes, *etc*.[5]

CPs are of particular interest because of their facile processing at ambient temperature and the rather easy tunability of the optical, electronic, mechanical or biologically relevant properties. These characteristics can be altered during the polymer synthesis process by changing the polymer backbone structure or the attached side chains.[6] Most synthetic routes towards CPs are rather simple and the most convenient synthesis pathway depends on the monomer composition. Push-pull conjugated polymers are for example typically synthesized via palladium catalysed Suzuki or Stille cross-coupling polymerization reactions, while poly(*p*-phenylene ethynylene)s (PPEs) are generally synthesized via Sonogashira cross-coupling reactions. Nickel catalysed Yamamoto polycondensations are often employed for the synthesis of polyfluorenes and Kumada catalyst-transfer condensation polymerization (KCTCP) is a well studied technique for the synthesis of polythiophenes. To improve on the environmental impact, more sustainable enzymatic and plasma polymerizations are recently studied as well.[7]

1.2 CONJUGATED POLYMERS FOR (BIO)SENSING

The interest in CPs for sensing purposes has grown over the last decades due to the excellent electrical and optical properties they exhibit. These properties make them sensitive to small variations in physicochemical conditions, like the pH, dielectric constant, humidity, temperature and chemical composition.[7] As a response to those small environmental variations, changes in optical, electrical and mechanical properties of the polymers can be measured and converted into readable output signals. Furthermore, the straightforward introduction of recognition sites onto the polymer chains improves the selectivity,[8] while the ability to make CPs soluble in almost any solvent makes them suitable for processing into polymeric solutions, films or dispersions.[7] Among the different interesting CP features, sensory signal amplification might be the most fascinating one. This effect is the result of the combined response of many conjugated units and is referred to as the 'molecular wire effect' (Figure 1).[9]

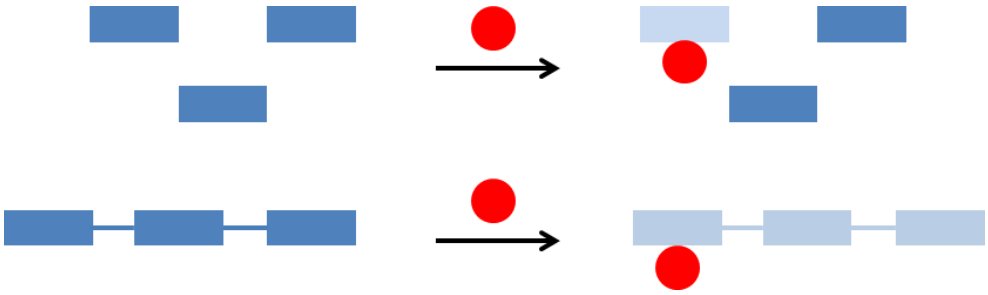

Figure 1: Illustration of the molecular wire effect.

When an analyte binds to a small molecule, its effect on the optical or electronical properties can only be displayed by one single small unit, while in a conjugated polymer different units are connected. Analyte binding somewhere onto the polymer backbone affects the whole polymer chain, leading to an amplification of the signal. Until now, conjugated polymer based sensors have shown their use in beverage and food control, medical diagnosis, the pharmaceutical industry, environmental monitoring and homeland security.[10] Sensor platforms are generally fabricated by immobilizing a receptor material, which detects the analyte, on the surface of a suitable transducer that converts

the binding event into a quantifiable output signal (Figure 2). CPs can be used as receptor layers but also as transducer materials.

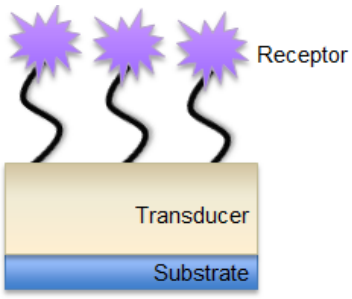

Figure 2: General sensor outline.

Many conjugated polymer structures have been synthesized for sensing purposes. Although the total number of different structures is high, the structural diversity remains rather modest. The polymer backbone is generally of the poly(*p*-phenylene vinylene) (PPV),[11] poly(3-alkylthiophene) (P3AT)[12] or PPE[13] type and some of the most frequently applied building blocks are simple phenylenes, fluorenes, iptycenes and benzothiadiazoles.[10,14] Surprisingly, there seems to be a poor cross-fertilization between the field of CP sensing and the development of CP semiconductors for other organic electronic applications, such as OLEDs, OFETs and OPVs.[15] Some of the targeted material features in these branches are, however, of relevance for sensing as well, such as emissive properties and/or high charge carrier mobilities.

1.3 CONJUGATED POLYMERS FOR BIO-IMAGING

Recently, the insight in biological processes and malfunctions has grown due to the development of novel imaging methodologies.[16] Optical and fluorescence imaging are appealing techniques due to their non-destructive nature, high signal-to-noise ratio and excellent temporal and spatial resolution. To successfully conduct these imaging techniques, highly photostable, bright and biocompatible fluorescent probes are needed.[17] Furthermore, specific cell or organelle targeting is of high importance and can be obtained by the immobilization of specific receptors onto the emissive probe. This specific

targeting makes the line between sensing and imaging rather thin, since imaging has no sense when the right target cannot be reached. In the last decade, conjugated polymer nanoparticles have emerged in the bio-imaging field due to their excellent fluorescence brightness, photostability, fast radiative decay, nonblinking behaviour and low cytotoxicity.[18] An in-depth overview of the field is provided in Chapter 2.

1.4 PPES AS MULTIFUNCTIONAL MATERIALS

PPEs are polymers in which phenylene moieties are separated by alkyne linkers (Figure 3). Their structure resembles the extensively studied PPV materials (Figure 3), but the properties of both types of polymers are clearly different. PPEs exhibit some superior properties compared to PPVs. They are for example stable up to 300 °C in air, they have an enhanced photostability and they are highly fluorescent both in solution and in the solid state.[19] Furthermore, the rigid rod-like backbone structure facilitates charge transport along the polymer chain.[20] A versatile side chain functionalization is also possible and therefore PPEs are ideal for studying the effect of side chain variations and functionalizations on sensing and imaging properties.

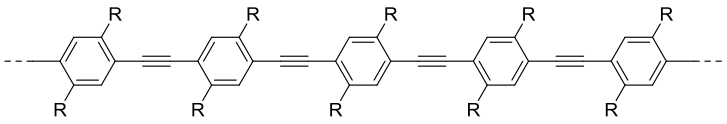

Poly(*p*-Phenylene Ethynylene) (PPE)

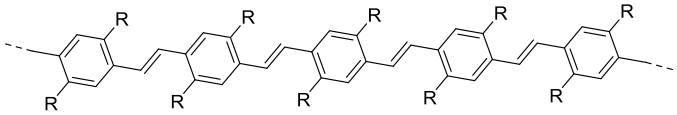

Poly(*p*-Phenylene Vinylene) (PPV)

Figure 3: Chemical structures of PPE and PPV.

PPEs are typically synthesized via two different routes, each with its own advantages and disadvantages. The Heck-Cassar-Sonogashira-Hagihara or simply Sonogashira cross-coupling reaction was first employed by Giesa and Schulz[21] to form polymers and is nowadays the most commonly used polymerization route towards PPEs (Scheme 1).

Overall reaction

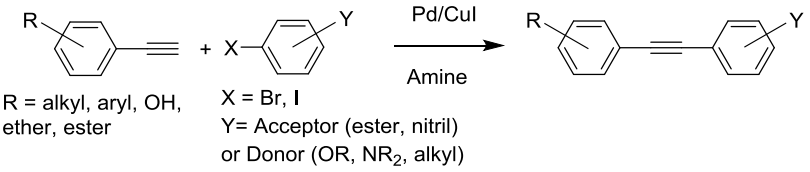

Catalyst activation

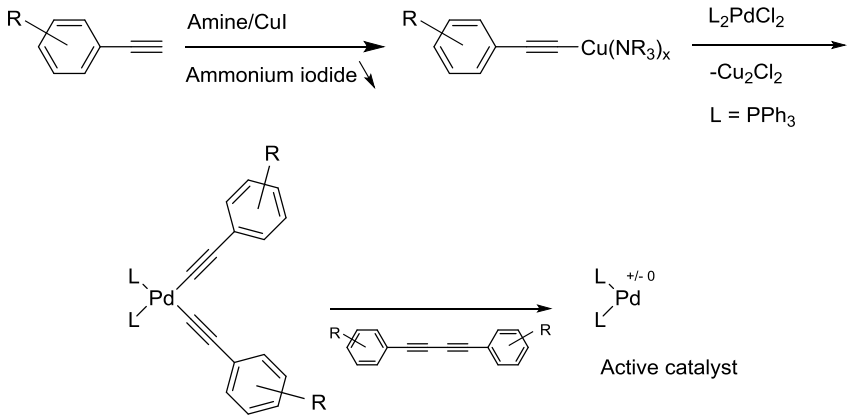

Catalytic cycle

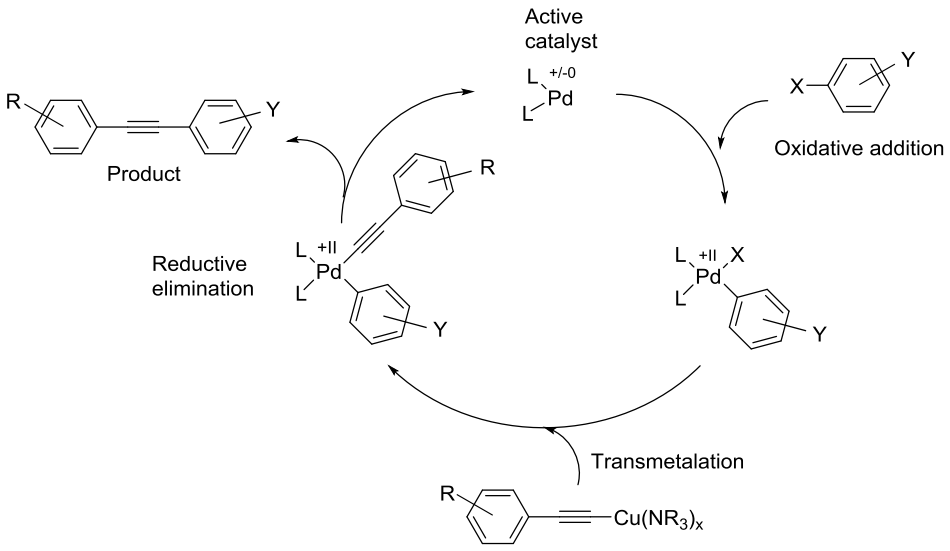

Scheme 1: Reaction mechanism for the Sonogashira cross-coupling reaction.[22]

In this coupling reaction, an aromatic diyne is coupled to an aromatic dihalide in an amine solvent, in the presence of a palladium catalyst ($Pd(PPh_3)_2Cl_2$ or $Pd(PPh_3)_4$) and CuI as cocatalyst.[22] The addition of a solvent (THF or toluene) can lead to higher molar masses and yields, although they are still smaller than those achieved for other polymers via other polymerization reactions.[23] Typical degrees of polymerization (P_n) are in the 20 to 50 range. Furthermore, the formation of butadiyne defects in the polymer chain is an unfortunate side effect that cannot be overcome when employing this polymerization route. However, the influence on the optical and electrical properties of the polymers can be neglected.[20]

A second synthetic approach, the acyclic diyne metathesis (ADIMET), was developed to achieve higher molar masses and degrees of polymerization (Scheme 2). This reaction was discovered by Mortreux and Blanchard in 1974[24b] and can be considered as an analogue of the acyclic diene metathesis reaction. Polymerization reactions based on this approach indeed lead to higher molar masses, but the use of the highly air and moisture sensitive tungsten catalysts (Schrock catalyst) complicates the use of this reaction in most organic synthesis labs.[20,25] Mortreux and Bunz were able to improve the applicability of this reaction by the development of a molybdenum catalyst that is formed *in situ* from $Mo(CO)_6$ and 4-chlorophenol and that can be used in nondried off-the-shelf solvents.[24,26] However, the higher reaction temperature (130 – 150 °C) and low tolerancy for heteroatoms make that this reaction is not suitable for every PPE synthesis.

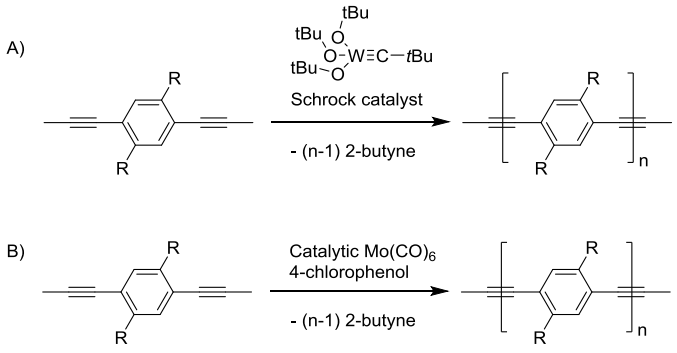

Scheme 2: ADIMET with A) the Schrock catalyst and B) the Mortreux-Bunz catalyst system.

1.5 OUTLINE OF THE THESIS

Conjugated polymers are not only of interest for organic electronics. Due to their unique optical properties, applications in bio-sensing and bio-imaging are emerging. Two main challenges that must be tackled in those fields are the selectivity of sensors and fluorescent probes and the fluorescence brightness. In this work, PPEs with azide functionalities on the side chains were designed and synthesized. These functional groups are of interest because of their facile click conjugation, with or without copper catalysis. This approach enables simple immobilization of small molecules or biomolecules that are selective towards a certain target. Click reaction onto the developed PPE polymers is shown as a proof-of-principle, both in solution and on nanoparticles. Furthermore, the influence of tetra(ethylene glycol) (TEG) side chains and azide functionalities on polymer synthesis, nanoparticle formation and the optical properties of the polymers in solution, thin film and particles were investigated. To obtain an improved photoluminescence quantum yield (PLQY) and brightness of PPE based conjugated polymer nanoparticles (CPNPs) for bio-imaging, a new approach including crosslinking of the polymer chains was developed. All nanoparticles synthesized were also tested for their cell cytotoxicity, cellular uptake and stability.

The above mentioned topics are divided over the different chapters of this thesis as follows:

Chapter 2 gives an introduction to CPNPs for bio-imaging purposes. Important aspects regarding fluorescence imaging techniques are described and an overview of the methods employed in literature to improve the PLQY is given. Since particle functionalization is important for specific targeting of cells or organelles, a wide variety of functional groups to achieve (bio)conjugation is highlighted, together with effective functionalization reactions.

Since PPEs are interesting materials to be used in biosensors as well as imaging probes, the investigation of different synthetic routes towards azide-functionalized PPEs is described in **Chapter 3**. The azide functionalities are interesting handles for post-polymerization functionalization with any (bio)conjugate via copper catalyzed alkyne-azide click (CuAAC) chemistry. The azide functionalities are introduced on the octyloxy polymer side chains in a pre-

or post-polymerization functionalization approach. The insertion of azide functionalities on the diiodo-substituted monomers before polymerization leads to the best results. Furthermore, as a proof-of-principle, a first click reaction onto the azidified polymer with phenylacetylene is performed in solution.

In **Chapter 4**, the synthesis and particle formation of three different PPEs with the same backbone structure but decorated with different side chains - i.e. regular octyloxy substituents, half of the octyloxy chains azide terminated or azide functionalized TEG side chains - is described. This work is the initial step towards highly fluorescent and selective CPNPs for bio-imaging purposes. The influence of the functionalization pattern on the size and the optical properties of the resulting PPE nanoparticles is studied using transmission electron microscopy, dynamic light scattering, UV-Vis absorption and fluorescence spectroscopy. The polymer containing azide functionalized TEG chains affords larger particles, which can be attributed to hydration of the outer layer and the interior of the more hydrophilic polymer particles. However, this does not impact the PLQY of the nanoparticles. The two azide functionalized PPE particles exhibit the highest quantum yields (13%). As a proof-of-principle, a fluorescent dye is clicked onto the CPNPs after particle formation.

In **Chapter 5**, a new technique to improve the PLQY of CPNPs is introduced. The synthesis of PPE networks, which are formed by the inclusion of 2D and 3D crosslinkers, is described. Furthermore, CPNPs are synthesized and the influence of crosslinking on the optical and biological properties of the particles is investigated. In general, larger crosslinker concentrations lead to brighter particles with higher PLQYs. Crosslinker incorporation seems to have a positive influence on particle internalization in cells as well. Cell viability and stability of the particles are excellent for all samples.

Since polymer functionalization is of huge importance to obtain high selectivity for sensing applications, CuAAC functionalization of a biological probe (protein A (SpA)) on PPE films was monitored via quartz-crystal microbalance with dissipation monitoring (QCM-D). The results are described in **Chapter 6**. A comparison between hydrophobic and more hydrophilic films (due to oligo(ethylene glycol) side chains) is made, but aspecific adsorption onto the polymer films made the interpretation of the results troublesome.

In **Chapter 7**, a general summary of the thesis is presented and an outlook is provided.

1.6 REFERENCES

[1] A. L. Andrady and M. A. Neal, *Philos. Trans. R. Soc. Lond. B Bio. Sci.*, 2009, **364**, 1977.

[2] (a) H. Shirakawa, E. J. Louis, A. G. MacDiarmid, C. K. Chiang and A. J. Heeger, *J. Chem. Soc.*, *Chem. Commun.*, 1977, 578. (b) C. K. Chiang, C. R. Fischer, Y. W. Park, A. J. Heeger, H. Shirakawa, E. J. Louis, S. C. Gau and A. G. MacDiarmid, *Phys. Rev. Lett.*, 1977, **39**, 1098. (c) H. Shirakawa, *Nobel lecture Chemistry 1996-2000*, World Scientific Publishing Co., Singapore, 2003.

[3] G. Malliaras and R. Friend, *Phys. Today*, 2005, **58**, 53.

[4] T. A. Skotheim and J. Reynolds, *Conjugated Polymers: Theory, Synthesis, Properties, and Characterization* (*Handbook of Conducting Polymers, Third Edition*); CRC Press, 2006.

[5] O. Ostroverkhova, *Chem. Rev.*, 2016, **116**, 13279.

[6] J. Rivnay, R. M. Owens and G. G. Malliaras, *Chem. Mater.*, 2014, **26**, 679.

[7] D. S. Correa, E. S. Medeiros, J. E. Oliveira, L. G. Paterno and L. H. C. Mattoso, *J. Nanosci. Nanotechnol.*, 2014, **14**, 6509.

[8] H. Kim, Y. Kim and J. Y. Chang, *Macromol. Chem. Phys.*, 2014, **215**, 1274.

[9] (a) Q. Zhou and T. M. Swager, *J. Am. Chem. Soc.*, 1995, **117**, 7017. (b) Q. Zhou and T. M. Swager, *J. Am. Chem. Soc.*, 1995, **117**, 12593.

[10] S. Rochat and T. M. Swager, *ACS Appl. Mater. Interfaces*, 2013, **5**, 4488.

[11] F. Chu and J. Yang, *Sens. Actuators A*, 2012, **175**, 43.

[12] (a) C. V. Goncalves and D. T. Balogh, *Sens. Actuators B*, 2012, **162**, 307. (b) L. H. Zhang, T. Jiang, L. B. Wu, J. H. Wan, C. H. Chen, Y. B. Pei, H. Lu, Y. Deng, G. F. Bian, H. Y. Qiu and G. Q. Lai, *Chem. Asian J.*, 2012, **7**, 1583. (c) C. Li and G. Shi, *ACS Appl. Mater. Interfaces*, 2013, **5**, 4503.

[13] (a) B. C. Englert, S. Bakbak and U. H. F. Bunz, *Macromolecules*, 2005, **38**, 5868. (b) J. H. Wosnick, C. M. Mello and T. M. Swager, *J. Am. Chem. Soc.*,

2005, **127**, 3400. (c) F. E. Alemdaroglu, S. C. Alexander, J. Dongmei, K. P. Deepak, M. Borsch and A. Herrmann, *Macromolecules*, 2009, **42**, 6529. (d) E. Kozma, F. Munno, D. Kotowski, F. Bertini, S. Luzzati and M. Catellani, *Synth. Met.*, 2010, **160**, 996. (e) J. Pecher, J. Huber, M. Winterhalder, A. Zumbusch and S. Mecking, *Biomacromolecules*, 2010, **11**, 2776. (f) S. G. Hahm, Y. Rho, J. Jung, S. H. Kim, T. Sajoto, F. S. Kim, S. Barlow, C. E. Park, S. A. Jenekhe, S. R. Marder and M. Ree, *Adv. Funct. Mater.*, 2013, **23**, 2060.

[14] (a) D. T. McQuade, A. E. Pullen and T. M. Swager, *Chem. Rev.*, 2000, **100**, 2537. (b) S. W. Thomas, G. D. Joly and T. M. Swager, *Chem. Rev.*, 2007, **107**, 1339.

[15] (a) Y. J. Cheng, S. H. Yang and C. S. Hsu, *Chem. Rev.*, 2009, **109**, 5868. (b) X. Zhao and X. Zhan, *Chem. Soc. Rev.*, 2011, **40**, 3728. (c) Y. Li, *Acc. Chem. Res.*, 2012, **45**, 723. (d) H. Zhou, L. Yang and Y. Wei, *Macromolecules*, 2012, **45**, 607. (e) P. Lin and F. Yan, *Adv. Mater.*, 2012, **24**, 34. (f) M. Zhu and C. Yang, *Chem. Soc. Rev.*, 2013, **42**, 4963.

[16] C. Wu and D. T. Chiu, *Angew. Chem. Int. Ed.*, 2013, **52**, 3086.

[17] Yao, M. Yang and Y. Duan, *Chem. Rev.*, 2014, **114**, 6130.

[18] (a) R. Ahmad Khanbeigi, T. F. Abelha, A. Woods, O. Rastoin, R. D. Harvey, M.-C. Jones, B. Forbes, M. A. Green, H. Collins and L. A. Dailey, *Biomacromolecules*, 2015, **16**, 733. (b) D. Tuncel and H. V. Demir, *Nanoscale*, 2010, **2**, 484.

[19] (a) C. E. Halkyard, M. E. Rampey, L. Kloppenburg, S. L. Studer-Martinez and U. H. F. Bunz, *Macromolecules*, 1998, **31**, 8655. (b) T. Miteva, L. Palmer, L. Kloppenburg, D. Neher and U. H. F. Bunz, *Macromolecules*, 2000, **33**, 652. (c) J. J. Lavigne, D. L. Broughton, J. N. Wilson, B. Erdogan and U. H. F. Bunz, *Macromolecules*, 2000, **36**, 7409. (d) J. N. Wilson, Y. Q. Wang, J. J. Lavigne and U. H. F. Bunz, *Chem. Commun.*, 2003, 1626.

[20] U. H. F. Bunz, Poly(arylene ethynylene)s: From synthesis to application, 2005, Springer.

[21] R. Giesa and R. C. Schulz, *Macromol. Chem. Phys.*, 1990, **191**, 857.

[22] U. H. F. Bunz, *Chem. Rev.*, 2000, **100**, 1605.

[23] (a) S. Thorand and N. Krause, *J. Org. Chem.*, 1998, **63**, 8551. (b) M. Moroni, J. LeMoigne and S. Luzzati, *Macromolecules*, 1994, **27**, 562.

[24] (a) U. H. F. Bunz and L. Kloppenburg, *Angew. Chem.*, 1999, **38**, 478. (b) A. Mortreux and M. Blanchard, *J. Chem. Soc.*, 1974, 786.

[25] N. Kaneta, K. Hikichi, S. Asaka, M. Uemura and M. Mori, *Chem. Lett.*, 1995, 1055.

[26] S. A. Krouse and R. R. Schrock, *Macromolecules*, 1989, **22**, 2569.

Chapter 2

Conjugated Polymer Nanoparticles for Bio-imaging

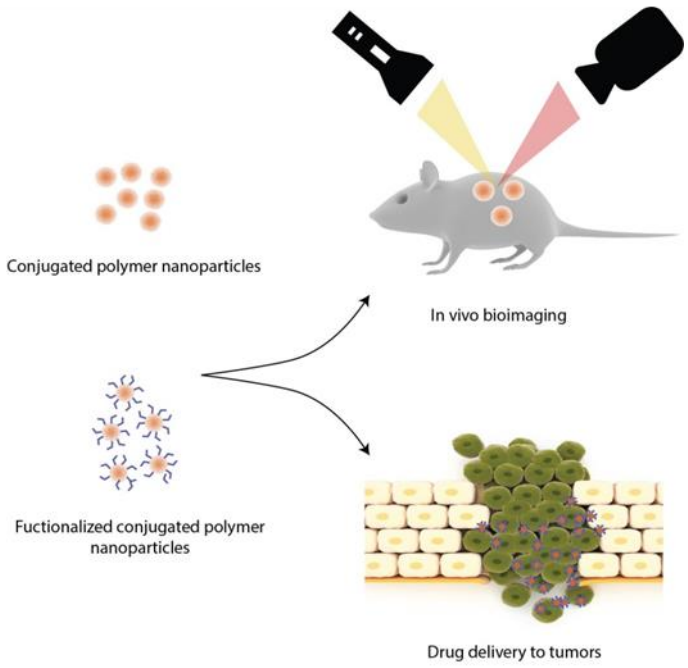

Y. Braeken, S. Cheruku, A. Ethirajan and W. Maes, *manuscript submitted.*

ABSTRACT

During the last decade, conjugated polymers have emerged as an interesting class of fluorescence imaging probes. They generally show high fluorescence brightness, high photostability, fast emission rates, non-blinking behavior and low cytotoxicity. The main concern related to most conjugated polymers is their lack of hydrophilicity and thereby poor bio-availability. This can, however, be overcome by the formulation of conjugated polymer nanoparticles in aqueous medium. This chapter provides an overview of the different techniques employed for the preparation of conjugated polymer nanoparticles, together with methods to improve their photoluminescence quantum yields. For selective targeting of specific cells, dedicated surface functionalization protocols have been developed, using different functional groups for ligand immobilization. Finally, conjugated polymer nanoparticles have recently also been employed for theranostic applications, wherein the particles are simultaneously used as fluorescent probes and carriers for anti-tumor drugs.

2.1 INTRODUCTION

Bio-imaging is a powerful method to gain insights in biological processes and malfunctions.[1] Over the past decades, several techniques were developed to create images of organs, veins and cells, such as magnetic resonance imaging (MRI),[2] X-ray computerized tomography (CT),[3] ultrasound imaging[4] and positron emission tomography (PET)[5]. Nevertheless, the search for improved cost-effective, time dependent and safe bio-imaging techniques with an excellent spatial resolution is still ongoing.

Fluorescence imaging allows the visualization of biological processes from the cellular down to the molecular level in an easy and non-destructive way.[6] As a result, fluorescence-based diagnosis of diseases and fluorescence image guided surgery have been shown to be successful applications.[7] Different types of fluorescent probes have been reported. Fluorescent organic dyes can exhibit high photoluminescence quantum yields (PLQYs) and a large variety of dyes with tunable optical characteristics are readily available. However, those small molecules generally exhibit a low stability and photobleaching often presents a problem.[8–11] The stability of the fluorescent probes can be improved by the use of inorganic quantum dots, consisting of heavy metals like lead, cadmium or indium, but the presence of those metals significantly increases the cytotoxicity.[8,12,13] Conjugated polymers (CPs) have recently gained considerable interest as they are generally stable and non-cytotoxic and their structure can be readily adapted to tune the optical characteristics.[14,15] CPs have a backbone of alternating σ- and π-bonds, inducing semi-conductivity. The bandgap of the polymer strongly depends on its composition. In the field of organic electronics, those CPs have been studied extensively over the past decades. The introduction of an alternating 'push-pull' or 'donor-acceptor' copolymer structure has been used frequently to lower the bandgap.[16] Typical push/donor entities are electron-rich monomers with high-lying energy levels, whereas pull/acceptor moieties have low-lying energy levels. This concept allows to stretch the absorption and emission spectra of CPs as far as the near infra-red (NIR) region. This wavelength range is obviously attractive for bio-imaging as it enables deep tissue penetration and minimal background autofluorescence. Moreover, low energy optical waves are non-destructive for tissues.[17] However, for

applications in biological environment, it is imperative that the fluorescent probes are water-soluble. Since CP backbones are generally hydrophobic, strategies have to be implemented to make them operable in aqueous media. One particular approach uses the introduction of charged moieties on the polymer side chains, creating conjugated polyelectrolytes (CPEs).[18,19] These CPEs are soluble in water and can hence be used individually as fluorescent probes. Other strategies link the CP to biological structures such as human serum albumin (HSA) or liposomes.[20,21] A more common technique is to prepare a polymer dispersion in water or a buffer solution. Small conjugated polymer nanoparticles (CPNPs), also known as polymer dots (Pdots), are thus created, stabilized by surfactant molecules.[22–24] A complication induced by the tight packing of the polymer chains in the particles is fluorescence quenching, which significantly decreases the PLQY and the brightness of the probe.
In this review, the focus lies on recent chemical developments in bio-imaging with CPNPs. Applied techniques for the improvement of the PLQY through reduction of quenching processes will be discussed in detail. Furthermore, some strategies employed for surface functionalization will be highlighted.

2.1.1 Theory and background on fluorescence

Fluorescence is the emission of light by a compound that is in an electronically excited state. Here, the visualization of an excited state will be done by molecular orbitals (MOs), mathematical regions where electrons in a molecule are most likely to be found. Every electronic state of a molecule can be described by a linear combination of its MOs. According to Pauli's principle, each orbital contains a maximum of 2 electrons and the spin of those electrons must be in opposite direction. To define the ground state of a molecule, MOs are filled with electrons following Pauli's principle, starting from the lowest to higher energy orbitals. An electronic excitation of a molecule can be seen as the movement of an electron from a lower to a higher energy MO and is often induced by the absorption of light. Mostly, not all of the MOs are involved in those electronic transitions. Typical energy absorption and emission processes occur in the highest occupied molecular orbital (HOMO) and lowest unoccupied molecular orbital (LUMO) levels of molecules.

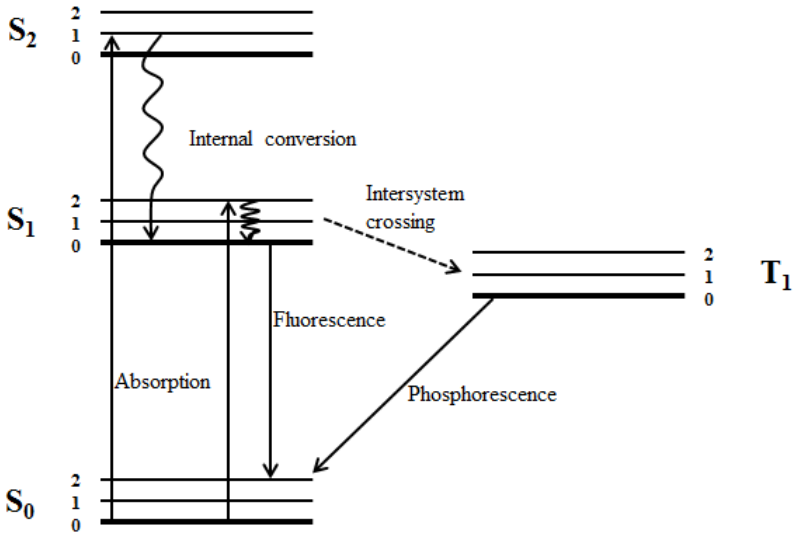

Figure 1: Jablonski diagram showing singlet and triplet electronic energy states (S_0, S_1, S_2 and T_1), each divided into vibrational energy levels (0, 1 and 2).

The movement of electrons to other energy levels is often visualized in Jablonski diagrams (Figure 1), showing the electronic states of a free molecule, ordered vertically according to their energy. When an absorbed photon promotes an electron from the ground state (S_0) to a higher energy level, the spin state of the electron is generally maintained. In that case, singlet excited states are formed (S_1, S_2 etc.). In rare cases, an inversion in electron spin is observed and then triplet excited states are formed (T_1, T_2 etc.). Triplet excited states can typically not be accessed from the ground state, so intersystem crossing (ISC) from excited singlet states is needed to populate the triplet states.

Furthermore, every electronic level is divided into vibrational energy levels because of the nuclear motion relative to the molecular coordinates. Thermal excitation from a lower vibrational state to one with higher energy is possible. However, at room temperature, the thermal energy is not sufficient to populate higher energy vibrational states. An electron can lose energy by the emission of a photon or by energy loss in the form of heat (internal conversion), after which it will fall back to the ground state. Fluorescent molecules have an efficient photon emission by an electron falling back from a singlet excited state into the ground state, while photons emitted from the triplet state are referred to as

phosphorescence.

Excitation typically happens in the femtosecond timescale (10^{-15} s), while relaxation processes often go slower. Internal conversion from higher vibronic states to the vibrational ground state happens in picoseconds (10^{-12} s), after which fluorescence or phosphorescence occur on a timescale of nanoseconds (10^{-9} s) and milliseconds (10^{-3} s) respectively.

Absorption maxima are generally blue shifted relative to emission spectra due to thermal energy loss during internal conversion. This shift in peak maximum is referred to as the Stokes shift. For bio-imaging purposes, a large stokes shift is beneficial because it reduces the overlap between the excitation and the emission wavelength and thus the background signal. In CPs, the π-bonds are considerably weaker than σ-bonds, leading to lower energy and thus easier excitations of the π-electrons. The energy gap between the π and π* orbitals is typically 1.5 to 3 eV, meaning that light absorption and emission is in the visible range of the spectrum. This interesting emission feature is, however, often compensated by the negative effect of fluorescence quenching whenever multiple molecules closely interact with each other, for example in the solid state or within nanoparticles. Excited state reactions, resonance energy transfer (Förster and Dexter mechanisms), intersystem crossing, collisional quenching (mainly in the gas state and in solution), photoinduced electron transfer (PET) and ground state complex formation are typical fluorescence quenching processes that have been described in literature. Although the latter two are the most frequently discussed mechanisms for conjugated polymers in the solid state, the quenching process can differ from one system to another and often different mechanisms are playing at the same time.[25-28]

2.1.2 Preparation of CPNPs

Different techniques have been employed for the synthesis of CPNPs. The solvent exchange method is most frequently used (Figure 2a). In this procedure, the CP is dissolved in a good, water miscible solvent, e.g. THF. The polymer solution is subsequently added into water while sonicating. When the polymer solution is added to the water phase, the solubility of the polymer drops drastically and the polymer precipitates in very small particles. As such, this

technique is also often referred to as the nanoprecipitation method. Afterwards, the organic solvent residues are removed by evaporation and the CPNPs remain dispersed in water. In general, particles smaller than 40 nm are formed by this approach and the size can be tuned by the polymer concentration, water temperature and solubility of the polymer.

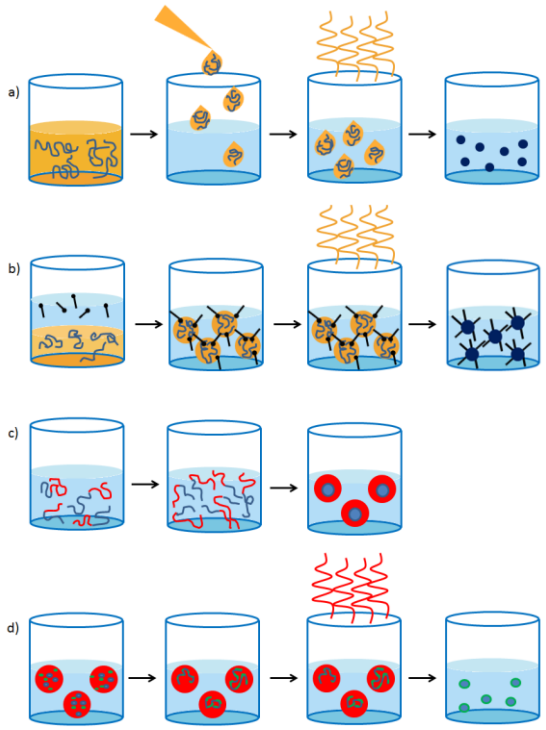

Figure 2: CPNP formulation via a) the solvent exchange technique, b) the mini-emulsion technique, c) self-assembly and d) emulsion polymerization.

CPNPs are less commonly prepared via the mini-emulsion technique (Figure 2b). Here, a continuous phase and a dispersed phase are combined. The former consists out of a surfactant dissolved in water and the latter contains the polymer in a water-immiscible solvent, e.g. chloroform. By applying strong shear forces via ultra-sonication to the two phase system, the dispersed phase is bursting into small droplets containing the CP and packed by the surfactant on the outside. The size of the nanoparticles can be adjusted by varying the polymer:surfactant ratio and typically ranges from 40–500 nm. Also in this method, the water-immiscible organic solvent is removed via evaporation in the

final step. Even less employed techniques are the self-assembly method (Figure 2c), in which the polymers assemble into predefined structures due to specific molecular interactions, and the emulsion polymerization technique (Figure 2d), in which the polymer is readily synthesized in preformed emulsion droplets.[22,29] In 2014, Yoon et al.[30] developed a new nanoparticle formation technique in which phase-separated films of CPs and phospholipids were split up in particles by sonication. However, this technique is not considered as a standard particle synthesis method. Table 1 provides an overview of the preparation methods of the particles discussed further on in this review article.

Table 1: Overview of CPNPs used in bio-imaging.

Polymer	NP/Hybrid	Hybrid material	Preparation method	Particle size (nm)	PLQY (%)	Other applications	Ref.
28-**29**	NP		Solvent exchange	4-264	14-26	/	48
5-**7**, **30**	NP		Solvent exchange	23	1-36	/	38
44-**47**	NP		Solvent exchange	58-87	/	/	58
38	NP		Solvent exchange	42-57	/	/	52
8-**11**, **31**	NP		Solvent exchange	22	47	/	39
5-6	NP		Solvent exchange	16	13, 19	/	37
15	Hybrid NP	PEG	Solvent exchange	80	27	/	43
39	Hybrid NP	Silica	Solvent exchange	5-50	1.5	/	53
18-**21**	NP		Solvent exchange	50-100	76	/	45
14	Hybrid NP	PEG	Solvent exchange	56	/	/	41
2	Hybrid NP	PEG and dye	Solvent exchange	45	45	/	35
16-**17**	Hybrid NP	PCL-*b*-POEGMA	Solvent exchange	50-500	26	/	44
12-13	Hybrid NP	PEG	Solvent exchange	28	14	/	40
42-43	Hybrid NP	PS-PEG	Solvent exchange	13	57	/	56
34-37	Hybrid NP	PSMA	Solvent exchange	30	3-78	/	51
52-53	Hybrid NP	DSPE-PEG	Solvent exchange	30	23	Theranostic	63
32	NP		Solvent exchange	30	14	/	49
25-27	NP		Solvent exchange	16-21	17-30	/	47
22-**24**	NP		Emulsion polymerization	25-73	56	/	46
48	NP		Self-assembly	117	/	Theranostic	59
51	NP		Self-assembly	24	3	Theranostic	62
1	NP		Mini-emulsion	2.9	1.7	/	31
3-4	NP		Mini-emulsion	116-117	3	/	36
15-17	NP		Mini-emulsion	78-188	8-13	/	42
33	Hybrid NP	PEG	Mini-emulsion	20	46	/	50
40	Hybrid NP	Azide-funct. PEG	Mini-emulsion	130	4	/	54
41	Hybrid NP	HPG	Mini-emulsion	40-210	23	/	55
42	Hybrid NP	Peptide	Mini-emulsion	40	37-42	/	57
49	Hybrid NP	Fe_3O_4	Ligand exchange	26	21.5	Theranostic	60
50	NP		1 polymer brush/NP	20-54	20-30	Theranostic	59

2.2 RECENT DEVELOPMENTS IN CPNP BIO-IMAGING

Fluorescent dyes are often added in a few mass percent to non-conjugated polymer or silica matrices to form fluorescent nanoparticles. Nevertheless, problems concerning leaching of the dye out of the matrix and poor photostability have stimulated research into alternative strategies. By replacing typical small molecule fluorescent dyes by conjugated polymers, leaching can be overcome. Furthermore, since the polymers themselves serve as fluorescent probes, no external matrix material is needed anymore to fixate the probe in the particles. During the last decade, many different CPs have been studied as fluorescent imaging probes. Highly complicated polymer structures with uncommon monomer moieties, nowadays developed for organic electronics, are not widely used in this application. Polymer backbone structures are overall simple and easy to synthesize. Poly(*p*-phenylene ethynylene)s (PPEs) and poly(*p*-phenylene vinylene)s (PPVs) are typical examples of such polymers. However, since their emission spectrum does not reach into the attractive first NIR window (650–1000 nm), push-pull conjugated polymers are also emerging in the bio-imaging field.

The most often employed polymers are based on fluorene, copolymerized together with benzothiadiazole, quinoxaline and/or thiophene. The influence of monomer ratios and side chain variations on the optical properties, particle formation, stability and *in vitro/in vivo* imaging have been widely studied (*vide infra*). Hong et al.[31] pushed the emission of their NPs into the second NIR window (1000–1350 nm) by developing a push-pull conjugated polymer (**1**) (Figure 3) based on a strong fluorinated thieno[3,4-*b*]thiophene acceptor. The polymer was formed into small particles via the mini-emulsion technique and the CPNPs were stabilized with a PEGylated surfactant. While the absorption maximum was found at λ = 654 nm, an impressive Stokes shift of 400 nm was observed with an emission peaking at λ = 1047 nm. This long emission wavelength is beneficial for bio-imaging because of a lower autofluorescence and reduced photon scattering in biological tissues, resulting in a higher spatial resolution and deeper tissue penetration. A drawback of CPNPs with emission peaks in the second optical window is the decrease in PLQY. CPNPs synthesized from **1** (Figure 3) exhibit a poor PLQY of 1.7%, which might be high for

fluorophores emitting in this long wavelength region, but low in comparison to emitters in the first NIR-window (Table 1). Hong and coworkers were, however, able to monitor arterial blood flow *in vivo* due to the excellent time resolution (20 ms) that could be obtained with these particles.[31] Since the cardiac cycle in mice takes 200 ms, changes in blood velocity during this cycle could be observed. Furthermore, the outstanding spatial resolution obtained with those CPNPs enabled tracking of blood flow in capillary vessels with a sub-10 μm diameter, which had not been realized before with traditional ultrasound and optical coherence tomography (OCT). This real-time haemodynamic imaging can be of high importance to improve our understandings of cardiovascular diseases and to design treatments accordingly.

Recently, much more interest has gone into two photon excitation microscopy, where a single excitation is the result of the simultaneous absorption of two photons with longer wavelength. Because typical excitation wavelengths are in the NIR regime, the beam can penetrate deeper into tissue (1 mm) and it causes less damage to the biological tissue. The probability of emission increases drastically (non-linear) when the excitation beam intensity is high. This means that scattered light does not contribute to the output signal, leading to a high optical resolution.[32] Most conjugated polymers have shown to be good two photon excitation probes.[33,34] This was also illustrated by Lv et al.,[35] who combined fluorene based CP **2** (Figure 3) with a perylene diimide (PDI) dye, creating particles that can be excited at λ = 800 nm, while emission occurs at λ = 730 nm. Peters et al.[36] also investigated two photon excitation of their PPV-based NPs (**3** and **4**; Figure 3) and they were able to excite the particles at 830 nm, while the fluorescence maximum lies at 580 nm.

For some applications, multiple targets have to be detected simultaneously, which is referred to as spectral multiplexing. To carry this out, probes with narrow emission peaks are needed, to prevent emission overlay. Rong and coworkers[37] developed boron dipyrromethene (BODIPY) based push-pull conjugated polymers (**5** and **6**; Figure 3) with emission peak widths at half maximum of only 40–55 nm, which is 1.5 to 2 times narrower than the emission peak widths of conventional CPNPs.[9] This can be achieved by the efficient intraparticle energy transfer to the BODIPY units, which are known to be narrow

emissive species. This property is transferred onto the BODIPY containing polymers.

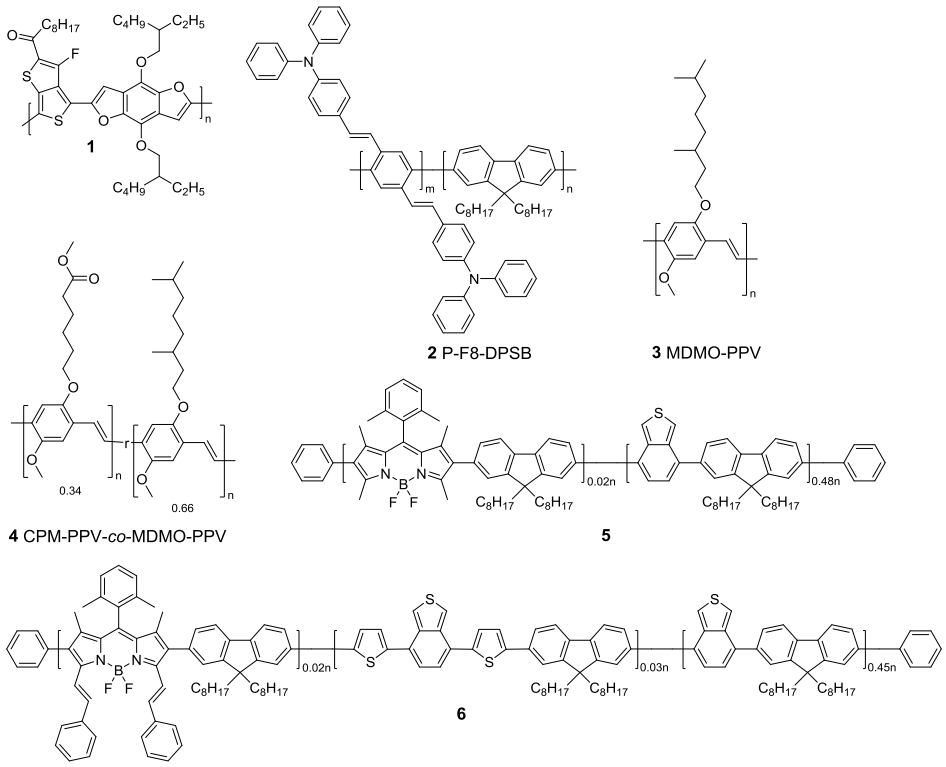

Figure 3: Structures of conjugated polymers with absorption in the NIR region because of the strong donor-strong acceptor approach (**1**), two photon excitation (**2**-**4**) and extra narrow emission peaks (**5**-**6**).

2.3 IMPROVING THE PLQY

All conjugated polymers discussed in this section are developed to increase the PLQYs and their structures are gathered in Figure 4. PLQYs of CPNPs are in general smaller than those of their molecularly dissolved CP counterparts. This can mainly be attributed to quenching processes due to the close proximity of multiple polymer chains. The main strategy employed to diminish quenching is to increase the polymer inter-chain distances within one particle. Different approaches have been investigated but the most convenient method is to include (bulky) side chains onto the polymer backbone, which limit stacking by imposing steric hindrance.

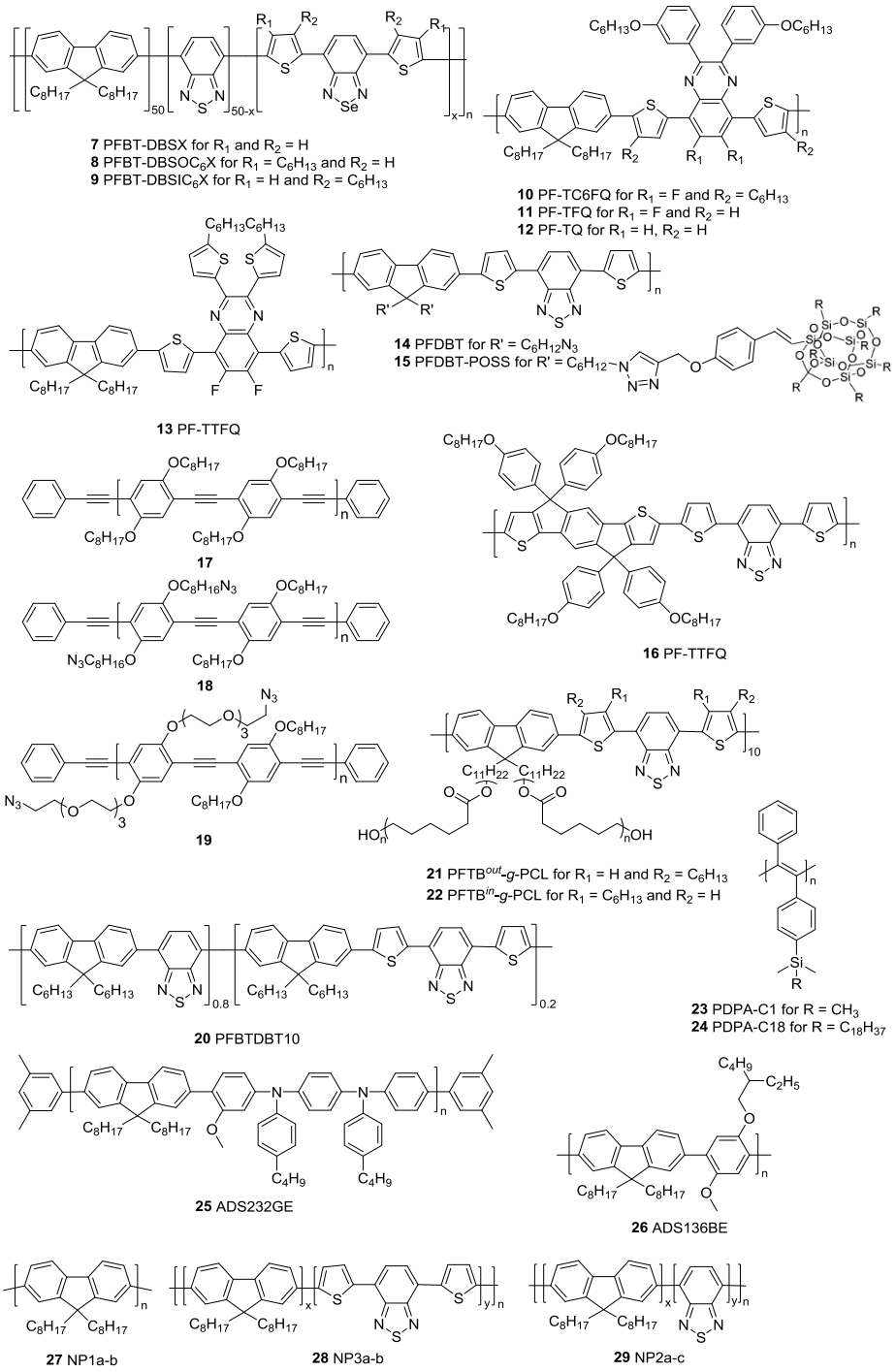

Figure 4: CPs affording improved PLQYs in CPNP form.

Chen et al.[38] illustrated this approach by the introduction of hexyl side chains onto dithienylbenzoselenadiazole (DBS) based polymers **7**-**9**. Alkyl substitution on the thiophene subunits improved the QY from 2% for the non-substituted derivative to 8% for polymer **9**, where the hexyl chains point toward the DBS unit. A maximum of 15% was even obtained for polymer **8**, where the side chains point outwards from DBS.

Liu et al.[39] developed a series of quinoxaline based polymers **10**-**13**. Substitution of the phenyl rings on the quinoxaline 2,3-positions (**11**) by thiophene moieties (**13**) reduced the PLQY from 11 to 8%. On the other hand, a red shift of both the absorption and emission spectra could be observed due to the extension of the conjugated system in the thiophene rings. Also the effect of substitution on the polymer backbone was investigated. The introduction of fluorine atoms on the quinoxaline 6,7-positions slightly raised the PLQY from 9 (**12**) to 11% (**13**). Also in this work, the introduction of hexyl side chains pointing outwards from the quinoxaline unit afforded a strong increase in PLQY, from 11% for polymer **11** to 47% for polymer **10**.

The introduction of the bulky polyhedral oligomeric silsesquioxane (POSS) side chain increased the PLQY of poly{[9,9-di(hexyl)fluorene]-*alt*-[4,7-bis(thiophen-2'-yl)-2,1,3-benzothiazole]} (PFDBT, **14**) NPs from 2 to 14% (PFDBT-POSS **15**).[40] A 4-octyloxyphenyl side chain was introduced by the same group onto the indacenothiophene units of polymer **16**.[41] The bulkiness of those side chains hinders efficient π-π stacking, which is beneficial for the fluorescence efficiency due to the inhibition of charge transfer induced fluorescence quenching. Also smaller functional groups can have an influence on the quantum efficiency of CPNPs. This was illustrated by D'Olieslaeger et al.[42] who designed PPEs with azides on the octyloxy (**18**) and tetra(ethylene glycol) (TEG) (**19**) side chains. The PLQYs of the resulting NPs increased from 8% for **17**, the reference PPE containing no azide groups, to 13% for **18** and **19**. The influence of the TEG side chains on the PLQY is minimal but almost no cell penetration was observed for the CPNPs consisting of **19**, which can be ascribed to low protein adsorption on the polymer surface. Furthermore, cell viabilities for the azide containing CPNPs were comparable to those of the particles containing no azide functionalities, indicating a non-toxic effect of the azide functionalization.

Furthermore, co-precipitation of the CP with PEG isolates the polymer chains from each other, again preventing stacking and thus fluorescence quenching. Co-precipitation of polymer **2** with a non-conjugated folic acid functionalized amphiphilic triblock copolymer was described by Lv et al.[35] A bis(diphenylaminostyryl)benzene (DPSB) based CP (**2**) was developed and acts as a FRET (Förster resonance energy transfer) donor in the CPNPs. A PDI dye was chosen as the acceptor material since it is emitting NIR light and the energy transfer efficiency from the donor to the acceptor material exceeds 90%. The co-precipitation of the different materials diminishes the stacking probablity, together with the large DPSB groups and the octyl side chains on the fluorene subunit. The success of this approach is illustrated by a PLQY of 45% for the hybrid NPs.

Ding et al.[43] also employed the co-precipitation technique to achieve a PLQY of 27% for CPNPs containing 50 mol% of **20** and 50 mol% of a non-conjugated PEG matrix material. Likewise, the formation of brush-like polymer structures can prevent aggregation of the CP chains. In this case, the brushes form a protecting outer layer around the CP backbone, isolating every single chain from each other. Yang et al.[44] showed in their recent work that the introduction of polycaprolactone (PCL) side chains, acting as the brushes, can improve the PLQY up to 5 times (to ~26% for **21**). The length of the PCL side chains had a small influence on the quantum efficiency, with the best PLQYs obtained for the longest PCL brushes. Also in this work, the effect of hexyl side chains on the thiophene rings was investigated and again the best results were obtained for polymer **22**, in which the hexyl groups point outwards.

A very promising technique was introduced by Kim et al.,[45] who showed that the freezing of polydiphenylacetylene (PDPA, **23** and **24**) into CPNPs in their relaxed state can lead to an extremely high PLQY of 76%. PDPA is an amorphous polymer and the effect of relaxed state freezing is very specific for this polymer of which the backbone is rigid, but highly twisted because of the steric hindrance caused by the phenyl side chains. The twisted and sterically hindered structure can only undergo weak intermolecular interactions, meaning that intermolecular stacking is difficult. However, the phenyl rings on the polymer's side chain can undergo intermolecular stacking, leading to fluorescence quenching in solid state films (PLQY of 1%). When **23** or **24** is

dissolved in a good solvent like THF, the polymer chains become more flexible, reducing the intermolecular stacking and increasing the PLQY to 31%. However, in solution, collisional quenching and vibrational relaxation is still possible. Those quenching processes were reduced by freezing **23** in its relaxed state in CPNPs, leading to a PLQY of 76%. The quantum efficiency of CPNPs of **23** and **24** was compared to those of commercially available 'highly emissive' fluorene based polymers **25** and **26**. Their PLQY did not exceed 7%.

Behrendt et al.[46] tuned the quantum efficiency of fluorene based CPNPs by varying the amount of benzothiadiazole (BT) acceptor. Polymer **28** was prepared with 5 and 10% of thiophene-BT-thiophene and the PLQYs were compared to the emission of **27**. In general, a decrease in the PLQY could be observed after the introduction of BT. However, the decrease was more pronounced for larger amounts of the acceptor unit. In polymer **29**, the introduction of 5−50% of BT was examined. A maximal PLQY of 56% was obtained for the 10% BT polymer, while lower amounts led to significantly lower PLQYs. This can be ascribed to a more effective FRET from fluorene-fluorene moieties to BT-fluorene units for higher BT amounts. The perfectly alternating donor-acceptor polymer showed the lowest PLQY, which was only 12%.

2.4 SURFACE FUNCTIONALIZATION

The functionalization of CPNPs can be a great asset to guide the particles to specific cells or organelles. For this purpose, probes that specifically bind receptors on the targeted cells can be covalently bound to the particle surfaces. Multiple strategies have been investigated to achieve such probe immobilization. All polymer structures discussed below are gathered in Figure 5. The most convenient technique is to functionalize the CP side chains, enabling straightforward covalent linking of the probe. The most widely used functional groups are carboxylic acid and *N*-hydroxysuccinimide (NHS) groups, allowing easy covalent linkage through the formation of amide bonds. In the case of the carboxylic acids, the acids react with 1-ethyl-3-(3-dimethylaminopropyl)carbodiimide (EDC) to form *o*-acylisourea active esters. NHS, on the other hand, is already an activated ester. Both groups can then react with a primary amine to form the desired amide bond.

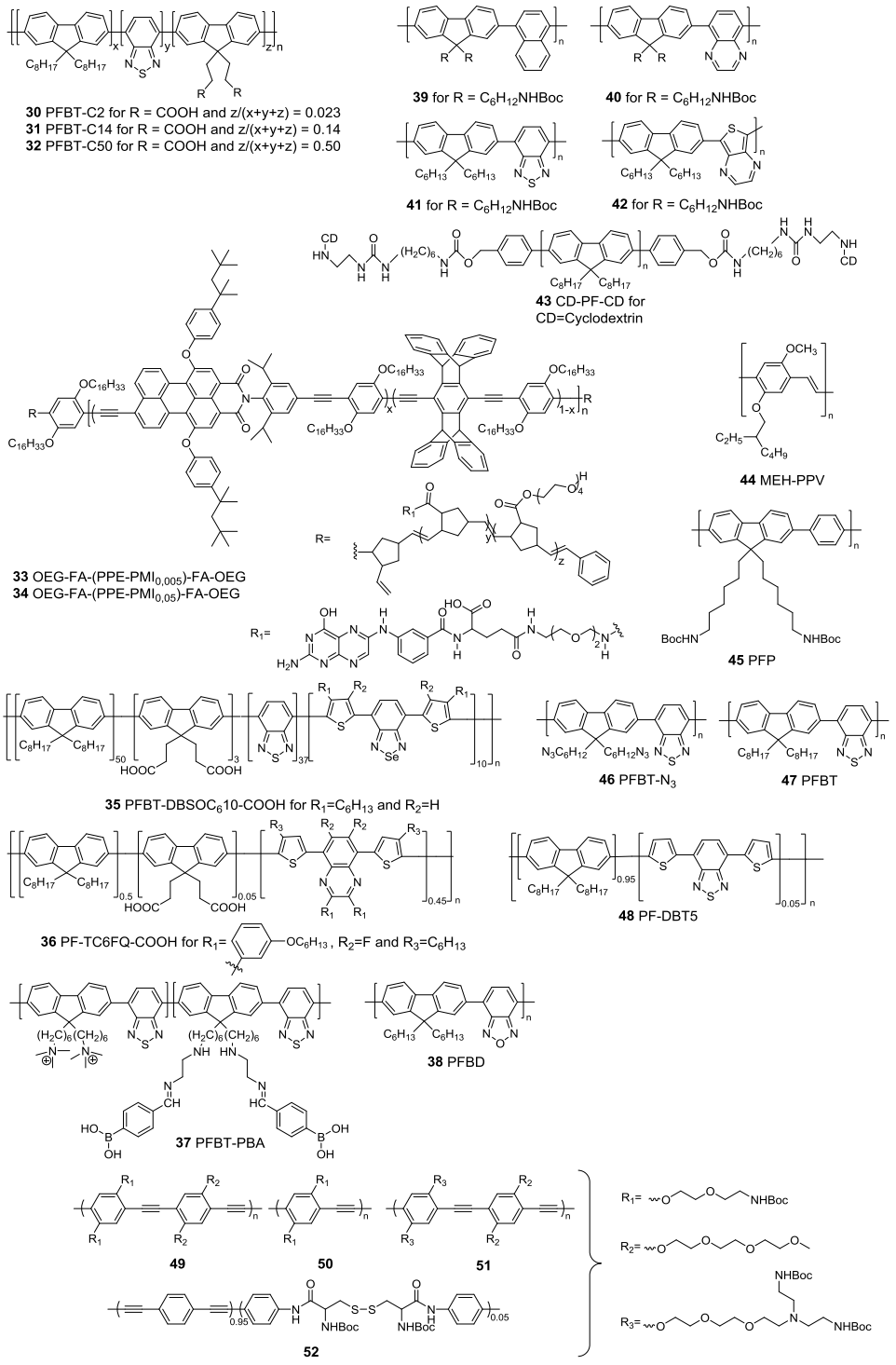

Figure 5: Functionalized CPNPs for covalent or non-covalent probe immobilization to target specific cells or organelles.

Zhang et al.[47] investigated the influence of the carboxylic acid side chain density of poly[(9,9-dioctylfluorenyl-2,7-diyl)-*co*-(1,4-benzo[2,1',3]thiadazole)]s (PFBTs **30**-**32**) on particle formation, colloidal stability, internal structure, fluorescence brightness and non-specific cell adsorption. PFBT polymers with carboxylic acid molar fractions of 2.3, 14 and 50% were synthesized. The PLQY of the CPNPs decreased with higher functionalization degrees, from 30% for polymer **30** to 17% for **32**. The same trend could be observed for the single particle fluorescence brightness (defined as the product of the extinction coefficient at the relevant wavelength and the PLQY). The non-specific adsorption was highest for the densely functionalized particles while it was nihil for particles prepared from **30**. The overall performance was best for the CPNPs synthesized from PFBT **30**. Those particles were then covalently bound to streptavidin and successful imaging of HER2-overexpressed breast cancer cells (SKBR-3) was achieved.

Ahmed et al.[48] developed a pentablock copolymer (**33** and **34**) of an ABCBA structure in which a fluorescent PPE core (block C) comprising 0.5 to 5% of perylene monoimide is coupled to an NHS functionalized block (B). Block A is an oligo(ethylene glycol) structure to improve water solubility, stealth-like and anti-fouling properties. Since folate receptors (FR) are overexpressed on cell membranes of many different cancer cell types (e.g. in ovarian, breast, brain and lung cancer), the authors chose to covalently bind folate to the polymer side chains via NHS chemistry. After particle formation, the hydrophobic A block is situated in the core of the particles, whereas the hydrophilic blocks form a shell around the hydrophobic core, exposing the folate groups to the surrounding medium. The FA-functionalized CPNPs can be seen as a "Trojan Horse", because the activation of the FR induces endocytosis, leading to cancer cell internalization of the CPNPs. The particles with 5% PMI loading exhibited a lower PLQY of 14%, whereas the particles with only 0.5% of PMI loading showed an excellent quantum efficiency of 26%. Cell uptake of particles of **33** and **34** in KB cells (a sub-line of the HeLa tumor cell line) was 3 to 6 times higher compared to those of non-functionalized particles. Furthermore, at high concentrations, the cytotoxicity of the non-functionalized particles was higher due to the high reactivity of the NHS groups. Folate-functionalized NPs, on the other hand, showed no significant cell cytotoxicity.

Chen et al.[38] also introduced carboxylic acid functions onto the side chains of their CPs (**35**) and they were able to covalently bind streptavidin onto the CPNPs via EDC catalyzed coupling. Streptavidin has an extremely high affinity for biotin, which enables the labelling of cellular and subcellular structures when biotinylated receptor ligands of interest are administered. Their theory was confirmed by the imaging of subcellular microtubules in HeLa cells after incubation with a biotinylated monoclonal anti-α-tubulin antibody and by the imaging of MCF-7 cell membranes after incubation with biotinylated primary antihuman CD326 EpCAM antibody. The Pdots are able to bind the biotinylated receptor ligands selectively due to the presence of streptavidin. Moreover, no non-specific adsorption was observed in any of the studied cases.
Liu et al.[39] employed the same technique for streptavidin immobilization on CPNPs of the similar quinoxaline based polymer **36**.

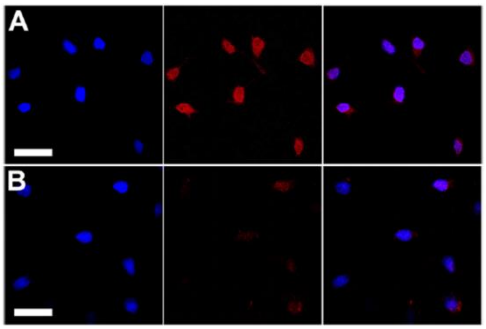

Figure 6: Confocal fluorescence images of SKOV-3 cells labeled by Pdot-folate conjugates and the flow cytometry results using MCF-7 cells. (A) The blue fluorescence results from the nuclear counterstain Hoechst 34580, and the red fluorescence is due to the Pdot-folate conjugates. The right panel shows the overlay of the blue and red fluorescence. (B) Images of negative control samples in which cells were incubated with bare Pdots without folate functionalization. The scale bars are 30 μm. Reproduced with permission.[39] Copyright 2015, American Chemical Society.

These CPNPs showed the same selectivity for the imaging of microtubules in HeLa cells and the imaging of MCF-7 cell membranes. In addition, they utilized receptor mediated endocytosis to label ovarian cancer cells with overexpressed

folate receptors (SKOV-3 cells). This was possible after surface functionalization of the Pdots with folic acid. Strong red fluorescence was observed for cells stained with folate functionalized Pdots, while a significantly lower intensity red fluorescence was observed for cells treated with the bare, non-functionalized Pdots (Figure 6).

Peters et al.[36] prepared PPV based (**3** and **4**, Figure 3) CPNPs and noticed that some of the ester functions on copolymer **4** were hydrolyzed during the washing steps following particle formation. As a proof-of-concept, they immobilized a gold-labeled antibody to the NP surface by means of EDC coupling. The success of the reaction was shown by TEM and was confirmed by energy-dispersive X-ray (EDX) spectroscopy.

Liu et al.[49] introduced phenylboronic acid (PBA) groups on a poly(fluorene-*alt*-benzothiadiazole) polymer (**37**). PBA is known to undergo a pH driven reversible esterification reaction with *cis*-diol compounds to form cyclic boronates. This reaction can be of interest for the selective targeting of sialic acid (SA, a 9-C monosaccharide) overexpressed cancer cells like DU-145 (prostate cancer cell line). Unfortunately, PBA has no preference for SA over other monosaccharides. This problem was solved by SA-template imprinting in the CPNPs during co-precipitation. SA was subsequently removed by adjusting the pH followed by dialysis. The cavities formed on the surface of the CPNPs perfectly fit SA, leading to a selective targeting of cancer cells with SA overexpression.

Sometimes, functional groups are not directly bound to the CP, but to surfactant or matrix molecules. Li et al.[50] prepared CPNPs from poly(fluorene-*co*-benzoxadiazole) **38** via the mini-emulsion technique, using PEG-COOH as the surfactant. Remarkably small CPNPs were formed, with a hydrodynamic diameter of only 20 nm. No broadening of the absorption spectra of the CPNPs of **38** in water compared to the molecularly dissolved polymer (in dichloromethane) was observed. This indicates a low amount of inter-chain aggregates in the particles, which can explain the exceptionally high PLQY of 46%. Bioconjugation with a cyclic amine labeled RGDfK peptide was achieved in the presence of EDC and *N*-hydroxysulfosuccinimide (sulfo-NHS). After incubation of HT-29 human colon cancer cells, the particles were found to clearly bind to the cells, whereas for the non-labeled NPs no fluorescence was observed (Figure 7).

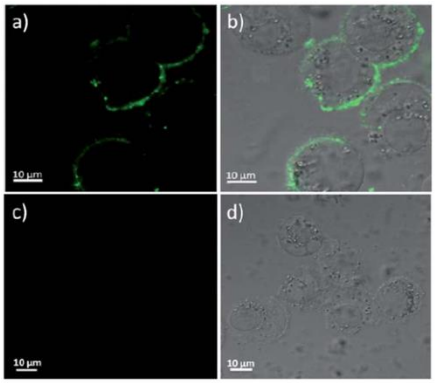

Figure 7: Confocal fluorescence images of HT-29 cells labeled with cyclic RGDfK tagged PEG-PFBD 33 dots after 15 min incubation at room temperature (top row) and non-functionalized PEG-PFBD dots (bottom row). Scale bar: 10 µm. Reproduced with permission.[50] Copyright 2012, Royal Society of Chemistry.

Feng et al.[51] developed 4 different CPNPs with four different colors. To achieve this, they co-precipitated fluorene based alternating copolymers **39**-**42** with poly(styrene-*co*-maleic anhydride) (PSMA). After particle formation, modification of the surface with carboxyl groups was conducted. Different antibodies were then successfully immobilized onto the particle surfaces via amide coupling. This variety in functionalized CPNPs enabled a double-antibody recognition mode for the specific detection of cancer cells. In this work, differentiation between SK-BR3, MCF-7 and HeLa cells was demonstrated. One batch of CPNP41 was functionalized with anti-EpCAM and another with anti-ErbB2. Treatment of SK-BR3, MCF-7 and HeLa cells with the particles was performed and only SK-BR3 and MCF-7 cells were stained with the anti-EpCAM particles, while the anti-ErbB2 particles only stained the HeLa cells. All three cell types could be distinguished, even though the SK-BR3 and MCF-7 belong to the same breast cancer cell lines.
Sun et al.[52] introduced β-cyclodextrin (CD) units on the outer ends of every polyfluorene (**43**) chain. They modified the CPNPs via the typical host-guest interaction between CD and adamantane (ADA), which was introduced on the chain ends of 4 different glycopolymers. The glycopolymer functionalized NPs (Lac-NP) showed an excellent binding to lectines like e.g. galectin-3 (GAL), which has been shown to be crucial in cell-cell interactions related to many diseases like cancer. Gal-NP specifically entered Hep-G2 cells (liver cancer cells)

that express the Gal-specific ASGP receptor on their surface, which enables specific targeting of turmeric tissue.

In some other studies, functional groups for NP modification were introduced onto matrix materials instead of the CP itself. Joshi et al.[53] encapsulated PPV-based (**44**) CPNPs with a porous silica matrix to increase the stability of the particles. Silica is a well-known carrier that is biocompatible, non-interfering, transparent to visible light and easy to functionalize. Modification of the silica coated PPV-CPNPs was achieved by coating the particles with (3-aminopropyl)triethoxysilane (APTES), an amine modified silane layer. After modification, the zeta-potential of the particles rose from -41 to 18 mV, indicating that the surface hydroxyl groups are exchanged by amine groups pointing outwards. Covalent linking of ligands onto the particles was not shown in this work.

Copper catalyzed azide-alkyne click (CuAAC) functionalities are bio-orthogonal, indicating that no reactions occur between those functional moieties and bio-available functional groups. This is a remarkable asset compared to regularly employed functional groups such as carboxylic acids or amines that are reactive in living cells. The inert nature of those bio-orthogonal groups generally makes them less cytotoxic than for example NHS-coupled counterparts and non-specific adsorption is often reduced as well. Li et al.[54] developed hybrid CPNPs consisting of poly(fluorene-*co*-phenylene) **45** (PFP) combined with an azide-functionalized PEG-chain (PLGA-PEG-N_3). Because of the hydrophobic nature of the PFP and the hydrophilicity of PLGA-PEG-N_3, a fluorescent PFP core is formed and the azide functionalities are pointing outwards due to the hydrophilic nature of the PEG. Plerixafor (PLE) is an FDA approved drug, known to inhibit endocytosis of CXCR4 transmembrane proteins and this makes it the ideal ligand for cell membrane labelling. Alkyne functionalities were introduced onto PLE and a CuAAC reaction was performed between the CPNPs and PLE. The CPNPs were found to effectively locate on the cell membrane.

Liu et al.[40,41] designed CPNPs synthesized from polymers **14**, **15** or **16** (Figure 4) in a matrix of 1,2-distearoyl-*sn*-glycero-3-phosphoethanolamine-*N*-[methoxy(polyethylene glycol)-2000] (DSPE-PEG_{2000}) and its maleimide modified derivative DSPE-PEG_{2000}-Mal. A hydrophobic core consisting of the conjugated polymer (**14**, **15** or **16**) was formed, while the hydrophilic PEG and PEG-Mal

point outwards. Click functionalization of the maleimide groups with anti-HER2 affibody (for **14** and **15** based CPNPs) or human immunodeficiency virus type 1 (HIV-1) trans-activating transcriptional activator (Tat, for **16** based CPNPs) was performed to increase the HER2-overexpressed SKBR-3 breast cancer cell (CPNP**14** and CPNP**15**) or HepG2 liver cancer cell (for CPNP**16**) internalization efficiency compared to the non-functionalized CPNPs. The fluorescence intensity of SKBR-3 cells incubated with affibody functionalized and non-functionalized CPNP**14** and CPNP**15** was compared (Figure 8). Few non-bioconjugated particles are able to enter the cancer cells due to their PEG shell, which inhibits nonspecific cellular internalization (Figure 8 A and B). While for CPNP**14**-Mal, no fluorescence could be observed, some weak fluorescent dots appeared for CPNP**15**-Mal. A strong increase of fluorescence brightness was observed for CPNP**15**-Affibody (Figure 8D). For both, the increase in emission can be ascribed to the remarkably higher PLQY of the CPNPs formed by the POSS-functionalized polymer **15**. The introduction of affibody on the CPNPs surface induces specific cell uptake of the particles (compare Figure 8C and A, D and B).

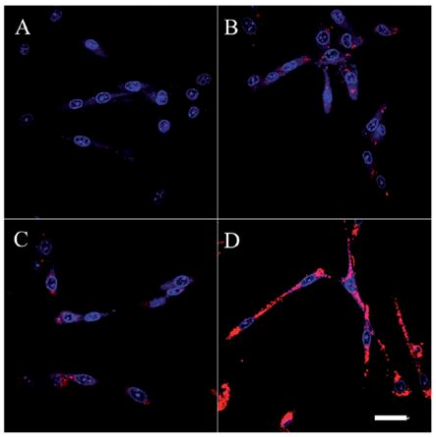

Figure 8: Confocal laser scanning microscopy (CLSM) images of fixed SKBR-3 breast cancer cells incubated with CPNP14-Mal (A), CPNP15-Mal (B), CPNP14-Affibody (C) and CPNP15-Affibody (D) at 37 °C overnight. All images share the same scale bar of 30 µm. Reproduced with permission.[40] Copyright 2013, Royal Society of Chemistry.

Liu et al.[40] also showed that the affibody-bioconjugated CPNP**15**s were able to specifically enter HER2-overexpressed breast cancer cells (SKBR-3), while no uptake in non-HER2-overexpressed breast cancer cells (MCF-7) and normal cells (MIH-3T3 fibroblasts) could be observed (Figure 9). With CPNP**16**, in vivo monitoring of liver tumor growth was possible up to 27 days because of the long residence time of the particles in the body (Figure 10).

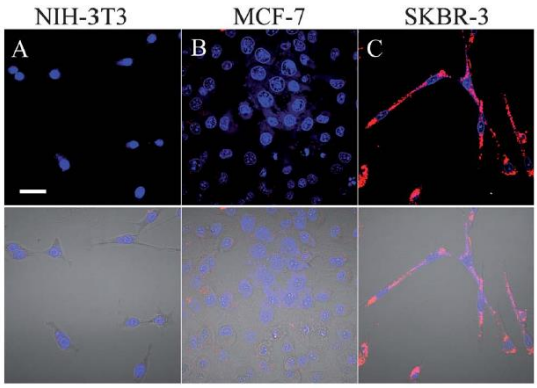

Figure 9: CLSM fluorescence (top) and fluorescence/transmission overlay (bottom) images of fixed NIH-3T3 (A), MCF-7 (B) and SKBR-3 (C) cells incubated overnight with 5 nM CPNP15 at 37 °C. All images share the same scale bar of 30 µm. Reproduced with permission.[40] Copyright 2013, Royal Society of Chemistry.

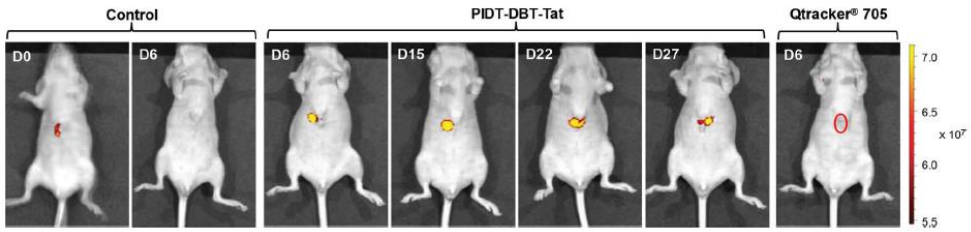

Figure 10: Representative in vivo fluorescence images of a mouse transplanted with 4 × 10^6 of HepG2 cells labeled by CPNP**13** and Qtracker 705. Control images were obtained from a nude mouse that underwent the same surgical operation without injection of labeled HepG2 cells. The images were taken on designated days post cell injection (λ_{ex} = 640 nm, 720/20 nm filter). Reproduced with permission.[41] Copyright 2015, Wiley.

In 2012, Zhou et al.[55] introduced CPNPs embedded in a covalently bound hydroxyl-containing matrix material. By copper-free thermally initiated click chemistry they were able to form NPs from azide functionalized copolymer **46** with alkyne-functionalized hyperbranched polyglycerol (HPG). The size of the particles could be adjusted from 40 to 210 nm and PLQYs up to 23% were obtained. MCF-7 breast cancer cells were treated with the particles and efficient internalization was observed. Unfortunately, no bioconjugation of the CPNPs was shown.

Somewhat later, Koner et al.[56] co-precipitated commercially available polymers **47** and **48** with polystyrene (PS) decorated with either hydroxyl or carboxylic acid terminated PEG side chains. The hydrophobic PS backbone entangles in the hydrophobic CP core of the particles, while the functionalized PEG chains point outwards. The particles exhibited an excellent PLQY of 57% and high stability. After particle formation, the hydroxyl groups were activated with 1,1'-carbonyldiimidazole (CDI), which allows further reactions with amines to form carbamates. Particle functionalization with streptavidin was performed and HeLa cervical cancer cells were incubated with biotin and the carboxylic acid or hydroxyl functionalized CPNPs. Biotinylated cells were clearly marked by the fluorescent Pdots. Non-biotinylated cells were non-specifically bound by the carboxylic acid functionalized particles, whereas no binding was observed for the hydroxyl terminated particles. The introduction of hydroxyl groups on the CPNP surface thus reduces non-specific cell binding.

Ding et al.[43] prepared functionalized CPNPs via co-precipitation of polymer **20** (Figure 4) with DSPE-PEG_{2000} and FA-functionalized PEG (DPSE-PEG_{5000}-FA). This approach is interesting because no post-NP-formation functionalization is needed, thus leaving out one synthesis step. MCF-7 breast cancer cells with overexpressed FR and NIH/3T3 fibroblast normal cells with low FR expression were incubated with the FA-functionalized and non-functionalized Pdots. A remarkably more intense fluorescence (x1.8) could be observed for the MCF-7 cells treated with the FA-functionalized particles, showing that active transport of the NPs via FR is occurring. Furthermore, when free FA is available in the medium, less NP internalization in the MCF-7 cells was observed, indicating that the FA groups on the particle surface mediate cell entrance. The functionalized and non-functionalized NPs exhibited an equal fluorescence intensity after

NIH/3T3 staining due to the low FR expression in those cells.

The introduction of amphiphilic peptides as capping ligands was demonstrated by Almeida et al.[57] Three different peptide sequences were conjugated to a branched aliphatic chain by their N-terminus, enabling embedding of the aliphatic tail in the CP core (**47**), while the peptide sequences are exposed to the medium. The first sequence was the positively charged cell penetrating TAT sequence (2-hexyldecane-GRKKRRQRRRPQ-amide), the second one the negatively charged anti-TAT sequence (2-hexyldecane-GDEEDDQDDDPQ-amide, designed to mimic the TAT sequence) and the third a zwitterionic PEK peptide (2-hexyldecane-PPPPEKEKEKEK-amide), which is known to inhibit cellular uptake. HeLa cells were treated with the peptide-functionalized particles (TAT/NP, anti-TAT/NP and PEK/NP) and after 30 min, internalization of TAT/NP into the perimembraneous region was observed. After 2 h of incubation, the particles migrated to the cytoplasmic region, whereas after 24 h, accumulation in the perinuclear region was noticed. The anti-TAT/NP and PEK/NP showed minimal cell internalization due to the negative charges on the peptide chains. Furthermore, they showed altered emission colors through the use of other CPs, although the cellular uptake of the particles remained the same. Via this multi-color imaging, Almeida and coworkers were able to point out that cell internalization of negatively charged particles was facilitated by TAT/NPs when cells were treated with both particles at the same time.

Another strategy was employed by Mendez et al.,[58] who obtained subcellular localization of PPE-based (**49**-**52**) CPNPs (denoted as CPNP-1 to CPNP-4, respectively) driven by the type of functional groups on the CP side chains. The presence of primary amine groups (CPNP-2) and a higher flexibility of the polymer backbone (CPNP-4) increased Golgi localization, whereas the presence of short ethylene glycol side chains (CPNP-1) and tertiary amine groups (CPNP-3) decreased Golgi localization (Figure 11). Moreover, the cell cytotoxicity for CPNP-1 and CPNP-3 was higher.

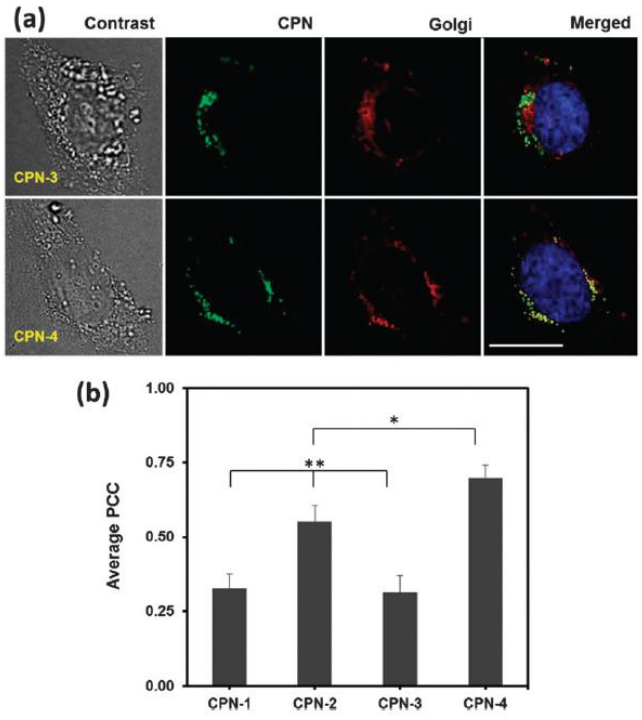

Figure 11: (a) Microscopic images of HeLa cells incubated with CPNP-3 and CPNP-4, followed by Golgi (red) and nucleus (blue) staining. The scale bar is 20 μm. CPNP-4 exhibits a higher overlap with Golgi than CPNP-3. (b) Quantitative analysis of co-localization using the PCC algorithm. Co-localization with Golgi is dependent on the side chain and backbone structures. The error bar represents ±standard deviation (n = 3). *<0.05 when CPNP-4 compared with CPN-2. **<0.0005 when CPNP-1 and CPNP-3 are compared with CPNP-2 and CPNP-4 (n = 3). Reproduced with permission.[58] Copyright 2013, Royal Society of Chemistry.

2.5 THERANOSTIC CPNPS

Theranostic agents combine diagnosis and therapy. The theranostic properties of CPNPs have been investigated in multiple cases where the fluorescence brightness of the particles leads to diagnosis (e.g. cancer) due to specific binding of the CPNPs to specific receptors (e.g. FR). When the particles are loaded with a drug, it can immediately be delivered and released at the site of interest. On the

other hand, controlled and located release of the pharmaceuticals can also decrease the toxicity to healthy cells. All structures discussed in this section are gathered in Figure 12.

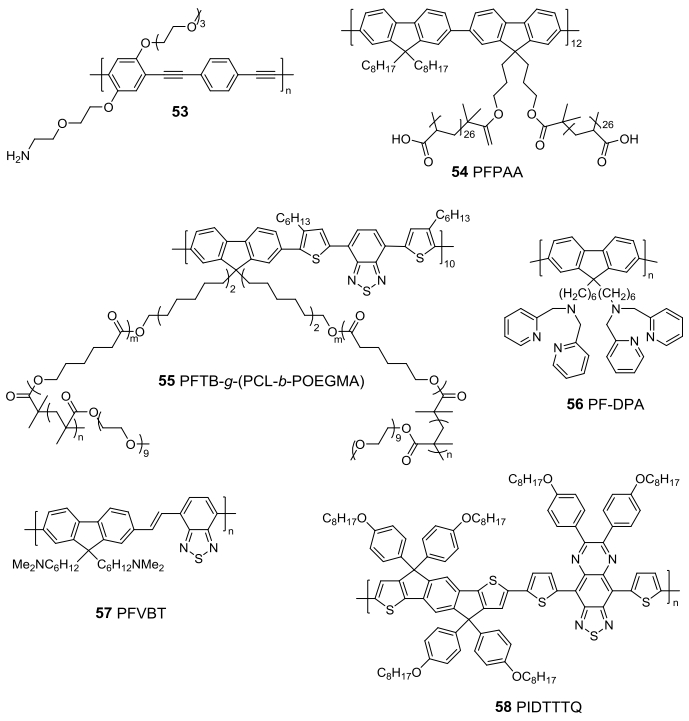

Figure 12: CPs used to form theranostic CPNPs.

Chen et al.[59] developed self-assembled NPs from the amphiphilic PPE copolymer **53**. The hydrophobic CP backbone will form the core of the particles, while the hydrophilic triethylene glycol monomethyl ether side chains and the amine groups will point outwards. Internalization of the CPNPs in human prostate cancer cells (PC3) was illustrated, and the cell cytotoxicity was found to be low. Because of the rigid and hydrophobic nature of the polymer backbone, it was possible to load the particles with the anti-cancer drug doxorubicin (DOX), which is internalized via strong intermolecular π-π stacking interactions. A loading capacity of 5.1% was achieved. In vitro drug release studies have been performed by staining of the PC3 cells with the loaded CPNPs. After particle internalization, slow DOX release was observed. Furthermore, cell viabilities

decreased with increasing DOX loading. It should be noted that the loaded CPNPs had a lower cytotoxicity to the PC3 cells than free DOX at the same dose due to the prolonged release of DOX from the PPE-NPs. This is also reflected in the IC50 value for the PPE-NPs (4.23 µg/mL), which is higher than the value for free DOX (1.71 µg/mL). Overall, the growth of cancer cells could be inhibited by the use of the loaded CPNPs, while the toxicity of the drug could be reduced.

Lu et al.[60] synthesized fluorine copolymer **54**, a grafted CPE with multiple carboxylate groups on the brush-like side chains. These carboxylic acid groups served as a polydentate ligand to bind and thus stabilize magnetic Fe_3O_4 nanoparticles (MNPs). The CP is highly fluorescent, leading to MNPs with a PLQY of 21%, which is boosted by the brush-like polymer structure, preventing inter-chain aggregation and thus fluorescence quenching. Due to the superparamagnetic properties of the particles, imaging via MRI is possible and the delivery of the particles to target sites via an external applied magnetic field can be performed while monitoring with a fluorescent microscope. Low cytotoxicity of the MNPs was observed after treatment of NIH-3T3 fibroblasts. Due to the brush-like structure of **54**, more DOX molecules can be accommodated, leading to high drug loadings of 10 wt%. BGC-823 human gastric cancer cells were incubated with the DOX-loaded MNPs and a good therapeutic efficiency was observed. After 10 h, only 30% of the cancer cells survived, while a 90% cell viability of the cells treated with DOX-free particles was noted. Furthermore, drug release was shown to be pH dependent, with better results in more acidic environment. This is beneficial for therapeutic use in cancer cells because their cytoplasm is slightly acidic.

The pH dependent DOX release was also observed by Yang et al.[61] They synthesized a poly(fluorene-*alt*-benzothiadiazole) copolymer (**55**) grafted with PCL and poly[oligo(ethylene glycol) methyl ether methacrylate] (POEGMA) block copolymers. Those bottlebrush-like polymers form highly fluorescent unimolecular micelles, with a PLQY up to 25% through prevention of intermolecular aggregation. The influence of the presence of a PCL block on the PLQY was investigated and an increase of 5% was observed, from 17 to 22%. Furthermore, the PCL block serves as a reservoir for DOX loading. The longer the PCL block, the more DOX could be loaded in the reservoir. Amounts up to 10 wt% could be achieved. On the other hand, DOX release was dependent on the

POEGMA chain length, with an optimal degree of polymerization of 29. Longer chains retarded the DOX release due to their bulkiness. The DOX-loaded unimolecular micelles showed a low cytotoxicity for normal cells (L929), whereas the toxicity for cervical cancer cells (HeLa cells) was remarkably higher. This effect could be attributed to the pH dependent DOX release, which is higher for more acidic cells like cancer cells.

Muthuraj and co-workers developed polyfluorene based (**56**) CPNPs with dual state emission, but rather low PLQY of 3%.[62] These particles have the unique property of being toxic to melanoma (B16F10) and ovarian cancer (SKOV-3) cells, even without drug loading. On the other hand, the cytotoxicity to normal cells (NIH-3T3 and CHO cells) is minimal. These results were reflected in the IC50 values obtained for NIH-3T3 (>2000 µg/mL) and CHO cells (1851 µg/mL), which were higher than those of B16F10 (411 µg/mL) and SKOV-3 cells (766 µg/mL). A clear inhibition of cancer cell proliferation was observed, even for low concentrations (<200 µg/mL). This observation can be ascribed to a larger particle uptake in cancer cells compared to normal cells under the same treatment concentrations. The di(picolyl)amine (DPA) functionalities on the polymer side chains have been shown to trigger the formation of reactive oxygen species (ROS), which play a crucial role in cancer cell death. More ROS were produced in B16F10 cancer cells treated with the CPNPs compared to non-treated cells, leading to more cell death. Due to the multifunctional nature of the particles, no leaking of the highly toxic anti-cancer drug out of the particles is possible, preventing severe side effects for the patients to be treated.

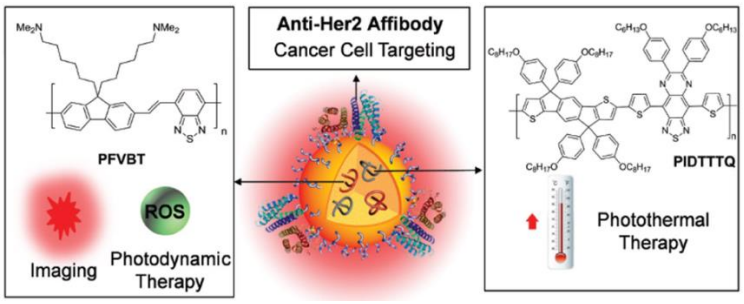

Figure 13: Schematic illustration of the components and functions of anti-HER2-CPNs consisting of **57**, **58** and DSPE-PEG_{2000}-maleimide. Reproduced with permission.[63] Copyright 2017, Wiley.

Multifunctional CPNPs consisting of two different CPs **57** and **58** in a DSPE-PEG_{2000}-maleimide matrix were very recently developed by Feng et al (Figure 13).[61] PFVBT **57** is highly fluorescent, leading to a PLQY of 23% for the formed CPNPs. Moreover, it can also efficiently transform light into ROS. On the other hand, PIDTTTQ **58** is a non-fluorescent material that can convert light into thermal heat, which makes the particles suitable for photothermal therapy. Since the CPNPs are toxic to biological tissue under irradiation, specific particle localization is of utmost importance. This was achieved by click immobilization of anti-HER2 affibody onto the particle surface. CPNPs internalization was only observed for HER2 overexpressed SKBR-3 breast cancer cells, while no uptake was noticed for MCF-7 breast cancer cells and NIH-3T3 normal fibroblast cells lacking HER2 expression (Figure 14). Successful tumor cell (SKBR-3) death was observed after incubation with the CPNPs and irradiation with NIR laser light and/or white light (Figure 14E), which can partly be ascribed to ROS formation. This was demonstrated by the cell permeable fluorescent dye dichlorofluorescein diacetate (DCF-DA), a ROS indicator that is rapidly oxidized to dichlorofluorescein (DCF), affording a bright green fluorescence (Figure 14D).

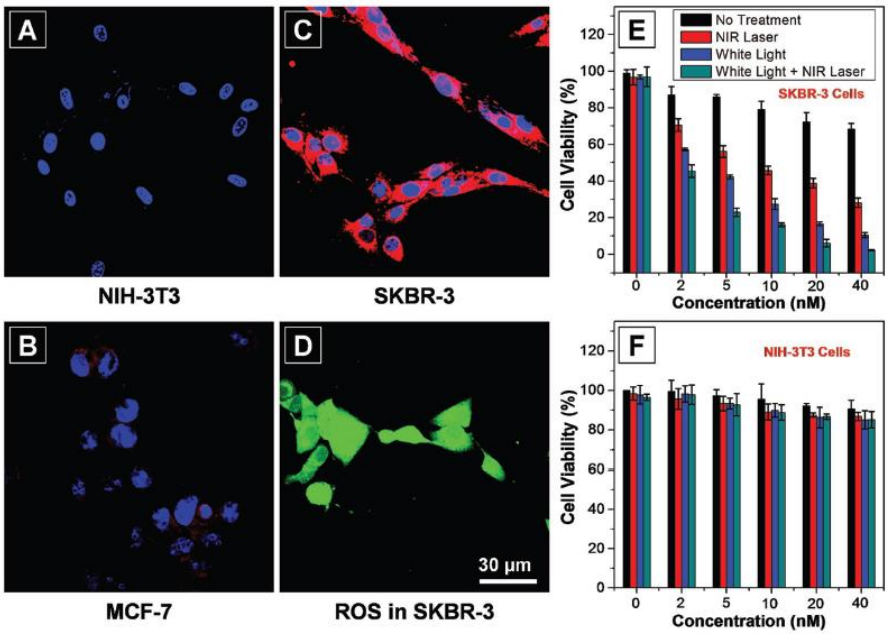

Figure 14: Confocal images of A) NIH-3T3, B) MCF-7, and C) SKBR-3 cells after 4 h incubation with anti-HER2-CPNPs (2 × 10−9 M). The red fluorescence of anti-HER2-CPNPs is collected above 505 nm upon excitation at 488 nm. The blue fluorescence of Hoechst from the nucleus is collected from 430 to 470 nm upon excitation at 405 nm. D) Detection of intracellular ROS generation by DCF-FA in SKBR-3 cells after incubation with anti-HER2-CPNPs (2 × 10^{-9} M, 4 h) followed by light irradiation (30 s). Images (A)–(D) share the same scale bar of 30 μm. Cell viabilities of E) SKBR-3 and F) NIH-3T3 cells after incubation with anti-HER2-CPNPs (2 × 10−9 M, 4 h) followed by photodynamic and photothermal treatment. Reproduced with permission.[63] Copyright 2017, Wiley.

2.6 CONCLUSIONS AND OUTLOOK

Conjugated polymer nanoparticles are attractive fluorescent probes due to their excellent optical properties and low cytotoxicity. Up until now, a whole range of polymer particles have been synthesized, with particle sizes ranging from the nano- to the micrometer scale and with colors covering the entire visible range. Most conjugated polymers used for imaging have a rather simple backbone structure, often based on fluorene.[31-36] On the other hand, a huge variety of

push-pull type semiconducting polymers have recently been studied for optoelectronic applications, notably organic photovoltaics.[64] We believe that multiple of those structures could be useful for imaging too. The combination of strong donor and acceptor monomers leads to low bandgap materials of which the absorption and emission maxima can be pushed toward the NIR region. This wavelength range is of particular interest for bio-imaging because of the low autofluorescence and deep tissue penetration of NIR light. Unfortunately, the photoluminescence quantum yield generally drops when the NIR regime is approached. Different techniques have been employed to boost the fluorescence intensity. Most of these techniques rely on the prevention or limitation of π-π stacking in the particles. Nevertheless, quantum efficiencies hardly reach values over 50%. The introduction of specific moieties known to exhibit aggregation induced emission seems to be an attractive alternative solution, since those materials exhibit higher emission efficiencies when tight packing can be obtained.[35,38-46]

Surface functionalization of the conjugated polymer nanoparticles is needed to target specific cells. Functional groups allowing bioconjugation have been introduced on the conjugated polymer backbone itself or on non-conjugated matrix materials such as PEG chains or silica. The most frequently introduced functional groups are carboxylic acids and amines. However, due to their pH dependent charge, functionalized particles experience difficulties to enter cells under certain conditions. Click functionalities like maleimides, alkynes and azides have been explored as alternatives. A vast range of immobilization methods have been studied so far, allowing the immobilization of nearly any ligand to the particle surfaces.[36,38-41,43,47-58]

Since specific cell targeting can be achieved, conjugated polymer nanoparticles are also of interest for therapeutic applications. The advantage of delivering cell-attacking drugs to the region of interest minimizes healthy cell destruction. Several conjugated polymer nanoparticles were loaded with doxorubicin, a well-known anti-tumor drug, via non-covalent interactions. The side chains of the conjugated polymers in these cases typically act as a reservoir for the drug molecules. Other examples use conjugated polymers known to generate reactive oxygen species, which are toxic for tumor cells.[59-63]

On the basis of the steady improvements on the brightness, stability, cell

viability, specificity and theranostic nature of many conjugated polymer nanoparticles reported in literature, a 'bright' future lies ahead for conjugated polymer nanoparticle bio-imaging.

2.7 REFERENCES

[1] C. Wu and D. T. Chiu, *Angew. Chem. Int. Ed.*, 2013, **52**, 3086.
[2] M. Carril, *J. Mater. Chem. B*, 2017, **5**, 4332.
[3] D. J. Brenner and E. J. Hall, *N. Engl. J. Med.*, 2007, **357**, 2277.
[4] V. Paefgen, D. Doleschel and F. Kiessling, *Front. Pharmacol.*, 2015, **6**, 197.
[5] K. Lameka, M. D. Farwell and M. Ichise, *Handbook of Clinical Neurology*, 2016, **35**, 209.
[6] J. Yao, M. Yang and Y. Duan, *Chem. Rev.*, 2014, **114**, 6130.
[7] G. M. van Dam, G. Themelis, L. M. A. Crane, N. J. Harlaar, R. G. Pleijhuis, W. Kelder, A. Sarantopoulos, J. S. de Jong, H. J. G. Arts, A. G. J. van der Zee, J. Bart, P. S. Low and V. Ntziachristos, *Nat. Med.*, 2011, **17**, 1315.
[8] U. Resch-Genger, M. Grabolle, S. Cavaliere-Jaricot, R. Nitschke and T. Nann, *Nat. Meth.*, 2008, **5**, 763.
[9] C. Wu, B. Bull, C. Szymanski, K. Christensen and J. McNeill, *ACS Nano*, 2008, **2**, 2415.
[10] J. Peng, X. He, K. Wang, W. Tan, Y. Wang and Y. Liu, *Anal. Bioanal. Chem.*, 2007, **388**, 645.
[11] H.-S. Peng, J. A. Stolwijk, L.-N. Sun, J. Wegener and O. S. Wolfbeis, *Angew. Chem. Int. Ed.*, 2010, **122**, 4342.
[12] X. Michalet, F. F. Pinaud, L. A. Bentolila, J. M. Tsay, S. Doose, J. J. Li, G. Sundaresan, A. M. Wu, S. S. Gambhir and S. Weiss, *Science*, 2005, **307**, 538.
[13] B. A. Kairdolf, A. M. Smith, T. H. Stokes, M. D. Wang, A. N. Young and S. Nie, *Annu. Rev. Anal. Chem.*, 2013, **6**, 143.
[14] R. Ahmad Khanbeigi, T. F. Abelha, A. Woods, O. Rastoin, R. D. Harvey, M.-C. Jones, B. Forbes, M. A. Green, H. Collins and L. A. Dailey, *Biomacromolecules*, 2015, **16**, 733.
[15] D. Tuncel and H. V. Demir, *Nanoscale*, 2010, **2**, 484.

[16] P.-L. T. Boudreault, A. Najari and M. Leclerc, *Chem. Mater.*, 2011, **23**, 456.

[17] E. Hemmer, A. Benayas, F. Légaré and F. Vetrone, *Nanoscale Horiz.*, 2016, **1**, 168.

[18] T. Klingstedt and K. P. R. Nilsson, *Biochim. Biophys. Acta*, 2011, **1810**, 286.

[19] N. Y. Kwon, D. Kim, G. Jang, J. H. Lee, J.-H. So, C.-H. Kim, T. H. Kim and T. S. Lee, *ACS Appl. Mater. Interfaces*, 2012, **4**, 1429.

[20] Z. Kahveci, R. Vázquez-Guilló, M. J. Martínez-Tomé, R. Mallavia and C. R. Mateo, *ACS Appl. Mater. Interfaces*, 2016, **8**, 1958.

[21] M. Ma, M. Lei, X. Tan, F. Tan and N. Li, *RSC Adv.*, 2016, **6**, 1945.

[22] J. Yu, Y. Rong, C.-T. Kuo, X.-H. Zhou and D. T. Chiu, *Anal. Chem.*, 2017, **89**, 42.

[23] Y.-H. Chan and P.-J. Wu, *Part. Part. Syst. Charact.*, 2015, **32**, 11.

[24] J. Pecher and S. Mecking, *Chem. Rev.*, 2010, **110**, 6260.

[25] J. L. Brédas, D. Beljonne, V. Coropceanu and J. Cornil, *Chem. Rev.*, 2004, **104**, 4971.

[26] S. Doose, H. Neuweiler and M. Sauer, *ChemPhysChem*, 2009, **10**, 1389.

[27] H. Klauk, Organic Electronics: Materials, Manufacturing and Applications, 2006, Wiley.

[28] J. R. Lakowicz, Principles of Fluorescence Spectroscopy, 2006, Springer US.

[29] L. Feng, C. Zhu, H. Yuan, L. Liu, F. Lv and S. Wang, *Chem. Soc. Rev.*, 2013, **42**, 6620.

[30] J. Yoon, J. Kwag, T. J. Shin, J. Park, Y. M. Lee, Y. Lee, J. Park, J. Heo, C. Joo, T. J. Park, P. J. Yoo, S. Kim and J. Park, *Adv. Mater.*, 2014, **26**, 4559.

[31] G. Hong, Y. Zou, A. L. Antaris, S. Diao, D. Wu, K. Cheng, X. Zhang, C. Chen, B. Liu, Y. He, J. Z. Wu, J. Yuan, B. Zhang, Z. Tao, C. Fukunaga and H. Dai, *Nat. Commun.*, 2014, **5**, 4206.

[32] W. Denk, J. Strickler and W. Webb, *Science*, 1990, **248**, 73.

[33] C. Wu, C. Szymanski, Z. Cain and J. McNeill, *J. Am. Chem. Soc.*, 2007, **129**, 12904.

[34] J. Pecher, J. Huber, M. Winterhalder, A. Zumbusch and S. Mecking, *Biomacromolecules*, 2010, **11**, 2776.

[35] Y. Lv, P. Liu, H. Ding, Y. Wu, Y. Yan, H. Liu, X. Wang, F. Huang, Y. Zhao and Z. Tian, *ACS Appl. Mater. Interfaces*, 2015, **7**, 20640.

[36] M. Peters, N. Zaquen, L. D'Olieslaeger, H. Bové, D. Vanderzande, N. Hellings, T. Junkers and A. Ethirajan, *Biomacromolecules*, 2016, **17**, 2562.

[37] Y. Rong, C. Wu, J. Yu, X. Zhang, F. Ye, M. Zeigler, M. E. Gallina, I.-C. Wu, Y. Zhang, Y.-H. Chan, W. Sun, K. Uvdal and D. T. Chiu, *ACS Nano*, 2013, **7**, 376.

[38] C.-P. Chen, Y.-C. Huang, S.-Y. Liou, P.-J. Wu, S.-Y. Kuo and Y.-H. Chan, *ACS Appl. Mater. Interfaces*, 2014, **6**, 21585.

[39] H.-Y. Liu, P.-J. Wu, S.-Y. Kuo, C.-P. Chen, E.-H. Chang, C.-Y. Wu and Y.-H. Chan, *J. Am. Chem. Soc.*, 2015, **137**, 10420.

[40] J. Liu, G. Feng, D. Ding and B. Liu, *Polym. Chem.*, 2013, **4**, 4326.

[41] J. Liu, K. Li and B. Liu, *Adv. Sci.*, 2015, **5**, 1500008.

[42] L. D'olieslaeger, Y. Braeken, S. Cheruku, J. Smits, M. Ameloot, D. Vanderzande, W. Maes and A. Ethirajan, *J. Colloid Interface Sci.*, 2017, **504**, 527.

[43] D. Ding, J. Liu, G. Feng, K. Li, Y. Hu and B. Liu, *Small*, 2013, **9**, 3093.

[44] C. Yang, H. Liu, Y. Zhang, Z. Xu, X. Wang, B. Cao and M. Wang, *Biomacromolecules*, 2016, **17**, 1673.

[45] B. S.-Il Kim, Y.-J. Jin, W.-E. Lee, D. J. Byun, R. Yu, S.-J. Park, H. Kim, K.-H. Song, S.-Y. Jang and G. Kwak, *Adv. Optical Mater.*, 2015, **3**, 78.

[46] J. M. Behrendt, J. A. Esquivel Guzman, L. Purdie, H. Willcock, J. J. Morrison, A. B. Foster, R. K. O'Reilly, M. C. McCairn and M. L. Turner, *React. Funct. Polym.*, 2016, **107**, 69.

[47] X. Zhang, J. Yu, C. Wu, Y. Jin, Y. Rong, F. Ye and D. T. Chiu, *ACS Nano*, 2012, **6**, 5429.

[48] E. Ahmed, S. W. Morton, P. T. Hammond and T. M. Swager, *Adv. Mater.*, 2013, **25**, 4504.

[49] R. Liu, Q. Cui, C. Wang, X. Wang, Y. Yang and L. Li, *ACS Appl. Mater. Interfaces*, 2017, **9**, 3006.

[50] Y. Li, J. Liu, B. Liu and N. Tomczak, *Nanoscale*, 2012, **4**, 5694.

[51] L. Feng, L. Liu, F. Lv, G. C. Bazan and S. Wang, *Adv. Mater.*, 2014, **26**, 3926.

[52] P. Sun, M. Lin, G. Chen and M. Jiang, *Sci. China Chem.*, 2016, **59**, 1616.

[53] P. B. Joshi and P. Zhang, *J. Mater. Sci.*, 2015, **50**, 3597.

[54] M. Li, C. Nie, L. Feng, H. Yuan, L. Liu, F. Lv and S. Wang, *Chem. Asian J.*, 2014, **9**, 3121.

[55] L. Zhou, J. Geng, G. Wang, J. Liu and B. Liu, *ACS Macro. Lett.*, 2012, **1**, 927.

[56] A. L. Koner, D. Krndija, Q. Hou, D. J. Sherratt and M. Howarth, *ACS Nano*, 2013, **7**, 1137.

[57] C. S. Almeida, I. K. Herrmann, P. D. Howes and M. M. Stevens, *Chem. Mater.*, 2015, **27**, 6879.

[58] E. Mendez and J. H. Moon, *Chem. Commun.*, 2013, **49**, 6048.

[59] T. Chen, W. Xu, Z. Huang, H. Peng, Z. Ke, X. Lu, Y. Yan and R. Liu, *J. Mater. Chem. B*, 2015, **3**, 3564.

[60] X. Lu, R. Jiang, M. Yang, Q. Fan, W. Hu, L. Zhang, Z. Yang, W. Deng, Q. Shen, Y. Huang, X. Liua and W. Huang, *J. Mater. Chem. B*, 2014, **2**, 376.

[61] C. Yang, S. Huang, X. Wang and M. Wang, *Polym. Chem.*, 2016, **7**, 7455.

[62] B. Muthuraj, S. Mukherjee, C. Ra. Patra and P. K. Iyer, *ACS Appl. Mater. Interfaces*, 2016, **8**, 32220.

[63] G. Feng, Y. Fang, J. Liu, J. Geng, D. Ding and B. Liu, *Small*, 2017, **13**, 1602807.

[64] C. Liu, K. Wang, X. Gong and A. J. Heeger, *Chem. Soc. Rev.*, 2016, **45**, 4825.

Chapter 3

Synthesis of a Multifunctional Poly(*p*-Phenylene Ethynylene) Scaffold with Clickable Azide-Containing Side Chains

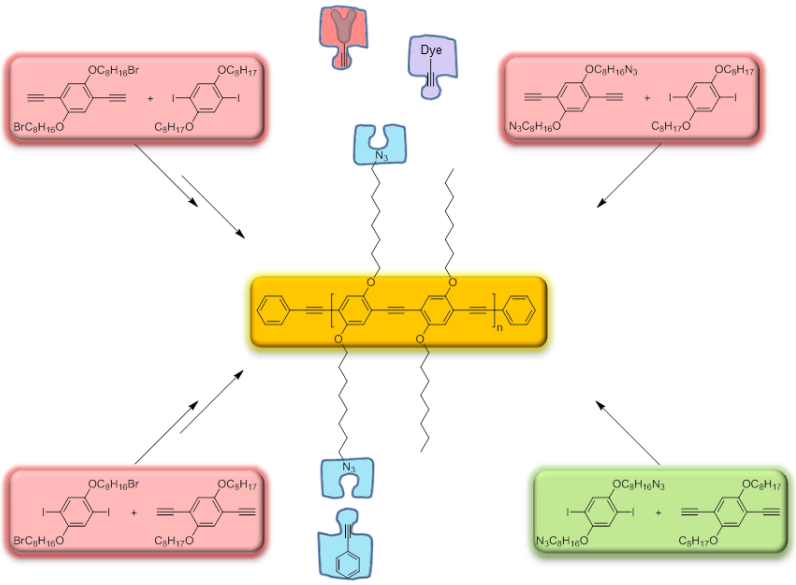

Y. Braeken, P. Verstappen, L. Lutsen, D. Vanderzande and W. Maes, *Polym. Chem.*, 2015, **6**, 6720.

ABSTRACT

Poly(*p*-phenylene ethynylene) (PPE) copolymers with alternating alkoxy and azide-functionalized alkoxy side chains are efficiently synthesized via Sonogashira polymerization and the materials are fully characterized. Among the different synthetic protocols investigated, best results are obtained when employing a pre-polymerization functionalization approach and upon implementing the azide-functionalized side chains on the diiodophenyl building block. End-capping of the conjugated polymer chains is shown to be essential to prevent side reactions. As a proof-of-principle, phenylacetylene is clicked in a nearly quantitative way on the polymer backbone. This illustrates the opportunities of these materials towards a variety of (bio)sensor applications.

3.1 INTRODUCTION

Due to their unique optoelectronic properties, conjugated polymers have attracted large interest over the last decades for numerous technological applications.[1] More recently, also the field of sensors based on conjugated polymers is receiving more attention.[2] Progress in the field of (bio)sensors based on conjugated polymers is stimulated by the insights achieved in popular domains such as polymer-based organic light-emitting diodes and photovoltaics, which has fostered significant synthetic progress and deepened understandings of structure-property relations for various classes of conjugated (co)polymer materials. Versatile adaptability of the physicochemical properties, the ability to print these semiconducting materials, the (consequent) low overall production costs and the appealing mechanical features (e.g. flexibility) of the resulting devices are some of the major driving forces to apply conjugated polymers in sensors.[2c] Furthermore, conjugated polymers are able to translate a binding or unbinding event into an easily measurable optical or electrochemical response and they display sensory signal amplification compared to small molecule counterparts, resulting from a 'molecular wire effect'.[3]

A typical sensor contains three different parts: (i) the receptor which binds the analyte, preferably selectively, (ii) a transducer which translates the binding event into a readable output signal, and (iii) a read-out system. Since the start-up of the field, poly(arylene ethynylene)s (PAE's) are widely used as transducer materials.[4–7] The main reason for this resides in the ease of their synthesis, their strong absorbance and high fluorescence quantum yield, and the rigid rod-like structure which is beneficial for charge carrier transport and thus increases the sensitivity of the overall device.[2,6,7] Receptors immobilized onto the polymer backbone introduce sensor selectivity because they are prone to bind only to the target analyte.[8] This immobilization is mostly obtained via rather complex synthetic routes.[9] For biomolecular receptors (proteins, nanobody proteins, …), non-site specific coupling techniques are usually applied, for example *N*-hydroxysuccinimide (NHS) chemistry[10] for covalent bonding or physical adsorption[11] if covalent linkage is not essential. Non-specific coupling methods with amines, thiols or carboxylic acid groups can, however, induce distortion of the biomolecule's tertiary structure, inhibiting the activity of the receptor,

whereas non-covalent couplings are reversible and often have an influence on the reproducibility of the sensors.[12]

To overcome the problems associated with the commonly used receptor immobilization techniques, in particular for biomolecular receptors, herein the synthesis of a universal and multifunctional transducer material based on a poly(*p*-phenylene ethynylene) (PPE) conjugated polymer scaffold with azide-functionalized side chains is reported. Any type of alkyne-functionalized receptor can be clicked to the polymer surface by means of copper(I)-catalyzed alkyne-azide click (CuAAC) chemistry, a simple chemical reaction that can be performed under mild conditions with a high efficiency and specificity and a lack of side reactions.[13] Moreover, this coupling reaction can be performed in aqueous media and is fully bio-orthogonal, which is highly beneficial for biosensor applications. The length of the linker between the polymer backbone and the azide functionality can be adjusted to the sensor type (*e.g.* shorter for Fluorescence Resonance Energy Transfer (FRET) sensors and longer for biosensors to maintain the activity of the biomolecule) and the side chain chemical composition can be optimized to enhance the affinity of the analyte for the surface of the sensor platform.

3.2 RESULTS AND DISCUSSION

The general synthetic strategy towards the envisaged azide-functionalized PPE copolymer platform is shown in Scheme 1. The desired polymers can be synthesized via both a pre- and a post-polymerization functionalization approach to introduce the azide moieties. Furthermore, two different strategies for the Sonogashira polymerization reaction were applied, with either the functionalized or the non-functionalized side chains on the diiodo-substituted phenyl building block. The results achieved upon application of the different synthetic routes are discussed in detail below.

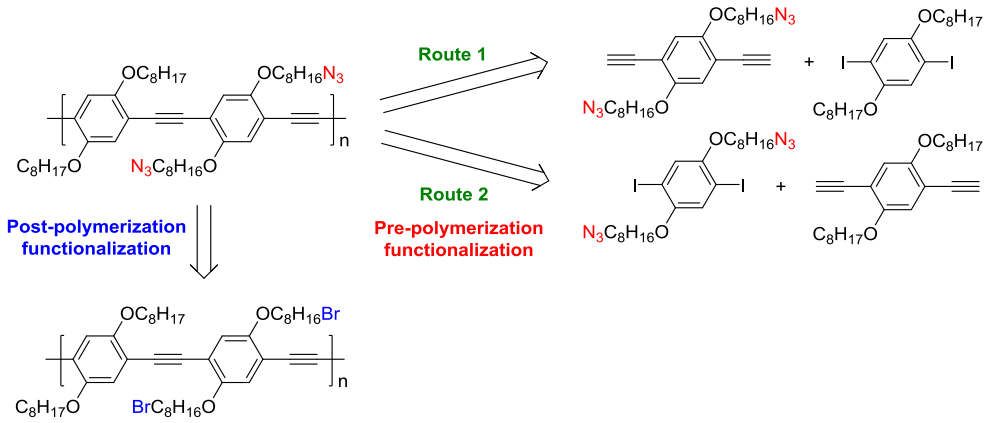

Scheme 1: Pre- and post-polymerization functionalization routes towards azide-functionalized PPE copolymers (retrosynthetic analysis).

3.2.1 Monomer synthesis

Route 1

Both monomers (**5** and **7**) needed for the Sonogashira polymerization reaction were synthesized via similar pathways (Scheme 2). The first step involves a Williamson ether synthesis in which *p*-hydroquinone (**1**) was dialkylated with 1,8-dibromooctane[14] or bromooctane,[15] respectively. A large excess of 1,8-dibromooctane was used to prevent two-fold reaction on one alkyl chain and potassium carbonate was found to give better yields than sodium hydroxide[16] or sodium hydride. Iodination of dialkylated precursors **2** and **6** with iodine and potassium iodate in acidic medium[17] gave products **3** and **7** in acceptable yields (62 and 77%, respectively). The alkyne entities on compound **4** were then introduced via a Sonogashira reaction with trimethylsilylacetylene (TMSA) in the presence of triethylamine. $Pd(PPh_3)Cl_2$ was used as the catalyst and CuI as co-catalyst.[18] From ^1H NMR analysis it was observed that some of the bromine atoms on the alkyl side chains were replaced by iodine during this reaction, leading to an extra triplet at 3.18 ppm (Figure S2). The amount of iodinated product depends on the amount of co-catalyst causing the halogen-halogen exchange. Because iodine is anyway easier substituted later on, this exchange does not pose any problems for the further reaction sequence. The product

mixture was used as starting material for the alkyne deprotection reaction. Tetra-*n*-butylammonium fluoride (TBAF) was initially used for this purpose.[19] However, besides the desired reaction, also halogen exchange occurred leading to fluorinated alkyl side chains (Figure S2). Because this side reaction poses reactivity problems for the azidation to follow, deprotection was performed with potassium hydroxide in a methanol/THF mixture at 0 °C, affording 2,5-diethynylbenzene derivative **4** in ~65% yield (Sonogashira + deprotection step, mixture of iodo- and bromo-substituted side chains).[20] The azide groups were finally introduced by reaction of **4** with sodium azide in DMSO, yielding monomer **5** in over 80% yield.[21]

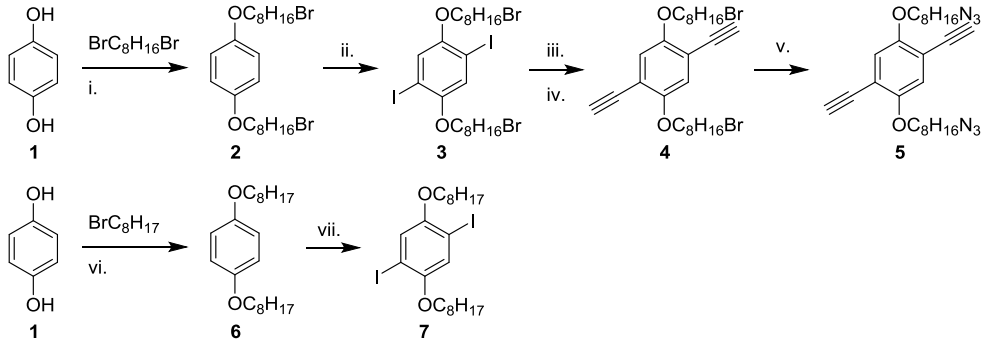

Scheme 2: Synthetic pathways towards monomers **5** and **7**: i. K_2CO_3, acetone, 50 °C, 12 h, 53%; ii. I_2, KIO_3, H_2SO_4, AcOH, reflux, 12 h, 62%; iii. TMSA, $Pd(PPh_3)_2Cl_2$, CuI, Et_3N, THF, 40 °C, 12 h; iv. KOH, MeOH, THF, 0 °C, 3 h, ~65% overall yield after iii. + iv.; v. NaN_3, DMSO, r.t., 12 h, ~84%; vi. KOH, EtOH, reflux, 12 h, 69%; vii. I_2, KIO_3, H_2SO_4, AcOH, reflux, 12 h, 77%.

Route 2

For the second possible building block combination, monomers **8** and **9** could readily be synthesized from products **3** and **7**, respectively (Scheme 3). The azide functionalities were introduced on precursor **3** in a highly efficient manner (96% yield) using the same reaction conditions as applied for compound **4**, and the Sonogashira reaction on 2,5-diiodobenzene derivative **7** was conducted in

the same way as mentioned above, in this case with TBAF as deprotection agent,[19] yielding 2,5-diethynylbenzene monomer **9** in 72% yield.

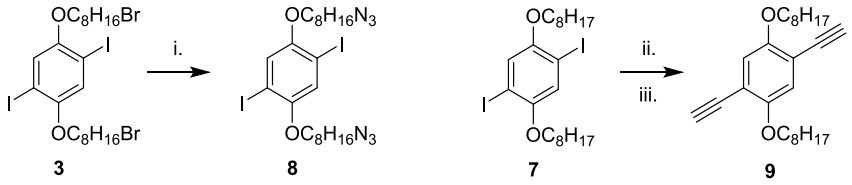

Scheme 3: Synthetic pathways towards monomers **8** and **9**: i. NaN_3, DMSO, THF, r.t., 12 h, 96%; ii. TMSA, $Pd(PPh_3)_2Cl_2$, CuI, Et_3N, THF, 40 °C, 12 h; iii. TBAF, THF, CH_2Cl_2, 0 °C, 20 min, 72% overall yield for ii. + iii.

3.2.2 Polymer synthesis and characterization

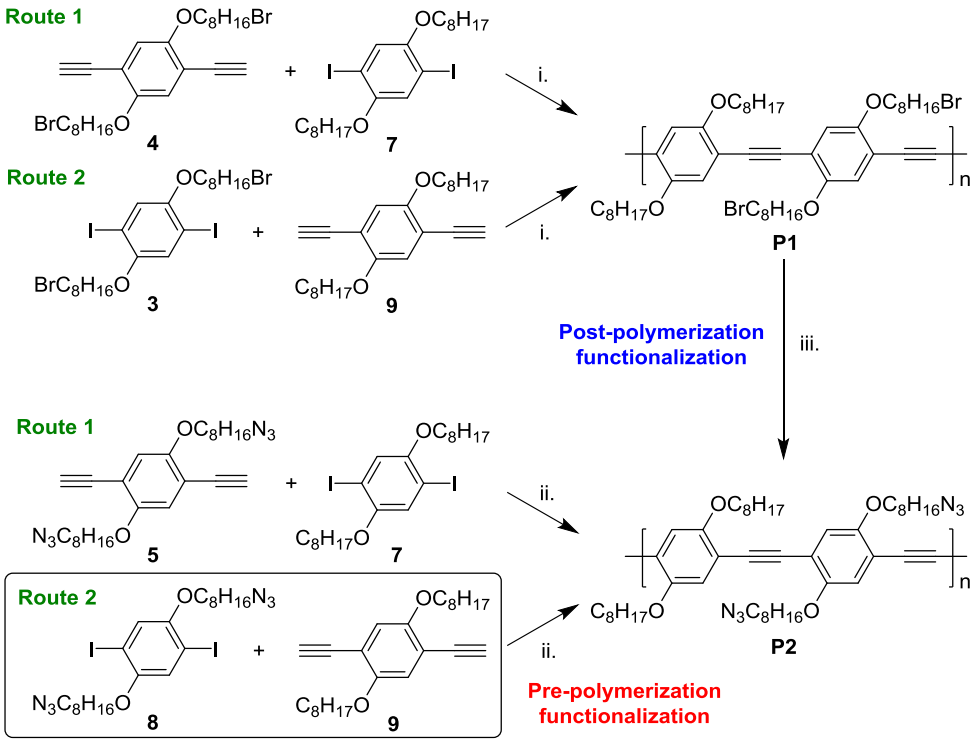

Scheme 4: Synthetic procedures towards azide-functionalized PPE copolymers **P2**: i. $Pd(PPh_3)_2Cl_2$, CuI, DIPA, toluene, 70 °C, 12 h; ii. $Pd(PPh_3)_2Cl_2$, CuI, DIPA, toluene, 70 °C, 2 h; iii. NaN_3, DMF, THF, r.t., 72 h.

The different polymerization routes employed towards the desired azide-functionalized PPE copolymer platform are summarized in Scheme 4. For the pre-polymerization functionalization route, monomers **8** and **9**, with the azide groups on 2,5-diiodobenzene monomer **8** (route 2), were copolymerized via Sonogashira polymerization with $Pd(PPh_3)2Cl_2$ as a catalyst and CuI as co-catalyst. The reaction was performed in a toluene/diisopropylamine (DIPA) mixture at 70 °C.[22] The same reaction was also done starting from monomers **5** and **7**, in this case with the azide functions on the 2,5-diethynylbenzene building block (route 1). When the polymerization reactions were continued overnight, insoluble gels were formed. This gel formation might be due to cross-linking (1,3-cycloaddition reaction) of the pendant azide groups with terminal alkynes from the polymer backbone.

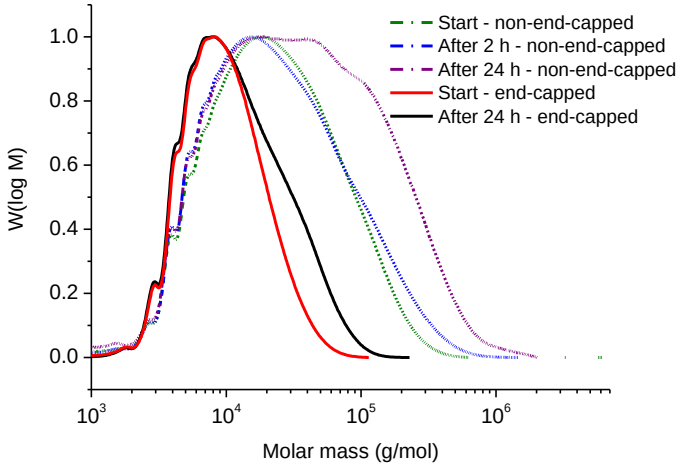

Figure 1: SEC profiles for a non-end-capped (dashed lines) and end-capped (solid lines) PPE copolymer **P2** upon exposure to a temperature of 70 °C for 24 h (in THF solution).

Cross-linking was further analyzed by stirring two separate solutions of end-capped (with phenyl groups, *vide infra*) and non-end-capped copolymers (as prepared from monomers **8** and **9** for the end-capped PPE and monomers **5** and **7** for the non-end-capped PPE) in THF at 70 °C for 24 hours. In the size exclusion chromatography (SEC) profiles, a clear shift of the peak maximum

could be observed for the non-end-capped copolymer, whereas for the end-capped copolymer there is no shift of the peak maximum, only a small shoulder at higher molar mass (Figure 1). This indicates that terminal moieties indeed play a role in gel formation. The availability of terminal alkyne moieties should thus be prevented when the polymer is exposed to high temperatures and/or cuprous salts. Furthermore, Mendez *et al.* stated that terminal alkyne groups can also undergo solid-state cross-linking after drying, leading to insoluble solids.[23] Also this side reaction can be prevented by end-capping the polymers.

Gelation could also be avoided by carefully monitoring the reaction time of the Sonogashira polymerization and following the reaction progress by SEC. The chromatograms revealed that chain elongation actually already stopped after ~1 hour (Figure 2). In most literature precedents, an end-capper is added to the reaction mixture from the start to control the polymer molar mass.[24] In this case, however, end-capping species were added after chain elongation finished to avoid inherent molar mass limitations. All further polymerization reactions employing azide-functionalized precursors were hence run for two hours before the end-capping reagents were added, first iodobenzene and, after stirring for 30 min at 70 °C, phenylacetylene. This final solution was then stirred at 70 °C for only 15 more minutes to prevent clicking of the end-capper on the azide-functionalized side chains. End-capped copolymers are indicated with an ' throughout the proceeding of this chapter.

None of the polymers were purified by soxhlet extraction because elevated temperatures can cause cross-linking via thermally activated Huisgen cycloaddition.[25] The polymers were precipitated in methanol and subsequently in acetone to remove catalyst residues and low molar mass fractions. The polymerization of monomers **5** and **7** yielded a PPE copolymer **P2a'** with a number average molar mass (M_n) of 17.8 kg/mol and a dispersity ($Đ$) of 2.3 (Table 1). On the other hand, copolymer **P2b'** was synthesized from monomers **8** and **9** and showed an M_n of 28.6 kg/mol with a dispersity of 2.4.

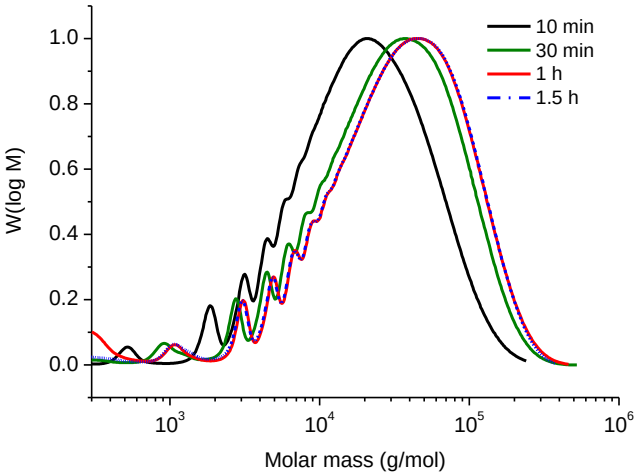

Figure 2: Evolution of molar mass during Sonogashira polymerization of monomers **8** and **9**.

For the post-polymerization functionalization route, the same catalyst and solvent system were used. The absence of azide functionalities reduces the risk of cross-linking, so these polymerization reactions were continued overnight. Copolymerization of monomers **4** and **7** yielded bromine-functionalized copolymer **P1a'** with an M_n of 12.5 kg/mol and a dispersity of 2.1, whereas combination of **3** and **9** yielded copolymer **P1b'** with an M_n of 19.3 kg/mol and a dispersity of 2.1 (Table 1).

Table 1: Overview of the PPE copolymers prepared and their molar mass data.

Polymer	Functionalization route	Monomer	Comonomer	M_n (kg/mol)	$Đ$
P1a'	Post-polymerization – route 1	**4**	**7**	12.5	2.1
P1b'	Post-polymerization – route 2	**3**	**9**	19.3	2.1
P2a'	Pre-polymerization – route 1	**5**	**7**	17.8	2.3
P2b'	Pre-polymerization – route 2	**8**	**9**	28.6	2.4

Both polymers (**P1a'** and **P1b'**) were then post-polymerization functionalized with sodium azide in a DMF/THF mixture under stirring for 72 hours at room temperature.[26] Functionalization was achieved in a nearly quantitative way, as

confirmed by NMR (Figure S2) and IR spectroscopy (Figure S4). The change in alkyl side chain end groups has a noticeable effect on the thermal properties of the PPE copolymers, as analyzed by rapid heat-cool calorimetry (RHC).[27] Whereas bromine-functionalized copolymer **P1b'** shows clear semi-crystalline features (complex melting behavior over a broad range, depending on the thermal history; melting peak maximum at 195 °C, T_g at 35–45 °C), no enthalpic effects are seen anymore after substitution of all bromine groups with azide moieties (Figure 3).

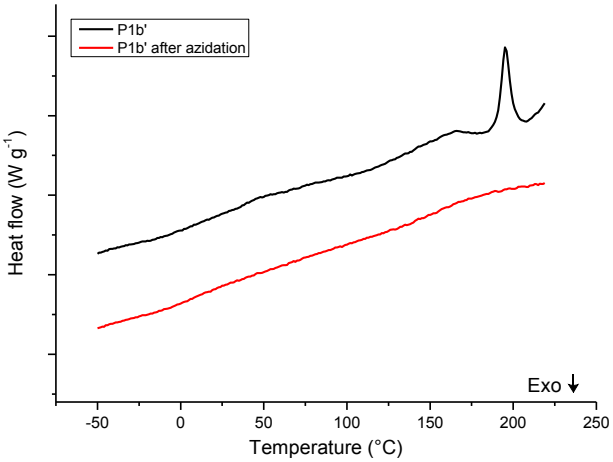

Figure 3: RHC profiles for bromine-functionalized PPE copolymer **P1b'** and the corresponding azide-functionalized analogue (first heating, curves shifted vertically for clarity).

Polymerization reactions for which the functionalized side chains were present on the iodine-containing species (route 2; **P1b'** and **P2b'**) showed higher M_n values than their counterparts for which the functionalized side chains were present on the alkynylated monomers (route 1; **P1a'** and **P2a'**). Furthermore, the polymers synthesized by the pre-polymerization strategy (**P2a'** and **P2b'**) had higher M_n values than their post-polymerization functionalization counterparts (compare **P1a'** to **P2a'** and **P1b'** to **P2b'**). The trends in molar masses for the different polymerization routes were confirmed by duplo experiments. Dispersities were comparable for all PPE's synthesized. Overall, the pre-polymerization route applied towards copolymer **P2b'** (Scheme 4, black rectangle) seems to be the most suitable approach for the synthesis of the

azide-functionalized target PPE. ^{1}H NMR spectra were obtained for all copolymers and clearly show the different protons present (see SI). The optical properties of the bromine- and azide-functionalized copolymers were found to be very similar, with a maximal absorption at 446 nm in solution ($CHCl_3$) and at 487 nm in thin film and a stokes shift of 29 nm in solution and 46 nm in film (Figure 4). Also the optical and electrochemical bandgaps are comparable (Table 2).

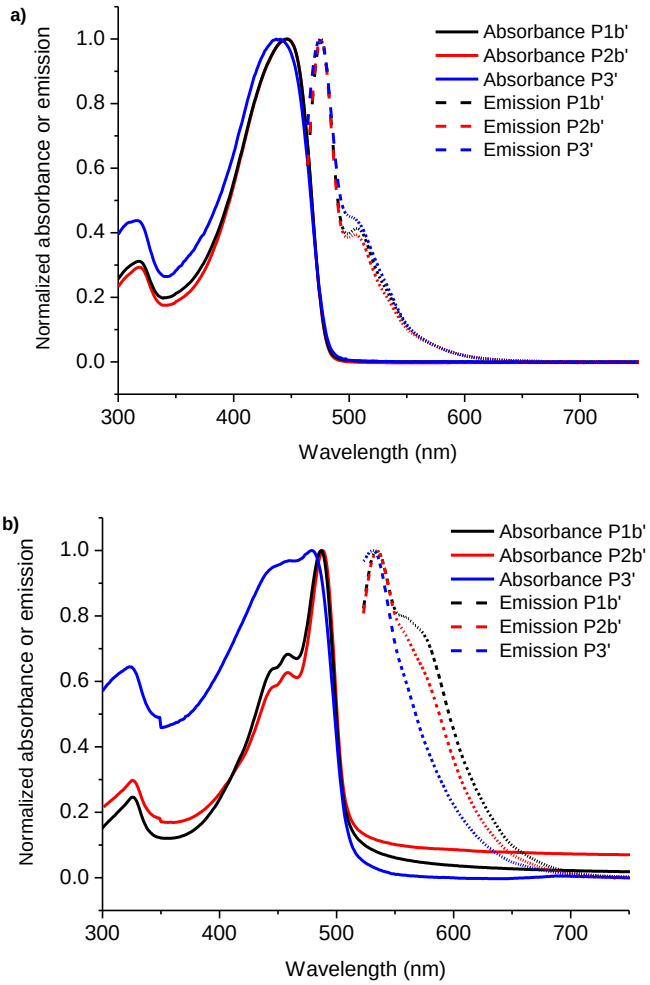

Figure 4: Absorption and emission spectra (normalized) of PPE copolymers **P1b'**, **P2b'** and **P3'** (Scheme 5 for structure) in a) $CHCl_3$ and b) film.

Table 2: Experimental optical and electrochemical data for PPE copolymers **P1b'**, **P2b'** and **P3'**.

Polymer	λ_{max}[a] (nm) solution	λ_{max}[b] (nm) film	E_g^{OPc} (eV)	HOMO[d] (eV)	LUMO[d] (eV)	E_g^{ECe} (eV)
P1b'	446	487	2.44	-5.74	-2.89	2.85
P2b'	446	487	2.43	-5.71	-2.88	2.83
P3'	437	479	2.43	-5.70	-2.93	2.77

[a] In $CHCl_3$. [b] Films were prepared by drop casting a solution of the polymer in $CHCl_3$ onto a quartz disc. [c] Optical bandgap, determined by the onset of the solid-state UV-Vis spectrum. [d] Determined from the onset of oxidation/reduction in cyclic voltammetry. [e] Electrochemical bandgap.

Homo-coupling is known to be a common side reaction in Sonogashira reactions. This oxidative coupling can be caused by the presence of oxygen in the reaction vessel or occurs during the reduction of the stable Pd(II) into the active Pd(0) species.[28] By MALDI-TOF mass spectrometry, it is possible to observe the presence of homo-coupling and other possible defects in the polymer chains. For the end-capped copolymer **P2b'** (low molar mass batch to improve resolution; M_n = 7.7 kg/mol, $Đ$ = 1.5), most chains have no defects in their backbone (Figure 5). A smaller part of the polymer chains has one homo-coupling or one distortion in the copolymer structure, and only a minor amount of polymer chains with more than one defect are observed. Furthermore, it is noticeable that only successfully end-capped polymer chains can be seen. Polymer chains with iodine or alkyne termini are not detected. For a non-end-capped copolymer **P2a** (M_n = 14.2 kg/mol, $Đ$ = 2.1), the same trend in homo-couplings was observed (Figure S1).

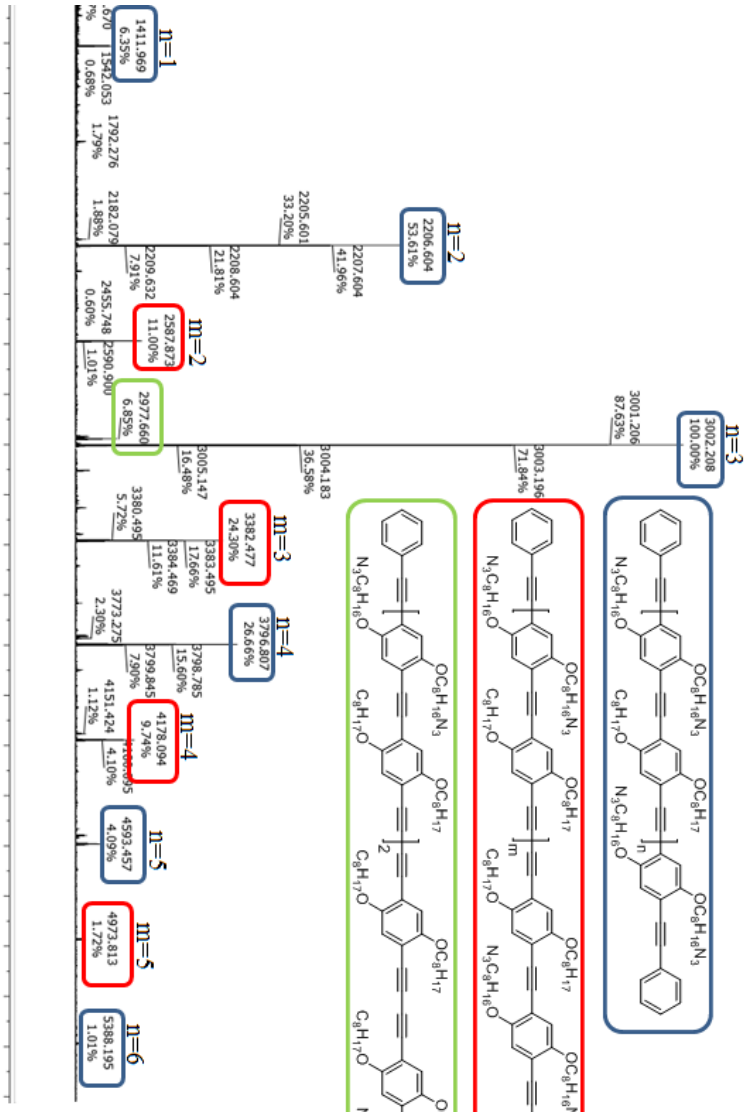

Figure 5: MALDI-TOF mass spectrum for N_3-functionalized PPE copolymer **P2b'** (M_n = 7.7 kg/mol, $Đ$ = 1.5), with product labels for the major signals observed. The exact position of the homo-couplings within the polymer backbone is unsure, but the number of homo-couplings per product is correct for every signal.

3.2.3 CuAAC functionalization

To the best of our knowledge, only a few cases of PPE-type copolymers with click functionalities suitable for CuAAC reactions have been reported before. Bunz et al. prepared a PPE with alkyne functionalities on the side chains,[29] and the click reaction of azide-functionalized mannose molecules onto those types of polymers was explored within the same research group.[30] Zhao and co-workers on the other hand demonstrated a click reaction on an azide-functionalized diethynylbenzene monomer before polymerization.[31] Bunz *et al.* also reported on an azide-functionalized PPE which was cross-linked at 300 °C to form a bubble array,[32] but no trials were done on CuAAC reactions with external alkyne-substituted molecules.

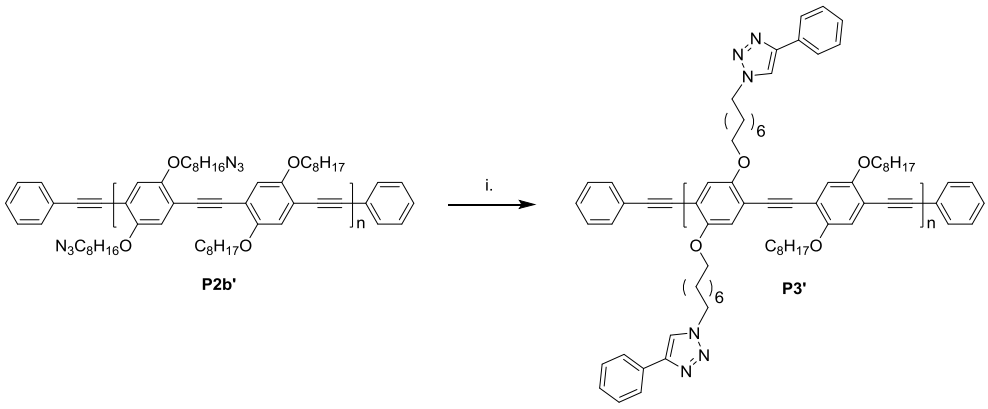

Scheme 5: Synthetic procedure for the CuAAC reaction on PPE copolymer **P2b'**: i. phenylacetylene, CuBr, PMDETA, DMF, THF, r.t., 1 h.

In our present work, for the first time, a nearly quantitative CuAAC click reaction on an azide-functionalized PPE scaffold was explored. To this extent, azide-functionalized copolymer **P2b'** was reacted with phenylacetylene in the presence of CuBr and PMDETA (*N,N,N',N'',N''*-pentamethyldiethylenetriamine) as a proof-of-principle reaction for the PPE click functionalization (Scheme 5). After one hour, all of the azide functions had reacted, as indicated by FT-IR spectroscopy (Figure 6). The typical azide vibration at 2093 cm^{-1} could not be observed anymore, which points out that the CuAAC reaction on the polymer is

accomplished in an effective way. This was confirmed in the ^{1}H NMR spectrum (Figure SI p 88) of the clicked PPE copolymer **P3'**, with a clear and complete shift of the signals of the neighbouring methylene groups (from 3.2 to 4.3 ppm) when exchanging the azide end groups for triazole moieties. The maximal absorption of **P3'** compared to this of azide-functionalized copolymer **P2b'** is slightly blue-shifted (437 nm in solution and 479 nm in film, Figure 4 and Table 2), whereas the optical bandgap (2.43 eV) and electrochemical properties remained very similar (Table 2).

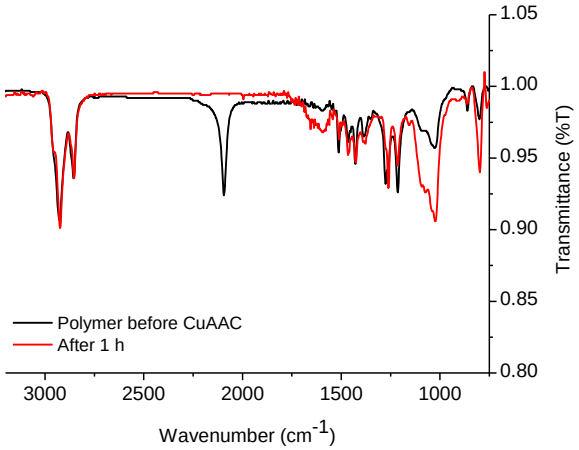

Figure 6: FT-IR spectra of PPE copolymer **P2b'** before and after CuAAC reaction with phenylacetylene.

3.3 CONCLUSIONS

A versatile PPE copolymer scaffold with clickable azide-functionalized side chains was efficiently synthesized. Both pre- and post-polymerization functionalization routes were explored with the functional moieties on either of the two phenyl building blocks (diiodo vs diethynyl). For all of the obtained copolymers, dispersities were comparable ($Đ$ = 2.1−2.4), but some variations in the molar masses of the PPEs synthesized via the different routes were observed. Best results were obtained via the pre-polymerization functionalization route and upon applying functionalized diiodobenzene monomers. Furthermore, terminal alkynes were shown to have a serious impact on the amount of gelation

occurring during the reaction (work-up) or processing of the polymers at elevated temperature. Therefore, all of the synthesized copolymers were end-capped. Proof-of-principle CuAAC reaction of phenylacetylene on the azide-functionalized PPE copolymer was achieved in a nearly quantitative way. The possibility of immobilizing different types of alkyne-functionalized molecules/receptors onto the novel PPE framework via a general and versatile CuAAC approach opens a number of opportunities to improve on both the sensitivity and selectivity of (bio)sensor platforms.

3.4 EXPERIMENTAL SECTION

3.4.1 General materials and methods

NMR chemical shifts (δ, in ppm) were determined relative to the residual $CHCl_3$ (7.26 ppm) absorption or the ^{13}C resonance shift of $CDCl_3$ (77.16 ppm). High resolution electrospray ionization mass spectrometry (ESI-MS) was performed using an LTQ Orbitrap Velos Pro mass spectrometer equipped with an atmospheric pressure ionization source operating in the nebulizer assisted electrospray mode. The instrument was calibrated in the m/z range 220−2000 using a standard solution containing caffeine, MRFA and Ultramark 1621. Reported masses are the 100% intensity isotope peaks. MALDI-TOF mass spectra were recorded on a Bruker Daltonics Ultraflex II Tof/Tof. 1 µL of the matrix solution (4 mg/mL DTCB (*trans*-2-[3-(4-*tert*-butylphenyl)-2-methyl-2-propenylidene]malononitrile) in $CHCl_3$) was spotted onto an MTP Anchorchip 600/384 MALDI plate. The spot was allowed to dry and 1 µL of the analyte solution (0.5 mg/mL in $CHCl_3$) was spotted on top of the matrix. Melting points were measured with an electrothermal IA9000 series digital melting point apparatus. Solid-state FT-IR spectra were recorded in transmission mode. UV-Vis measurements were performed on a VARIAN Cary 5000 UV-Vis-NIR spectrophotometer at a scan rate of 600 nm/min. The films for the UV-Vis measurements were prepared by drop casting a solution of the polymer in chloroform on a quartz substrate. The solid-state UV-Vis spectra were used to estimate the optical bandgaps (from the wavelength at the intersection of the tangent line drawn at the low energy side of the absorption spectrum with the baseline: E_g (eV) = 1240/(wavelength in nm)). Lamp corrected steady-state

emission spectra were recorded on a fluorimeter using a band pass of 1 nm for the excitation monochromator and a scanning speed of 1 nm/s. Spectra were collected at r.t. at an excitation wavelength of 446 nm for **P1b'** and **P2b'** in $CHCl_3$ and 488 nm for the films (without deoxygenation). For **P3'**, 440 nm was used as the excitation wavelength in solution and 479 nm for the film. Analysis of the molar masses and molar mass distributions of the polymers was performed on a Tosoh EcoSEC System, comprising of an autosampler, a PSS guard column SDV (50 x 7.5 mm), followed by three PSS SDV analytical linear XL columns (5 µm, 300 x 7.5 mm) and a UV-detector using THF as the eluent at 40 °C with a flow rate of 1.0 mL/min. The SEC system was calibrated using linear narrow polystyrene standards ranging from 474 to 7.5 x 10^6 g/mol (K= 14.1 x 10^{-5} dL/g and α = 0.70). Rapid heat-cool calorimetry experiments were performed on a prototype RHC of TA Instruments, equipped with liquid nitrogen cooling and specifically designed for operation at high scanning rates.[27] RHC measurements were performed at 500 K min^{-1} in aluminum crucibles, using helium (10 mL min^{-1}) as a purge gas. Electrochemical measurements (cyclic voltammetry) were performed with an Eco Chemie Autolab PGSTAT 30 potentiostat/galvanostat using a three-electrode microcell with a platinum working electrode, a platinum counter electrode and a $Ag/AgNO_3$ reference electrode (silver wire dipped in a solution of 0.01 M $AgNO_3$ and 0.1 M NBu_4PF_6 in anhydrous acetonitrile). The reference electrode was calibrated against ferrocene/ferrocenium as an external standard. Samples were prepared by dip coating the platinum working electrode in the respective polymer solutions (also used for the solid-state UV-Vis measurements). The CV measurements were done on the resulting films with 0.1 M NBu_4PF_6 in anhydrous acetonitrile as electrolyte solution. To prevent air from entering the system, the experiments were carried out under a curtain of argon. Cyclic voltammograms were recorded at a scan rate of 100 mV s^{-1}. For the conversion of V to eV, the onset potentials of the first oxidation/reduction peaks were used and referenced to ferrocene/ferrocenium, which has an ionization potential of -4.98 eV *vs.* vacuum. This correction factor is based on a value of 0.31 eV for Fc/Fc^+ *vs.* SCE[33a] and a value of 4.68 eV for SCE *vs.* vacuum[33b]: $E_{HOMO/LUMO}$ (eV) = -4.98 - $E_{onset\ ox/red}^{Ag/AgNO3}$ (V) + $E_{onset\ Fc/Fc+}^{Ag/AgNO3}$ (V).

3.4.2 Monomer synthesis

1,4-Bis(8-bromooctyloxy)benzene (2). Prepared according to a reported procedure.[14]

1,4-Bis(8-bromooctyloxy)-2,5-diiodobenzene (3). To a suspension of 1,4-bis(8-bromooctyloxy)benzene (**2**) (2.00 g, 4.06 mmol) in acetic acid (24 mL), water (2.4 mL), sulfuric acid (0.62 mL), iodine (0.86 g, 3.42 mmol) and potassium iodate (0.36 g, 1.70 mmol) were added. The mixture was refluxed overnight, after which it was cooled down to room temperature in an ice bath. The precipitate was filtered off and washed with a saturated Na_2SO_3 solution. The residue was dissolved in CH_2Cl_2 and washed with water (2x) and brine (1x). After drying over $MgSO_4$ and filtration, the solvent was removed under reduced pressure and the remaining solid was purified by column chromatography (silica, petroleum ether:CH_2Cl_2 6:4), yielding a white solid (1.88 g, 62%). ^{1}H NMR (400 MHz, $CDCl_3$), δ (ppm): 7.17 (s, 2H), 3.92 (t, *J* = 6.3 Hz, 4H), 3.41 (t, *J* = 6.8 Hz, 4H), 1.91–1.74 (m, 8H), 1.55–1.32 (m, 16H); ^{13}C NMR (75 MHz, $CDCl_3$), δ (ppm): 152.9, 122.9, 86.4, 70.3, 34.2, 32.9, 29.20, 29.18, 28.8, 28.2, 26.1; HRMS (ESI): calcd: 766.8892 measured: *m/z* 766.8896 for $C_{22}H_{34}Br_2I_2O_2Na$ $[M+Na]^+$; Mp: 92 °C.

1,4-Bis(8-bromooctyloxy)-2,5-diethynylbenzene (4). 1,4-Bis(8-bromooctyloxy)-2,5-diiodobenzene (**3**) (2.000 g, 2.69 mmol) was dissolved in THF/Et_3N (1/1, 10 mL). After purging the solution with nitrogen for 10 min, CuI (25.7 mg, 5 mol%), $PdCl_2(PPh_3)_2$ (94.4 mg, 5 mol%) and trimethylsilylacetylene (0.554 g, 5.64 mmol) were added, and the mixture was stirred overnight at 40 °C under inert atmosphere. After removal of the solvent under reduced pressure, the residue was purified by filtration through a silica plug with CH_2Cl_2 as the eluent. The solvent was evaporated, yielding a yellow solid, which was precipitated in methanol, yielding a beige solid which was dissolved in a mixture of MeOH (200 mL) and THF (200 mL). The solution was cooled down to 0 °C before adding an aqueous KOH solution (20% m/V, 37.5 mL). The reaction mixture was stirred for 3 h after which the solvent was removed under reduced pressure. The residue was dissolved in CH_2Cl_2 and the organic phase was washed with water (2x) and brine (1x), dried over $MgSO_4$, filtered and

evaporated to dryness. The resulting solid was purified by column chromatography (silica, petroleum ether:CH_2Cl_2 1:1) to yield a pale yellow solid (0.993 g), containing a mixture of iodo- and bromo-functionalized side chains. ^{1}H NMR (300 MHz, $CDCl_3$), δ (ppm): 6.95 (s, 2H), 3.97 (t, *J* = 6.5 Hz, 4H), 3.41 (t, *J* = 6.8 Hz, 1.8H, CH_2Br), 3.34 (s, 2H), 3.19 (t, *J* = 7.0 Hz, 2.2H, CH_2I), 1.92−1.72 (m, 8H), 1.52−1.32 (m, 16H); ^{13}C NMR (75 MHz, $CDCl_3$), δ (ppm): 154.0, 117.8, 113.3, 82.6, 79.9, 69.6, 34.2, 33.6, 32.9, 30.5, 29.22 (2C), 29.17, 28.8, 28.6, 28.2, 25.9, 7.5 (CH_2I); HRMS (ESI): calcd: 563.0960, measured: *m/z* 563.0955 for $C_{26}H_{36}Br_2O_2Na$ $[M+Na]^+$ (dibromo); calcd: 609.0841, measured: *m/z* 609.0829 for $C_{26}H_{36}BrIO_2Na$ $[M+Na]^+$ (1x Br, 1x I); calcd: 657.0703, measured: *m/z* 657.0683 for $C_{26}H_{36}I_2O_2Na$ $[M+Na]^+$ (diiodo); IR (NaCl, mixture), ν_{max} (cm^{-1}): 3281, 2934, 2912, 2859.

1,4-Bis(8-azidooctyloxy)-2,5-diethynylbenzene (5). 1,4-Bis(8-bromooctyloxy)-2,5-diethynylbenzene (as a mixture with the mono- and diiodo compound) (0.320 g) was dissolved in DMSO (9 mL) and stirred at room temperature while NaN_3 (0.096 g, 1.48 mmol) was added. After stirring overnight, the solution was quenched carefully with water leading to a rise in temperature. When the aqueous solution was cooled down to room temperature, it was extracted with diethyl ether. The combined organic phases were washed with water (2x) and brine (1x), dried over $MgSO_4$ and filtered. The solvent was removed under reduced pressure and the residue was purified by column chromatography (silica, gradient $CHCl_3$:petroleum ether 1:1 to 100% $CHCl_3$), yielding a white solid of pure monomer **5** (290 mg, 84%). ^{1}H NMR (400 MHz, $CDCl_3$), δ (ppm): 6.95 (s, 2H), 3.97 (t, *J* = 6.6 Hz, 4H), 3.34 (s, 2H), 3.26 (t, *J* = 7.0 Hz, 4H), 1.85–1.75 (m, 4H), 1.65–1.55 (m, 4H), 1.53–1.43 (m, 4H), 1.42−1.30 (m, 12H); ^{13}C NMR (75 MHz, $CDCl_3$), δ (ppm): 154.0, 117.8, 113.3, 82.6, 79.9, 69.6, 51.6, 29.3 (2C), 29.2, 29.0, 26.8, 25.9; HRMS (ESI): calcd: 487.2798, measured: *m/z* 487.2784 for $C_{26}H_{36}N_6O_2Na$ $[M+Na]^+$; Mp: 69 °C; IR (NaCl), ν_{max} (cm^{-1}): 3287, 2939, 2908, 2866, 2854, 2175, 2086.

1,4-Bis(octyloxy)benzene (6). Adapted from a literature procedure:[15] 1-Bromooctane was added directly to the hydroquinone solution. After extraction, the product was purified by column chromatography (silica, hexanes:CH_2Cl_2 5:1) and the excess 1-bromooctane was removed by vacuum distillation (p = $9*10^{-3}$

bar, T = 90 °C), yielding the product as a pure white solid (4.37 g, 69%). ^{1}H NMR (300 MHz, $CDCl_3$): δ (ppm) 6.82 (s, 4H), 3.90 (t, *J* = 6.6 Hz, 4H), 1.79–1.71 (m, 4H), 1.48–1.40 (m, 4H), 1.40−1.25 (m, 16H), 0.89 (t, *J* = 6.8 Hz, 6H).

1,4-Diiodo-2,5-bis(octyloxy)benzene (7). Adapted from a literature procedure:[17] After extraction, the crude product was purified by column chromatography (silica, petroleum ether:CH_2Cl_2 6:4), yielding the product as a white pure solid (0.672 g, 77%). ^{1}H NMR (300 MHz, $CDCl_3$): δ (ppm) 7.17 (s, 2H), 3.92 (t, *J* = 6.4 Hz, 4H), 1.85–1.73 (m, 4H), 1.55−1.40 (m, 4H), 1.40−1.20 (m, 16H), 0.89 (t, *J* = 6.8 Hz, 6H).

1,4-Bis(8-azidooctyloxy)-2,5-diiodobenzene (8). 1,4-Bis(8-bromooctyloxy)-2,5-diiodobenzene (0.500 g, 0.67 mmol) was dissolved in a mixture of DMSO (10 mL) and THF (10 mL). The solution was stirred at room temperature and NaN_3 (0.109 g, 1.68 mmol) was added. After stirring overnight, the solution was quenched carefully with water leading to a rise in temperature. When the aqueous solution was cooled down to room temperature, it was extracted with diethyl ether. The combined organic phases were washed with water (2x) and brine (1x), dried over $MgSO_4$ and filtered. The solvent was removed under reduced pressure and the residue was purified by column chromatography (silica, $CHCl_3$:petroleum ether 2:3), yielding a pure white solid (430 mg, 96%). ^{1}H NMR (300 MHz, $CDCl_3$), δ (ppm): 7.17 (s, 2H), 3.92 (t, *J* = 6.3 Hz, 4H), 3.26 (t, *J* = 6.9 Hz, 4H), 1.85−1.74 (m, 4H), 1.67−1.57 (m, 4H), 1.55–1.45 (m, 4H), 1.44–1.31 (m, 12H); ^{13}C NMR (75 MHz, $CDCl_3$), δ (ppm): 152.9, 122.9, 86.4, 70.4, 51.6, 29.2 (2C), 29.0, 26.8, 26.1; HRMS (ESI): calcd: 691.0731, measured: *m/z* 691.0724 for $C_{22}H_{34}I_2N_6O_2Na$ $[M+Na]^+$; Mp: 37 °C; IR (NaCl), ν_{max} (cm^{-1}): 2931, 2905, 2834, 2093.

1,4-Diethynyl-2,5-bis(octyloxy)benzene (9). Modified procedure:[19] 1,4-Diiodo-2,5-bis(octyloxy)benzene (**7**) (1.00 g, 1.70 mmol) was dissolved in dry THF/Et_3N (1/1, 6 mL). After purging with nitrogen for 10 min, CuI (16.2 mg, 0.085 mmol), $Pd(PPh_3)_2Cl_2$ (59.8 mg, 0.085 mmol) and trimethylsilylacetylene (0.51 mL, 3.58 mmol) were added and the reaction mixture was stirred overnight at 40 °C under inert atmosphere. After removal of the solvent, the mixture was purified by filtration through a silica plug with CH_2Cl_2 as the eluent

and the residue was precipitated in methanol yielding a solid with a golden lustre. This solid was redissolved in CH_2Cl_2 (20 mL), the solution was cooled down to 0 °C and TBAF (3.58 mL, 1M in THF) was added. After stirring at this temperature for 20 min, the solution was washed with water (2x) and brine (1x), dried over $MgSO_4$, filtered and evaporated to dryness. The residue was purified by column chromatography (CH_2Cl_2:hexanes 2:8), yielding the product as a pure yellow solid (0.47 g, 72%). ^{1}H NMR (300 MHz, $CDCl_3$) δ (ppm): 6.95 (s, 2H), 3.97 (t, *J* = 6.6 Hz, 4H), 3.33 (s, 2H), 1.86−1.73 (m, 4H), 1.51−1.42 (m, 4H), 1.40−1.19 (m, 16H), 0.88 (t, *J* = 6.8 Hz, 6H).

3.4.3 Polymer synthesis

P1a'. A mixture of dry toluene (4.8 mL) and diisopropylamine (2 mL) was degassed for 5 min. 1,4-Bis(octyloxy)-2,5-diiodobenzene (**7**) (0.108 g, 0.19 mmol), 1,4-bis(8-bromooctyloxy)-2,5-diethynylbenzene (**4**) (0.100 g, 0.19 mmol), CuI (2.1 mg, 5 mol%) and $Pd(PPh_3)_2Cl_2$ (6.6 mg, 5 mol%) were added and the mixture was stirred overnight at 70 °C. The polymer was end-capped by adding an excess of iodobenzene (2 drops), after which the reaction mixture was stirred for 30 more min at 70 °C. Then, an excess of phenylacetylene (2 drops) was added and the mixture was stirred again for 15 min at 70 °C. After cooling down to room temperature, the resulting polymer was precipitated in MeOH and filtered off. The resulting orange solid was redissolved in CH_2Cl_2 and precipitated again in acetone, yielding an orange solid (111 mg, 69%). SEC (THF): M_n 12.5 kg/mol, $Đ$ 2.1; ^{1}H NMR (300 MHz, $CDCl_3$): δ (ppm) 7.02 (s, 4H), 4.06–3.95 (m, 8H), 3.40−3.32 (m, 3.5H; bromooctyl), 3.18–3.08 (m, 0.5H; iodooctyl), 1.90–1.68 (m, 8H), 1.60−1.20 (m, 40H), 0.90–0.82 (m, 6H).

P1b'. A mixture of dry toluene (3.8 mL) and diisopropylamine (1.6 mL) was degassed for 5 min. 1,4-Bis(octyloxy)-2,5-diethynylbenzene (**9**) (0.050 g, 0.131 mmol), 1,4-bis(8-bromooctyloxy)-2,5-diiodobenzene (**3**) (0.097 g, 0.131 mmol), CuI (1.2 mg, 5 mol%) and $Pd(PPh_3)_2Cl_2$ (4.5 mg, 5 mol%) were added and the mixture was stirred overnight at 70 °C. The polymer was end-capped by adding an excess of iodobenzene (2 drops), after which it was stirred for 30 min at 70 °C. Then, an excess of phenylacetylene (2 drops) was added and the mixture was stirred again for 15 min at 70 °C. After cooling down to room temperature,

the resulting polymer was precipitated in MeOH and filtered off. The resulting orange solid was redissolved in CH_2Cl_2 and precipitated again in acetone, yielding an orange solid (98 mg, 86%). SEC (THF): M_n 19.3 kg/mol, $Đ$ 2.1; ^{1}H NMR (300 MHz, $CDCl_3$), δ (ppm): 7.02 (s, 4H), 4.04 (t, J = 6.1 Hz, 8H), 3.38 (t, J = 6.8 Hz, 4H), 1.96–1.75 (m, 8H), 1.66–1.17 (m, 40H), 0.87 (t, J = 6.5 Hz, 6H); ^{13}C NMR (75 MHz, $CDCl_3$), δ (ppm): 153.6, 117.4, 114.4, 91.7, 69.8, 69.7, 34.0, 32.9, 32.0, 29.6, 29.5, 29.4, 28.9, 28.3, 26.2, 26.1, 26.0, 22.8, 14.3; IR (NaCl), v_{max} (cm^{-1}): 2987, 2960, 2927, 2888, 2854.

P2a'. A mixture of dry toluene (6.3 mL) and diisopropyl amine (2.6 mL) was degassed for 5 min. 1,4-Bis(8-azidooctyloxy)-2,5-diethynylbenzene (**5**) (0.100 g, 0.215 mmol), 1,4-diiodo-2,5-bis(octyloxy)benzene (**7**) (0.132 g, 0.226 mmol), CuI (2.1 mg, 5 mol%) and $Pd(PPh_3)_2Cl_2$ (7.7 mg, 5 mol%) were added and the mixture was stirred at 70 °C for 2 h. The polymer was end-capped by adding an excess of iodobenzene (2 drops), after which the reaction mixture was stirred for 30 more min at 70 °C. Then, an excess of phenylacetylene (2 drops) was added and the mixture was stirred again for 15 min at 70 °C. After cooling down to room temperature, the polymer was precipitated in MeOH and filtered off. The resulting orange solid was redissolved in CH_2Cl_2 and precipitated again in acetone, yielding an orange solid (0.135 g, 79%). SEC (THF): M_n 17.8 kg/mol, $Đ$ 2.3; ^{1}H NMR (300 MHz, $CDCl_3$), δ (ppm): 7.02 (s, 4H), 4.06–4.00 (m, 8H), 3.25–3.20 (m, 4H), 1.93–1.75 (m, 8H), 1.65−1.20 (m, 40H), 0.92–0.80 (m, 6H).

P2b'. A mixture of dry toluene (4.4 mL) and diisopropyl amine (1.7 mL) was degassed for 5 min. 1,4-Bis(8-azidooctyloxy)-2,5-diiodobenzene (**8**) (0.100 g, 0.150 mmol), 1,4-diethynyl-2,5-bis(octyloxy)benzene (**9**) (0.057 g, 0.150 mmol), CuI (1.4 mg, 5 mol%) and $Pd(PPh_3)_2Cl_2$ (5.2 mg, 5 mol%) were added and the mixture was stirred at 70 °C for 2 h. The polymer was end-capped by adding an excess of iodobenzene (2 drops), after which the reaction mixture was stirred for 30 more min at 70 °C. Then, an excess of phenylacetylene (2 drops) was added and the mixture was stirred again for 15 min at 70 °C. After cooling down to room temperature, the polymer was precipitated in MeOH and filtered off. The resulting orange solid was redissolved in CH_2Cl_2 and precipitated again in acetone, yielding an orange solid (0.063 g, 53%). SEC (THF): M_n 28.6 kg/mol,

Đ 2.4. ^{1}H NMR (300 MHz, $CDCl_3$), δ (ppm): 7.02 (s, 4H), 4.07–4.00 (m, 8H), 3.23 (t, *J* = 6.9 Hz, 4H), 1.92–1.79 (m, 8H), 1.63–1.19 (m, 40H), 0.92–0.80 (m, 6H); ^{13}C NMR (75 MHz, $CDCl_3$), δ (ppm): 153.6, 117.4, 114.4, 91.7, 69.9, 69.7, 51.6, 32.0, 29.9, 29.6, 29.5, 29.4, 29.3, 29.0, 26.8, 26.2, 26.10, 26.05, 22.8, 14.3; IR (NaCl), ν_{max} (cm^{-1}): 2927, 2854, 2093.

Standard procedure for the post-polymerization azidation reaction

The PPE copolymer with bromine functions on the side chains (**P1a'** or **P1b'**) was dissolved in a THF:DMF mixture (2:1 ratio, 9 mL/0.05 mmol repeating units; one unit contains a bromine-functionalized monomer coupled to an alkoxy-functionalized monomer) and NaN_3 (5 equiv) was added under continuous stirring. After stirring for 72 h at r.t., the reaction was quenched by the addition of water. The polymer was extracted with $CHCl_3$ (3x) and the combined organic phases were washed with water (2x) and brine (1x), dried over $MgSO_4$ and filtered. After evaporation of the solvent, the polymer was precipitated in MeOH and filtered off, yielding an orange solid. ^{1}H NMR (300 MHz, $CDCl_3$), δ (ppm): 7.02 (s, 4H), 4.07–4.01 (m, 8H), 3.23 (t, *J* = 6.9 Hz, 4H), 1.92–1.75 (m, 8H), 1.63–1.43 (m, 8H), 1.42–1.19 (m, 32H), 0.92–0.80 (m, 6H); ^{13}C NMR (75 MHz, $CDCl_3$), δ (ppm): 153.6, 117.4, 114.5, 91.6, 69.9, 69.7, 51.6, 32.0, 29.6, 29.5, 29.4, 29.3, 26.8, 26.2, 22.8, 14.3; IR (NaCl), ν_{max} (cm^{-1}): 2928, 2855, 2095.

Click reaction with phenylacetylene on polymer P2b'

Polymer **P2b'** (0.050 g, 0.0628 mmol repeating units, M_n = 7.8 kg/mol, *Đ* = 1.7) was dissolved in a DMF:THF mixture (1:1, 5 mL, dry and degassed) to which phenylacetylene (14.5 µL, 0.132 mmol), Cu(I)Br (45 mg, 0.314 mmol) and PMDETA (65 µL, 0.314 mmol) were added. After stirring at room temperature for 1 h, $CHCl_3$ was added and the organic phase was washed with an aqueous EDTA solution (3x) until a colorless water layer was obtained. Afterwards, the organic phase was washed with water (2x) and brine (1x), dried over $MgSO_4$ and filtered. After removal of the solvent, an orange solid was obtained. SEC (THF): M_n 8.2 kg/mol, *Đ* 1.7. ^{1}H NMR (400 MHz, $CDCl_3$), δ (ppm): 7.88–7.77 (m, 4H), 7.74 (s(br), 2H), 7.56–7.28 (m, 6H), 7.06–6.93 (m, 4H),

4.36–4.23 (m, 4H), 4.08–3.91 (m, 8H), 1.95–1.72 (m, 8H), 1.59–1.11 (m, 40H), 0.92–0.75 (m, 6H). ^{13}C NMR (100 MHz, $CDCl_3$), δ (ppm): 153.5, 147.6, 131.5, 130.7, 128.8, 128.6, 128.3, 128.0, 125.6, 123.4, 117.3, 114.3, 94.9, 91.7, 85.9, 69.7, 69.5, 50.3, 31.8, 29.34, 29.27, 29.1, 29.02, 28.98, 26.3, 26.0, 25.9, 22.6, 14.1.

3.5 REFERENCES

[1] T. A. Skotheim and J. Reynolds, in *Conjugated Polymers: Theory, Synthesis, Properties, and Characterization* (*Handbook of Conducting Polymers*), CRC Press, 3rd edn., 2006.

[2] a) D. T. McQuade, A. E. Pullen and T. M. Swager, *Chem. Rev.*, 2000, **100**, 2537. b) S. W. Thomas, G. D. Joly and T. M. Swager, *Chem. Rev.*, 2007, **107**, 1339. c) H. Dong, X. Cao and C. M. Li, *ACS Appl. Mater. Interfaces*, 2009, **1**, 1599. d) S. Rochat and T. M. Swager, *ACS Appl. Mater. Interfaces*, 2013, **5**, 4488.

[3] a) J. S. Yang and T. M. Swager, *J. Am. Chem. Soc.*, 1998, **120**, 5321. b) J. S. Yang and T. M. Swager, *J. Am. Chem. Soc.*, 1998, **120**, 11864.

[4] U. H. F. Bunz, K. Seehafer, M. Bender and M. Porz, *Chem. Soc. Rev.*, 2015, **44**, 4322.

[5] a) H. Huang, F. Shi, G. Wang, S. M. Shah and X. Su, *Analyst*, 2012, **137**, 1481. b) A. Ricci, M. Chiarini, C. L. Sterzo, R. Pizzoferrato and S. Paoloni, *J. Photochem. Photobiol. A*, 2014, **298**, 1.

[6] C. Zhu, L. Liu, Q. Yang, F. Lv and S. Wang, *Chem. Rev.*, 2012, **112**, 4687.

[7] a) Q. Zhou and T. M. Swager, *J. Am. Chem. Soc.*, 1995, **117**, 7017. b) Q. Zhou and T. M. Swager, *J. Am. Chem. Soc.*, 1995, **117**, 12593. c) Y. Kim and T. M. Swager, *Macromolecules*, 2006, **39**, 5177. d) A. Narayanan, O. P. Varnavski, T. M. Swager and T. Goodson, *J. Phys. Chem. C*, 2008, **112**, 881. e) A. I. Costa, H. D. Pinto, L. F. V. Ferreira and J. V. Prata, *Sens. Actuat. B-Chem.*, 2012, **161**, 702.

[8] a) Y. Zhang, N. Islam, R. G. Carbonell and O. J. Rojas, *ACS Appl. Mater. Interfaces*, 2013, **5**, 8030. b) D. Pangeni and E. E. Nesterov, *Macromolecules*, 2013, **46**, 7266. c) Y.-X. Wu, J.-B. Li, L.-H Liang, D.-Q. Lu, J. Zhang, G.-J. Mao,

L.-Y. Zhou, X.-B. Zhang, W. Tan, G.-L. Shen and R.-Q. Yu, *Chem. Commun.*, 2014, **50**, 2040.

[9] a) I.-B. Kim, B. Erdogan, J. N. Wilson, U. H. F. Bunz, *Chem. Eur. J.*, 2004, **10**, 6247. b) J. P. Amara and T. M. Swager, *Macromolecules*, 2005, **38**, 9091. c) C. Li, C. Zhou, H. Zheng, X. Yin, Z. Zuo, H. Liu and Y. Li, *J. Polym. Sci. A: Polym. Chem.*, 2008, **46**, 1998. d) X. Yong, W. Wan, M. Su, W. You, X. Lu, Y. Yan, J. Qu, R. Liu and T. Masuda, *Polym. Chem.*, 2013, **4**, 4126.

[10] J. H. Wosnick, C. M. Mello and T. M. Swager, *J. Am. Chem. Soc.*, 2005, **127**, 3400.

[11] J. A. Camarero, *Biopolymers*, 2008, **90**, 450.

[12] a) L. S. Wong, J. Thirlway and J. Micklefield, *J. Am. Chem. Soc.*, 2008, **130**, 12456. b) L. S. Wong, F. Khan and J. Micklefield, *Chem. Rev.*, 2009, **109**, 4025. c) S. H. North, E. H. Lock, C. J. Cooper, J. B. Franek, C. R. Taitt and S. G. Walton, *ACS Appl. Mater. Interfaces*, 2010, **2**, 2884. d) E. Steen Redeker, D. T. Ta, D. Cortens, B. Billen, W. Guedens and P. Adriaensens, *Bioconjug. Chem.*, 2013, **24**, 1761.

[13] a) V. D. Bock, H. Hiemstra and J. H. van Maarseveen, *Eur. J. Org. Chem.*, 2006, **1**, 51. b) C. Barner-Kollowik, F. E. Du Prez, P. Espeel, C. J. Hawker, T. Junkers, H. Schlaad and W. Van Camp, *Angew. Chem. Int. Ed.*, 2011, **50**, 60. c) L. Liang and D. Astruc, *Coord. Chem. Rev.*, 2011, **255**, 2933.

[14] G. Saikia, A. K. Dwivedi and P. K. Iyer, *Anal. Methods*, 2012, **4**, 3180.

[15] J. C. Florès, M. A. Lacour, X. Sallenave, F. Serein-Spirau, J. P. Lère-Porte, J. J. E. Moreau, K. Miqueu, J. M. Sotiropoulos and D. Flot, *Chem. Eur. J.*, 2013, **19**, 7532.

[16] H. Cui, G. He, H. Wang, X. Sun, T. Liu, L. Ding and Y. Fang, *ACS Appl. Mater. Interfaces*, 2012, **4**, 6035.

[17] J. Hou, F. Song, L. Wang, G. Wei, Y. Chang and C. Zhu, *Macromolecules*, 2012, **45**, 7835.

[18] C. S. Andersen and K. V. Gothelf, *Org. Biomol. Chem.*, 2009, **7**, 58.

[19] P. Gerstel, S. Klumpp, F. Hennrich, A. Altintas, T. R. Eaton, M. Mayor, C. Barner-Kowollik and M. M. Kappes, *Polym. Chem.*, 2012, **3**, 1966.

[20] M. J. Plater, J. P. Sinclair, S. Aiken, T. Gelbrich and M. B. Hursthouse, *Tetrahedron*, 2004, **60**, 6385.

[21] A. Qin, C. K. W. Jim, W. Lu, J. W. Y. Lam, M. Häussler, Y. Dong, H. H. Y. Sung, I. D. Williams, G. K. L. Wong and B. Z. Tang, *Macromolecules*, 2007, **40**, 2308.

[22] N. Cheminet, T. Jarrosson, J.-P. Lère-Porte, F. Serein-Spirau, L. Cury, J. Moreau, L. Viau and A. Vioux, *J. Mater. Chem.*, 2011, **21**, 13588.

[23] J. D. Mendez, M. Schroeter and C. Weder, *Macromol. Chem. Phys.*, 2007, **208**, 1625.

[24] a) C. Weder and M. S. Wrighton, *Macromolecules*, 1996, **29**, 5157. b) C. Weder, M. S. Wrighton, R. Spreiter, C. Bosshard and P. Günter, *J. Phys. Chem.*, 1996, **100**, 18931. c) J. S. Kim, S. K. McHugh and T. M. Swager, *Macromolecules*, 1999, **32**, 1500.

[25] a) R. Huisgen, *Proc. Chem. Soc.*, 1961, 357. b) K. V. Gothelf and K. A. Jorgensen, *Chem. Rev.*, 1998, **98**, 863. c) V. R. Vsevolod, L. G. Green, V. V. Fokin and K. B. Sharpless, *Angew. Chem. Int. Ed.*, 2002, **41**, 2596.

[26] N. Zaquen, J. Vandenbergh, M. Schneider, L. Lutsen, D. Vanderzande and T. Junkers, *Polymers*, 2015, **7**, 418.

[27] a) R. L. Danley, P. A. Caulfield and S. R. Aubuchon, *Am. Lab.*, 2008, **40**, 9. b) S. Wouters, F. Demir, L. Beenaerts and G. Van Assche, *Thermochim. Acta*, 2012, **530**, 64. c) T. Ghoos, J. Brassinne, C.-A. Fustin, J.-F. Gohy, M. Defour, N. Van den Brande, B. Van Mele, L. Lutsen, D. J. Vanderzande and W. Maes, *Polymer*, 2013, **54**, 6293.

[28] U. H. F. Bunz, *Chem. Rev.*, 2000, **100**, 1605.

[29] B. C. Englert, S. Bakbak and U. H. F. Bunz, *Macromolecules*, 2005, **38**, 5868.

[30] a) R. L. Phillips, I.-B. Kim, L. M. Tolbert and U. H. F. Bunz, *J. Am. Chem. Soc.*, 2008, **130**, 6952. b) U. W. F. Bunz, *Synlett.*, 2013, **24**, 1899.

[31] Y. Pourghaz, P. Dongare, D. W. Thompson and Y. Zhao, *Chem. Commun.*, 2011, **47**, 11014.

[32] B. Erdogan, L. Song, J. N. Wilson, J. O. Park, M. Srinivasarao and U. H. F. Bunz, *J. Am. Chem. Soc.*, 2004, **126**, 3678.

[33] a) J. Bard and L. R. Faulkner, *Electrochemical methods: fundamentals and applications*, Wiley, 2nd edn., 2001. b) S. Trasatti, *Pure Appl. Chem.*, 1986, **58**, 955.

3.6 SUPPORTING INFORMATION

3.6.1. MALDI-TOF mass spectrum of copolymer P2a

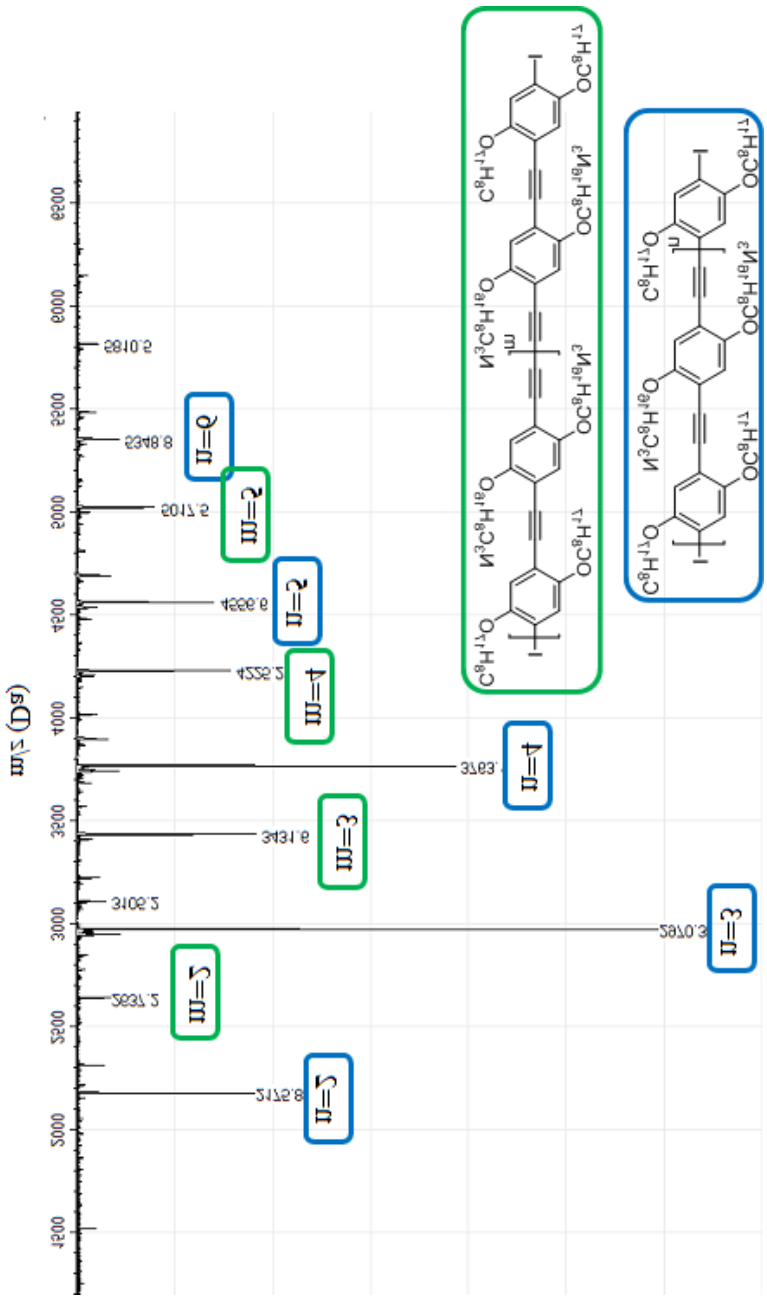

Figure S1: MALDI-TOF mass spectrum of (non-end-capped) copolymer **P2a** (M_n = 14 kg/mol, $Đ$ = 2.1). The majority of the polymer chains is defect-free, whereas a smaller part contains one homo-coupling somewhere along the polymer backbone.

3.6.2. ^{1}H and ^{13}C NMR spectra of monomers and polymers (in $CDCl_3$)

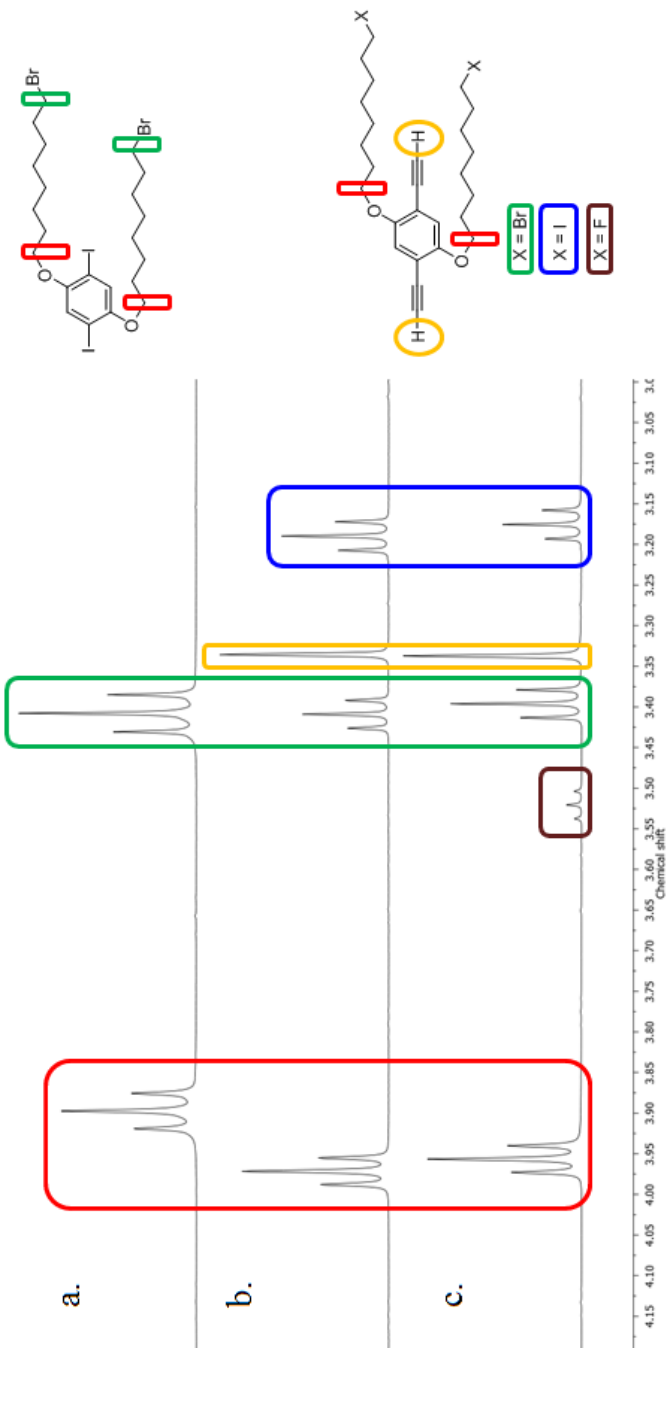

Figure S2: ^{1}H NMR spectra (zoom from 3.0 to 4.2 ppm) illustrating the different products formed upon performing the Sonogashira reaction with TMSA on diiodobenzene precursor **3** and subsequent deprotection: a) Precursor **3** (the triplets of the CH_2 groups next to the O and Br atoms are indicated in red and green, respectively), b) after Sonogashira coupling and deprotection with K_2CO_3 (a new triplet at 3.19 ppm from the CH_2 group next to I appears), c) after Sonogashira coupling and deprotection with TBAF (a new triplet at 3.52 ppm from the CH_2 group

PPE copolymer **P1a'**

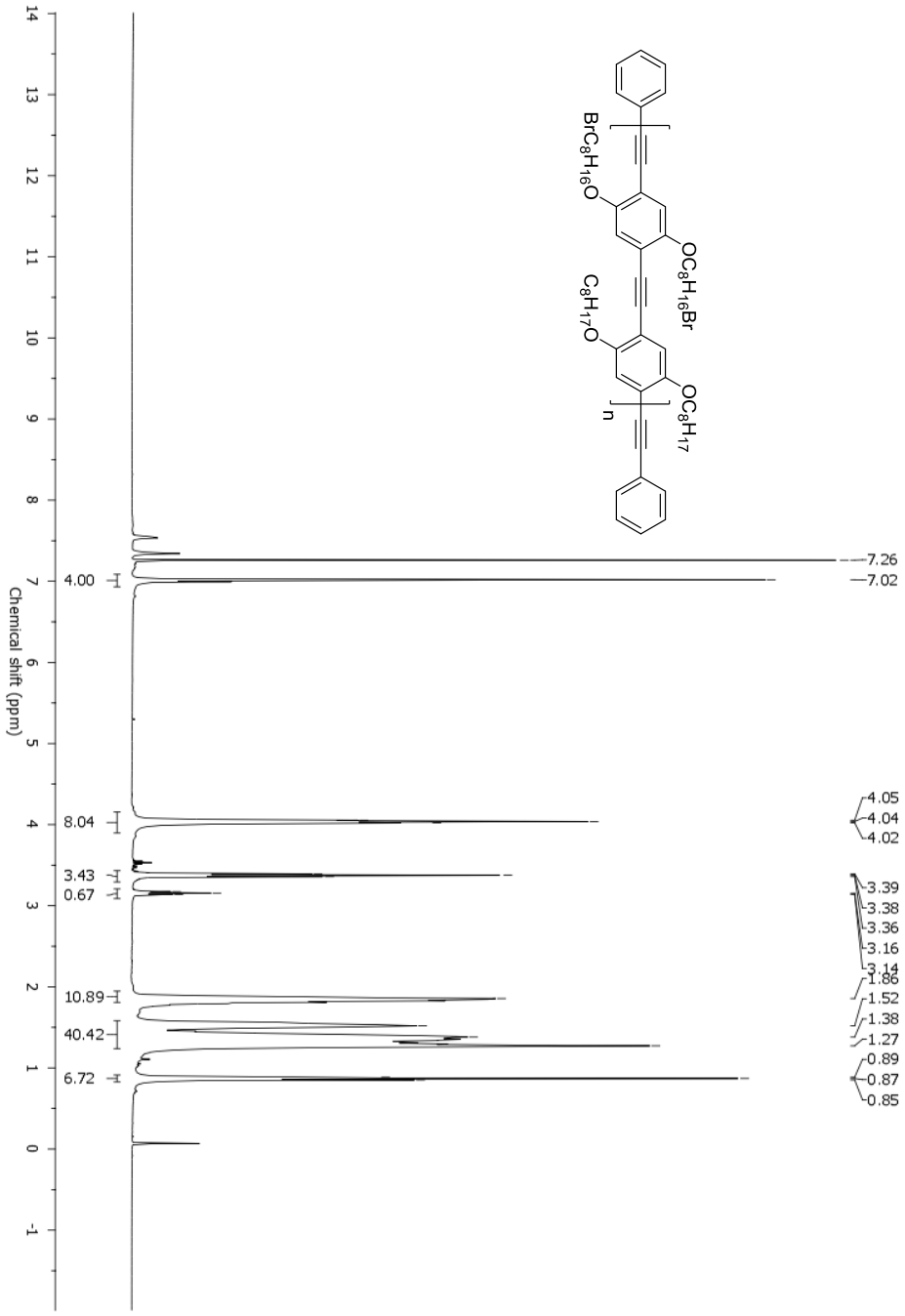

PPE copolymer **P1b'**

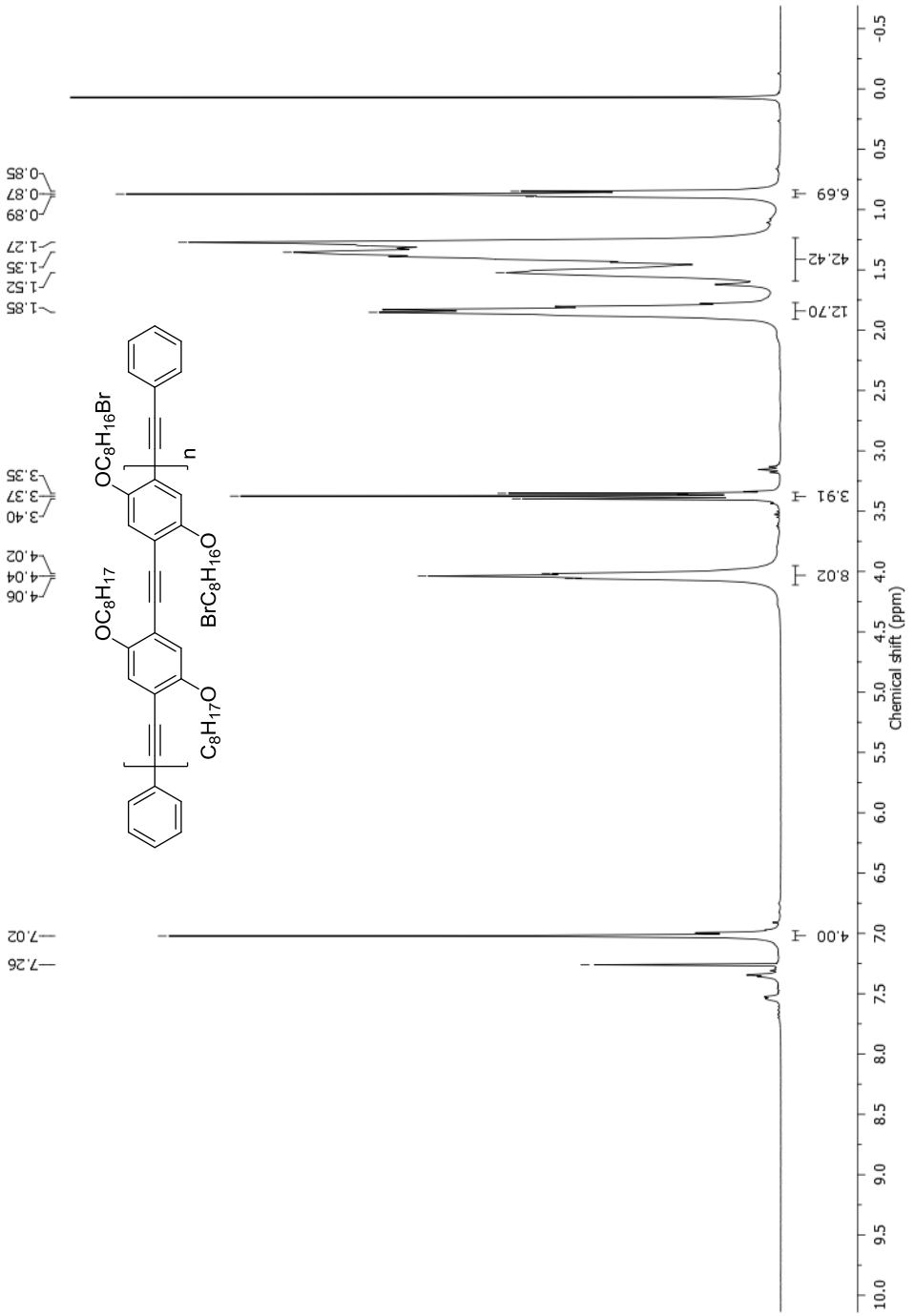

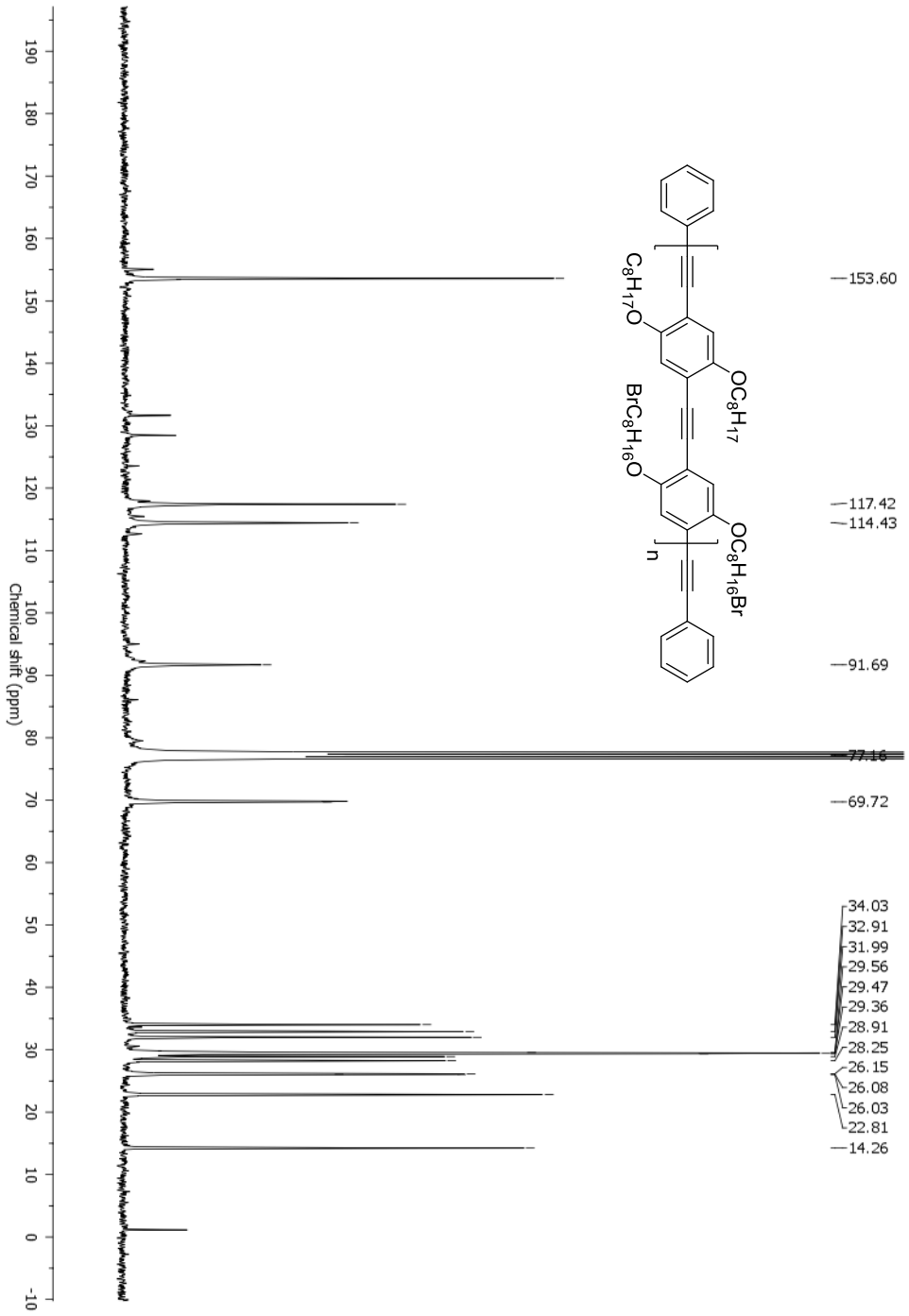
Chemical shift (ppm)
190
180
170
160
150
140
130
120
110
100
90
80
70
60
50
40
30
20
10
0
-10
153.60
117.42
114.43
91.69
77.16
69.72
34.03
32.91
31.99
29.56
29.47
29.36
28.91
28.25
26.15
26.08
26.03
22.81
14.26
C8H17O
OC8H17
BrC8H16O
OC8H16Br
n

PPE copolymer **P1b'** after post-polymerization functionalization with NaN_3

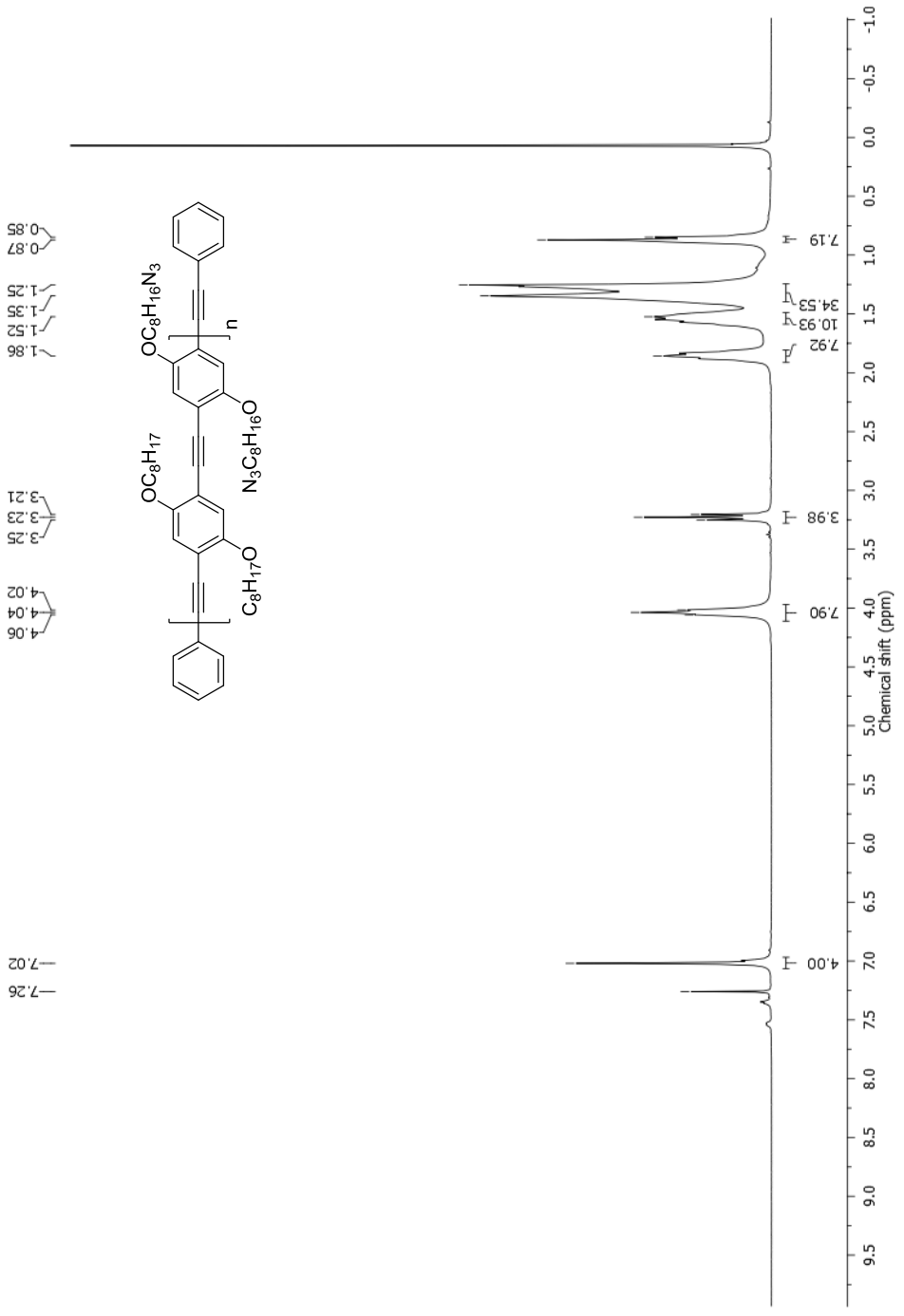

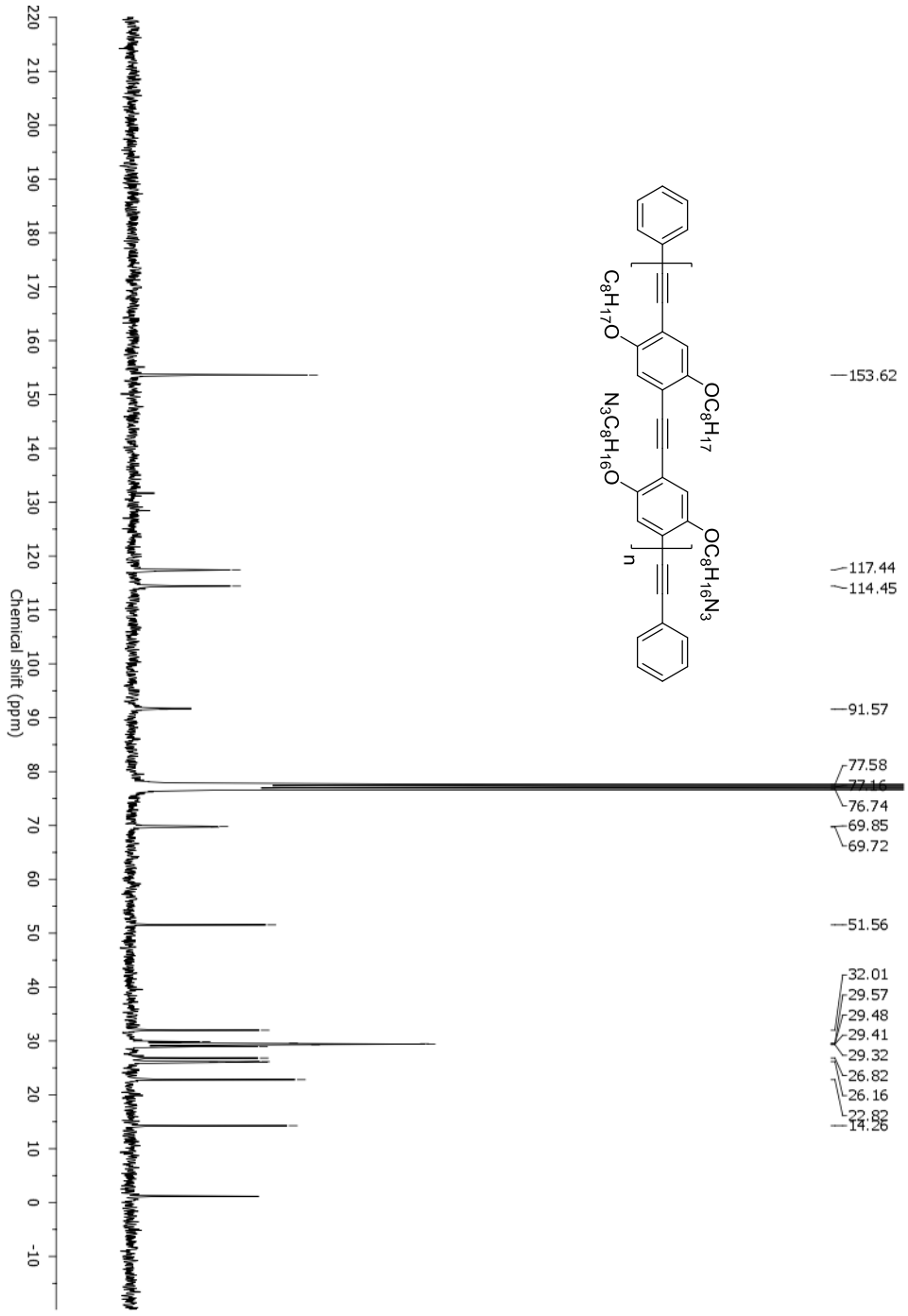
Chemical shift (ppm)
220 210 200 190 180 170 160 150 140 130 120 110 100 90 80 70 60 50 40 30 20 10 0 -10
153.62
117.44
114.45
91.57
77.58
77.16
76.74
69.85
69.72
51.56
32.01
29.57
29.48
29.41
29.32
26.82
26.16
22.82
14.26
C8H17O
OC8H17
N3C8H16O
OC8H16N3
n

PPE copolymer **P2a'**

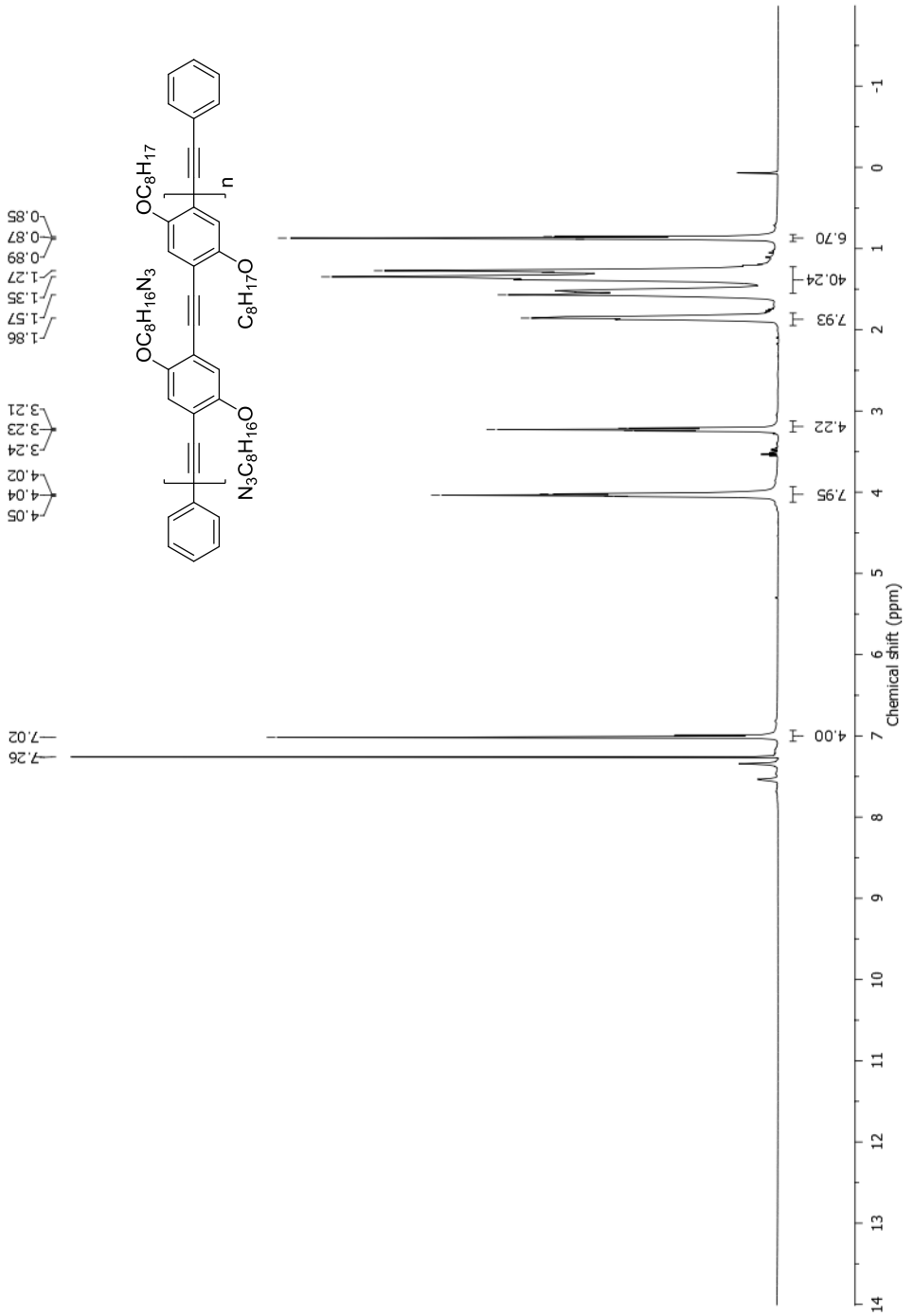

PPE copolymer **P2b'**

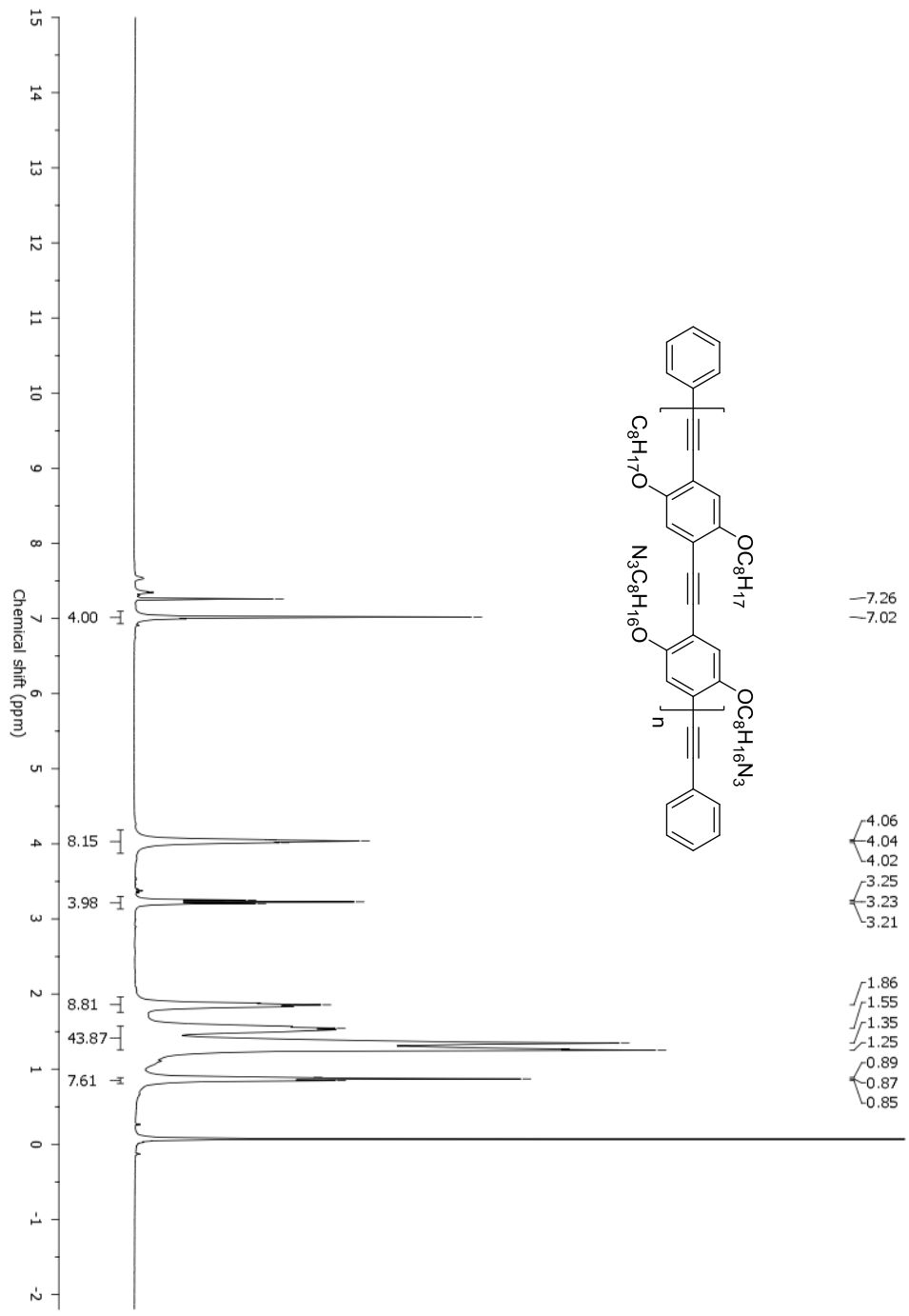

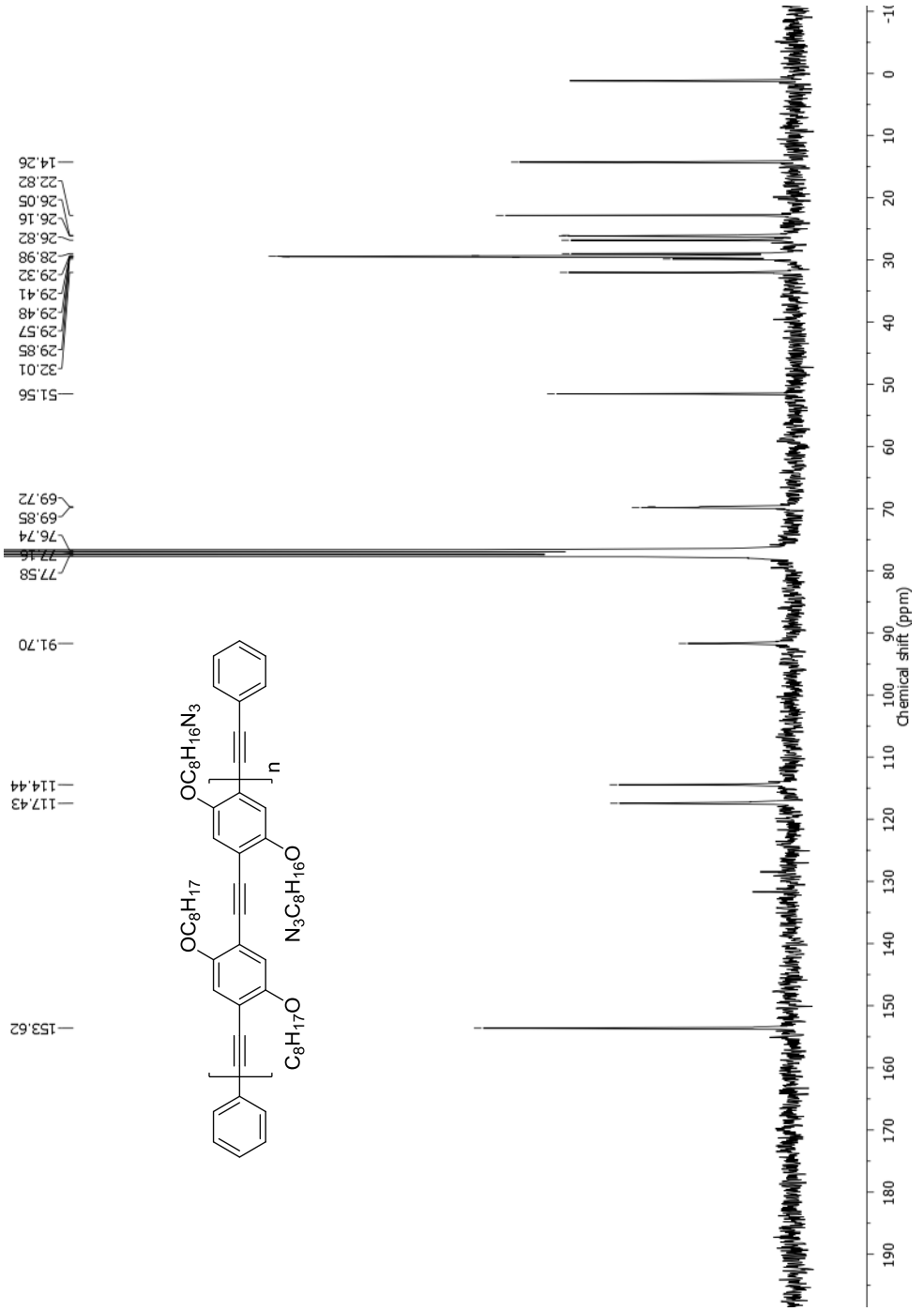
14.26
22.82
26.05
26.16
26.82
28.98
29.32
29.41
29.48
29.57
29.85
32.01
51.56
69.72
69.85
76.74
77.16
77.58
91.70
114.44
117.43
153.62
Chemical shift (ppm)
OC8H16N3
n
OC8H17
N3C8H16O
C8H17O

PPE copolymer **P3'**

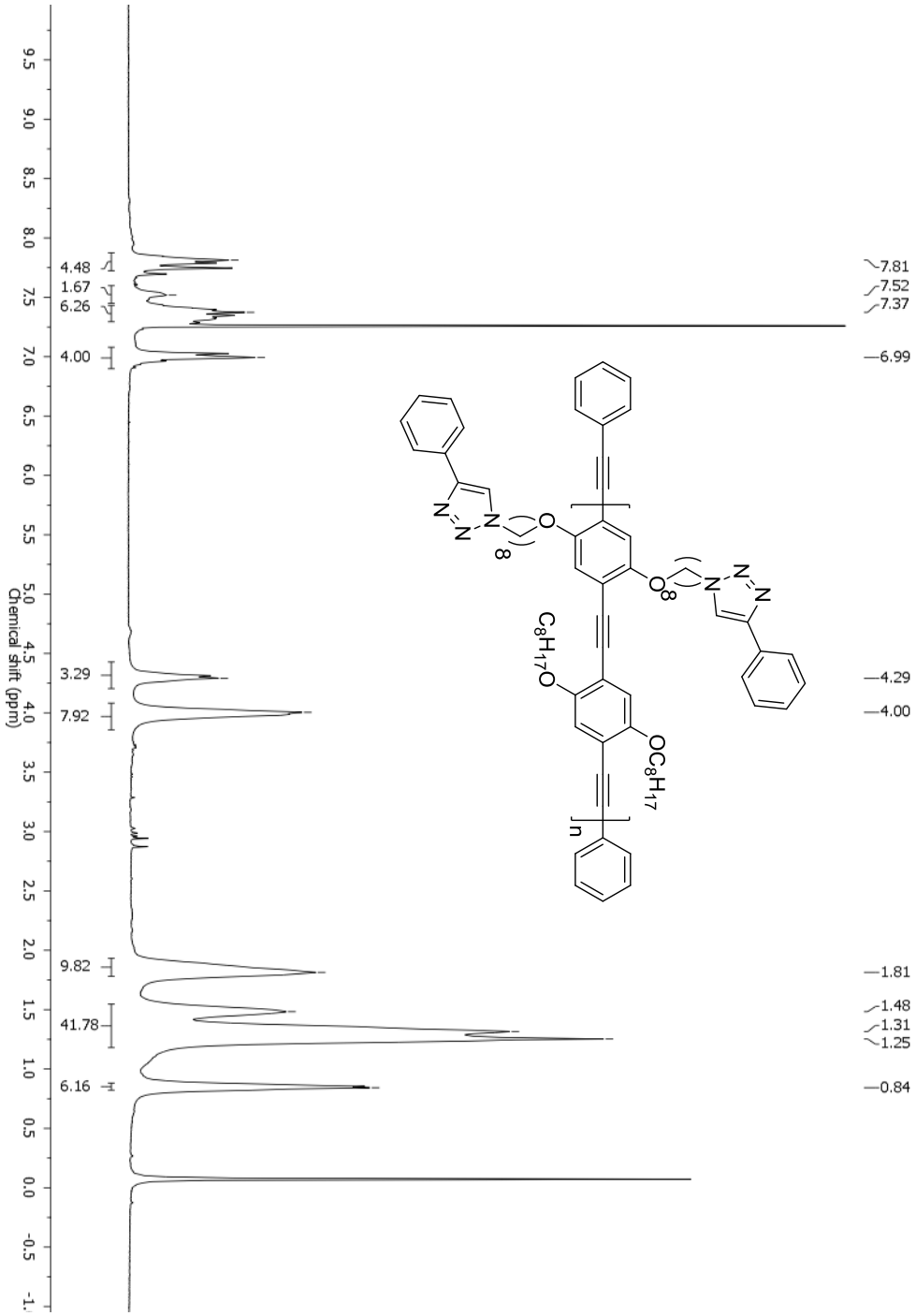

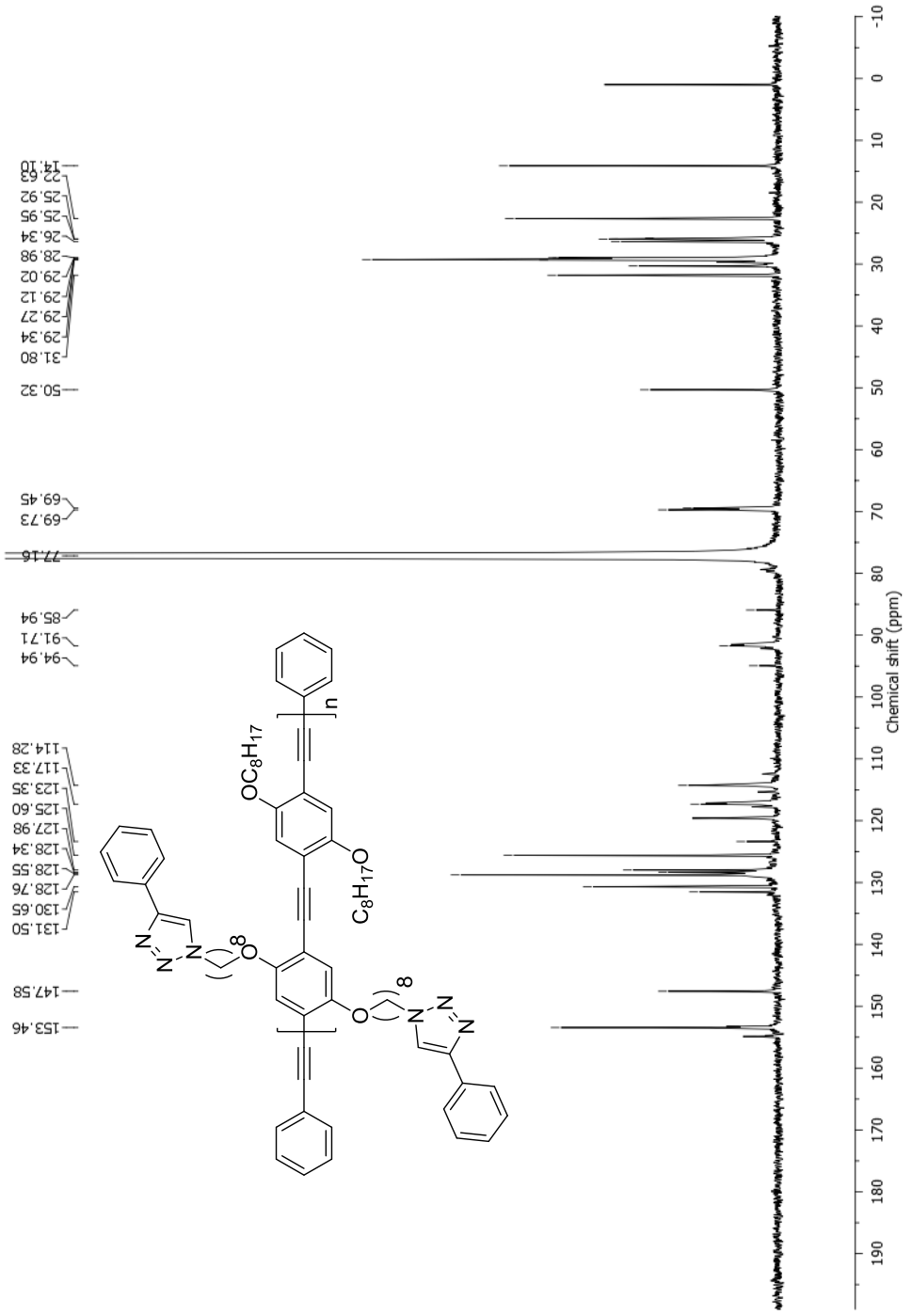
14.10
22.63
25.92
25.95
26.34
28.98
29.02
29.12
29.27
29.34
31.80
50.32
69.45
69.73
77.16
85.94
91.71
94.94
114.28
117.33
123.35
125.60
127.98
128.34
128.55
128.76
130.65
131.50
147.58
153.46
OC_8H_{17}
$C_8H_{17}O$
n
8
8
Chemical shift (ppm)

3.6.3. Cyclic voltammograms

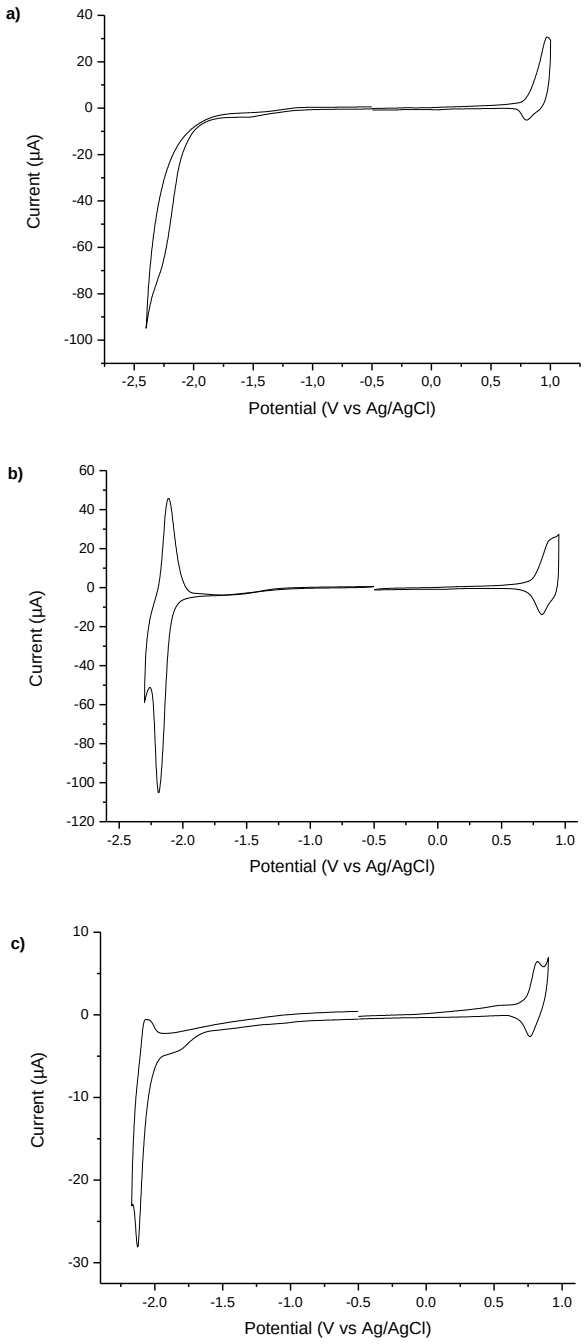

Figure S3: Cyclic voltammograms of a) **P1b'**, b) **P2b'** and c) **P3'** (in film).

3.6.4. FT-IR spectra

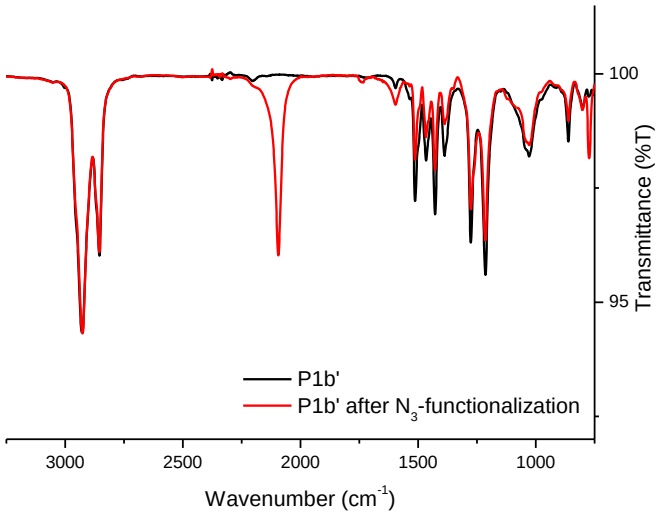

Figure S4: FT-IR spectra of copolymer **P1b'** before (black) and after (red) post-polymerization functionalization with azide moieties.

Chapter 4

Tuning the Optical Properties of Poly(*p*-Phenylene Ethynylene) Nanoparticles as Bio-imaging Probes by Side Chain Functionalization

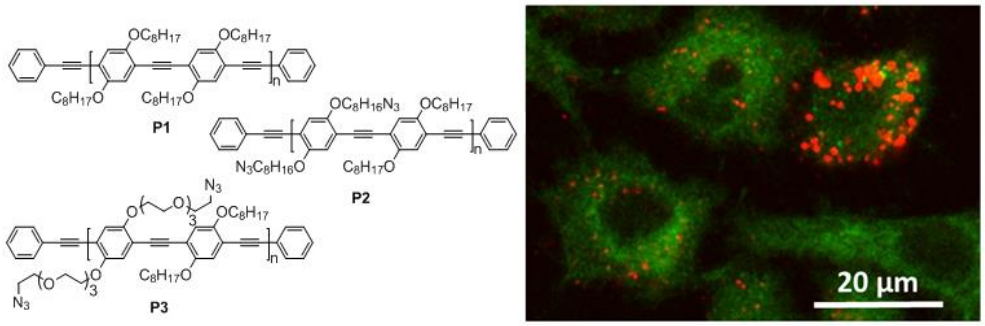

L. D'Olieslaeger*, Y. Braeken*, S. Cheruku, J. Smits, M. Ameloot, D. Vanderzande, W. Maes and A. Ethirajan, *J. Colloid Interface Sci.*, 2017, **504**, 527.
(* shared first authorship)

ABSTRACT

Conjugated polymers are versatile bio-imaging probes as their optical properties can be readily fine-tuned. In this chapter, the fabrication of fluorescent conjugated polymer nanoparticles using three different poly(*p*-phenylene ethynylene) (PPE) derivatives is described. The polymers have the same backbone but carry different side chains, i.e. regular octyloxy substituents, half of the octyloxy chains azide terminated, or azide functionalized tetraethylene glycol (TEG) moieties. The azide groups are specifically chosen to allow coupling of (bio)molecules to the surface of the particles using straightforward azide-alkyne click reactions, enabling different bioconjugation and targeting strategies. The influence of the functionalization pattern on the size and optical properties of the nanoparticles is studied using transmission electron microscopy, dynamic light scattering, UV-Vis absorption and fluorescence spectroscopy. The polymer containing the azide functionalized TEG chains affords larger particles, which can be attributed to hydration of the outer layer of the more hydrophilic polymer particles. However, this does not impact the fluorescence quantum yield. The two azide functionalized PPE particles exhibit the highest quantum yields (13%). Despite the presence of azide groups on two of the three materials, all particles are biocompatible and taken up by A549 human lung carcinoma cells. A proof of concept click reaction was performed as well.

4.1 INTRODUCTION

In the last decades, tremendous efforts have been done to visualize a broad range of biological activities in living systems, such as protein transport, gene expression and regulatory pathways.[1-3] The implementation of those imaging methods not only expanded our general knowledge in the fields of biology and medicine, but also enables us to detect and treat life-threatening diseases.[4-6] Fluorescence imaging techniques provide a very high spatial and temporal resolution and an excellent signal-to-noise ratio. A large collection of fluorescence imaging agents has been developed for this purpose, *e.g.* traditional organic dyes,[7] semiconductor quantum dots,[7-9] carbon dots, dye-doped polymer nanoparticles (NPs),[10] metal nanoclusters,[11] nanodiamonds,[12] and dye-embedded silica nanoparticles[13]. However, despite great efforts, each material system suffers from its own intrinsic limitations and drawbacks. For example, low molecular weight organic dyes and fluorescent proteins generally exhibit poor photostability.[14] Encapsulation of the dyes in polymer or silica nanoparticles can offer a solution, but in this case problems like dye leaking and self-quenching occur.[15,16] Semiconducting quantum dots possess a higher brightness, are very photostable and have a size and composition dependent narrow emission. However, their use for in vitro and in vivo applications is still controversial because of their intrinsic cytotoxicity and chemical instability (leaching).[8] Fluorescent nanodiamonds combine the advantages of semiconductor quantum dots (small size, high photostability, bright multicolor fluorescence) with biocompatibility and non-toxicity required for bio-imaging applications. However, dispersing nanodiamonds into single particles without contamination is demanding.[12]

In this regard, the use of fluorescent conjugated polymers forms a promising alternative. Although these polymers were originally designed for opto-electronic devices, they have recently also attracted lots of attention for biological applications because of their excellent optical properties, such as a good fluorescence brightness and photostability, a fast emission rate and non-blinking behaviour.[17,18] However, most conjugated polymers are highly hydrophobic and are only soluble in (toxic) organic solvents, thereby limiting their use in biological environment. A possible solution can be to transform the conjugated

polymers into water-based nanoparticle (NP) dispersions. Many research groups already synthesized conjugated polymer NP dispersions using miniemulsion, reprecipitation or self-assembly techniques. To date, mainly polyfluorenes,[19,20] poly(*p*-phenylene vinylene)s (PPVs)[21-24] and donor-acceptor type polymers[25-27] have been studied in nanoparticulate form.[28] Variation of the polymer side chains has a substantial impact on the optical properties of the NPs and their interaction with biological systems. Attaching bulky side chains to the polymer backbone generally improves the photoluminescence quantum yield (PLQY), which can be attributed to the change in packing density when formulating the polymer into NPs.[29] Moreover, it was found that variation of the density of hydrophilic carboxyl groups on poly(fluorene-*alt*-benzothiadiazole) NPs has a significant impact on the stability, fluorescence brightness and non-specific binding properties.[30]

Among the different types of conjugated polymers, PPEs are a very interesting class of materials for biomedical applications, including bio-imaging.[14,31-36] They have a rigid backbone and therefore generally exhibit high fluorescence quantum yields, combined with large molar extinction coefficients and a high photostability.[14,37] Moreover, the synthetic versatility of PPEs offers a wide selection of possible functionalized side chains, allowing to couple (bio)molecules as per demand. A few PPE based NPs have been reported before. Liu *et al.* synthesized particles by self-assembly of novel amphiphilic PPEs,[33] whereas Moon *et al.* showed that chemical modifications in the PPE side chains changed the cellular toxicity and subcellular localization of the NPs.[31] However, the influence of the chemical modifications on the optical properties of the NPs was not studied.

In the present study, the influence of azide functionalized hydrophilic and hydrophobic side chains on the optical properties of PPE NPs, their colloidal stability and morphology, and their interaction with biological systems is investigated for the first time. Particles containing azide groups show the important advantage to enable coupling of all kind of alkyne functionalized (bio)molecules to the NP surface. In this way any functional moiety can be selectively introduced onto the particles via an easy click chemistry protocol (that can be performed in water). Most often, not all surface groups undergo coupling, thereby leaving some of the excess functionalities unaffected. This can

be critical when the surface groups are known to cause purported cytotoxic effects. In general, the surface functionality of NPs plays a decisive role (among other factors) in determining their cellular toxicity and cellular uptake.[38-41]

In here, we present the optical properties of three functionalized PPE nanoparticles and the results of their biocompatibility and cellular uptake studies using the human lung cancer carcinoma A549 cell line, which is crucial towards the use of these particles for bio-imaging applications. As a proof-of-principle, the azide functionalities present at the periphery of the PPE-NP surface were used to click an alkyne functionalized megastokes dye using the copper(I)-catalyzed azide-alkyne 1,3-dipolar cycloaddition (CuAAC) reaction[42-44].

4.2 RESULTS AND DISCUSSION

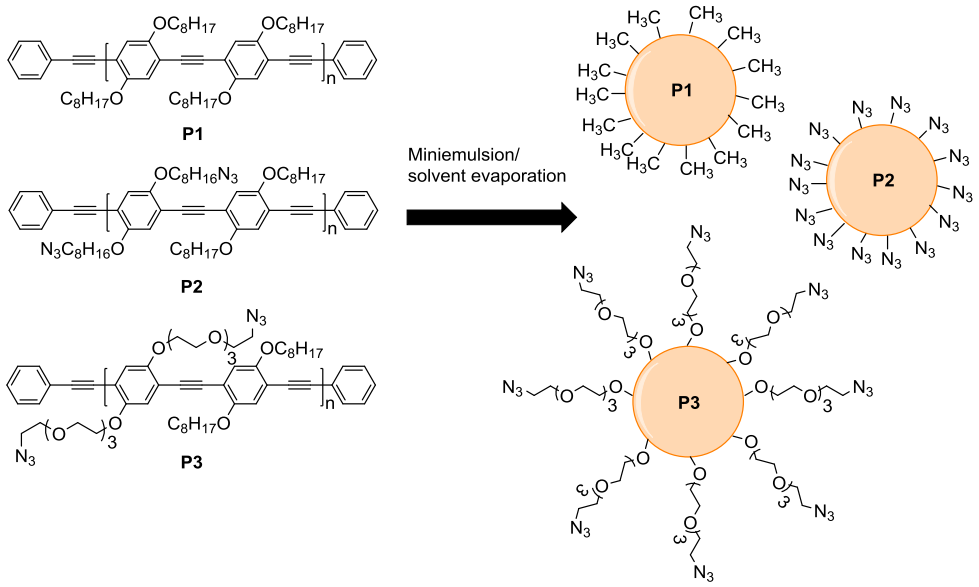

Scheme 1: Overview of the different synthesized PPE derivatives formulated into nanoparticles.

All three PPE derivatives compared in this work have the same backbone structure, but variation is introduced in the polymer side chains (Scheme 1). On the first polymer (**P1**), hydrophobic octyloxy side chains are introduced.[50] The second polymer (**P2**) is similar, but 50% of the octyloxy side chains are

terminated with an azide group.[45] The third polymer (**P3**) was designed to be more hydrophilic by the introduction of azide functionalized tetraethylene glycol (TEG) side chains.

4.2.1 Monomer and polymer synthesis

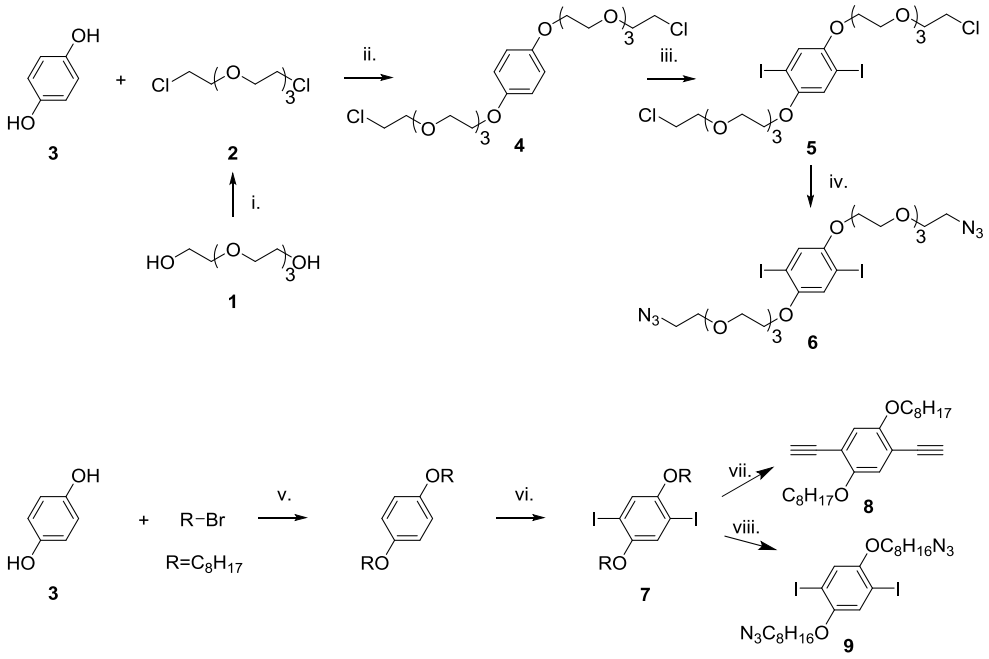

Scheme 2: Synthetic pathways towards PPE monomers **6**–**9**: i. $SOCl_2$, pyridine, $CHCl_3$, reflux, 3 h, 84%; ii. K_2CO_3, MeCN, reflux, 36 h, 63%; iii. ICl, MeOH, reflux, 4 h, 69%; iv. NaN_3, DMF, 70 °C, 3 d, full conversion; v. K_2CO_3, acetone, 50 °C, on; vi. I_2, KIO_3, AcOH, H_2O, H_2SO_4, reflux, on; vii. a) TMS-acetylene, $Pd(PPh_3)_2Cl_2$, CuI, THF, Et_3N, 40 °C, on; b) KOH, MeOH/THF, 0 °C, 3 h; viii. NaN_3, DMSO, rt, on.

For all monomers required for the final PPE polymers, the applied synthetic approach is comparable (Scheme 2), starting from hydroquinone (**3**), on which side chains are introduced via a Williamson ether protocol. Then, two iodine groups are added to enable either the introduction of alkyne functionalities or direct Sonogashira polymerization. On one of the monomers, azide moieties

were introduced at the outer end of the octyloxy side chains by a simple substitution reaction. Work-up and purification of this product (**9**) had to be done with care because it has a tendency to degrade when stored at room temperature. For diethynyl monomer **8**, two trimethylsilyl (TMS) protected alkyne functionalities were initially introduced on the phenyl ring via a Sonogashira cross coupling reaction. The TMS groups were afterwards removed with KOH. Deprotection was performed at 0 °C to prevent side product formation. Finally, monomer **6** was also synthesized from hydroquinone through introduction of a chlorine functionalized TEG side chain in both the 1- and 4-position. Precursor **4** was iodinated twice by means of ICl. In the last step, the chlorine end groups on the TEG side chains were substituted by azides.

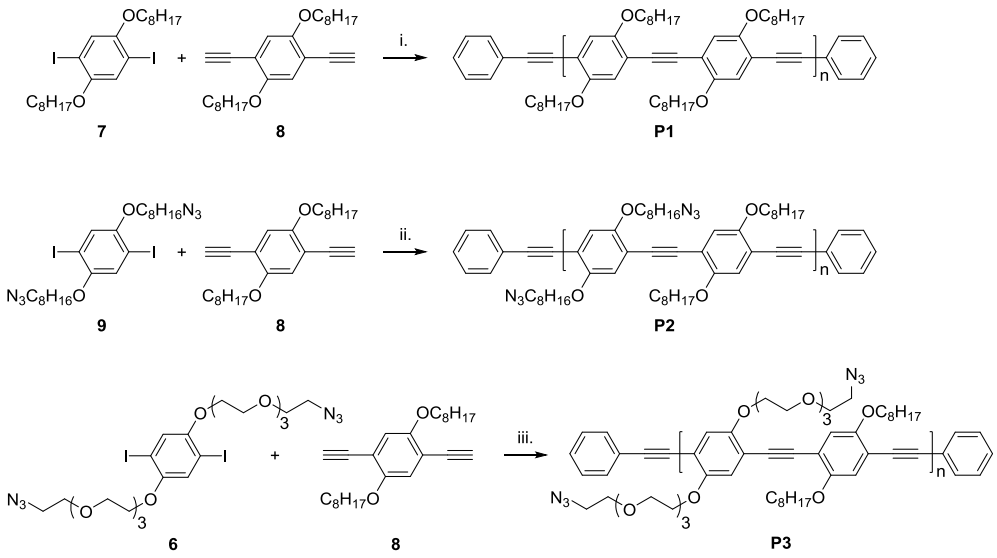

Scheme 3: Synthetic procedures towards PPE copolymers **P1**, **P2** and **P3**: i. $Pd(PPh_3)_2Cl_2$, CuI, DIPA, toluene, 70 °C, 2 h, 91%; ii. $Pd(PPh_3)_2Cl_2$, CuI, DIPA, toluene, 70 °C, 2 h, 73%; iii. $Pd(PPh_3)_4$, CuI, DIPA, toluene, microwave, 70 °C, 40 min, 93%.

The synthesis of PPE polymers **P1** and **P2** was reported previously (Scheme 3).[45,50] Both materials were successfully resynthesized here, affording polymers with (number-averaged) molar masses (M_n) of 16.0 kg/mol ($Đ$ = 1.9) and 14.0 kg/mol ($Đ$ = 1.9) for **P1** and **P2**, respectively. The synthesis of the novel

TEGylated polymer **P3** (Scheme 3) was slightly more complicated due to the oily character of the monomers, which rendered their purification and polymerization less straightforward. This is also reflected in the molar mass of **P3**. When $Pd(PPh_3)_2Cl_2$ was used as the catalyst, only oligomers were obtained, whereas the use of Pd_2dba_3 led to insoluble polymer gels. $Pd(PPh_3)_4$ finally afforded the best results (M_n = 8.2 kg/mol, $Đ$ = 2.3) and microwave irradiation was applied to stimulate the polymerization reaction. To prevent crosslinking during storage of all polymers containing azide functionalities (**P2** and **P3**), end-capping of the polymers was performed (with phenyl groups).[45] For the uniformity of all three polymers compared in this work, **P1** was also end-capped. **P3** was purified from catalyst residues by precipitation in ice-cold hexane. Soxhlet extraction was not performed to prevent crosslinking at elevated temperatures.[45]

4.2.2 Nanoparticle synthesis and characterization

NPs were then synthesized from the three PPE derivatives using the combined miniemulsion and emulsion/solvent evaporation technique (Figure 1).[51,52] Briefly, a two-phase system is created consisting of a dispersed phase, containing the polymer dissolved in chloroform, and a continuous phase, containing water and surfactant molecules. On this system, high shear forces are applied by ultrasonication to form droplets of the dispersed phase in the continuous phase. Afterwards, the solvent is evaporated, resulting in precipitation of the polymer chains in the form of NPs.

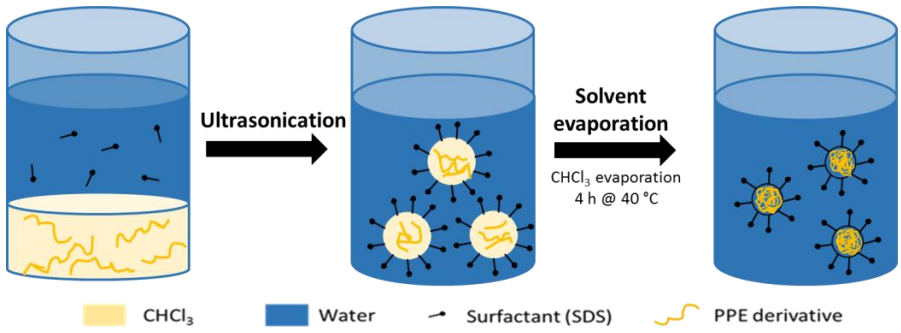

Figure 1: Schematic representation of the combined miniemulsion/solvent evaporation technique.

Table 1: Mean size, polydispersity index (PDI) and zeta potential of the different PPE NPs measured in water.

Sample	Size ± standard deviation (nm)	PDI	Zeta potential ± standard deviation (mV)
P1-NPs	78 ± 0.4	0.083	−40.24 ± 0.50
P2-NPs	87 ± 0.4	0.062	−22.49 ± 0.72
P3-NPs	188 ± 2.5	0.097	−1.56 ± 1.23

The solid content of the NP dispersions, after surfactant removal, was in the range of 0.14 to 0.36%. The characteristics of the different particles are summarized in Table 1. The sizes of the **P1**- and **P2**-NPs as observed by DLS are similar (Figure S8), whereas the **P3**-NPs are significantly larger due to the presence of the hydrophilic TEG chains, favouring the aqueous environment (as expected). However, the fact that the size is approximately two times larger for the latter particles indicates hydration of the polymer chains within the volume of the particles, as the hydration of the outer layer of the particles alone is insufficient to explain such an increased size. As the size of the TEG units is about 1.12 nm (4x0.28 nm, where 4 is the number of monomeric units in TEG and 0.28 nm is the length of one monomer unit in the crystal unit cell of PEG[53,54]), it is highly unlikely that the outer layer hydration alone would give such a pronounced swelling. Because of the combination of low molecular weight polymer chains (M_n 8.2 kg/mol) and the presence of TEG chains on each repeating unit, we hypothesize that the particles are not as compact as the other two nanoparticle types formulated using **P1** and **P2**, and the volume of the particles is very hydrated (hydrogel-like) in the dispersed state, resulting in a large hydrodynamic size in DLS.

The zeta potential values of the washed samples are negative due to the presence of the anionic surfactant SDS. It can be seen that for the **P1**- and **P2**-NPs, adequate washing does not remove all of the anionic surfactant. The presence of the functional groups does aid in the removal of the surfactant, as can be seen in the case of the **P2**- and **P3**-NPs where the zeta potential values (magnitude) are lowered, the effect being most significant in case of the latter.

In Figure 2, TEM images of the different particles are presented. In these

images, the size and the morphology of all particles look similar. The **P3**-NPs, however, have a smaller size as compared to what was measured in DLS due to the fact that the particles are imaged in the dried state. Under dry conditions the hydrated TEG chains will collapse, resulting in a smaller size and thereby reflecting the earlier observation that the particles might exist as hydrogels in the dispersion.

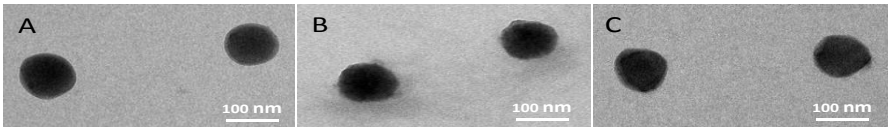

Figure 2: TEM images of the different nanoparticles: **P1**-NPs (A), **P2**-NPs (B) and **P3**-NPs (C).

42.3 Optical properties

The optical properties of the different PPEs, in molecularly dissolved (MD) and NP form, were studied in detail using UV-Vis absorption and fluorescence spectroscopy and the resulting data are gathered in Table 2. The absorbance and emission of the MD polymer chains were measured in chloroform and their respective NPs were analysed in water (Figure 3). The absorption profiles of the MD polymers are very similar (as expected). For the NPs, there is more dissimilarity, which can be assigned to the different packing of the polymers when formulated into particles as a result of the different side chain patterns. The absorption spectra of the NPs are broadened, red-shifted and have a different shape as compared to the spectra of the free polymer chains, which can be attributed to the aggregation/stacking of the chains within the particles, causing torsion, kinking and bending of the polymer backbone.[55] All synthesized PPE NPs have a broad absorption band ranging from 350 to over 500 nm, which is interesting for bio-imaging applications using two-photon excitation. Also in the emission, a strong red-shift can be observed for the NPs because of a change from intra- to interchain emission when the conjugated polymers aggregate, during the evaporation of the solvent, into NPs.[55] The occurring red shift is due to overlap of the π-orbitals during aggregation, leading to delocalization of the π-electrons across several chains and thereby causing

the formation of new electronic species with lower band gaps. This strong bathochromic shift reflects in a large Stokes shift (Table 2), which is desirable for fluorescence microscopy applications as it eliminates spectral overlap between absorption and emission and allows for a better detection of the fluorescence signal.

For all three PPE NPs, a decrease in PLQY is observed as compared to their MD counterparts: from 66 to 8% for **P1**, from 64 to 13% for **P2** and from 56 to 13% for **P3**. In general, aggregation of polymer chains results in fluorescence quenching by interchain interactions, resulting in excitations reaching quenching sites more easily and thereby opening an effective relaxation path.[55] The PLQYs of the different NPs depend on the amount of interchain interactions and thus on the packing/stacking of the polymer chains in the aggregated form.[21,56] The beneficial effect on the PLQY of attaching bulky side chains onto the conjugated backbone is already reported in literature.[29,57] Based on our results, the presence of azide groups has a significant impact on the PLQY of PPEs when formulated into NPs. **P1** only contains hydrophobic octyloxy side chains with no affinity for the water phase (reflected in the particle size as observed by DLS), resulting in a high packing density of the polymer chains. However, the reasonably high PLQY observed for the **P1**-NPs indicates that the octyloxy side chains can effectively introduce some spacing between the polymer backbones. The **P2**- and **P3**-NPs have increased PLQYs (by 5% as compared to the **P1**-NPs). However, this difference is not seen in case of the MD polymer chains. This indicates that the presence of the azide groups has a substantial impact on the fluorescence behaviour when formulated into NPs. Although the affinity of the polymer chains to the water phase in case of **P3** is foreseen due to the presence of the TEG units (as also observed by DLS), the unexpected similarity in PLQY between the **P2**- and **P3**-NPs indicates that the azide groups strongly influence the packing of the polymer chains within the NPs, resulting in a decreased packing density in both NP types. Apart from introducing steric hindrance during packing within the particles, the affinity of the polymer chains for the water phase might also be influenced by the presence of the azide groups, thereby changing the packing arrangement/conformation during the precipitation of the polymer chains while the NP is being formed. Based on the PLQY results, irrespective of the hydration due to the TEG chains in polymer **P3**, the similarity

between the **P2**- and **P3**-NPs indicates that it is likely that the dominant contribution to the PLQY arises from the hydrophobic conjugated polymer backbones constituting the volume of the particles, where the packing is hindered due to the side chain functional groups.

Apart from high PLQYs in NP form, the molar extinction coefficients are also very important for achieving high fluorescence brightness, which is defined as the PLQY multiplied by the mass extinction coefficient. As can be seen in Table 2, varying the composition of the repeating unit also influences the molar absorptivity. In all cases, the high values for the molar extinction coefficients together with the high PLQYs render these NP probes very suitable for bio-imaging applications.

Table 2: Optical characteristics of the different PPEs in molecularly dissolved and NP form.

Sample	λ_{max} emission (nm)	λ_{max} absorption (nm)	Stokes shift (nm)	PLQY (%)	Molar extinction coefficient ε (M^{-1} cm^{-1})	Fluorescence brightness (M^{-1} cm^{-1})
P1-NPs	579	450, 482	97	8	6×10^5	48×10^3
P1-MD	476	450	26	66	2×10^6	13×10^5
P2-NPs	538	443, 485	53	13	3×10^5	39×10^3
P2-MD	476	441	35	64	5×10^5	32×10^4
P3-NPs	534	464, 491	43	13	5×10^4	65×10^2
P3-MD	473	437	36	56	2×10^5	11×10^4

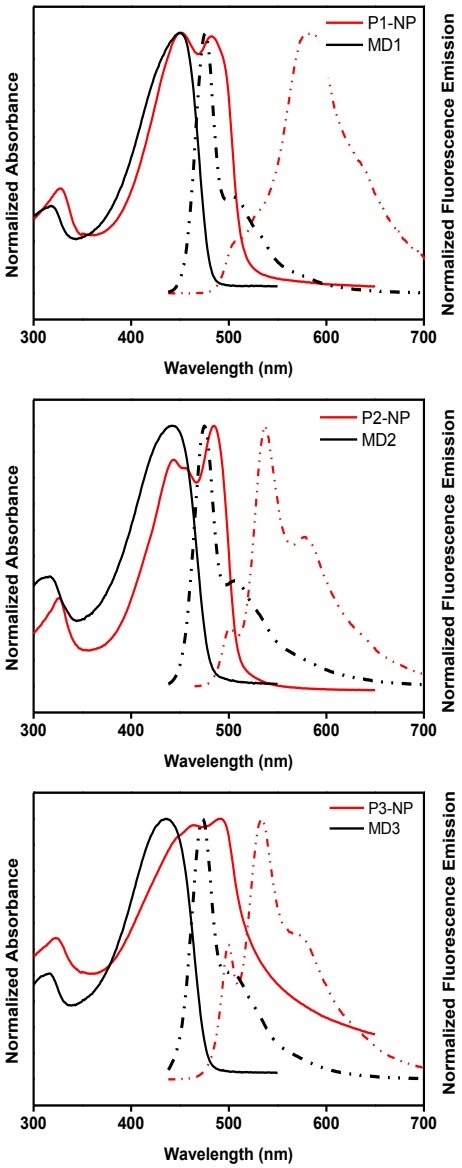

Figure 3: Absorption (solid lines) and emission (dotted lines) spectra of polymers **P1**, **P2** and **P3** in the molecularly dissolved (MD1, MD2, MD3) as well as NP form (**P1**-NP, **P2**-NP, **P3**-NP).

4.2.4 Cytotoxicity studies

Biocompatibility of the PPE NPs is obviously of high importance as they are being developed for bio-imaging applications. Therefore, the viability of A549 cells incubated with increasing amounts of the respective PPE NPs was studied using the Alamar blue assay (Figure 4). The cell viability remained over 90% for all the NPs tested after a 24 hour incubation with concentrations up to 100 µg/mL, thereby confirming the safety of the PPE NPs in terms of cellular viability for bio-imaging applications. As a control, A549 cells were treated the exact same way as all test samples, but with the exception that the NPs were not added. These cytotoxicity results are similar to those reported in other studies on conjugated polymers for biological applications.[58] As the surface functionality is usually a crucial factor in determining the cellular toxicity,[45,50-52] it is remarkable that, independent of the functionality present, all particles are biocompatible and the presence of azide groups has no negative effect.

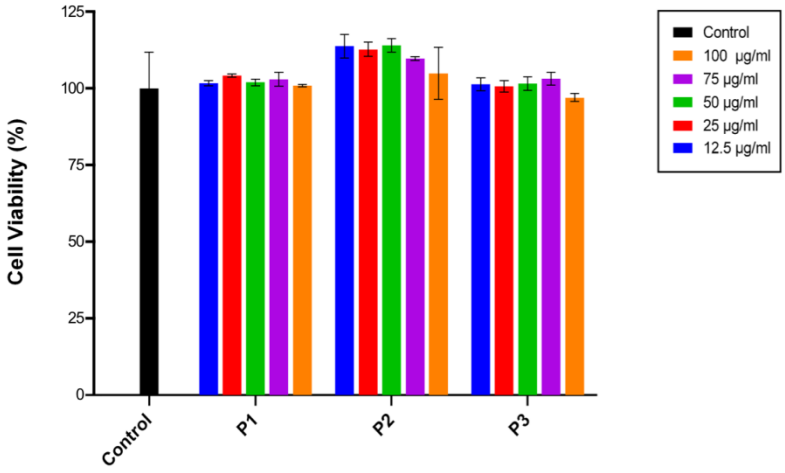

Figure 4: Dose dependent cytotoxicity of the different PPE NPs after 24 h of exposure, as determined by the Alamar blue assay on A549 cells, showing no significant cytotoxicity. Error bars show the standard deviation of the measurements (n = 3).

4.2.5 In vitro imaging

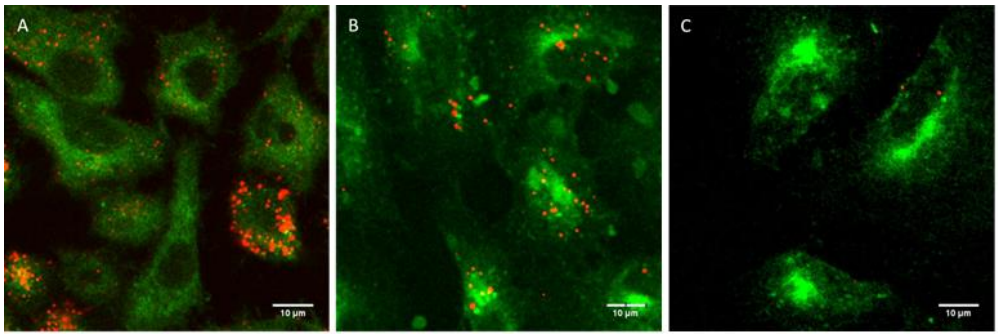

Figure 5: Confocal microscopy images of A549 cells treated with **P1**- (A), **P2**- (B) and **P3**-NPs (C) for 24 h (scale bar = 10 µm). The NPs (red) are seen distributed within the volume of the cell. The cell membrane is seen labelled in green. The images are single optical sections with the plane of imaging passing through the middle of the cells.

The cellular uptake and bio-imaging potential of the PPE NPs was then confirmed using a combination of two-photon and confocal laser scanning microscopy (Figure 5). The **P1**-NPs were taken up by the A549 cells after a 24 hour incubation period. The internalization of the NPs by the cells was confirmed by z-stacks (optical slice thickness = 0.52 µm) through the volume of the cells. Similarly, the **P2**-NPs were also internalized by the cells. The **P3**-NPs, however, exhibited a markedly lower uptake. This is likely due to the presence of the azide terminated TEG chains that play a role in the cellular uptake, resulting from one or a combination of following reasons. Azide end-capped hydrophilic TEG chains can lead to a larger hydrodynamic size of the NPs and/or render them sterically less susceptible to protein corona formation. The presence of the azide groups can itself also influence the interaction with the biological milieu. The presence of polyethylene glycol (PEG) chains of increasing lengths on NPs has previously been shown to lower their level of cellular uptake due to reduced protein adsorption on the surface.[59] However, for short TEG chains with azide end groups, a detailed study is lacking in literature. For all three polymers, no morphological changes were visually noted in cells incubated with their respective NPs as compared to control samples. This demonstrates the potential

to use the PPE NPs as fluorescent markers for both multi-colour and two-photon imaging.

4.2.6 Click reaction

Only a few PPE-type polymers with functionalities suitable for CuAAC click reactions have been reported before.[60-64] In previous work, we have shown that CuAAC reactions can be performed in a quantitative way in solution on azide functionalized PPE copolymers.[45] The success of the click reaction on **P2** with phenylacetylene was clearly indicated by ^{1}H NMR and FT-IR analysis (by disappearance of the typical azide vibration at 2093 cm^{-1}). As a proof-of-concept, the CuAAC reaction was now also performed on the **P2**-NPs with megastokes dye 735 (Scheme 4). The **P2**-NPs were chosen because of their high cellular uptake (compared to **P3**-NPs) and highest PLQY. When comparing the pure and the clicked **P2**-NPs, an increased absorption in the 550−800 nm range can be observed, indicating that the dye is also present on the NPs (Figure S9). Also in the corresponding emission spectra a shift is observed when the megastokes dye is attached onto the NPs (Figure S10).

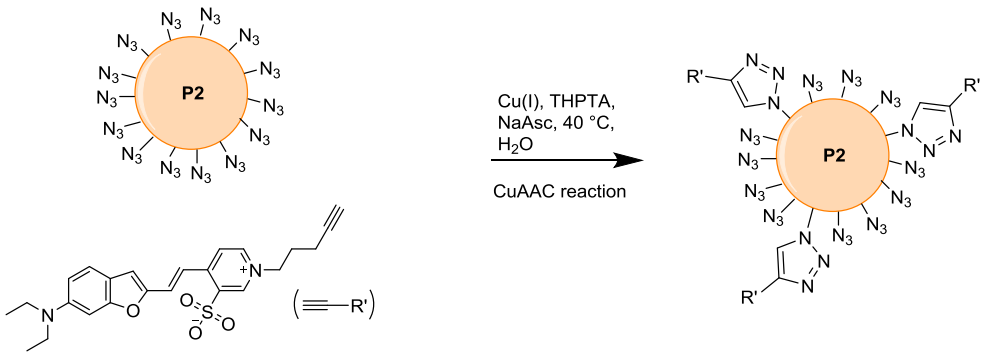

Scheme 4: Illustration of the CuAAC reaction to click an alkyne functionalized megastokes dye to the azide groups present at the surface of the NPs derived from PPE **P2**.

4.3 CONCLUSIONS

In this work, the influence of hydrophobic and hydrophilic side chain functionalization - including azide moieties for further click reactions - on the size, optical and biological properties of poly(*p*-phenylene ethynylene) (PPE) nanoparticles was investigated. Synthetic tuning of the polymer side chains can improve the optical properties of the resulting particles, as has been shown before.[29,30,57] However, the influence of azide functionalities on the aforementioned properties has not been evaluated before. Moreover, these click functionalities enable (bio)molecule binding on the particle surface, which can be beneficial for specific cell targeting. On the other hand, tetraethylene glycol units were incorporated to enhance the hydrophilicity of the polymer nanoparticles. Particles were synthesized from three different PPE polymers with varying side chain patterns using the combined miniemulsion and emulsion/solvent evaporation technique. It was shown that the introduction of azides significantly increases the fluorescence quantum yield of the nanoparticles (from 8 to 13%), while the presence of hydrophilic tetraethylene glycol chains leads to larger particle sizes (188 nm as observed by DLS for **P3**-NPs). Excellent cell viabilities comparable to other conjugated polymer nanoparticles discussed in literature[58] were observed for all three PPE nanoparticles at different concentrations. This clearly indicates that the particles are biocompatible, regardless of the presence of azide moieties. The cellular uptake was, however, dependent on the choice of the polymer, with the TEGylated nanoparticles exhibiting a relatively lower uptake. This effect has been discussed in literature before for PEGylated polymers[59] and is ascribed to reduced protein adsorption on the particle surface. A study for shorter ethylene glycol side chains was, however, missing in literature. As a proof of principle, the megastokes dye 735 was coupled to the azide functionalized **P2**-NPs.

4.4 EXPERIMENTAL SECTION

4.4.1 Materials and methods

Sodium dodecyl sulfate (SDS) was supplied by Merck Millipore. Spectrum Labs delivered Spectra/Por® 3 dialysis cellulose membranes (MWCO 3.5 kDa). Coumarin 153 (99%) and tetrahydrofuran (THF; 99.9%) were purchased from Sigma Aldrich. 9,10-Diphenylanthracene (DPA) was purchased from Janssen Chimica Belgium. Cyclohexane (99.9%) and chloroform (99.0%) were obtained from Analar Normapur. Copper(II) sulfate pentahydrate (≥ 98%), tris(3-hydroxypropyltriazolylmethyl)amine (THPTA; 95%), (+)-sodium L-ascorbate (≥ 98%) and the alkyne megastokes dye 735 were supplied by Sigma-Aldrich. The CellMask Green stain was purchased from Life Technologies. Alamar blue was supplied by Invitrogen. The modified eagle's medium with GlutaMAX and penicillin/streptomycin were obtained from Gibco and the non-heat inactivated fetal bovine serum (FBS) was purchased from Biochrom AG.

NMR chemical shifts (δ, in ppm) were determined relative to the residual $CHCl_3$ (7.26 ppm) absorption or the ^{13}C resonance shift of $CDCl_3$ (77.16 ppm). High resolution electrospray ionization mass spectrometry (HR ESI-MS) was performed using an LTQ Orbitrap Velos Pro mass spectrometer equipped with an atmospheric pressure ionization source operating in the nebulizer assisted electrospray mode. The instrument was calibrated in the m/z range 220−2000 using a standard solution containing caffeine, MRFA and Ultramark 1621. Reported masses are the 100% intensity isotope peaks. Melting points were measured with an electrothermal IA9000 series digital melting point apparatus. Solid-state FT-IR spectra were recorded in transmission mode. Analysis of the molar masses and molar mass distributions of the polymers was performed on a Tosoh EcoSEC System, comprising of an autosampler, a PSS guard column SDV (50 x 7.5 mm), followed by three PSS SDV analytical linear XL columns (5 µm, 300 x 7.5 mm) and a UV-detector using THF as the eluent at 40 °C with a flow rate of 1.0 mL/min. The SEC system was calibrated using linear narrow polystyrene standards ranging from 474 to 7.5 x 10^6 g/mol (K = 14.1 x 10^{-5} dL/g and α = 0.70).

4.4.2 Monomer and polymer synthesis

All known monomers (**7**−**9**) were synthesized according to literature procedures.[45-49]

1-Chloro-2-(2-(2-(2-chloroethoxy)ethoxy)ethoxy)ethane (2). Modified procedure:[46] A solution of thionyl chloride (43.9 mL, 605 mmol) in chloroform (40 mL) was added dropwise to a solution of tetraethylene glycol (40 mL, 233 mmol) and pyridine (37.5 mL, 465 mmol) in chloroform (160 mL) at 0 °C under inert atmosphere. After stirring at reflux for 3 h, the mixture was cooled down to room temperature, washed with water (2x) and brine (1x), and dried over MgSO4. After filtration of the drying agent and removal of the solvent under reduced pressure, the residue was purified by vacuum distillation (T = 145 °C, p = $2*10^{-2}$ mbar), yielding a colourless oil (45.0 g, 84%). ^{1}H NMR (400 MHz, $CDCl_3$): δ (ppm) 3.76 (t, *J* = 6.0 Hz, 4H), 3.67 (s, 8H), 3.63 (t, *J* = 6.1 Hz, 4H).

1,4-Bis(2-(2-(2-(2-chloroethoxy)ethoxy)ethoxy)ethoxy)benzene (4). Prepared according to a reported procedure.[47]

1,4-Bis(2-(2-(2-(2-chloroethoxy)ethoxy)ethoxy)ethoxy)-2,5-diiodobenzene (5).[48] 1,4-Bis(2-(2-(2-(2-chloroethoxy)ethoxy)ethoxy)ethoxy) benzene (0.55 g, 1.10 mmol) was added dropwise to a solution of iodine monochloride (0.90 g, 5.52 mmol) in methanol (25 mL) at 0 °C. After stirring at reflux for 4 h, the reaction mixture was cooled down to room temperature and diluted with CH_2Cl_2, after which it was washed with a saturated Na_2SO_3 solution. The separated organic phase was washed with water (2x) and brine (1x), dried over $MgSO_4$, filtered and evaporated to dryness. Then, the crude product was purified by flash chromatography (silica, ethyl acetate:CH_2Cl_2 2:8) and dried under vacuum, yielding a pale yellow solid (0.57 g, 69%). ^{1}H NMR (400 MHz, $CDCl_3$): δ (ppm) 7.23 (s, 2H), 4.10 (t, *J* = 4.0 Hz, 4H), 3.88 (t, *J* = 4.0 Hz, 4H), 3.79−3.74 (m, 8H), 3.71−3.68 (m, 12H), 3.64−3.61 (m, 4H); ^{13}C NMR (100 MHz, $CDCl_3$): δ (ppm) 153.2, 123.6, 86.5, 71.5, 71.3, 70.9, 70.83, 70.80, 70.4, 69.7, 42.9; HRMS: calcd for $C_{22}H_{34}Cl_2I_2NaO_8$: 772.9618, measured: *m/z* 772.9608 $[M + Na]^+$; *Mp* 58 °C.

1,4-Bis(2-(2-(2-(2-azidoethoxy)ethoxy)ethoxy)ethoxy)-2,5-diiodobenzene (6).[49] NaN_3 (0.30 g, 4.70 mmol) was added to a solution of 1,4-bis(2-(2-(2-(2-chloroethoxy)ethoxy)ethoxy)ethoxy)-2,5-diiodobenzene (0.35 g, 0.47 mmol) in DMF (2 mL). After stirring at 70 °C for 72 h, the reaction mixture was cooled down to room temperature and the solvent was removed by co-evaporation with toluene (3x 50 mL), after which the obtained product was redissolved in CH_2Cl_2, washed with water (2x) and brine (1x), and dried over $MgSO_4$. After filtration of the drying agent and removal of the solvent, the crude product was purified by flash chromatography (silica, ethyl acetate:CH_2Cl_2 3:17), yielding a faint yellow oil (0.36 g, full conversion). ^{1}H NMR (300 MHz, $CDCl_3$): δ (ppm) 7.23 (s, 2H), 4.11−4.08 (m, 4H), 3.89−3.86 (m, 4H), 3.80−3.76 (m, 4H), 3.71−3.64 (m, 16H), 3.40−3.36 (m, 4H); ^{13}C NMR (75 MHz, $CDCl_3$): δ (ppm) 153.2, 123.5, 86.5, 71.3, 70.9, 70.8 (2 C), 70.4, 70.1, 69.7, 50.8; IR (NaCl): ν_{max} (cm^{-1}) 2922, 2867, 2097; HRMS: calcd for $C_{22}H_{34}I_2NaN_6O_8$: 787.0425, measured: *m/z* 787.0428 $[M + Na]^+$.

1,4-Diiodo-2,5-bis(octyloxy)benzene (7). Prepared according to a reported procedure.[45]

1,4-Diethynyl-2,5-bis(octyloxy)benzene (8). Prepared according to a reported procedure.[45]

1,4-Bis(8-azidooctyloxy)-2,5-diiodobenzene (9). Prepared according to a reported procedure.[45]

P1. Modified synthesis procedure.[50] 1,4-Diethynyl-2,5-bis(octyloxy)benzene (**8**) (74.4 mg, 0.127 mmol) and 1,4-bis(octyloxy)-2,5-diiodobenzene (**7**) (50 mg, 0.131 mmol) were dissolved in dry toluene (3.8 mL) and diisopropylamine (1.6 mL) was added. The solution was purged with nitrogen for 10 min after which $Pd(PPh)_3Cl_2$ (4.5 mg, 5 mol%) and CuI (1.2 mg, 5 mol%) were added. After stirring for 2 h at 70 °C, an excess iodobenzene (2 drops) and phenylacetylene (2 drops) were added, with 10 min of stirring at 70 °C in between of the two additions. After stirring for 10 more min at 70 °C, the polymer was precipitated in methanol, redissolved in chloroform and then precipitated again in acetone to remove catalyst residues. An orange polymer was obtained (84 mg, 91%). SEC

(THF): M_n 16.0 kg/mol, $Đ$ 1.9; ^{1}H NMR (400 MHz, $CDCl_3$): δ (ppm) 7.02 (s, 2H), 4.03 (t, J = 6.4 Hz, 4H), 1.91–1.80 (m, 4H), 1.55–1.47 (m, 4H), 1.42–1.21 (m, 16H), 0.87 (t, J = 6.6 Hz, 6H).

P2. Prepared according to a reported synthesis procedure.[45] 1,4-Bis(8-azidooctyloxy)-2,5-diiodobenzene (**9**) (0.100 g, 0.150 mmol), 1,4-diethynyl-2,5-bis(octyloxy)benzene (**8**) (0.057 g, 0.150 mmol), CuI (1.4 mg, 5 mol%) and $Pd(PPh_3)_2Cl_2$ (5.2 mg, 5 mol%) were dissolved in dry toluene (4.4 mL) and diisopropylamine (1.7 mL) was added. An orange solid was finally obtained (0.087 g, 73%). SEC (THF): M_n 14.0 kg/mol, $Đ$ 1.9; ^{1}H NMR (300 MHz, $CDCl_3$): δ (ppm) 7.02 (s, 4H), 4.07–4.00 (m, 8H), 3.23 (t, J = 6.9 Hz, 4H), 1.92–1.79 (m, 8H), 1.63–1.19 (m, 40H), 0.92–0.80 (m, 6H).

P3. A mixture of dry toluene (2.5 mL) and diisopropylamine (1.0 mL) was degassed for 5 min. 1,4-Diethynyl-2,5-bis(octyloxy)benzene (**8**) (0.041 g, 0.108 mmol), 1,4-bis(2-(2-(2-(2-azidoethoxy)ethoxy)ethoxy)ethoxy)-2,5-diiodo benzene (**6**) (0.080 g, 0.105 mmol), CuI (1.0 mg, 5 mol%) and $Pd(PPh_3)_4$ (6 mg, 5 mol%) were added and the mixture was stirred under microwave irradiation for 40 min at 70 °C. The polymer was end-capped by adding an excess of iodobenzene (2 drops), after which it was stirred for 5 min at 70 °C under microwave irradiation. Then, an excess of phenylacetylene (2 drops) was added and the mixture was stirred again for 5 min at 70 °C under microwave irradiation. After cooling down to room temperature, the resulting polymer was precipitated in *n*-hexane at 0 °C and filtered off, yielding a sticky yellow-orange solid (87 mg, 93%). SEC (THF): M_n 8.2 kg/mol, $Đ$ 2.3; ^{1}H NMR (400 MHz, $CDCl_3$): δ (ppm) 7.08–6.98 (m, 4H), 4.25–4.17 (m, 4H), 4.07–3.98 (m, 4H), 3.93–3.87 (m, 4H), 3.81–3.74 (m, 4H), 3.66–3.60 (m, 16H), 3.34 (t, J = 5.0 Hz, 4H), 1.87–1.78 (m, 4H), 1.53–1.46 (m, 4H), 1.39–1.32 (m, 4H), 1.31–1.18 (m, 12H), 0.86 (t, J = 6.3 Hz, 6H); IR (NaCl): ν_{max} (cm^{-1}) 2966, 2925, 2186.

4.4.3 Nanoparticle synthesis

The three different PPE derivatives were formulated into NPs using a combination of the miniemulsion and emulsion/solvent evaporation technique (Figure 1).[51,52] The respective PPE polymer (25 mg) was dissolved in $CHCl_3$ (0.7

g) and then mixed with a solution consisting of SDS (5 mg) and water (1.7 g). After mechanical stirring for 1 h at 1000 rpm, the miniemulsion was prepared by ultrasonication for 180 s (30 s pulse, 20 s pause) at 60% amplitude under ice-cooling using a Branson 450 W digital sonifier with a 1/8" tip. The obtained miniemulsion was transferred into a round bottom flask with a wide neck and heated at 40 °C under mechanical stirring (1000 rpm) for 4 h. The time of chloroform evaporation was chosen by comparison with a reference system (the same amount of chloroform in a separate round bottom flask). Afterwards, the resulting dispersion was passed through filter paper (Whatman, pore size 4–7 µm) to remove large aggregates. Excess SDS was removed using dialysis membranes (MWCO 3.5 kDa).

4.4.4 Transmission electron microscopy (TEM)

The NP dispersions were diluted and drop casted on a carbon coated copper grid. TEM imaging was performed using a TECNAI spirit TEM of FEI operating at 120 kV.

4.4.5 Dynamic light scattering (DLS)

The size, size distribution and zeta potentials of all NPs were obtained by DLS using a Brookhaven Instruments Zetapals.

4.4.6 Stationary UV-Vis absorption and fluorescence spectroscopy

UV-Vis absorption spectra of the NPs were obtained using an Agilent Cary 5000 Scan UV-Vis-NIR spectrophotometer. The emission spectra were measured using a Horiba-Jobin Yvon FluoroLog-3 spectrofluorometer, with correction for the wavelength dependence of the throughput and sensitivity of the detection channel. A quantum counter was used to correct for temporal fluctuations in the excitation intensity as well as for the wavelength dependence of the excitation intensity. The absorption coefficients of the materials were calculated using Lambert-Beer's law by varying the concentration of the NPs in water or the polymers in $CHCl_3$. The fluorescence quantum yields of the polymers in $CHCl_3$ and the NPs in water were measured using coumarin 153 in ethanol as a

standard (FQY = 53%). Five dilutions were prepared for all samples as well as for the standard. The most concentrated sample had an absorbance of 0.1 at an excitation wavelength of 423 nm. Emission spectra were collected for all samples after which the absorption versus the integral of the emission spectra for each dilution and sample were plotted and trend lines were fitted. The resulting slope values (m) as well as the refractive indexes (η) of the solvents were used to determine the FQYs of the samples using following formula:

$$FQY_{sample} = FQY_{standard} \frac{m_{sample}}{m_{standard}} \frac{{\eta_{sample}}^2}{{\eta_{standard}}^2}$$

4.4.7 Cell cultures

A549 cells were cultured in modified eagle's medium (MEM) with GlutaMAX, supplemented with 10% non-heat inactivated fetal bovine serum (FBS) and 1% penicillin/streptomycin. They were incubated at 37 °C with 5% CO_2. The cells were sub-cultured at 80% confluence. Cells were seeded for 24 h before the addition of the NPs in 8-well µ-slides (Ibidi GmbH) at a density of $1x10^4$ cells/well for microscopic observations.

4.4.8 Cytotoxicity studies

The Alamar blue assay was used to assess cytotoxicity of the different PPE NPs. A549 cells were seeded at a density of 10^3 cells/well in a black 96-well plate and allowed to incubate for 24 h at 37 °C with 5% CO_2. PPE NPs were then added at concentrations of up to 100 µg/mL and incubated for a further 24 h. Subsequently, the cells were washed three times with phosphate buffered saline (PBS) and the Alamar blue reagent was added as per manufacturer's instructions. After incubation for 4 h, the plate was read using a fluorescence plate reader (Tecan).

4.4.9 In vitro imaging

A549 cells were grown on glass coverslips placed within 24-well cell culture plates. The cells were subsequently incubated at 37 °C with 5% CO_2 with **P1**, **P2**

and **P3** NPs at a concentration of 75 µg/mL for 24 h. The cells were then rinsed 3 times with PBS to remove free NPs. Thereafter, the cells were stained with a freshly prepared, 1x working solution of CellMask Green for 10 min at 37 °C, as per manufacturer's instructions. The cells were subsequently washed three times with PBS and fixed by incubating the cells with 4% paraformaldehyde at room temperature for 10 min.

Imaging was performed using a LSM 510 META (Zeiss) confocal laser scanning microscope (CLSM) on an inverted Axiovert 200 M motorized frame. The microscope was fitted with a LD C-Apochromat 40×/1.1 W Corr UV-Vis-IR water immersion objective. The NPs and CellMask stain were excited in separate channels by a femtosecond pulsed titanium-sapphire laser (MaiTai DeepSee, Spectra-Physics) tuned to a 900 nm laser and 543 nm He-Ne laser, respectively. The fluorescence emission was then channeled through a 565–615 nm band pass filter for the He-Ne channel and through a 650 nm low pass filter for the pulsed titanium-sapphire laser channel. The internal meta-detector and the non-descanned detector of the microscope were used for imaging each of the channels, respectively.

4.4.10 Click reaction

The CuAAC reaction was performed by clicking the alkyne functionalized megastokes dye 735 onto the **P2**-NPs. The amount of dye was calculated based on the amount of clickable groups present in a dispersion of **P2**-NPs with 0.1% solid content. As not all azide groups are available on the NP surface, a molar ratio of 1:0.5 (azide moieties in NP dispersion:dye) was used. For 1 µM alkyne, following ratios were maintained: 5 µM $CuSO_4$, 10 µM THPTA and 25 µM sodium L-ascorbate. The CuAAC reaction was performed at 40 °C to avoid aggregation of the dye as much as possible. After 42 h, 5% EDTA solution was added to stop the reaction. The unreacted dye was removed using multiple centrifugation steps. The particles were centrifuged down at 14000 rpm and the supernatant was removed. Afterwards, the pellet was redispersed in a 70:30 ethanol:water mixture to dissolve the unreacted dye. This was repeated 4 times to ensure all the unreacted dye was removed. After the last centrifugation step, the pellet was redispersed in pure water. Optical spectra of the NPs before and after the

click reaction, and of the alkyne-functionalized megastokes dye 735 dissolved in water, were obtained using UV-Vis absorption and fluorescence spectroscopy.

4.5 REFERENCES

[1] R. Pepperkok and J. Ellenberg, *Nat. Rev. Mol. Cell Biol.*, 2006, **7**, 690.

[2] X. S. Xie, J. Yu and W. Y. Yang, *Science*, 2006, **312**, 228.

[3] A. Yildiz, J. N. Forkey, S. A. McKinney, T. Ha, Y. E. Goldman and P. R. Selvin, *Science*, 2003, **300**, 2061.

[4] R. Weissleder, *Science*, 2006, **312**, 1168.

[5] R. Weissleder and M. J. Pittet, *Nature*, 2008, **452**, 580.

[6] E. A. Osborn and F. A. Jaffer, *Curr. Opin. Cardiol.*, 2008, **23**, 620.

[7] U. Resch-Genger, M. Grabolle, S. Cavaliere-Jaricot, R. Nitschke and T. Nann, *Nat. Meth.*, 2008, **5**, 763.

[8] X. Michalet, F. F. Pinaud, L. A. Bentolila, J. M. Tsay, S. Doose, J. J. Li, G. Sundaresan, A. M. Wu, S. S. Gambhir and S. Weiss, *Science*, 2005, **307**, 538.

[9] B. A. Kairdolf, A. M. Smith, T. H. Stokes, M. D. Wang, A. N. Young and S. Nie, *Annu. Rev. Anal. Chem.*, 2013, **6**, 143.

[10] S.-T. Yang, L. Cao, P. G. Luo, F. Lu, X. Wang, H. Wang, M. J. Meziani, Y. Liu, G. Qi and Y.-P. Sun, *J. Am. Chem. Soc.*, 2009, **131**, 11308.

[11] L.-Y. Chen, C.-W. Wang, Z. Yuan and H.-T. Chang, *Anal. Chem.*, 2015, **87**, 216.

[12] V. N. Mochalin, O. Shenderova, D. Ho and Y. Gogotsi, *Nat. Nanotechnol.*, 2012, **7**, 11.

[13] A. A. Burns, J. Vider, H. Ow, E. Herz, O. Penate-Medina, M. Baumgart, S. M. Larson, U. Wiesner and M. Bradbury, *Nano Lett.*, 2009, **9**, 442.

[14] C. Wu, B. Bull, C. Szymanski, K. Christensen and J. McNeill, *ACS Nano*, 2008, **2**, 2415.

[15] J. Peng, X. He, K. Wang, W. Tan, Y. Wang and Y. Liu, *Anal. Bioanal. Chem.*, 2007, **388**, 645.

[16] H.-S. Peng, J. A. Stolwijk, L.-N. Sun, J. Wegener and O. S. Wolfbeis, *Angew. Chem. Int. Ed.*, 2010, **122**, 4342.

[17] R. Ahmad Khanbeigi, T. F. Abelha, A. Woods, O. Rastoin, R. D. Harvey, M.-C. Jones, B. Forbes, M. A. Green, H. Collins and L. A. Dailey, *Biomacromolecules*, 2015, **16**, 733.

[18] D. Tuncel and H. V. Demir, *Nanoscale*, 2010, **2**, 484.

[19] Y.-H. Chan and P.-J. Wu, *Part. Part. Syst. Char.*, 2015, **32**, 11.

[20] M. Li, C. Y. Nie, L. H. Feng, H. X. Yuan, L. B. Liu, F. T. Lv and S. Wang, *Chem. Asian J.*, 2014, **9**, 3121.

[21] M. Peters, N. Zaquen, L. D'Olieslaeger, H. Bové, D. Vanderzande, N. Hellings, T. Junkers and A. Ethirajan, *Biomacromolecules*, 2016, **17**, 2562.

[22] W. Zhang, H. Sun, S. Yin, J. Chang, Y. Li, X. Guo and Z. Yuan, *J. Mater. Sci.*, 2015, **50**, 5571.

[23] J. Xu, Y. Zhou, G. Cheng, M. Dong, S. Liu and C. Huang, *Luminescence*, 2015, **30**, 411.

[24] M. Doshi, M. Krienke, S. Khederzadeh, H. Sanchez, A. Copik, J. Oyer and A. J. Gesquiere, *RSC Adv.*, 2015, **5**, 37943.

[25] J. Geng, C. Sun, J. Liu, L.-D. Liao, Y. Yuan, N. Thakor, J. Wang and B. Liu, *Small*, 2015, **11**, 1603.

[26] G. Hong, Y. Zou, A. L. Antaris, S. Diao, D. Wu, K. Cheng, X. Zhang, C. Chen, B. Liu, Y. He, J. Z. Wu, J. Yuan, B. Zhang, Z. Tao, C. Fukunaga and H. Dai, *Nat. Commun.*, 2014, **5**, 4206.

[27] Y. H. Seo, M. J. Cho, O. J. Cheong, W.-D. Jang, T. Y. Ohulchanskyy, S. Lee, D. H. Choi, P. N. Prasad and S. Kim, *Biomaterials*, 2015, **39**, 225.

[28] L. Feng, C. Zhu, H. Yuan, L. Liu, F. Lv and S. Wang, *Chem. Soc. Rev.*, 2013, **42**, 6620.

[29] J. Liu, G. Feng, D. Ding and B. Liu, *Polym. Chem.*, 2013, **4**, 4326.

[30] X. Zhang, J. Yu, C. Wu, Y. Jin, Y. Rong, F. Ye and D. T. Chiu, *ACS Nano*, 2012, **6**, 5429.

[31] E. Mendez and J. H. Moon, *Chem. Commun.*, 2013, **49**, 6048.

[32] G. Feng, D. Ding and B. Liu, *Nanoscale*, 2012, **4**, 6150.

[33] T. Chen, W. Xu, Z. Huang, H. Peng, Z. Ke, X. Lu, Y. Yan and R. Liu, *J. Mater. Chem. B*, 2015, **3**, 3564.

[34] K. Li and B. Liu, *J. Mater. Chem.*, 2012, **22**, 1257.

[35] P. Howes, M. Green, J. Levitt, K. Suhling and M. Hughes, *J. Am. Chem. Soc.*, 2010, **132**, 3989.

[36] J. Steverlynck, J. De Winter, P. Gerbaux, R. Lazzaroni, P. Leclère and G. Koeckelberghs, *Macromolecules*, 2015, **48**, 8789.

[37] I.-B. Kim, H. Shin, A. J. Garcia and U. H. F. Bunz, *Bioconjugate Chem.*, 2007, **18**, 815.

[38] L. Ruizendaal, S. Bhattacharjee, K. Pournazari, M. Rosso-Vasic, L. H. de Haan, G. M. Alink, A. T. Marcelis and H. Zuilhof, *Nanotoxicology*, 2009, **3**, 339.

[39] M. R. Lorenz, V. Holzapfel, A. Musyanovych, K. Nothelfer, P. Walther, H. Frank, K. Landfester, H. Schrezenmeier and V. Mailänder, *Biomaterials*, 2006, **27**, 2820.

[40] O. Lunov, T. Syrovets, C. Loos, J. Beil, M. Delacher, K. Tron, G. U. Nienhaus, A. Musyanovych, V. Mailänder, K. Landfester and T. Simmet, *ACS Nano*, 2011, **5**, 1657.

[41] V. Mailänder and K. Landfester, *Biomacromolecules*, 2009, **10**, 2379.

[42] V. D. Bock, H. Hiemstra and J. H. van Maarseveen, *Eur. J. Org. Chem.*, 2006, **1**, 51.

[43] C. Barner-Kowollik, F. E. Du Prez, P. Espeel, C. J. Hawker, T. Junkers, H. Schlaad and W. Van Camp, *Angew. Chem. Int. Ed.*, 2011, **50**, 60.

[44] L. Liang and D. Astruc, *Coord. Chem. Rev.*, 2011, **255**, 2933.

[45] Y. Braeken, P. Verstappen, L. Lutsen, D. Vanderzande and W. Maes, *Polym. Chem.*, 2015, **6**, 6720.

[46] H. Liu, Z.-B. Gao, Z. Yao, S. Zheng, Y. Li, W. Zhu, X. Tan, X. Luo, J. Shen, K. Chen, G.-Y. Hu and H. Jiang, *J. Med. Chem.*, 2007, **50**, 83.

[47] M. Asakawa, P. R. Ashton, S. E. Boyd, C. L. Brown, R. E. Gillard, O. Kocian, F. M. Raymo, J. F. Stoddart, M. S. Tolley, A. J. P. White and D. J. Williams, *J. Org. Chem.*, 1997, **62**, 26.

[48] P. I. Abronina, A. I. Zinin, A. V. Orlova, S. L. Sedinkin and L. O. Kononov, *Tetrahedron Lett.*, 2013, **54**, 4533.

[49] A. R. Gulur Srinivas, T. E. Kerr-Phillips, H. Peng, D. Barker and J. Travas-Sejdic, *Polym. Chem.*, 2013, **4**, 2506.

[50] C. Weder and M. S. Wrighton, *Macromolecules*, 1996, **29**, 5157.

[51] T. Kietzke, D. Neher, K. Landfester, R. Montenegro, R. Guntner and U. Scherf, *Nat. Mater.*, 2003, **2**, 408.

[52] K. Landfester, *Angew. Chem. Int. Ed.*, 2009, **48**, 4488.

[53] S. Nettesheim, D. Zeisel, M. Handschuh and R. Zenobi, *Langmuir*, 1998, **14**, 3101.

[54] Y. Takahashi and H. Tadokoro, *Macromolecules*, 1973, **6**, 672.

[55] B. J. Schwartz, *Annu. Rev. Phys. Chem.*, 2003, **54**, 141.

[56] L. D'Olieslaeger, M. Pfannmöller, E. Fron, I. Cardinaletti, M. Van Der Auweraer, G. Van Tendeloo, S. Bals, W. Maes, D. Vanderzande, J. Manca and A. Ethirajan, *Sol. Energy Mater. Sol. Cells*, 2017, **159**, 179.

[57] P. K. Kandel, L. P. Fernando, P. C. Ackroyd and K. A. Christensen, *Nanoscale*, 2011, **3**, 1037.

[58] C. S. Almeida, I. K. Herrmann, P. D. Howes and M. M. Stevens, *Chem. Mater.*, 2015, **27**, 6879.

[59] B. Pelaz, P. del Pino, P. Maffre, R. Hartmann, M. Gallego, S. Rivera-Fernandez, J. M. de la Fuente, G. U. Nienhaus and W. J. Parak, *ACS Nano*, 2015, **9**, 6996.

[60] B. C. Englert, S. Bakbak and U. H. Bunz, *Macromolecules*, 2005, **38**, 5868.

[61] R. L. Phillips, I.-B. Kim, L. M. Tolbert and U. H. Bunz, *J. Am. Chem. Soc.*, 2008, **130**, 6952.

[62] U. H. Bunz, *Synlett*, 2013, **24**, 1899.

[63] Y. Pourghaz, P. Dongare, D. W. Thompson and Y. Zhao, *Chem. Commun.*, 2011, **47**, 11014.

[64] B. Erdogan, L. Song, J. N. Wilson, J. O. Park, M. Srinivasarao and U. H. Bunz, *J. Am. Chem. Soc.*, 2004, **126**, 3678.

[65] D. T. Ta, E. Steen Redeker, B. Billen, G. Reekmans, J. Sikulu, J.-P. Noben, W. Guedens and P. Adriaensens, *Protein Eng. Des. Sel.*, 2015, **28**, 351.

4.6 SUPPORTING INFORMATION

4.6.1 ^{1}H and ^{13}C NMR spectra

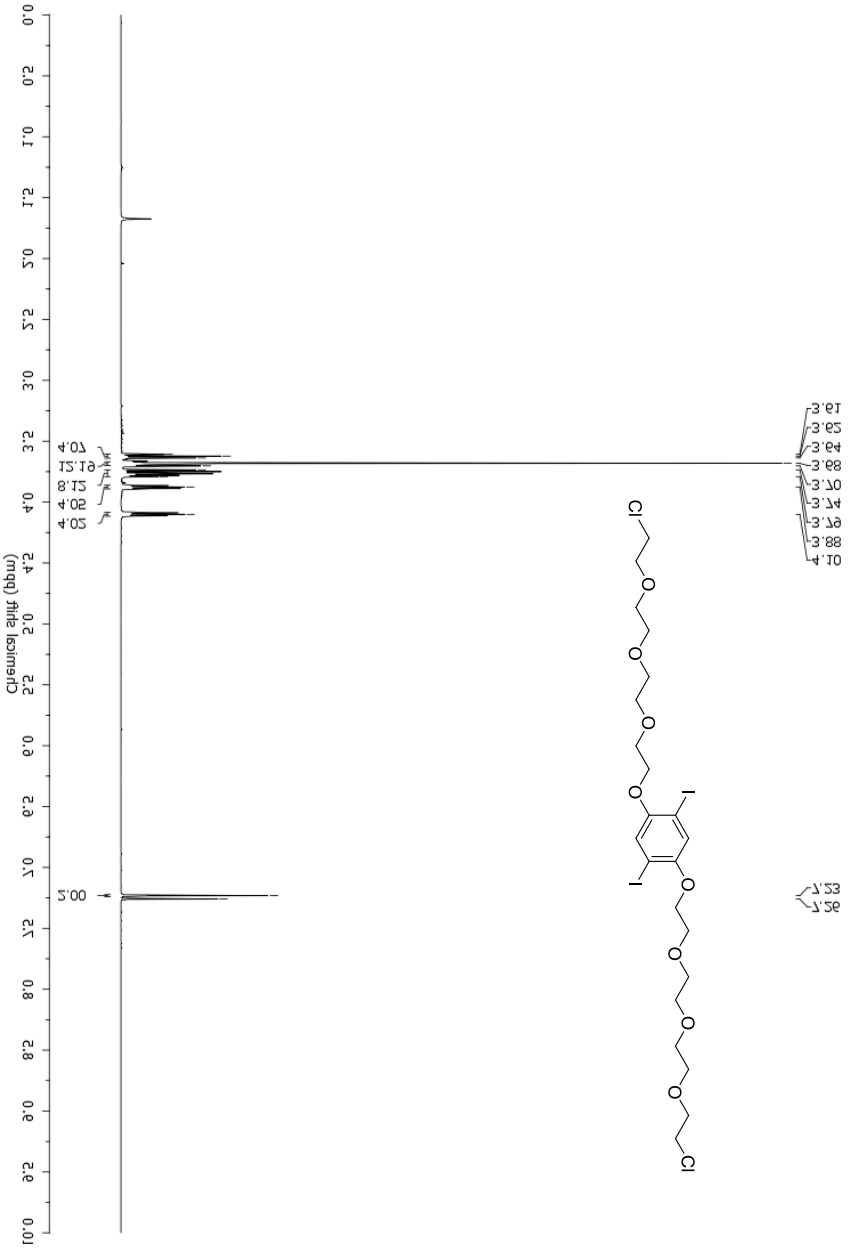

Figure S1: ^{1}H NMR spectrum of 1,4-bis(2-(2-(2-(2-chloroethoxy)ethoxy)ethoxy)ethoxy)-2,5-diiodobenzene (in $CDCl_3$).

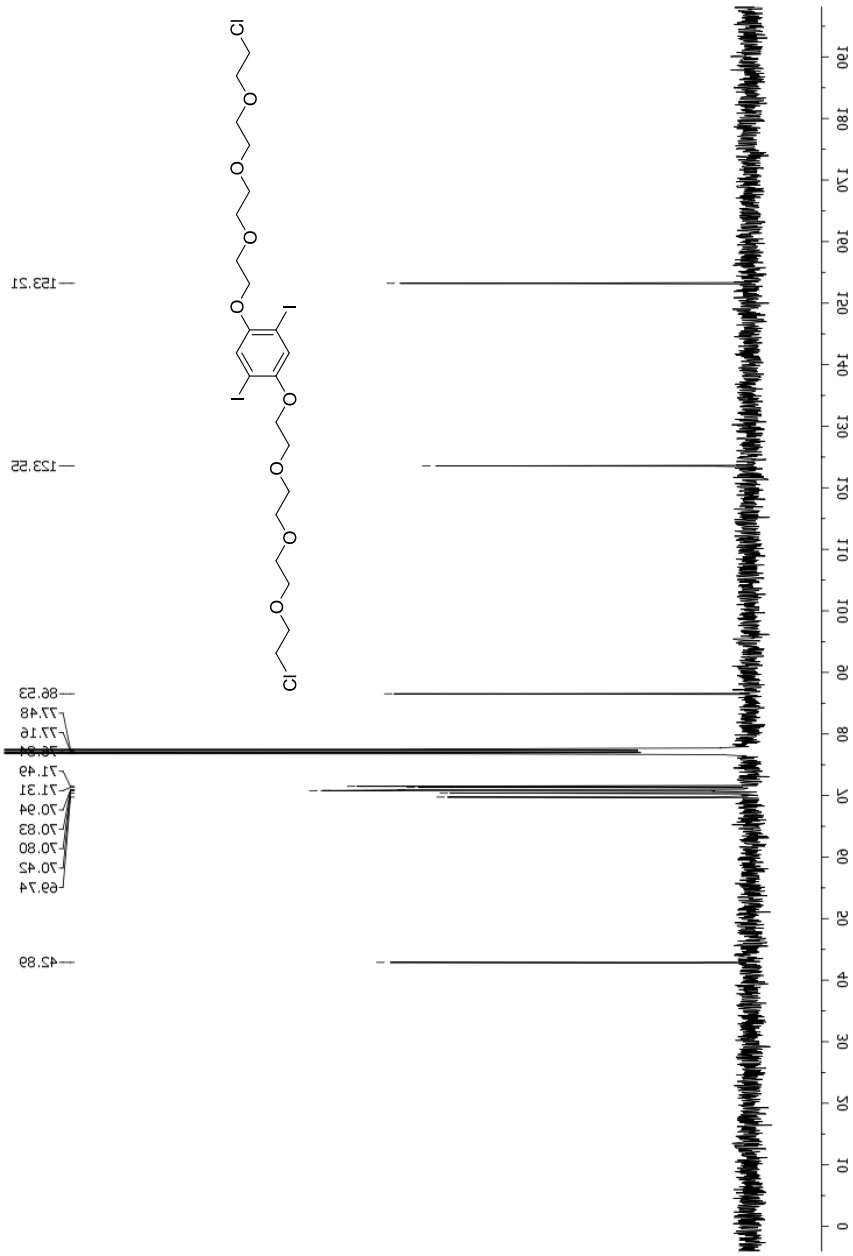

Figure S2: ^{13}C NMR spectrum of 1,4-bis(2-(2-(2-chloroethoxy)ethoxy)ethoxy)-2,5-diiodobenzene (in $CDCl_3$).

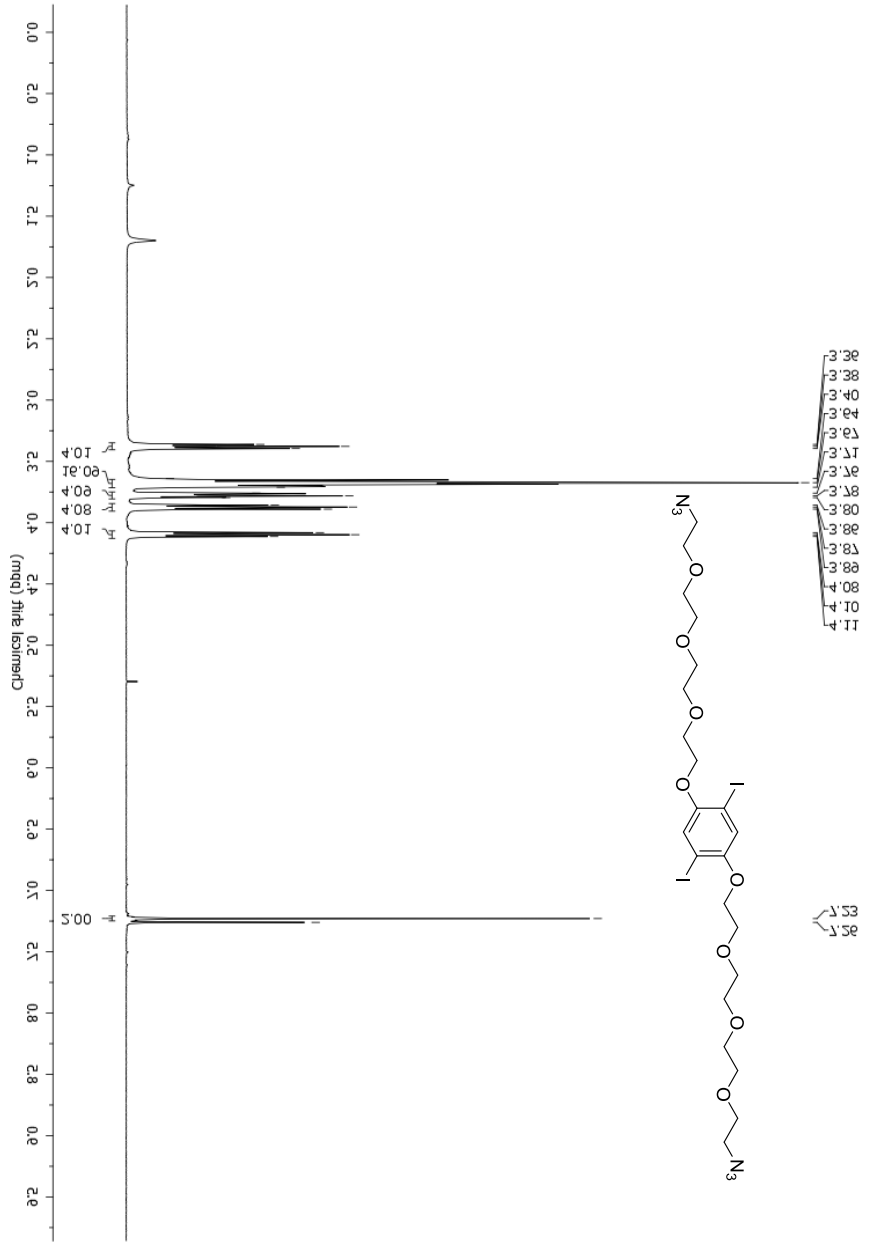

Figure S3: ^{1}H NMR spectrum of 1,4-bis(2-(2-(2-(2-azidoethoxy)ethoxy)ethoxy)ethoxy)-2,5-diiodobenzene (in $CDCl_3$).

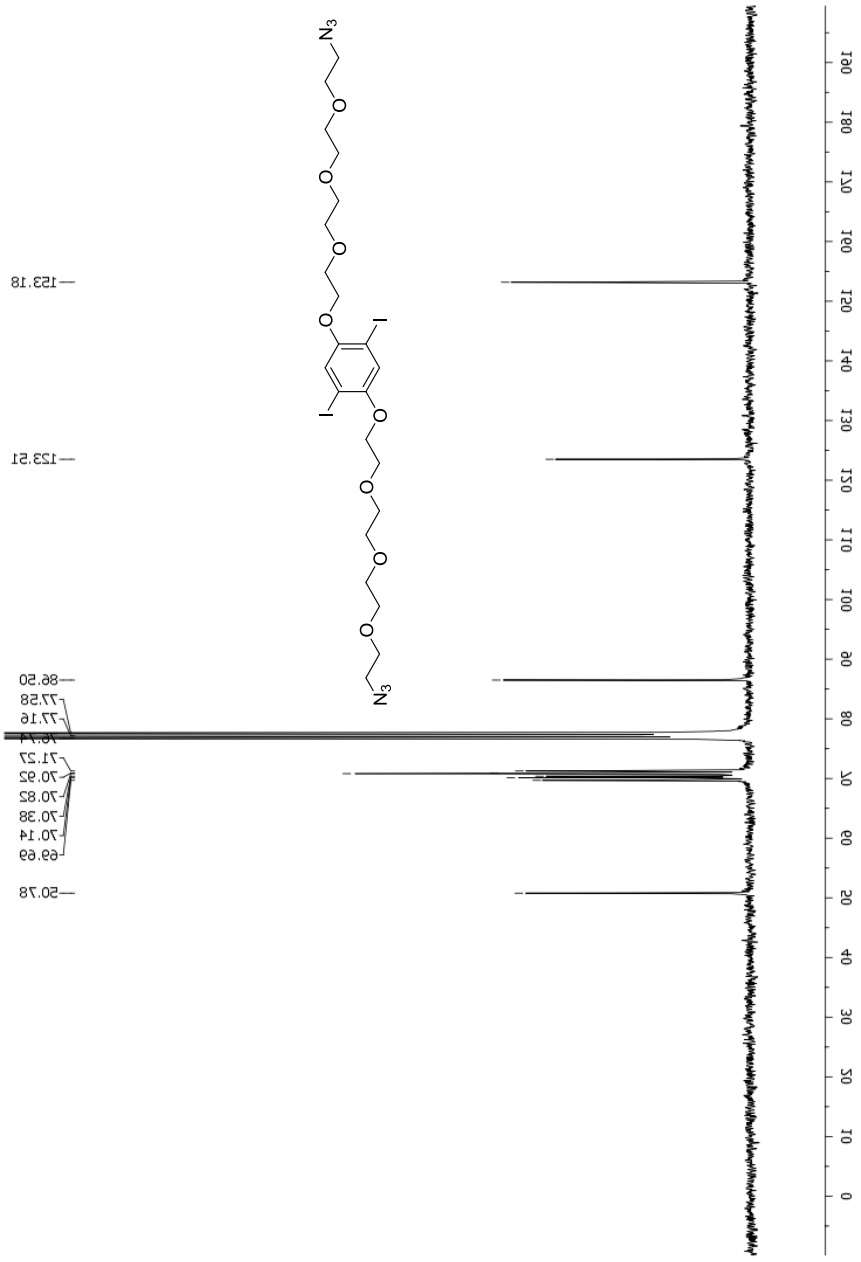

Figure S4: ^{13}C NMR spectrum of 1,4-bis(2-(2-(2-azidoethoxy)ethoxy)ethoxy)-2,5-diiodobenzene (in $CDCl_3$).

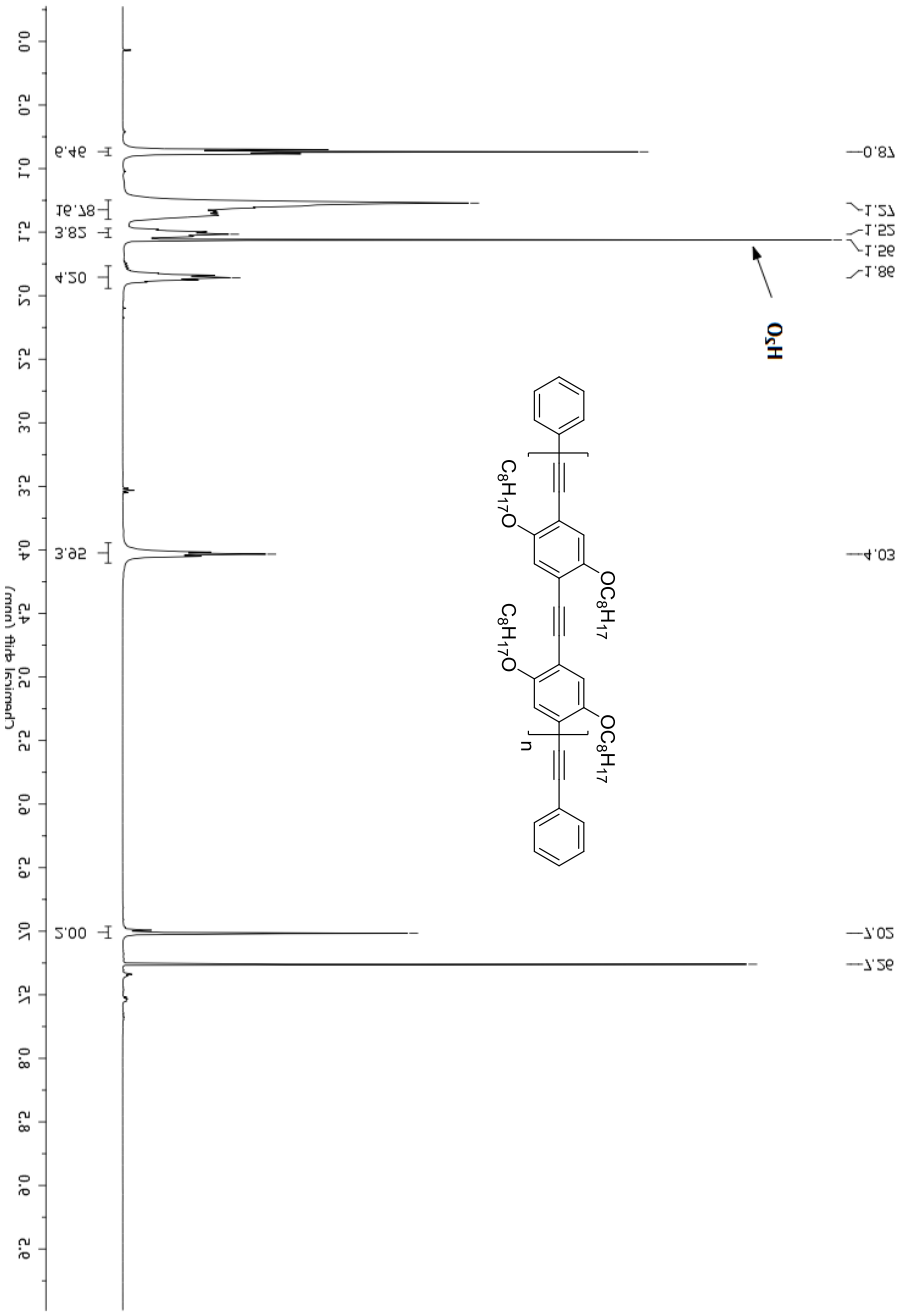

Figure S5: ^{1}H NMR spectrum of **P1** (in $CDCl_3$).

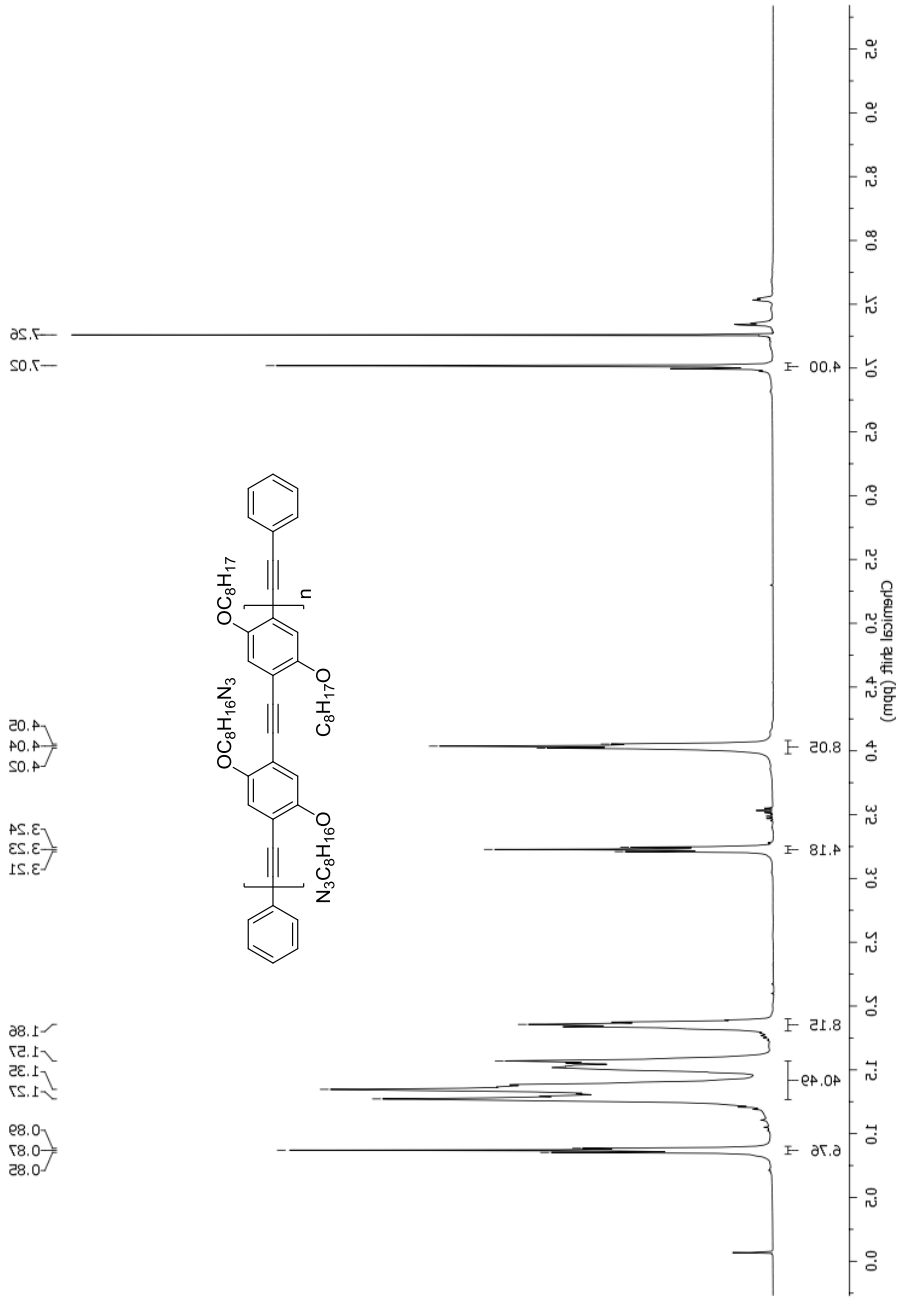

Figure S6: ^{1}H NMR spectrum of **P2** (in $CDCl_3$).

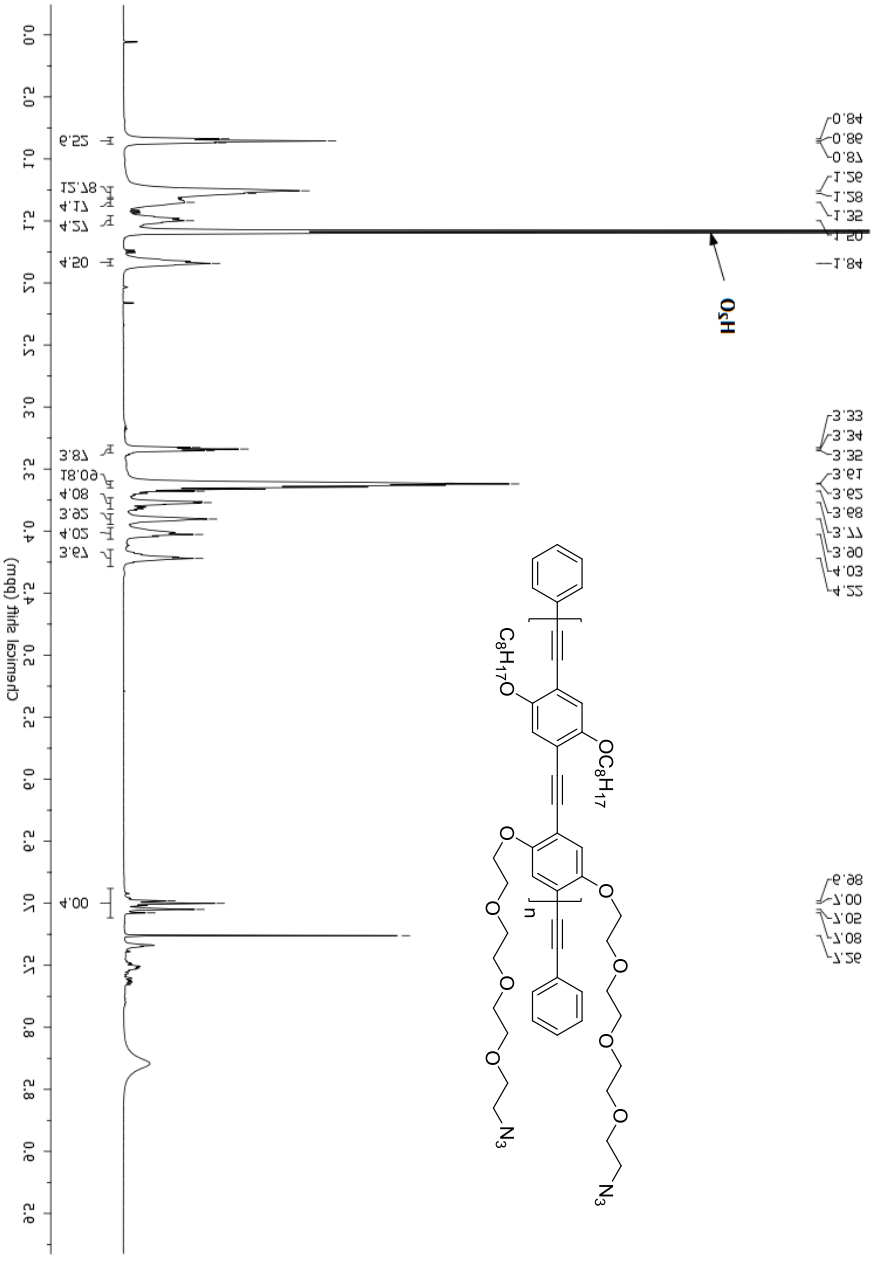

Figure S7: ^{1}H NMR spectrum of **P3** (in $CDCl_3$).

4.6.2 DLS size distributions

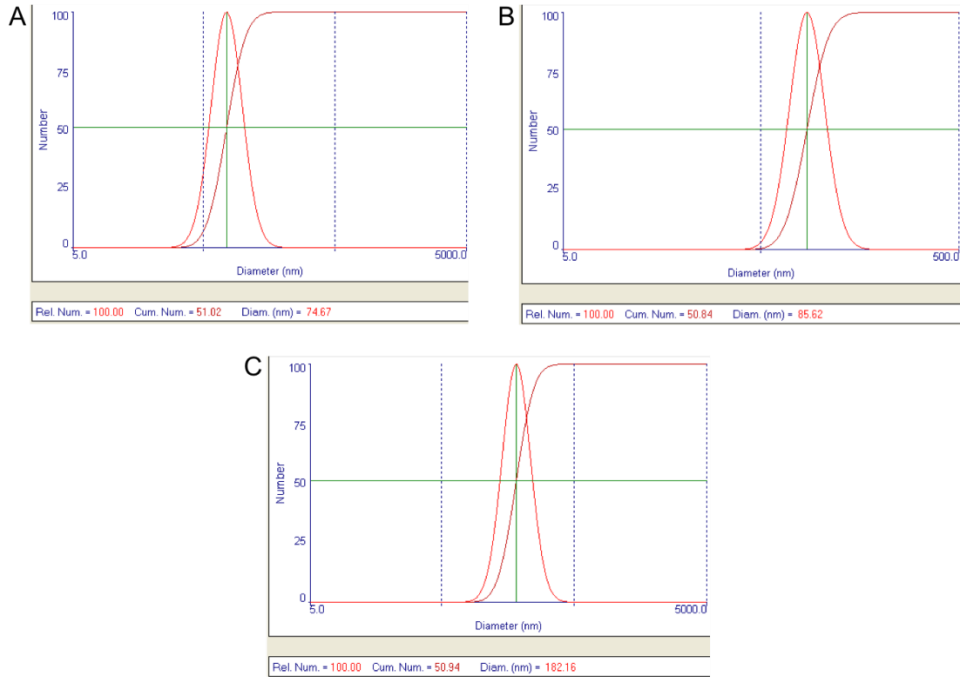

Figure S8: Number-average hydrodynamic size distributions of **P1**- (A), **P2**- (B) and **P3**-NPs (C) in an aqueous dispersion. The diameter values indicated are the modal hydrodynamic sizes as extracted from these distributions.

4.6.3 CuAAC reaction on P2-NPs

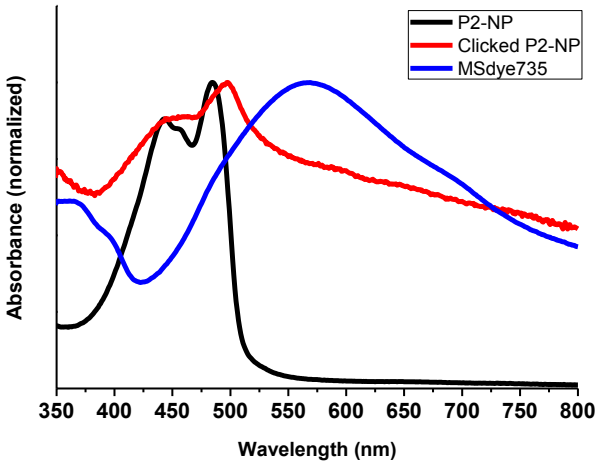

Figure S9: UV-Vis absorption spectra (normalized) of megastokes dye 735 (blue) and the **P2**-NPs before (black) and after (red) the CuAAC reaction.

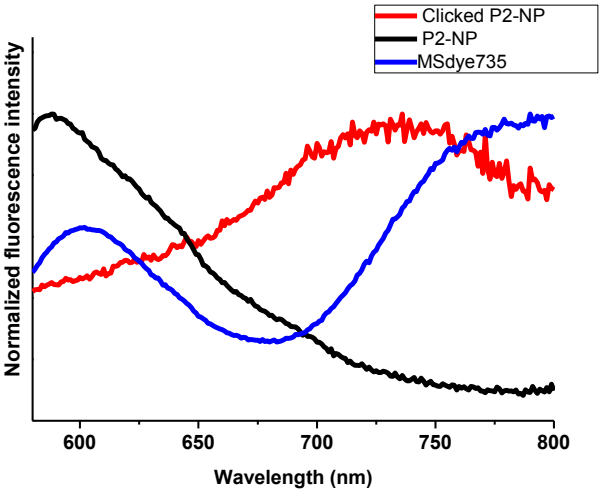

Figure S10: Fluorescence emission spectra (normalized) of megastokes dye 735 (blue) and the **P2**-NPs before (black) and after (red) the CuAAC reaction.

Chapter 5

The Influence of Crosslinking on the Optical Properties of Poly(*p*-Phenylene Ethynylene) Nanoparticles for Bio-imaging

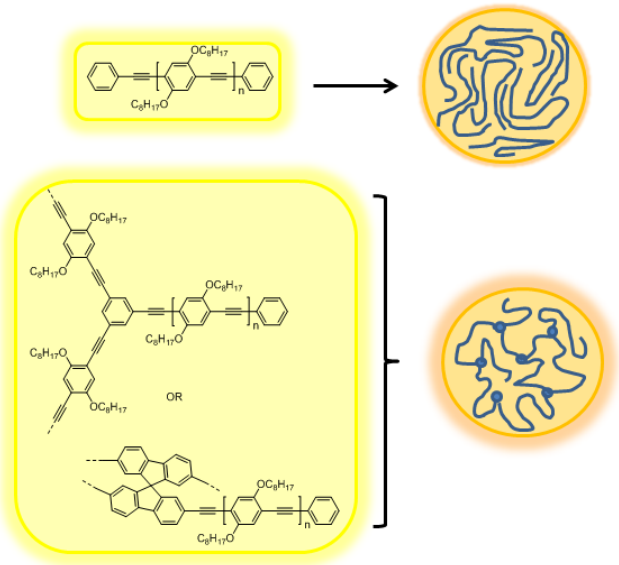

Y. Braeken, S. Cheruku, S. Seneca, L. Berden, L. Kruyfhooft, L. Lutsen, D. Vanderzande, A. Ethirajan and W. Maes, *manuscript submitted*.

ABSTRACT

Fluorescent conjugated polymers formulated in nanoparticles possess attractive properties to be used as bio-imaging probes. However, their fluorescence brightness is generally limited by quenching effects due to interchain aggregation in the confined nanoparticle space. In this chapter, slightly crosslinked conjugated polymer networks are investigated as a way to enhance the photoluminescence quantum yield of the resulting conjugated polymer nanoparticles. 1,3,5-Tribromobenzene and 2,2',7,7'-tetrabromo-9,9'-spirobifluorene are chosen as crosslinking moieties and added in 3 and 5 mol% to the poly(*p*-phenylene ethynylene) (PPE) synthesis. Nanoparticles of all samples are prepared via the combined mini-emulsion/solvent evaporation technique and the optical properties of the polymers in solution and in nanoparticle form are then compared to those of the linear PPE counterparts. The inclusion of crosslinkers increases the nanoparticle fluorescence quantum yield, from 5 to 11% for the sample containing 1,3,5-tribromobenzene. Furthermore, when 5 mol% of either crosslinker is used, the fluorescence brightness doubles. The nanoparticles also show low cytotoxicity, good particle uptake into cells and compatibility with two-photon imaging.

5.1 INTRODUCTION

Nowadays, many imaging techniques are routinely employed in hospitals and research institutes, such as positron emission tomography (PET),[1,2] computerized tomography (CT)[2] and magnetic resonance imaging (MRI)[3,4]. The main purpose of these techniques is the non-invasive visualization of different parts of the body to trace malfunctions. Furthermore, biological processes can be visualized as well, both in vitro and in vivo. Depending on the technique, information from the cellular down to the molecular level can be obtained. As such, a much deeper understanding of important processes such as protein transport, gene expression and regulatory pathways has been achieved.[5-7] Unfortunately, most of these imaging methods are quite expensive and they can also damage biological tissues. Research into new cost-effective and safe imaging techniques hence remains important. Because fluorescence imaging meets all of the above requirements,[8,9] the interest in the development of highly fluorescent and stable imaging probes has steadily grown. Many types of materials have been studied for this purpose, e.g. molecular organic dyes,[10] inorganic quantum dots,[10-12] carbon dots, nanodiamonds,[13] and combined particles in which organic dyes are embedded in polymer[14] or silica[15] matrices. Despite these research efforts, each of the listed materials suffers from specific drawbacks. Small organic dyes usually exhibit a low photostability,[16] whereas the combination of those dyes with matrix materials often leads to dye leaking and self-quenching.[17,18] The use of inorganic quantum dots for in vitro and in vivo applications is still under debate despite their elevated fluorescence brightness and high photostability because of their low chemical stability and intrinsic cytotoxicity.[11] Nanodiamonds seem to exhibit all the right characteristics for application as bio-imaging probes, but the dispersion of those materials in single particles often leads to contamination.[13]

Conjugated polymers (CPs) have attracted huge interest for applications such as organic photovoltaics (OPVs), organic photodetectors (OPDs), light-emitting diodes (OLEDs) and field-effect transistors (OFETs) due to their excellent opto-electronic properties. However, during the last decade, these materials have been proven to be successful imaging probes too. They often exhibit high fluorescence brightnesses and photostabilities and are generally non-

cytotoxic.[19,20] Furthermore, their absorption and emission features can readily be tuned and even pushed into the near-infrared (NIR) region,[21] where the background autofluorescence is low and deeper tissue penetration can be achieved.[22,23] Low energy wavelengths are also less damaging to tissue.[24] One of the issues that needs attention is the low solubility of regular CPs in aqueous environment. To overcome this, different methods have been used. The introduction of charges on the polymer side chains or backbone to create conjugated polyelectrolytes (CPEs) has proven to be a successful approach.[25,26] Limited cases in which the CPs are immobilized onto biological structures like human serum albumin (HSA) are also known.[27,28] The most employed strategy, however, is to prepare a dispersion of CPs in water.[29-31] The formulated particles are then referred to as conjugated polymers nanoparticles (CPNPs) or CP dots. Unfortunately, due to the tight packing of the polymer chains in those particles, fluorescence quenching readily occurs.[32-37] Multiple studies describe techniques to improve the photoluminescence quantum yield (PLQY) of CPNPs.[38] Most of them rely on a reduction of the intermolecular interactions between the different polymer chains. Co-precipitation of the CP with a non-conjugated and non-fluorescent matrix material has also been employed,[23,39,40] as well as the introduction of bulky side chains onto the polymer backbone.[41-45] Furthermore, optimizing the monomer ratios[46] or freezing the polymer in the relaxed state[47] can improve the optical properties as well.

In the presented work, the introduction of crosslinkers is proposed as an alternative strategy to enhance the fluorescence brightness of CPNPs. Because the crosslinkers are added to the polymerization reaction, no complicated additional synthesis steps nor matrix materials are required. Poly(*p*-phenylene ethynylene)s (PPEs) were selected as the CP materials of choice because of their simple but rigid backbone structure, relatively high PLQYs, large molar extinction coefficients and high photostability.[16,48] By the introduction of acceptor moieties in the backbone, the bandgap can eventually be lowered and their emission can be pushed into the NIR region. Moreover, the pending (solubilizing) side chains enable introduction of specific (e.g. click) functionalities, which can be interesting in terms of specific cell targeting.[38,45,49] So far, only a few studies have been devoted to PPE-type NPs. Liu et al. prepared particles from amphiphilic PPEs via self-assembly,[50] while other reports comment on the

influence of side chain modifications on cytotoxicity, subcellular localization and optical properties.[45,51] Ponzio et al.[52] introduced a crosslinked non-conjugated matrix material to yield high-strength rigid particles which withstand dissolution by organic solvents. The influence of crosslinking of the CP itself on the optical properties of any type of CPNPs has, however, not been investigated before. In the present study, a linear PPE with octyloxy side chains (**P1**, see Scheme 1) was chosen as a reference. 1,3,5-Tribromobenzene (**3**) and 2,2',7,7'-tetrabromo-9,9'-spirobifluorene (**4**) were added as crosslinkers in 3 or 5 mol% during the polymerization reaction and CPNPs were prepared from each sample via the mini-emulsion/solvent evaporation technique. The influence of crosslinking on the optical properties of the NPs, their morphology and interaction with human lung carcinoma A549 cells was then carefully evaluated.

5.2 RESULTS AND DISCUSSION

To improve the PLQY of PPE CPNPs, two different crosslinking moieties, 1,3,5-tribromobenzene (**3**) and 2,2',7,7'-tetrabromo-9,9'-spirobifluorene (**4**), were incorporated into the backbone of a linear PPE polymer (**P1**) in 3 and 5 mol% ratios (Scheme 1). Because compound **3** has a flat structure, the polymer chains will extend in the same plane, forming a two-dimensional network. Compound **4**, on the other hand, can extend the polymer in 2 different planes, creating a three-dimensional network. The influence of these different types of crosslinkers on the optical properties of PPE-type CPNPs was then investigated.

5.2.1 Polymer synthesis and characterization

The required monomers **1** and **2** were synthesized according to previously reported procedures.[49] The polymers were obtained by Sonogashira polymerizations. The reaction conditions were based on a reported procedure,[45] but the amounts of the monomers were adjusted according to the amount of crosslinker added (3/5%). Since the crosslinker concentrations are very small, the proton signals of these moieties could not be detected in the ^{1}H NMR spectra (see supporting material). However, the polymers became more gel-like and viscous when 3 mol% of any of the crosslinkers was used and this effect was even more pronounced for the polymers with 5 mol% crosslinker. Higher (7.5

mol%) crosslinker concentrations led to insoluble polymer gels that could not be processed and characterized. The influence of the crosslinker is also reflected in the molar masses of the different polymers. **P1** has a number-average molar mass (M_n) of 33.0 kg/mol, while the molar mass increases after the inclusion of 3 mol% (M_n = 45.0 kg/mol for **P2**) and 5 mol% (M_n = 60.0 kg/mol for **P3**) of the trifunctional benzene core **3**. When using spirobifluorene **4** as crosslinker, the increasing trend was observed as well.

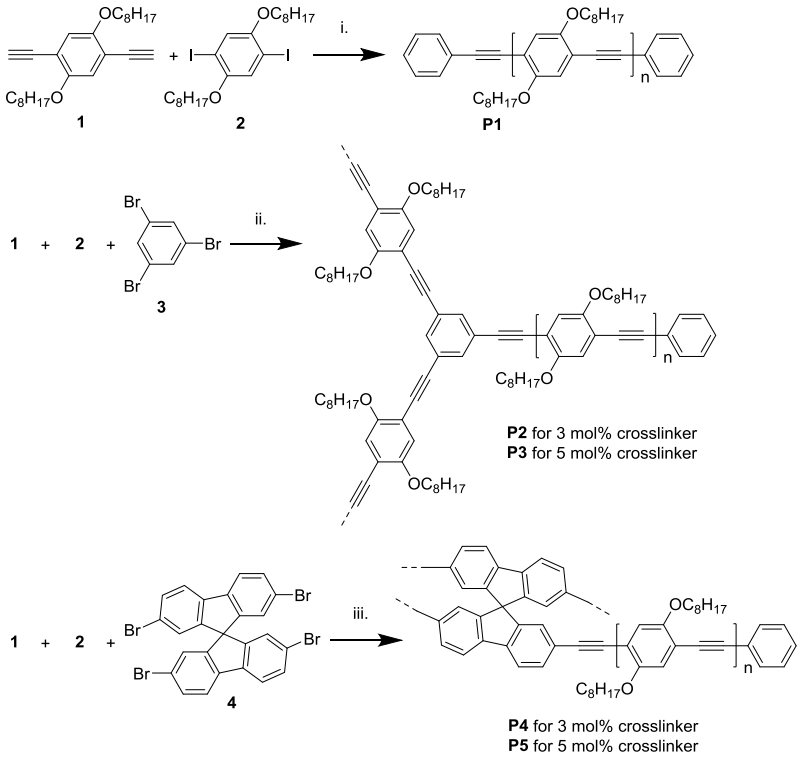

Scheme 1: Synthetic procedures towards the PPE polymers without crosslinker (**P1**), with 3 and 5 mol% 1,3,5-tribromobenzene (**P2** and **P3**) or 3 and 5 mol% 2,2',7,7'-tetrabromo-9,9'-spirobifluorene (**P4** and **P5**): i) $Pd(PPh_3)_2Cl_2$, CuI, DIPA, toluene, 70 °C, 2 h; 82%; ii. $Pd(PPh_3)_2Cl_2$, CuI, DIPA, toluene, 70 °C, 2 h; 79% for 3 mol% **3** and nearly quantitative for 5 mol% **3**; iii. $Pd(PPh_3)_4$, CuI, DIPA, toluene, 70 °C, 40 min; 89% for 3 mol% **4** and nearly quantitative for 5 mol% **4**.

Normalized absorption and emission spectra of all polymers in chloroform solution are shown in Figure 1 and an overview of the optical properties of the different samples is provided in Table 1.

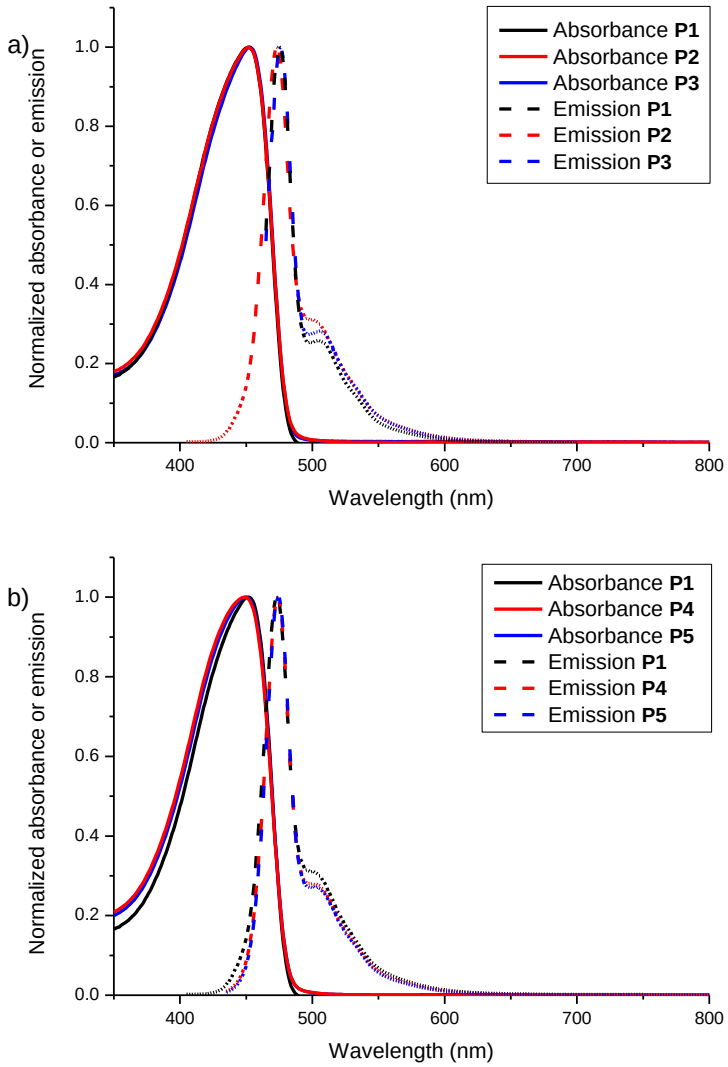

Figure 1: Normalized absorption and emission spectra of a) **P1**, **P2** and **P3**, and b) **P1**, **P4** and **P5** dissolved in chloroform.

Since the conjugated backbone of all polymers is the same, comparable spectra are to be expected. The absorption (449−452 nm) and emission (473−476 nm) maxima are indeed nearly the same for all samples, and so is the Stokes shift (21−25 nm). The PLQY of PPEs **P2** and **P4** slightly lowers in comparison to **P1**, while higher values are reached when higher amounts of any of the crosslinkers are used. The PLQY multiplied by the mass extinction coefficient gives the fluorescence brightness of the samples. Overall, these are the best for the samples in which 5 mol% of crosslinker is used (53 L cm^{-1} g^{-1} for **P3** and 55 L cm^{-1} g^{-1} for **P5**), although the values remain close.

Table 1: Summary of the optical properties of PPEs **P1**−**P5** dissolved in chloroform.

Sample	λ_{max} absorption (nm)	λ_{max} [a] emission (nm)	Stokes shift (nm)	PLQY[a] (%)	Mass extinction coefficient ε [a] (L cm^{-1} g^{-1})	Fluorescence brightness[a] (L cm^{-1} g^{-1})
P1	452	475	23	66	72	48
P2	452	473	21	61	76	46
P3	452	476	24	69	77	53
P4	449	474	25	63	78	49
P5	449	474	25	69	80	55

[a] Upon excitation at 423 nm.

5.2.2 NP synthesis and characterization

NPs of all polymer samples were then prepared via the mini-emulsion/solvent evaporation technique. A dispersed phase consisting of the CP dissolved in chloroform was added to a continuous phase of surfactant (sodium dodecyl sulfate, SDS) in water. The two phases were then ultrasonicated, creating small droplets of the dispersed in the continuous phase. Because chloroform is damaging to cells, it was removed via evaporation at 40 °C. A dispersion of the CPNPs in water was hence obtained. The excess SDS was removed via multiple washing cycles.

The characteristics of the different CPNPs are summarized in Table 2. All particles had comparable sizes, ranging from 123 to 153 nm (see Figure S7). Zeta potentials ranged from -26.20 mV to -34.80 mV. The negative zeta

potentials can be attributed to the presence of residual SDS, despite the afore-mentioned washing steps. The amount of crosslinker present in the polymer however does not seem to have an influence on the zeta potential values.

Table 2: Mean size, polydispersity index (PDI) and zeta potential of the different PPE NPs measured in water.

Sample	Size ± standard deviation (nm)	PDI	Zeta potential ± standard deviation (mV)
P1-NPs	123 ± 0.6	0.042	-26.20 ± 0.78
P2-NPs	131 ± 0.7	0.065	-34.28 ± 0.83
P3-NPs	153 ± 0.6	0.050	-32.95 ± 1.51
P4-NPs	133 ± 0.7	0.051	-34.80 ± 1.61
P5-NPs	141 ± 0.4	0.050	-21.89 ± 2.65

In Figure 2, TEM micrographs of the different particles are shown. The general morphology of the various NP samples appear to be similar and the sizes of the different NPs correspond with those measured by DLS. The difference in size as compared to the DLS measurements can be attributed to the dried particle state in the TEM micrographs, whereas the hydrodynamic radius is probed by DLS.

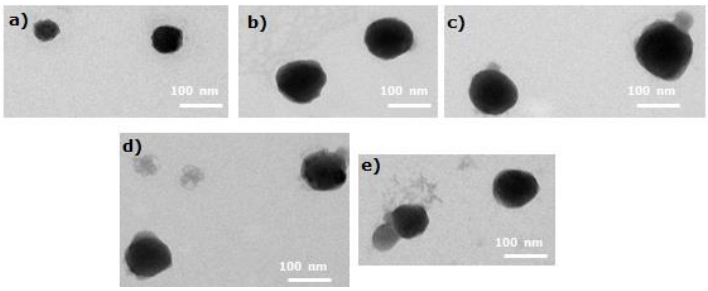

Figure 2: TEM images of the different nanoparticles: **P1**-NPs (a), **P2**-NPs (b), **P3**-NPs (c), **P4**-Nps (d) and **P5**-NPs (e).

5.2.3 Optical properties of the CPNPs

The absorption and emission spectra of all CPNPs dispersed in water are shown in Figure 3 and the optical properties are summarized in Table 3.

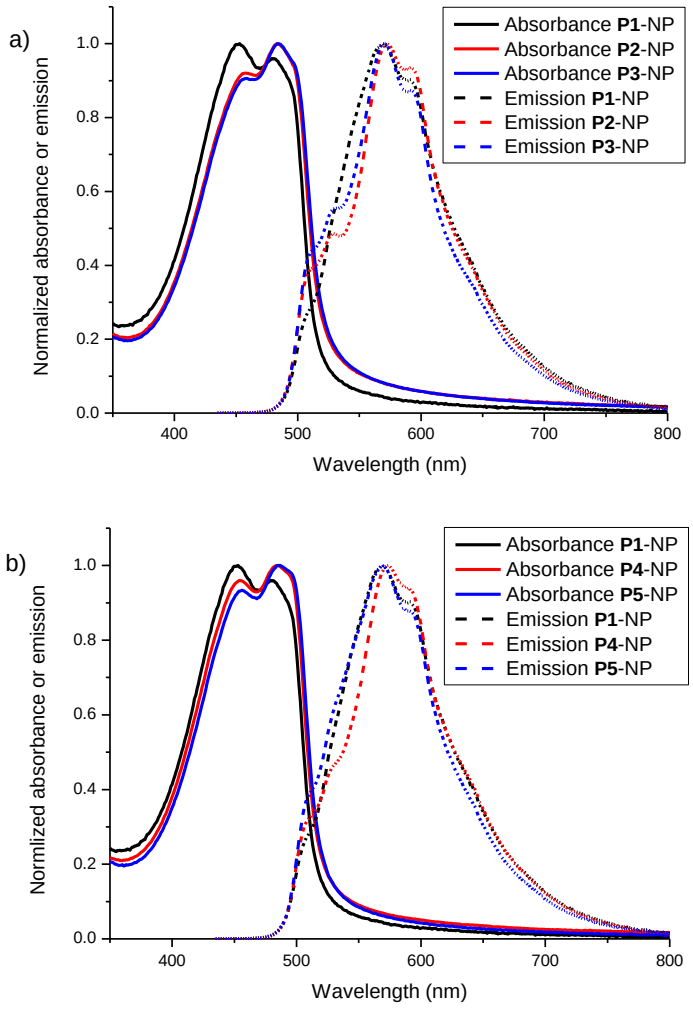

Figure 3: Normalized absorption (solid lines) and emission (dotted lines) spectra of the different PPEs in NP form.

The spectra of all samples are very similar. Compared to the spectra of the molecularly dissolved PPE polymers, the absorption bands are broader and a pronounced shoulder appears, which can be ascribed to the aggregation

(stacking) of the different polymer chains inside the NPs. The overlap of the π-orbitals of the polymer chains lowers the bandgap and thus causes a bathochromic shift in the absorption spectrum.[37] The absorption range from 400 to 500 nm is interesting for fluorescence imaging applications employing two-photon excitation mechanisms.[39,53] Furthermore, the large Stokes shifts (~90 nm; Table 3) are beneficial for detection of the signal without interference of the excitation wavelength when single photon excitations are envisioned. The PLQYs of the CPNPs dispersed in water increase with crosslinker concentration (Table 3). This effect is most pronounced for 1,3,5-tribromobenzene, where a PLQY of 11% is reached at 5 mol% crosslinker concentration. This trend is illustrated in Figure 4. Samples with equal absorbance at the excitation wavelength (423 nm) were prepared. The corresponding emission spectra are depicted and the area under the curve relates to the PLQY. In Figure 4a, the area under the emission curve increases with increasing 1,3,5-tribromobenzene concentration. The same trend can be observed in Figure 4b for an increasing amount of 2,2',7,7'-tetrabromo-9,9'-spirobifluorene. The integrated emission area for the **P3**-NPs is larger than for the **P5**-NPs, which is also reflected in the PLQYs of the samples.

Table 3. Overview of the optical properties of the different PPEs in NP form.

Sample	λ_{max} absorption (nm)	λ_{max} emission (nm)	Stokes shift (nm)	PLQY[a] (%)	Mass extinction coefficient[a] (ε, L cm^{-1} g^{-1})	Fluorescence brightness[a] (L cm^{-1} g^{-1})
P1-NP	481	569	88	5	22	1.1
P2-NP	483	572	89	8	15	1.2
P3-NP	484	572	88	11	19	2.1
P4-NP	484	573	89	7	19	1.3
P5-NP	484	573	89	8	29	2.3

[a] at 423 nm.

The absorption and emission spectra were also measured at constant concentration (see Figure S6). Mass extinction coefficients were then calculated and multiplied with the PLQYs to obtain the fluorescence brightnesses of all NP samples. The inclusion of a small amount (3 mol%) of either crosslinker has a

minor effect on the brightness. However, for the larger crosslinker amounts (5 mol%), the brightness doubles, regardless of the crosslinker's chemical composition, which is a highly relevant result toward bio-imaging and illustrates the success of the envisaged approach.

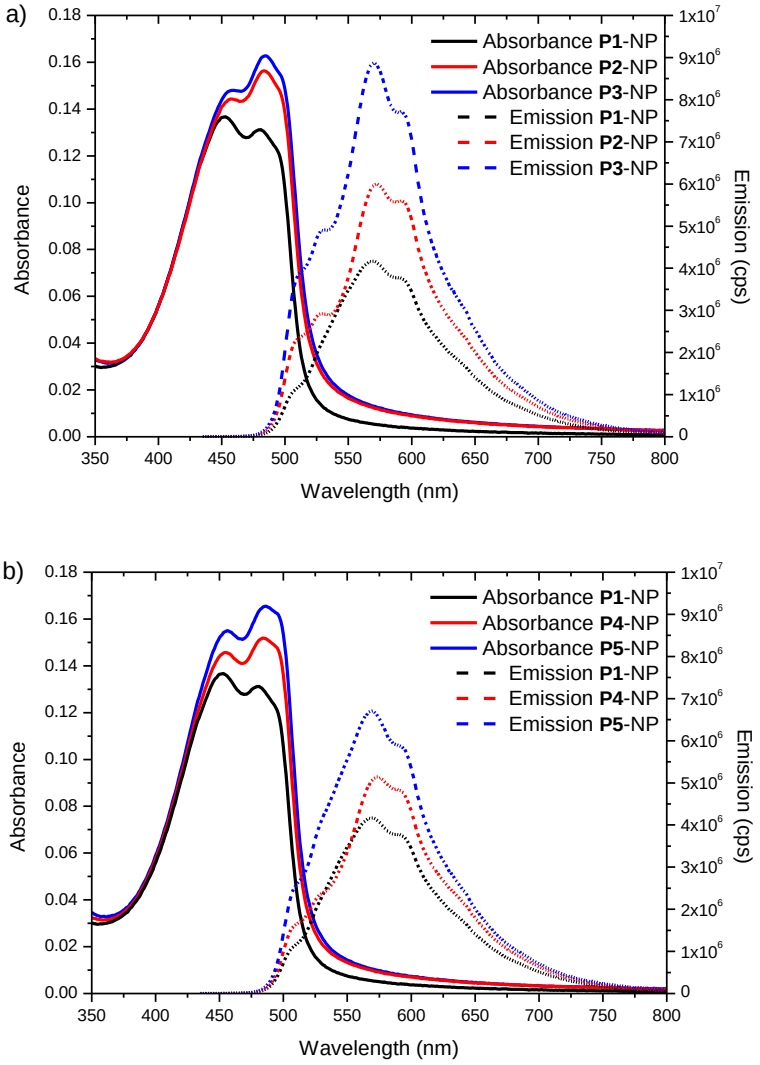

Figure 4: Absorption (solid lines) and emission (dotted lines) spectra of the different PPE-NP dispersions in water with equal absorbance at the excitation wavelength (423 nm). The area under the emission curve is representative for the photoluminescence efficiency.

5.2.4 Cytotoxicity studies

As a potential biological imaging probe, the cytotoxicity of the NP samples is of utmost importance. Those studies were performed on the samples with the highest and thus most interesting brightnesses (**P3**-NPs and **P5**-NPs). The results were compared to those of **P1**-NPs. Cytotoxicity was tested on A549 cells using the Alamar blue assay. A549 cells incubated with increasing amounts of the various PPE NPs were assessed for their cell viability (Figure 5). The cell viability remained over 88% for all the NPs tested after a 24 hour incubation with concentrations up to 100 µg/mL. This confirms the safety of the PPE NPs in terms of cellular viability for bio-imaging applications, as typical concentrations used for this purpose do not exceed 75 µg/mL. These cytotoxicity results are also similar to those reported in other studies of conjugated polymers for biological applications[36,45].

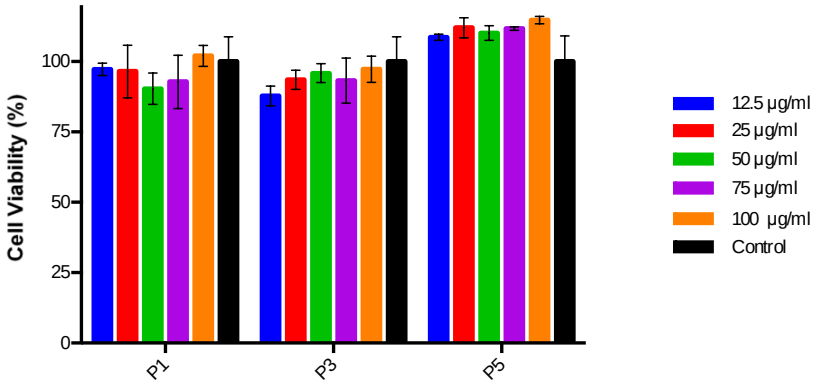

Figure 5: Dose dependent cytotoxicity of the **P1**-, **P3**- and **P5**-NPs on A549 cells after 24 hour exposure, as determined by an Alamar blue assay, showing no notable cytotoxicity. Error bars show the standard deviation of the measurements (n = 3).

5.2.5 In vitro imaging

The cellular uptake and bio-imaging potential of **P1**-, **P3**- and **P5**-NPs was then confirmed using two-photon microscopy (Figure 6). All three NPs were taken up

by the A549 cells after a 6 hour incubation period and could still be imaged after 24 hours (Figure S8). The Internalization of the NPs by the cells after 6 hours was furthermore confirmed by z-stacks (optical slice thickness = 0.46 μm) through the volume of the cells.

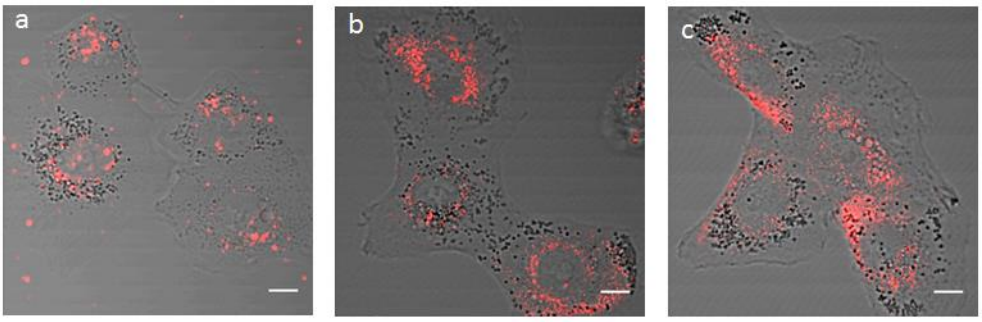

Figure 6: Two-photon microscopy images of A549 cells incubated with **P1**- (a), **P3**- (b) and **P5**-NPs (c) for 6 h. The NPs (red) are seen distributed within the volume of the cell. The transmission images are visualized in gray. These images are single optical sections, with the plane of imaging passing through the volume of the cells. Scale bar: 10 μm

5.3 CONCLUSIONS

Because of their synthetic versatility, the optical properties of conjugated polymers can be fine-tuned toward specific applications, for instance bio-imaging.[19,20] The poor solubility of these materials in aqueous environment can be overcome by the formation of nanoparticles dispersed in water.[29-31] However, the tight packing of the conjugated polymer chains in those particles generally leads to fluorescence quenching by strong interchain interactions. Some solutions have been suggested, but they often require additional synthesis steps or different types of matrix materials.[23,39-47] In this work, a simple synthetic solution is provided, avoiding extra synthesis steps or complicated materials. Two different crosslinking moieties, 1,3,5-tribromobenzene and 2,2',7,7'-tetrabromo-9,9'-spirobifluorene, were introduced in low molar ratios (3 and 5 mol%, to prevent gelation) during the Sonogashira polymerization reactions to form poly(*p*-phenylene ethynylene)s. The crosslinkers covalently connect the different polymer chains and thereby prevent tight stacking in the

nanoparticles. The optical properties of the different crosslinked polymers were then compared to those of the linear reference polymer, both in solution and in nanoparticle form. The photoluminescence quantum yield of the nanoparticles doubled (from 5 to 11%) when 5 mol% of 1,3,5-tribromobenzene was introduced and also the fluorescence brightness doubled for each of the crosslinkers when added in 5 mol%. Those improvements on the NP brightness are of great importance to the performance of conjugated polymers in bio-imaging applications. The negligible cytotoxicity exhibited by all the particles even at a concentration higher than those typically used for bio-imaging confirmed the biocompatibility of these particles. Two-photon microscopy showed that the **P1**-, **P3**- and **P5**-NPs are well suited for bio-imaging, given their excellent cell uptake and photo-stability. Furthermore, the fact that these NPs are compatible with two-photon excitation affords two inherent benefits. Firstly, the near-infrared radiation used in two-photon excitation suffers from significantly less absorption in biological samples[23,39] and secondly, since two-photon microscopy affords self-sectioning by limiting the excitation volume this eliminates the need for a confocal microscope for optical sectioning[55].

5.4 EXPERIMENTAL SECTION

5.4.1 Materials and methods

1,3,5-Tribromobenzene was provided by Fischer Scientific. 2,2',7,7'-Tetrabromo-9,9'-spirobifluorene was obtained from Fluorochem. Sodium dodecyl sulfate (SDS) was supplied by Merck Millipore. Spectrum Labs delivered the Spectra/Por® 3 dialysis cellulose membranes (MWCO 3.5 kDa). Coumarin 153 (99%) and tetrahydrofuran (THF; 99.9%) were purchased from Sigma Aldrich. 9,10-Diphenylanthracene (DPA) was obtained from Janssen Chimica Belgium. Cyclohexane (99.9%) and chloroform (99.0%) were purchased from Analar Normapur. The CellMask Green stain was obtained from Life Technologies. Alamar blue was supplied by Invitrogen. The modified eagle's medium with GlutaMAX and penicillin/streptomycin were obtained from Gibco and the non-heat inactivated fetal bovine serum (FBS) was purchased from Biochrom AG.
NMR chemical shifts (δ, in ppm) were determined relative to the residual $CHCl_3$ (7.26 ppm) absorption or the ^{13}C resonance shift of $CDCl_3$ (77.16 ppm). Analysis

of the molar masses and molar mass distributions of the polymers was conducted on a Tosoh EcoSEC System, consisting of an autosampler, a PSS guard column SDV (50 x 7.5 mm), three PSS SDV analytical linear XL columns (5 µm, 300 x 7.5 mm) and a UV detector. THF was used as the eluent at 40 °C with a flow rate of 1.0 mL/min. The SEC system was calibrated using linear narrow polystyrene standards ranging from 474 to 7.5 x 10^6 g/mol (K = 14.1 x 10^{-5} dL/g and α = 0.70).

5.4.2 Monomer and polymer synthesis

The required monomers (**1** and **2**) were synthesized according to literature procedures.[49]

P1. Prepared according to a reported procedure.[45] An orange PPE polymer was obtained (0.076 g, 82%). SEC (THF): M_n 33.0 kg/mol, $Đ$ 2.0; ^{1}H NMR (400 MHz, $CDCl_3$): δ (ppm) 7.02 (s, 2H), 4.03 (t, J = 6.4 Hz, 4H), 1.91–1.80 (m, 4H), 1.55–1.47 (m, 4H), 1.42–1.21 (m, 16H), 0.87 (t, J = 6.6 Hz, 6H).

General polymerization procedure for P2, P3, P4 and P5. 1,4-Diethynyl-2,5-bis(octyloxy)benzene (**1**), 1,4-bis(octyloxy)-2,5-diiodobenzene (**2**) and crosslinker (either 1,3,5-tribromobenzene (**3**) or 2,2',7,7'-tetrabromo-9,9'-spirobifluorene (**4**)) were dissolved in dry toluene and diisopropylamine was added. The solution was purged with nitrogen for 10 min after which $Pd(PPh)_3Cl_2$ (5 mol%) and CuI (5 mol%) were added. After stirring for 2 h at 70 °C, an excess of iodobenzene (2 drops) and phenylacetylene (2 drops) was added, with 10 min of stirring at 70 °C in between of the two additions. After stirring for 10 more min at 70 °C, the polymer was precipitated in methanol, redissolved in chloroform and then precipitated again in acetone to remove catalyst and monomer residues.

P2. 1,4-Diethynyl-2,5-bis(octyloxy)benzene (**1**) (50.0 mg, 0.1307 mmol), 1,4-bis(octyloxy)-2,5-diiodobenzene (**2**) (73.0 mg, 0.1249 mmol), 1,3,5-tribromobenzene (**3**) (1.23 mg, 0.0039 mmol), $Pd(PPh)_3Cl_2$ (4.6 mg, 5 mol%), CuI (1.2 mg, 5 mol%), dry toluene (2.5 mL) and diisopropylamine (1.0 mL) were used. An orange solid was obtained (0.072 g, 79%). SEC (THF): M_n 45.0

kg/mol, *Đ* 5.4; ^{1}H NMR (400 MHz, $CDCl_3$): *δ* (ppm) 7.02 (s, 2H), 4.03 (t, *J* = 6.3 Hz, 4H), 1.90−1.79 (m, 4H), 1.55−1.44 (m, 4H), 1.40−1.23 (m, 16H), 0.87 (t, *J* = 6.6 Hz, 6H).

P3. 1,4-Diethynyl-2,5-bis(octyloxy)benzene (**1**) (50.0 mg, 0.1307 mmol), 1,4-bis(octyloxy)-2,5-diiodobenzene (**2**) (71.0 mg, 0.1209 mmol), 1,3,5-tribromobenzene (**3**) (2.05 mg, 0.0065 mmol), $Pd(PPh)_3Cl_2$ (4.6 mg, 5 mol%), CuI (1.2 mg, 5 mol%), dry toluene (2.5 mL) and diisopropylamine (1.0 mL) were used. An orange solid was obtained in nearly quantitative yield (0.089 g). SEC (THF): M_n 60.0 kg/mol, *Đ* 2.8; ^{1}H NMR (400 MHz, $CDCl_3$): *δ* (ppm) 7.02 (s, 2H), 4.03 (t, *J* = 6.3 Hz, 4H), 1.90−1.79 (m, 4H), 1.55−1.44 (m, 4H), 1.40−1.23 (m, 16H), 0.87 (t, *J* = 6.6 Hz, 6H).

P4. 1,4-Diethynyl-2,5-bis(octyloxy)benzene (**1**) (100.0 mg, 0.2614 mmol), 1,4-bis(octyloxy)-2,5-diiodobenzene (**2**) (146.0 mg, 0.2497 mmol), 2,2',7,7'-tetrabromo-9,9'-spirobifluorene (**4**) (4.9 mg, 0.0078 mmol), $Pd(PPh)_3Cl_2$ (9.2 mg, 5 mol%), CuI (2.5 mg, 5 mol%), dry toluene (5.0 mL) and diisopropylamine (2.0 mL) were used. An orange solid was obtained (0.162 g, 89%). SEC (THF): M_n 12.0 kg/mol, *Đ* 2.3; ^{1}H NMR (400 MHz, $CDCl_3$): *δ* (ppm) 7.02 (s, 2H), 4.03 (t, *J* = 6.3 Hz, 4H), 1.90−1.79 (m, 4H), 1.55−1.44 (m, 4H), 1.40−1.23 (m, 16H), 0.87 (t, *J* = 6.6 Hz, 6H).

P5. 1,4-Diethynyl-2,5-bis(octyloxy)benzene (**1**) (100.0 mg, 0.2614 mmol), 1,4-bis(octyloxy)-2,5-diiodobenzene (**2**) (141.8 mg, 0.2418 mmol), 2,2',7,7'-tetrabromo-9,9'-spirobifluorene (**4**) (8.2 mg, 0.0130 mmol), $Pd(PPh)_3Cl_2$ (9.2 mg, 5 mol%), CuI (2.5 mg, 5 mol%), dry toluene (5.0 mL) and diisopropylamine (2.0 mL) were used. An orange solid was obtained in nearly quantitative yield (0.178 g). SEC (THF): M_n 59.0 kg/mol, *Đ* 2.2; ^{1}H NMR (400 MHz, $CDCl_3$): *δ* (ppm) 7.02 (s, 2H), 4.03 (t, *J* = 6.3 Hz, 4H), 1.90−1.79 (m, 4H), 1.55−1.44 (m, 4H), 1.40−1.23 (m, 16H), 0.87 (t, *J* = 6.6 Hz, 6H).

5.4.3 Nanoparticle synthesis

A combination of the miniemulsion and the emulsion/solvent evaporation technique was employed for the preparation of nanoparticles from the five

different PPE polymer samples. To achieve this, a continuous phase was initially established by preparing a solution of SDS (72 mg) in deionized water (24 g). 1.7 g of this mixture was combined with the dispersive phase, obtained by dissolving the respective PPE polymers (25 mg) in chloroform (0.7 g). This was then mechanically stirred using a magnetic stirrer at 550 rpm for 45 min. Miniemulsions were subsequently formed by ultrasonication for 3 min (30 s pulse followed by 20 s pause) at 60% amplitude using a Branson 450 W digital sonifier equipped with a 1/4" tip. The resulting miniemulsions were then transferred to round bottom flasks with wide necks. Heating of the samples was subsequently done in oil baths at 40 °C, while simultaneously being mechanically stirred at 1000 rpm for a duration of 4 hours. The final solutions were filtered with filter paper (Whatman Grade 595½, pore size 4-7 µm). In the last step, the samples were centrifuged 20 successive times for 20 min to remove any excess of SDS left. This was done at a temperature of 4 °C at 2000 rpm using Amicon Ultra-4 centrifugal filter devices (MWCO = 30 kDa).

5.4.4 Transmission electron microscopy (TEM)

Transmission electron microscopy (TEM) images of the NP dispersions were obtained using a TECNAI Spirit TEM from FEI, operating at an accelerating voltage of 120 kV. A drop of the NP aqueous dispersion (solid content of about 0.01 wt%) was drop-casted onto a carbon coated copper grid and dried under ambient conditions.

5.4.5 Dynamic light scattering (DLS)

The size, size distribution and zeta potentials of all NPs were obtained by DLS using a Brookhaven Instruments Zetapals.

5.4.6 Stationary UV-Vis absorption and fluorescence spectroscopy

UV-Vis absorption spectra were obtained using an Agilent Cary 5000 Scan UV-Vis-NIR spectrophotometer. The fluorescence spectra were measured with a Horiba-Jobin Yvon FluoroLog-3 spectrofluorometer, with correction for the wavelength dependence of the throughput and sensitivity of the detection

channel. A quantum counter was employed to correct for temporal fluctuations in the excitation intensity and for the wavelength dependence of the excitation intensity. The absorption coefficients of the materials were calculated using Lambert-Beer's law by varying the concentration of the polymers in $CHCl_3$ or the NPs in water. The PLQYs of the polymers in $CHCl_3$ and the NPs in water were measured using the dye coumarin 153 in ethanol as a standard (QY = 53%). Five dilutions were prepared for all samples as well as for the standard. The most concentrated sample had an absorbance of 0.1 at an excitation wavelength of 423 nm. Emission spectra were collected for all samples after which the absorption versus the integral of the emission spectra for each dilution and sample were plotted and trend lines were fitted. The resulting slope values (m) as well as the refractive indexes (η) of the solvents were used to determine the PLQYs of the samples using following formula:

$$FQY_{sample} = FQY_{standard} \frac{m_{sample}}{m_{standard}} \frac{{\eta_{sample}}^2}{{\eta_{standard}}^2}$$

5.4.7 Cell cultures

A549 human lung carcinoma cells were cultured in modified eagle's medium (MEM) with GlutaMAX, supplemented with 10% non-heat inactivated fetal bovine serum (FBS) and 1% penicillin/streptomycin. The cells were incubated at 37 °C with 5 % CO_2 and the cell cultures were sub-cultured at 80% confluence. For microscopic observation, the cells were seeded and incubated for 24 h before the addition of the NPs into 8 well µ-slides (Ibidi GmbH) at a density of $1x10^4$ cells/well.

5.4.8 Cytotoxicity studies

An Alamar blue assay was used to determine the cytotoxicity of the different PPE NPs. A549 cells were seeded at an intial density of 103 cells/well in a black 96-well plate and allowed to incubate for 24 h at 37 °C with 5% CO_2. The **P1**-, **P3**- and **P5**-NPs were subsequently added at five different concentrations up to 100 µg/mL and incubated for an additional 24 h. Following this, the cells were washed three times with phosphate buffered saline (PBS) and the Alamar blue

reagent was added as per manufacturer's instructions. After incubation for 4 h, the plate was analyzed using a fluorescence plate reader (Tecan). The data were then normalized and tabulated.

5.4.9 In vitro imaging

A549 cells were grown in 8 well µ-slides. The cells were subsequently incubated at 37 °C with 5% CO_2 with the **P1**-, **P3**- and **P5**-NPs individually at a concentration of 50 µg/mL for 6 and 24 h (see supporting material for details on the imaging after 24 h incubation). The cells were then rinsed 3 times with PBS to remove free nanoparticles. Imaging after 6 h of incubation was performed using a LSM 880 (Zeiss) confocal laser scanning microscope (CLSM) on an inverted Axio observer motorized frame. The microscope was fitted with a LD C-Apochromat 40×/1.1 W Corr M27 water immersion objective. The NPs were excited by a femtosecond pulsed titanium-sapphire laser (MaiTai DeepSee, Spectra-Physics) tuned to 850 nm. The fluorescence emission was then channeled through a 650 nm low pass filter. The BiG-2 (Zeiss) non-descanned detector attached to the microscope was used for capturing the fluorescence images. A T-PMT (Zeiss) was simultaneously used to capture the transmission images of the cells.

5.5 REFERENCES

[1] N. de Jonge and F. Ross, *Nat. Nanotechnol.*, 2011, **6**, 695.

[2] D. Brooks, *Neurotherapeutics*, 2005, **2**, 226.

[3] C. Alric, J. Taleb, G. Duc, C. Mandon, C. Billotey, A. Meur-Herland, T. Brochard, F. Vocanson, M. Janier, P. Perriat, S. Roux and O. Tillement, *J. Am. Chem. Soc.*, 2008, **130**, 5908.

[4] M. Seemann, *Circulation*, 2005, **112**, 329.

[5] A. Boni, A. Politi, P. Strnad, W. Xiang, M. Hossain and J. Ellenberg, *J. Cell. Biol.*, 2015, **209**, 705.

[6] R. Day, *Mol. Cell. Endocrinol.*, 2005, **230**, 1.

[7] M. Wachsmuth, C. Conrad, J. Bulkescher, B. Koch, R. Mahen, M. Isokane, R. Pepperkok and J. Ellenberg, *Nat. Biotechnol.*, 2015, **33**, 384.

[8] J. Yao, M. Yang and Y. Duan, *Chem. Rev.*, 2014, **114**, 6130.

[9] G. M. van Dam, G. Themelis, L. M. A. Crane, N. J. Harlaar, R. G. Pleijhuis, W. Kelder, A. Sarantopoulos, J. S. de Jong, H. J. G. Arts, A. G. J. van der Zee, J. Bart, P. S. Low and V. Ntziachristos, *Nat. Med.*, 2011, **17**, 1315.

[10] U. Resch-Genger, M. Grabolle, S. Cavaliere-Jaricot, R. Nitschke and T. Nann, *Nat. Meth.*, 2008, **5**, 763.

[11] X. Michalet, F. F. Pinaud, L. A. Bentolila, J. M. Tsay, S. Doose, J. J. Li, G. Sundaresan, A. M. Wu, S. S. Gambhir and S. Weiss, *Science*, 2005, **307**, 538.

[12] B. A. Kairdolf, A. M. Smith, T. H. Stokes, M. D. Wang, A. N. Young and S. Nie, *Annu. Rev. Anal. Chem.*, 2013, **6**, 143.

[13] V. N. Mochalin, O. Shenderova, D. Ho and Y. Gogotsi, *Nat. Nanotechnol.*, 2012, **7**, 11.

[14] S.-T. Yang, L. Cao, P. G. Luo, F. Lu, X. Wang, H. Wang, M. J. Meziani, Y. Liu, G. Qi and Y.-P. Sun, *J. Am. Chem. Soc.*, 2009, **131**, 11308.

[15] A. A. Burns, J. Vider, H. Ow, E. Herz, O. Penate-Medina, M. Baumgart, S. M. Larson, U. Wiesner and M. Bradbury, *Nano Lett.*, 2009, **9**, 442.

[16] C. Wu, B. Bull, C. Szymanski, K. Christensen and J. McNeill, *ACS Nano*, 2008, **2**, 2415.

[17] J. Peng, X. He, K. Wang, W. Tan, Y. Wang and Y. Liu, *Anal. Bioanal. Chem.*, 2007, **388**, 645.

[18] H.-S. Peng, J. A. Stolwijk, L.-N. Sun, J. Wegener and O. S. Wolfbeis, *Angew. Chem. Int. Ed.*, 2010, **122**, 4342.

[19] R. Ahmad Khanbeigi, T. F. Abelha, A. Woods, O. Rastoin, R. D. Harvey, M.-C. Jones, B. Forbes, M. A. Green, H. Collins and L. A. Dailey, *Biomacromolecules*, 2015, **16**, 733.

[20] D. Tuncel and H. V. Demir, *Nanoscale*, 2010, **2**, 484.

[21] P.-L. T. Boudreault, A. Najari and M. Leclerc, *Chem. Mater.*, 2011, **23**, 456.

[22] A. Smith, M. Mancini and S. Nie, *Nat. Nanotechnol.*, 2009, **4**, 710.

[23] D. Ding, J. Liu, G. Feng, K. Li, Y. Hu and B. Liu, *Small*, 2013, **9**, 3092.

[24] E. Hemmer, A. Benayas, F. Légaré and F. Vetrone, *Nanoscale Horiz.*, 2016, **1**, 168.

[25] T. Klingstedt and K. P. R. Nilsson, *Biochim. Biophys. Acta*, 2011, **1810**, 286.

[26] N. Y. Kwon, D. Kim, G. Jang, J. H. Lee, J.-H. So, C.-H. Kim, T. H. Kim and T. S. Lee, *ACS Appl. Mater. Interfaces*, 2012, **4**, 1429.

[27] Z. Kahveci, R. Vázquez-Guilló, M. J. Martínez-Tomé, R. Mallavia and C. R. Mateo, *ACS Appl. Mater. Interfaces*, 2016, **8**, 1958.

[28] M. Ma, M. Lei, X. Tan, F. Tan and N. Li, *RSC Adv.*, 2016, **6**, 1945.

[29] J. Yu, Y. Rong, C.-T. Kuo, X.-H. Zhou and D. T. Chiu, *Anal. Chem.*, 2017, **89**, 42.

[30] Y.-H. Chan and P.-J. Wu, *Part. Part. Syst. Charact.*, 2015, **32**, 11.

[31] J. Pecher and S. Mecking, *Chem. Rev.*, 2010, **110**, 6260.

[32] J. L. Brédas, D. Beljonne, V. Coropceanu and J. Cornil, *Chem. Rev.*, 2004, **104**, 4971.

[33] S. Doose, H. Neuweiler and M. Sauer, *ChemPhysChem*, 2009, **10**, 1389.

[34] H. Klauk, Organic Electronics: Materials, Manufacturing and Applications, 2006, Wiley.

[35] J. R. Lakowicz, Principles of Fluorescence Spectroscopy, 2006, Springer US.

[36] M. Peters, N. Zaquen, L. D'Olieslaeger, H. Bové, D. Vanderzande, N. Hellings, T. Junkers and A. Ethirajan, *Biomacromolecules*, 2016, **17**, 2562.

[37] B. Schwartz, *Annu. Rev. Phys. Chem.*, 2003, **54**, 141.

[38] Y. Braeken, S. Cheruku, A. Ethirajan and W. Maes, Conjugated Polymer Nanoparticles for Bio-imaging, *manuscript submitted*.

[39] Y. Lv, P. Liu, H. Ding, Y. Wu, Y. Yan, H. Liu, X. Wang, F. Huang, Y. Zhao and Z. Tian, *ACS Appl. Mater. Interfaces*, 2015, **7**, 20640.

[40] C. Yang, H. Liu, Y. Zhang, Z. Xu, X. Wang, B. Cao and M. Wang, *Biomacromolecules*, 2016, **17**, 1673.

[41] C.-P. Chen, Y.-C. Huang, S.-Y. Liou, P.-J. Wu, S.-Y. Kuo and Y.-H. Chan, *ACS Appl. Mater. Interfaces*, 2014, **6**, 21585.

[42] H.-Y. Liu, P.-J. Wu, S.-Y. Kuo, C.-P. Chen, E.-H. Chang, C.-Y. Wu and Y.-H. Chan, *J. Am. Chem. Soc.*, 2015, **137**, 10420.

[43] J. Liu, G. Feng, D. Ding and B. Liu, *Polym. Chem.*, 2013, **4**, 4326.

[44] J. Liu, K. Li and B. Liu, *Adv. Sci.*, 2015, **5**, 1500008.

[45] L. D'olieslaeger, Y. Braeken, S. Cheruku, J. Smits, M. Ameloot, D. Vanderzande, W. Maes and A. Ethirajan, *J. Colloid Interface Sci.*, 2017, **504**, 527.

[46] J. M. Behrendt, J. A. Esquivel Guzman, L. Purdie, H. Willcock, J. J. Morrison, A. B. Foster, R. K. O'Reilly, M. C. McCairn and M. L. Turner, *React. Funct. Polym.*, 2016, **107**, 69.

[47] B. S.-Il Kim, Y.-J. Jin, W.-E. Lee, D. J. Byun, R. Yu, S.-J. Park, H. Kim, K.-H. Song, S.-Y. Jang and G. Kwak, *Adv. Optical Mater.*, 2015, **3**, 78.

[48] I.-B. Kim, H. Shin, A. J. Garcia and U. H. F. Bunz, *Bioconjugate Chem.*, 2007, **18**, 815.

[49] Y. Braeken, P. Verstappen, L. Lutsen, D. Vanderzande and W. Maes, *Polym. Chem.*, 2015, **6**, 6720.

[50] T. Chen, W. Xu, Z. Huang, H. Peng, Z. Ke, X. Lu, Y. Yan and R. Liu, *J. Mater. Chem. B*, 2015, **3**, 3564.

[51] E. Mendez and J. H. Moon, *Chem. Commun.*, 2013, **49**, 6048.

[52] R. A. Ponzio, Y. L. Marcato, M. L. Gomez, C. V. Waiman, C. A. Chesta and R. E. Palacios, *Methods Appl. Fluoresc.*, 2017, **5**, 024001.

[53] W. Denk, J. Strickler and W. Webb, *Science*, 1990, **248**, 73.

5.6 SUPPORTING INFORMATION

5.6.1 ^{1}H NMR spectra

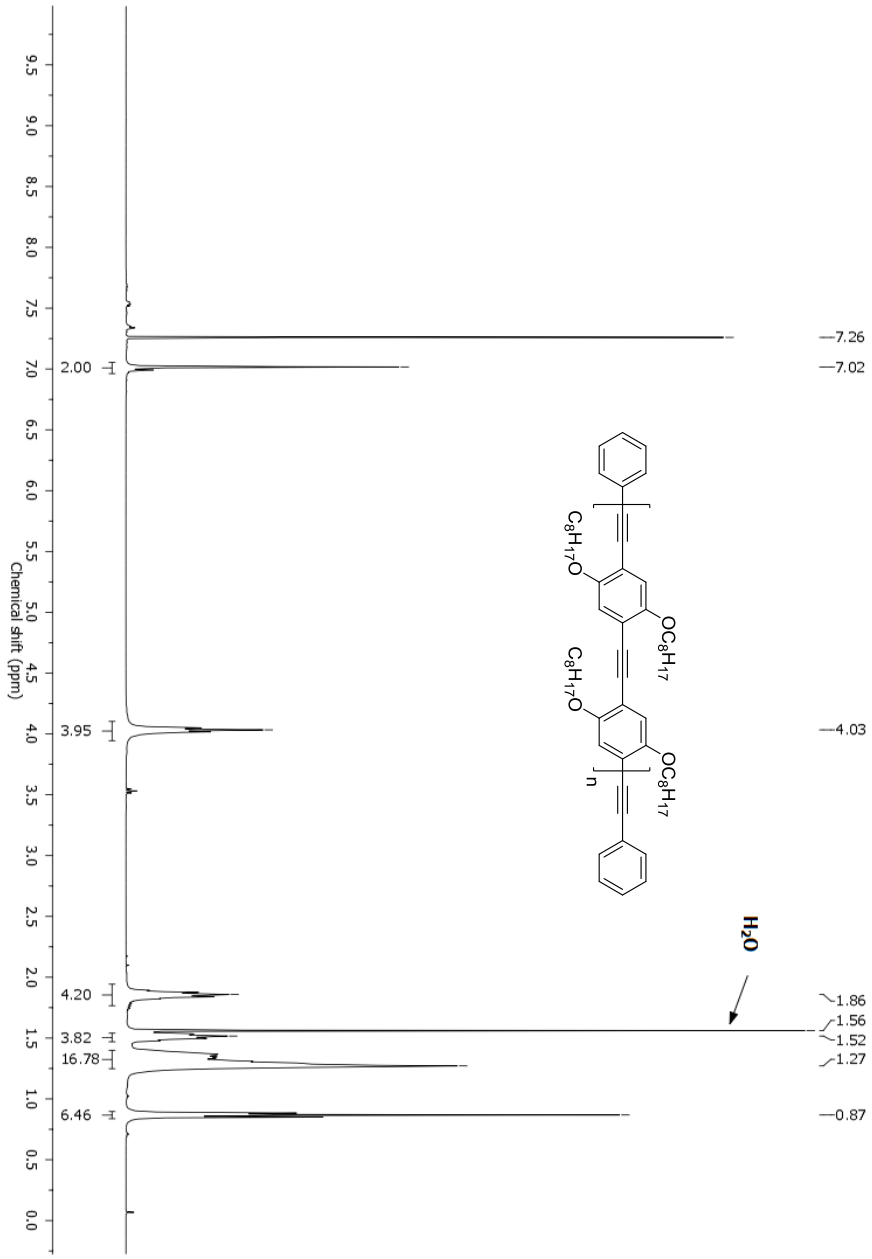

Figure S1: ^{1}H NMR spectrum of **P1** (in $CDCl_2$).

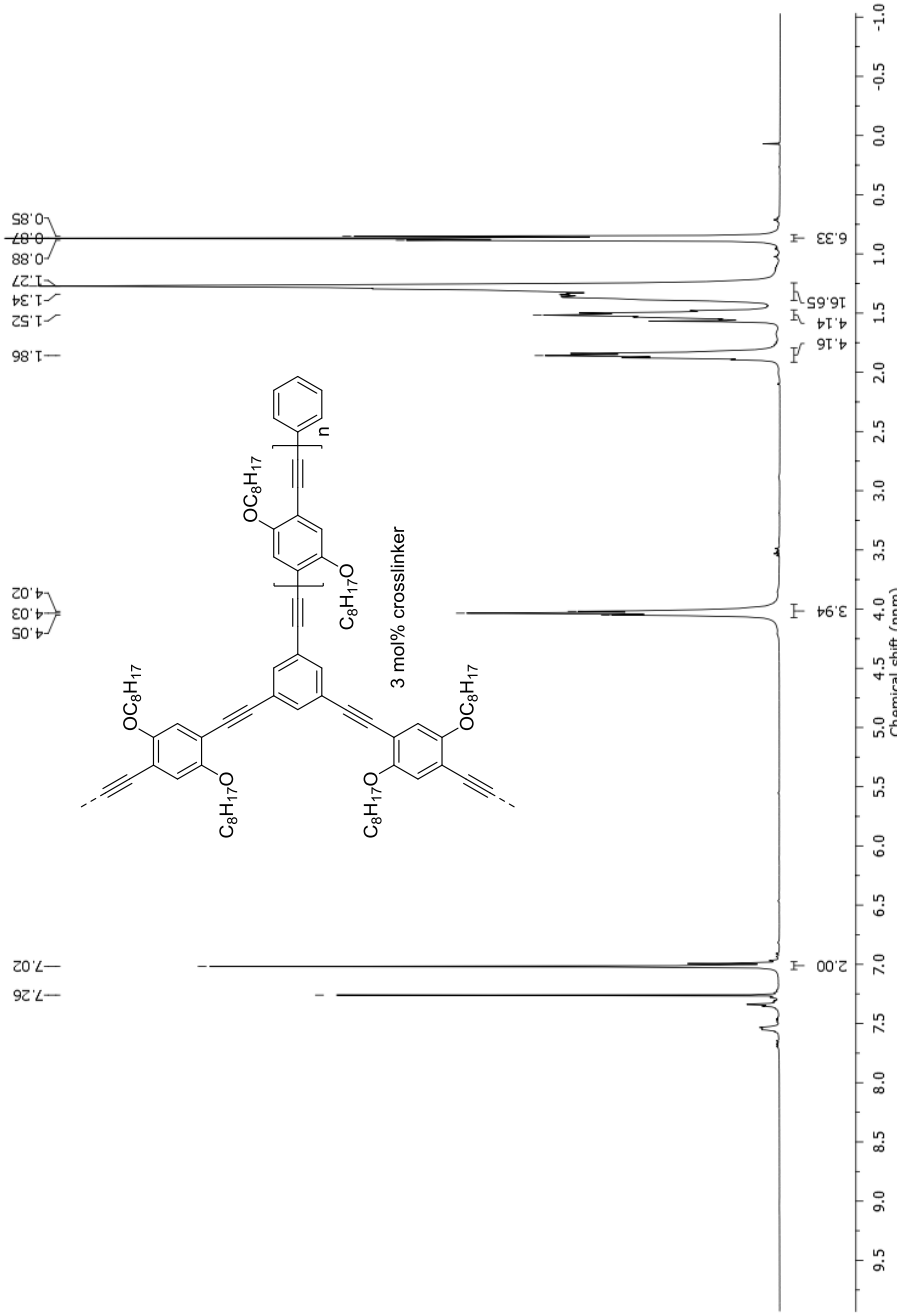

Figure S2: ^{1}H NMR spectrum of **P2** (in $CDCl_3$).

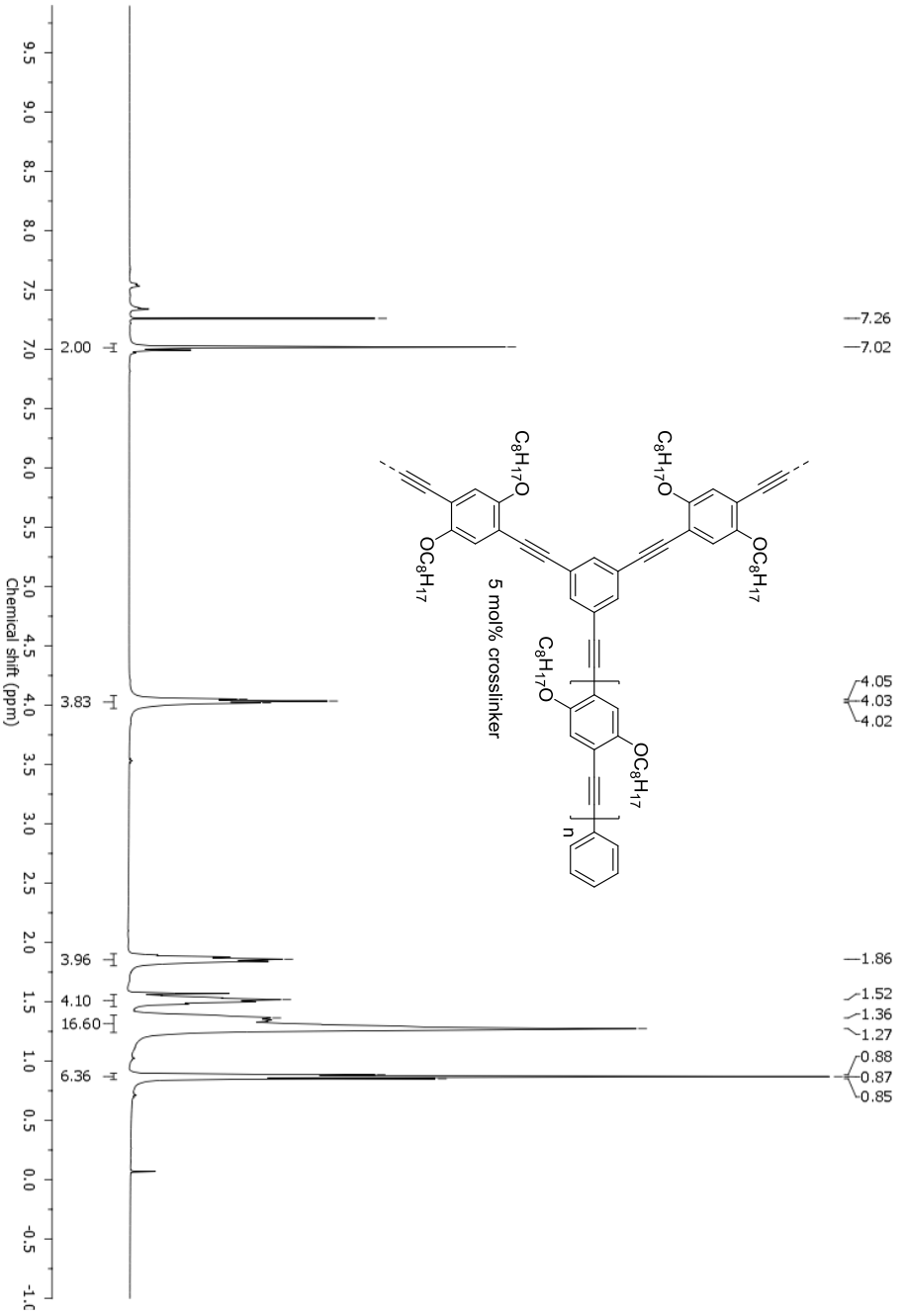

Figure S3: ^{1}H NMR spectrum of **P3** (in $CDCl_3$).

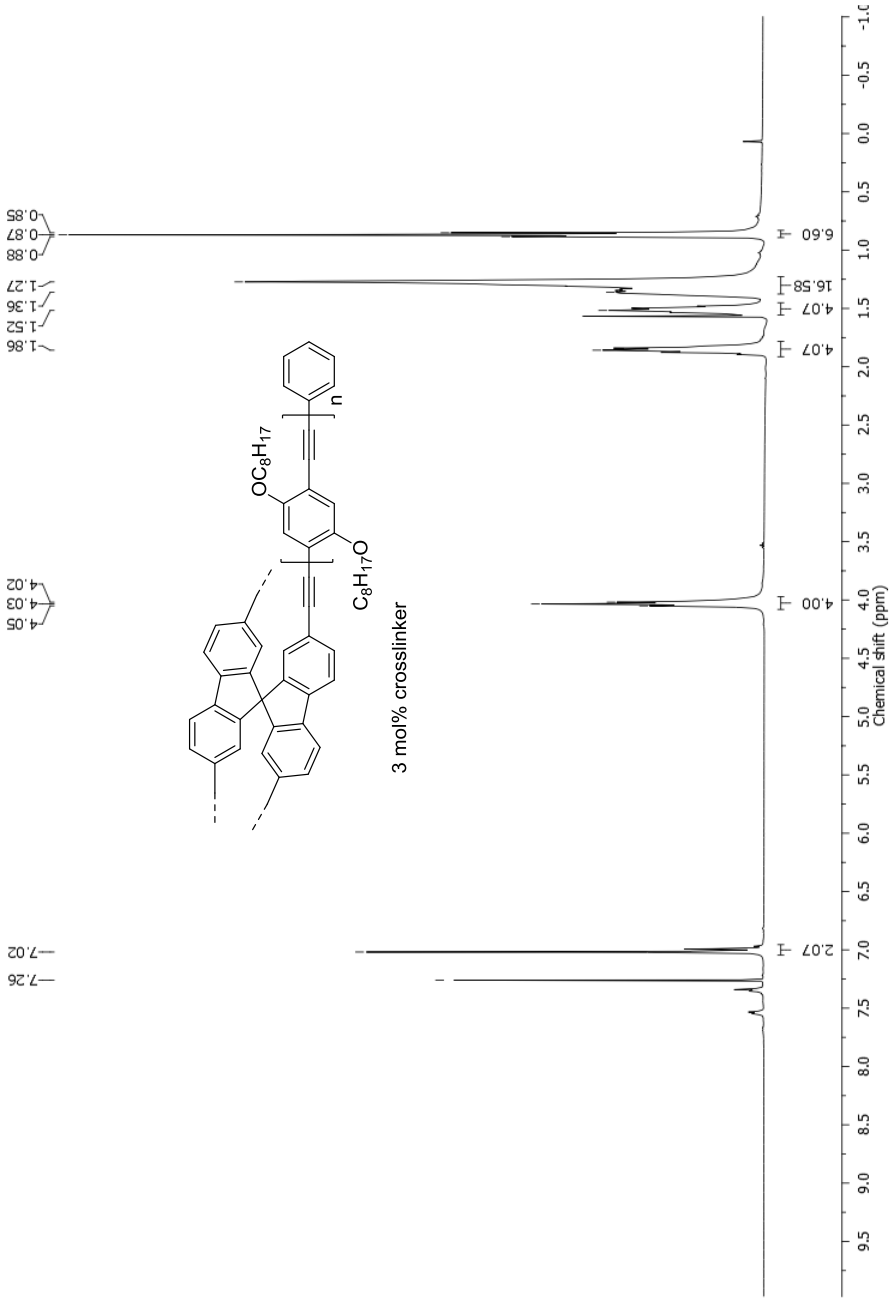

Figure S4: ^{1}H NMR spectrum of **P4** (in $CDCl_3$).

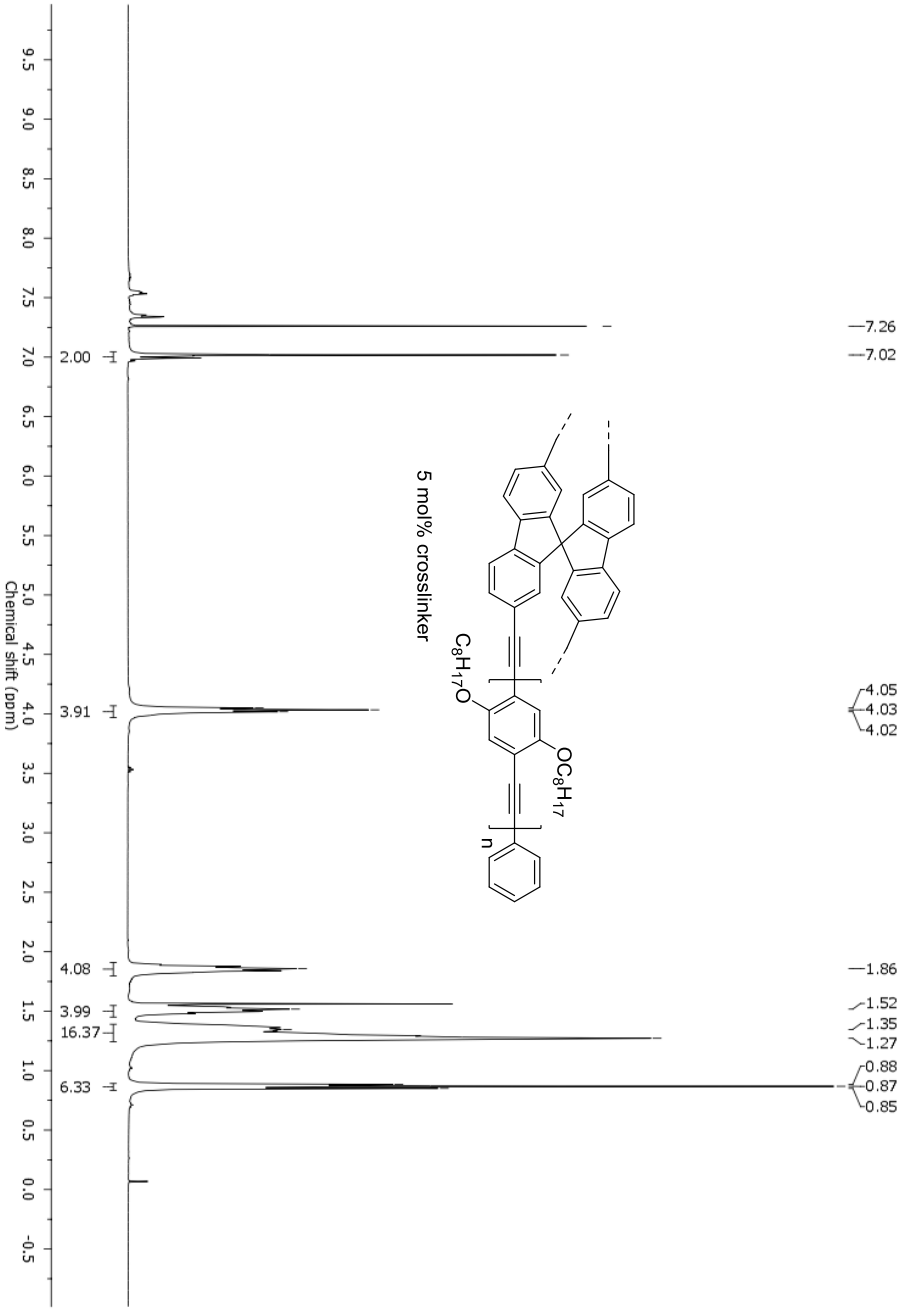

Figure S5: ^{1}H NMR spectrum of **P5** (in $CDCl_3$).

5.6.2 UV-Vis and fluorescence spectra of the PPE NPs at constant concentration

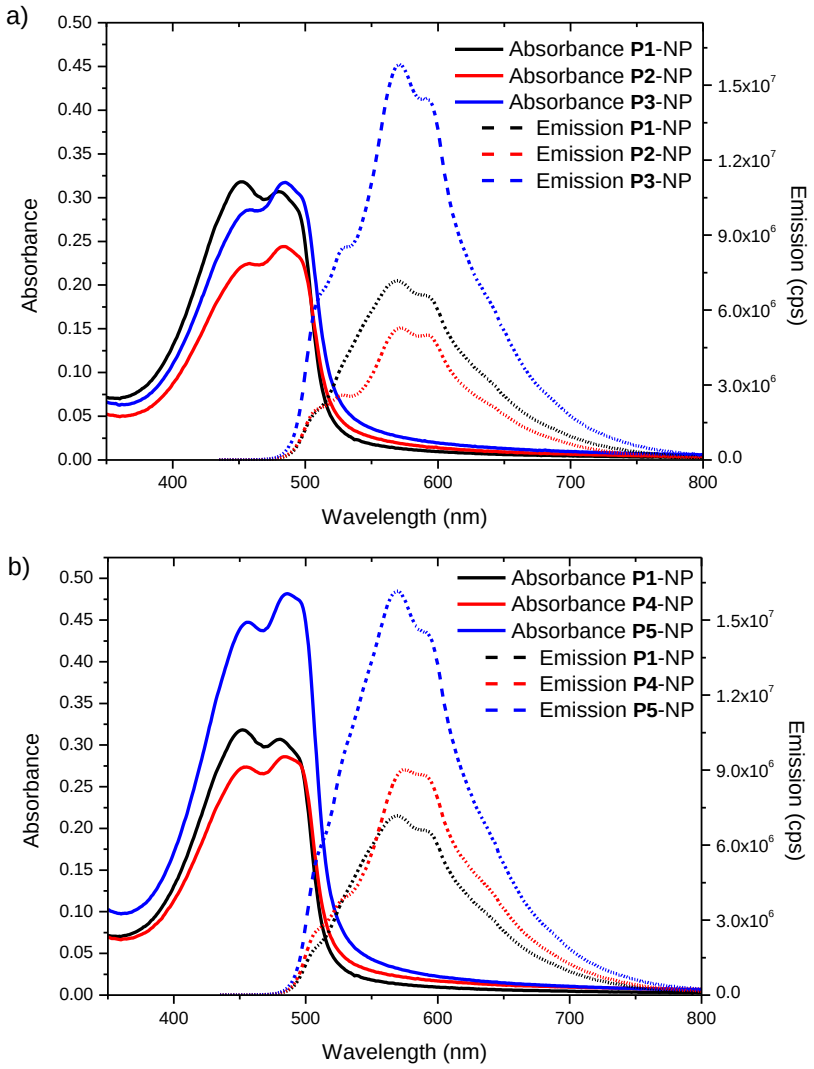

Figure S6: Absorption and emission spectra of the nanoparticles based on a) **P1**, **P2** and **P3**, and b) **P1**, **P4** and **P5** at a concentration of 10 mg/L.

5.6.3 DLS Size distributions

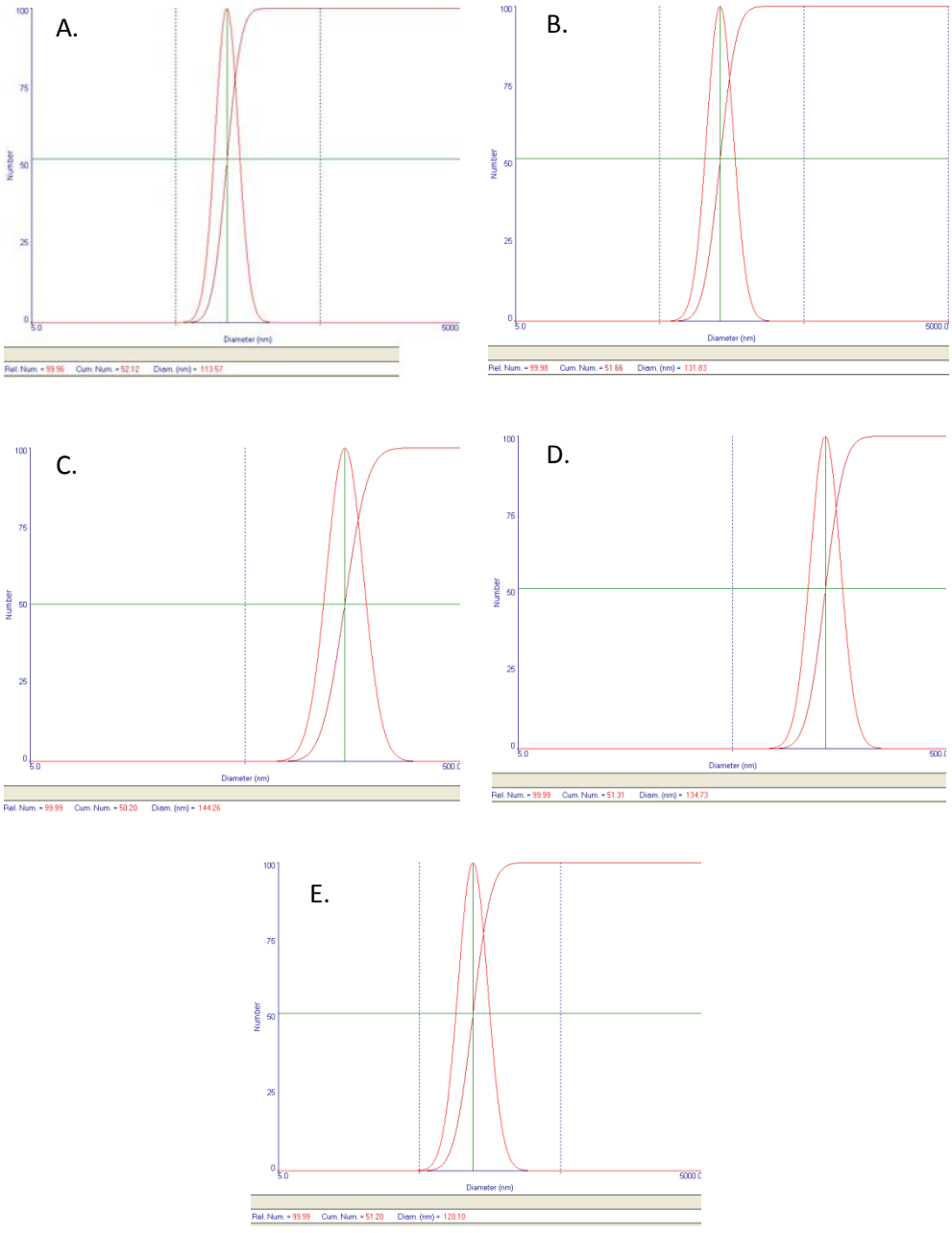

Figure S7: Number-average hydrodynamic size distributions of **P1**- (A), **P2**- (B), **P3**- (C), **P4**- (D) and **P5**-NPs (E) in an aqueous dispersion.

5.6.4 In vitro imaging methodology for imaging after 24 hour incubation with A549 cells

The imaging was performed using a LSM 510 META (Zeiss) confocal laser scanning microscope (CLSM) on an inverted Axiovert 200 M motorized frame. The microscope was fitted with a LD C-Apochromat 40×/1.1 W Corr UV-VIS-IR water immersion objective. The NPs were excited by a femtosecond pulsed titanium-sapphire laser (MaiTai DeepSee, Spectra-Physics) tuned to between 825 – 900 nm. The fluorescence emission was then channeled through a 650 nm low pass filter. The non-descanned detector of the microscope were used for capturing the image.

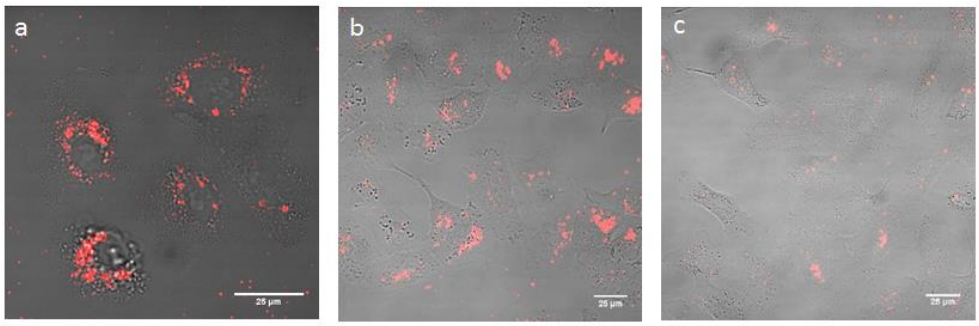

Figure S8: Two-photon microscopy images of A549 cells incubated with P1- (a), P3- (b) and P5-NPs (c) for 24 h. The NPs (red) are seen distributed within the volume of the cell. The transmission images are visualized in gray. Scale bar: 25 µm.

Chapter 6

Click Immobilization of Randomly Alkynylated Protein A on Poly(*p*-Phenylene Ethynylene) Films - Influence of Side Chain Hydrophilicity

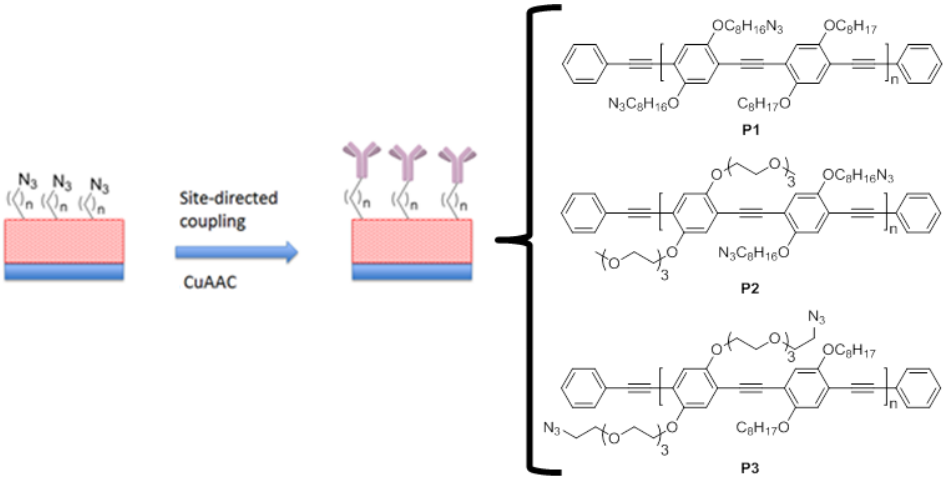

ABSTRACT

The use of biomolecular receptors is a viable way to improve sensor selectivity since these molecules are designed by nature to bind specific targets. To implement those natural materials, the development of reproducible immobilization techniques is imperative. In this work, thin films of three different conjugated polymers are employed, all with the same poly(*p*-phenylene ethynylene) backbone, but different side chains with variable hydrophilicity. Copper(I)-catalysed azide-alkyne click is chosen as the immobilization strategy due to the bio-orthogonality of the reactive functional groups and its possible application under mild conditions in water. The attempted immobilization of different molecules (randomly alkynylated SpA and nanobody BCII10 (NbBCII10), and alkynylated PEG_n-COOH) is monitored via quartz crystal microbalance with dissipation monitoring. None of the immobilization attempts was successful. For SpA, the polymer surface was saturated after 20 minutes due to aspecific interactions. Furthermore, it was not possible to wash off the protein afterwards, making reproducibility impossible. On the other hand, no interaction with the polymer surface was observed for the alkynylated NbBCII10 and PEG_n-COOH.

6.1 INTRODUCTION

Over the past few decades, the interest in conjugated polymer based biological and chemical sensors has steadily grown. One of the reasons for this widespread activity is the availability of different types of conjugated polymers, developed for flexible and light-weight optoelectronic devices like organic photovoltaics (OPV), organic light-emitting diodes (OLEDs) and organic field-effect transistors (OFETs). A broad scope of sensor applications can be covered due to the adaptability of these polymer backbones and side chains. Furthermore, conjugated polymers, and in particular poly(*p*-phenylene ethynylene)s (PPEs), exhibit excellent fluorescent properties,[1] high conductivities[2] and amplifying effects, which enables to use these materials not only as an immobilization matrix for the receptor but also as a transducer material.[3] Those properties together with the minimal production cost of the final products because of the availabilities of facile film-forming techniques, render those materials excellent candidates for sensor applications.

For the development of state-of-the-art biosensors, it is important to tackle three major aspects: (i) the sensitivity[3] of the sensors, which can be improved by high receptor loadings and a clever choice of transducer material, coupled to a suitable read-out technique, (ii) the selectivity of the sensor, which can be tailored by the use of biomolecules, designed by nature to probe a specific target [3], and (iii) the reproducibility of the sensor output.[4] Stability of the probe is therefore crucial, but also the coupling technique used for probe immobilization onto the transducer material is of higher importance.

Multiple examples of biosensors based on polymers have been described, but in many reported cases no covalent immobilization of the receptor onto the polymer was realised. However, in some more sophisticated sensory systems, biomolecule immobilization is needed and a number of immobilization techniques has thus been described. Most polymer based sensory systems comprise non-conjugated polymers. Receptors have been introduced on the polymer backbone via e.g. Michael addition, Schiff base reactions, proton coupling techniques, thiol-ene click chemistry and EDC/NHS chemistry.[5-10] All of those techniques have the big disadvantage that they bind the receptor non-site specifically. Copper catalysed alkyne azide click (CuAAC) immobilization of proteins on

polycaprolactone,[11] magnetic beads[12] and star polymers[13] has been reported as well and was proven to be successful. In these examples, the biomolecule is coupled site-directed onto the polymer backbone. For conjugated polymers, probe or receptor immobilization on the backbone is mostly achieved non-covalently,[14] although some cases are known in which a covalent coupling is described. Often, this coupling is achieved via NHS chemistry.[15] The conjugated polymers of choice in most of these cases are polypyrrole and polythiophene, because of their easy synthesis, high conductivity and stability in air.[16] To the best of our knowledge, only one example of CuAAC immobilization of a biomolecule on a conjugated polymer has been described and this was on the end groups of polythiophene.[17] Furthermore, this reaction was done in solution instead of on a film and the immobilized biomolecule was DNA rather than a large functional protein. However, protein immobilization on conjugated polymer films through CuAAC chemistry opens up opportunities for more sensitive and reproducible sensors.

In this work, a covalent coupling strategy was preferred because of its robustness. CuAAC was the reaction of choice because of the applicability in aqueous media. Furthermore, the mild reaction conditions, high yields and bio-orthogonality of the reactive groups, which prevent denaturation caused by side reactions with any of the proteins' natural available functional groups, make this reaction very attractive for biomolecule immobilization.[18] Bio-orthogonality of the immobilization strategy is also of major importance when working towards site-directed coupling of the probes. In this case, all the active binding sites of the biomolecules are maximally exposed to the medium (Figure 1), leading to a higher sensor sensitivity and reproducibility.[4] Furthermore, the covalent immobilization of biomolecules, which are designed by nature to target specific receptors, is also of importance for bio-imaging applications.[19]

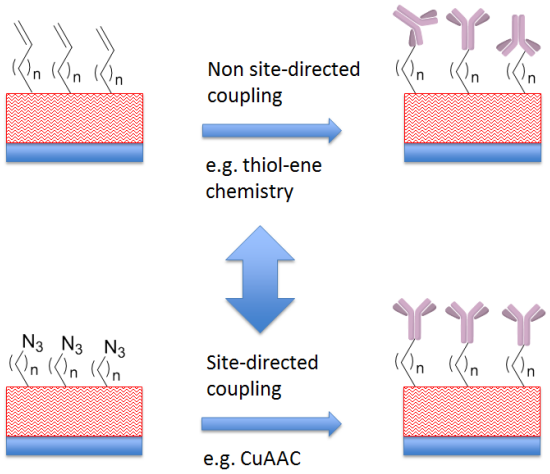

Figure 1: Non site-directed coupling compared to site-directed coupling, wherein all the recognition sites are optimally exposed to the medium.

In this work, the click reaction of randomly alkynylated protein A (SpA) onto conjugated polymer thin films was monitored. The influence of the side chain hydrophilicity on the effectiveness of the CuAAC reaction was investigated by the use of three different polymers **P1**-**P3** (Figure 2). **P1** has hydrophobic octyloxy side chains, in which half of the side chains are end-functionalized with azide groups. **P2** and **P3** have comparable backbone structures to **P1**, but on **P2** the non-functionalized octyloxy side chains are replaced by hydrophilic tetraethylene glycol (TEG) side chains, while on **P3** the azide functionalities are introduced on the TEG side chains.

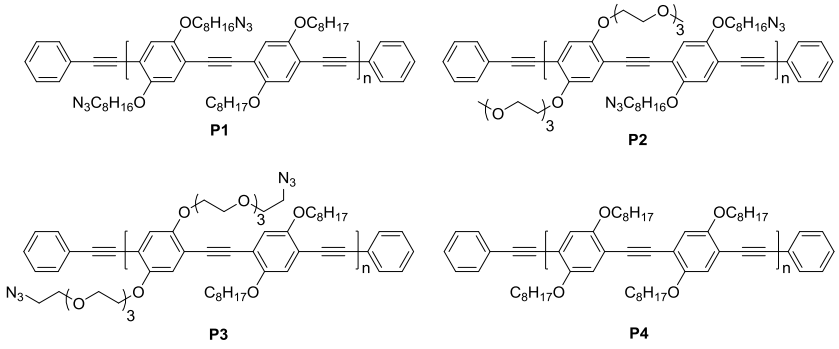

Figure 2: Chemical structures of PPE polymers **P1**–**P4**.

6.2 RESULTS AND DISCUSSION

The click immobilization of biomolecular probes to surfaces is a very important feature for the development of state-of-the-art biosensors. Different parameters must be optimized to obtain high probe loadings onto thin films. CuAAC immobilization of randomly alkynylated SpA on silicon surfaces was recently described.[20] The reaction conditions employed in that work were used as a starting point for the immobilization of randomly alkynylated SpA onto thin PPE films. Randomly alkynylated SpA was chosen to optimize the reaction conditions and to explore the effect of hydrophilic side chains on the binding capacity because it is easily accessible and random alkynylation of the protein is straightforward.

6.2.1 Polymer synthesis and characterization

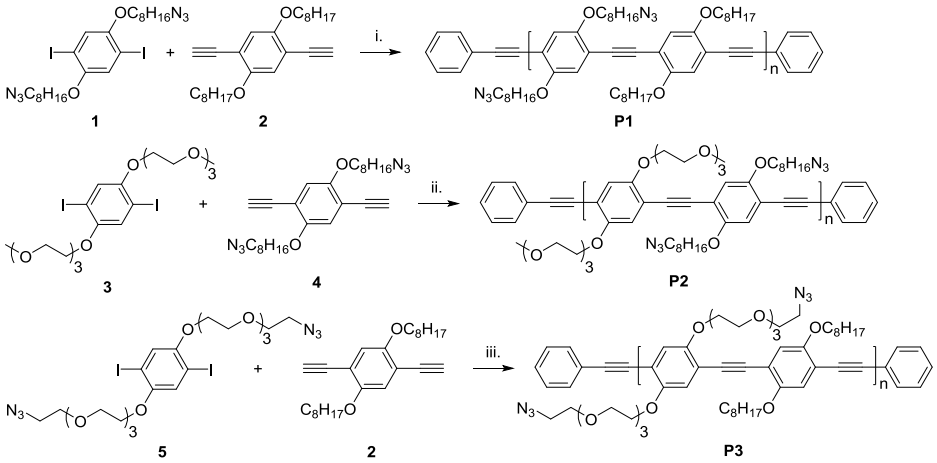

Scheme 1: Synthetic procedures towards azide-functionalized PPE copolymers **P1**, **P2** and **P3**: i. $Pd(PPh_3)_2Cl_2$, CuI, DIPA, toluene, 70 °C, 2 h; 53%; ii. $Pd(PPh_3)_4$, CuI, DIPA, toluene, 70 °C, 3 h; 59%; iii. $Pd(PPh_3)_4$, CuI, DIPA, toluene, microwave, 70 °C, 40 min; 93%.

All known monomers (**1**-**5**, Scheme 1) were synthesized according to literature procedures.[19,21-25] The synthesis of **P1** and **P2** was discussed in detail before.[19,25] The synthesis of **P2** was a bit more complicated due to the oily character of monomer **3**. This was also the case for **P3** and is reflected in the molar masses of both glycolated polymers when compared to **P1**. When

$Pd(PPh_3)_2Cl_2$ was used as the catalyst during the synthesis of **P2**, very low molar masses were obtained, while Pd_2dba_3 led to crosslinked insoluble polymer gels. Using $Pd(PPh_3)_4$ as the catalyst gave the best results (M_n 11.2, $Đ$ 1.8), which was also the case for polymer **P3** (M_n 6.4, $Đ$ 2.1)[19]. The polymer was purified from catalyst residues by precipitation in cold *n*-hexane. Soxhlet extraction was not performed due to the high risk for crosslinking at elevated temperatures.[25]

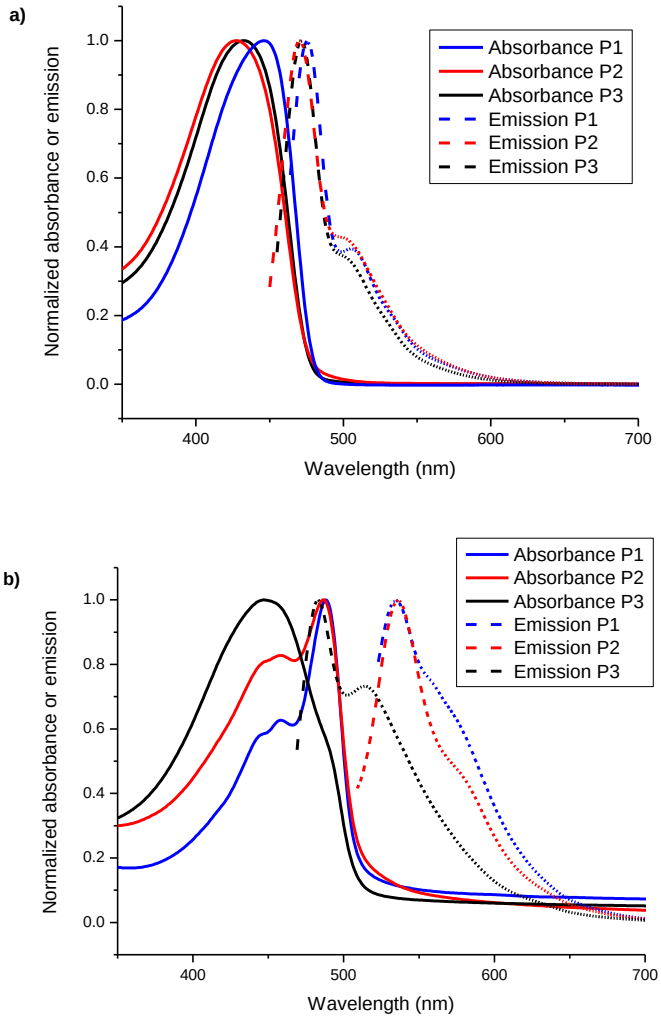

Figure 3: Absorption and emission spectra (normalized) of PPE copolymers **P1**, **P2** and **P3** in a) chloroform solution and b) thin film.

Full characterization of polymer **P2** was performed and the results were compared to those of **P1** and **P3**. The absorption and emission spectra for all three polymers in solution ($CHCl_3$) are comparable. For **P1**, the maximum in both the absorption and emission spectrum is slightly red-shifted as compared to **P2** and **P3** (Figure 3a). For the polymer films (Figure 3b), **P3** shows a different spectrum than **P2** and **P1**. The film characteristics of **P3** are comparable to those in solution (albeit broadened), while strong π-π stacking features appear in the thin films of **P1** and **P2**.
The optical and electrochemical bandgaps of all three polymers were also determined and compared (Table 1). While the optical bandgaps for all three polymers are alike, the electrochemical bandgap of **P1** is slightly larger.

Table 1: Optical and electrochemical data for PPE copolymers **P1−P3**.

Polymer	λ_{max}[a] (nm) solution	λ_{max}[b] (nm) film	E_g^{OPc} (eV)	HOMO[d] (eV)	LUMO[d] (eV)	E_g^{EC}[e] (eV)
P1	446	487	2.43	-5.71	-2.88	2.83
P2	428	486	2.42	-5.66	-3.00	2.66
P3	432	447	2.42	-5.65	-2.99	2.67

[a] In $CHCl_3$. [b] Films were prepared by drop casting a solution of the polymer in $CHCl_3$ onto a quartz disc. [c] Optical bandgap, determined by the onset of the solid-state UV-Vis spectrum. [d] Determined from the onset of oxidation/reduction in cyclic voltammetry. [e] Electrochemical bandgap.

To illustrate the difference in hydrophilicity of the different polymers (**P1** to **P3**) compared to a regular hydrophobic PPE polymer with only octyloxy side chains (**P4**), contact angles of a water drop onto the surface of thin polymer films were determined (Figure 4). The **P4** film (Figure 4a) is, as expected, the most hydrophobic one, with a contact angle of 104°. The **P1** film is more hydrophilic due to the presence of the azide functional groups, which is reflected in a slightly lower contact angle of 95° (Figure 4b). When the non-functionalized octyloxy side chains in **P1** are replaced by TEG chains in **P2**, the polymer film becomes very hydrophilic and a contact angle of only 16° is observed (Figure 4c). When the azide functionalized octyloxy side chains in **P1** are replaced by azide functionalized TEG chains (**P3**), a contact angle of intermediate value

(40°) is observed. The polymer film seems to be more hydrophilic than **P1**, which has no TEG side chains. Furthermore, it is observed that the polymer film is more hydrophobic than the **P2** film (Figure 4d).

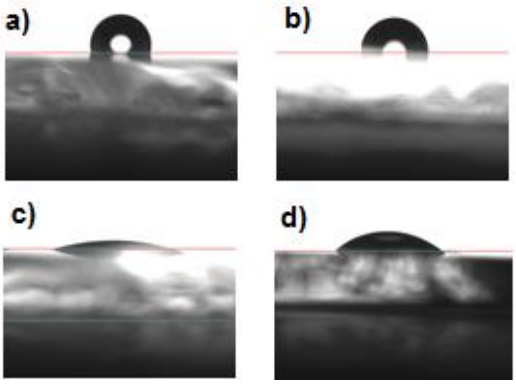

Figure 4: Side views of a water droplet on a) a **P4**, b) a **P1**, c) a **P2**, and d) a **P3** thin film (all deposited on a glass substrate).

6.2.2 Click immobilization of SpA

Thin films (~30 nm, as defined by profilometry) of PPE polymers **P1–P3** were then spin-coated on gold-coated quartz crystals, enabling in situ monitoring of the click reaction on the polymer surface via quartz crystal microbalance with dissipation monitoring (QCM-D) experiments. A range of SpA concentrations (0.1–1 μM) were examined, while the concentrations of $CuSO_4$, tris(3-hydroxypropyltriazolylmethyl)amine (THPTA) and sodium ascorbate (NaAsc) were kept constant.[20] QCM-D experiments for all samples were performed under a flow of 30 μL/min. First, the polymer thin films were rinsed with phosphate-buffered saline (PBS) until a stable baseline was obtained. Then, the reaction mixtures containing randomly alkynylated SpA were ran over the substrate. In all cases, a steep decrease in the oscillation frequency of the quartz crystal was observed. After saturation of the surface (after stabilization of the frequency), PBS was used to wash away any SpA adsorbed on the polymer surface. Only a minor amount of the SpA loosens from the surface, resulting in a small increase in the frequency, after which it stabilizes again. At this point, the mass immobilized on the polymer surface can be calculated by means of the

Sauerbrey equation for rigid layers.[26] To prove that the immobilized SpA is still active after the reaction under click conditions, a solution containing SpA antibody (2 µg/mL, ~ 0.1 nM) was run over the functional polymer surfaces, once again leading to a steep decrease in frequency. After rinsing with PBS, the frequency remained stable, indicating that SpA maintained its initial active form (Figure 5).[25]

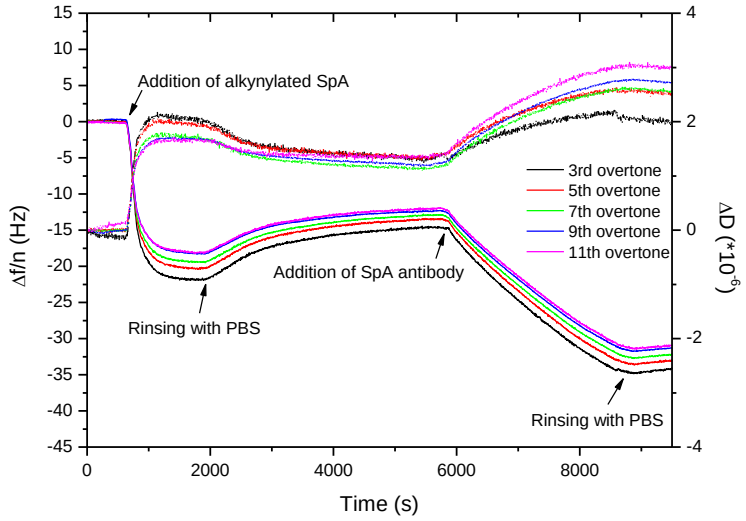

Figure 5: Example of the time evolution of Δ*f*/n and Δ*D* during a QCM-D experiment for the surface functionalization of a **P1** film with randomly alkynylated SpA.

For all samples, the shape of the frequency and dissipation curves in function of time appear quite similar, the only difference being the decrease in frequency after the introduction of the reaction mixtures and SpA antibody solution. This is a consequence of the different concentrations used in the reaction mixtures. A summary of the results can be seen in Figure 6.

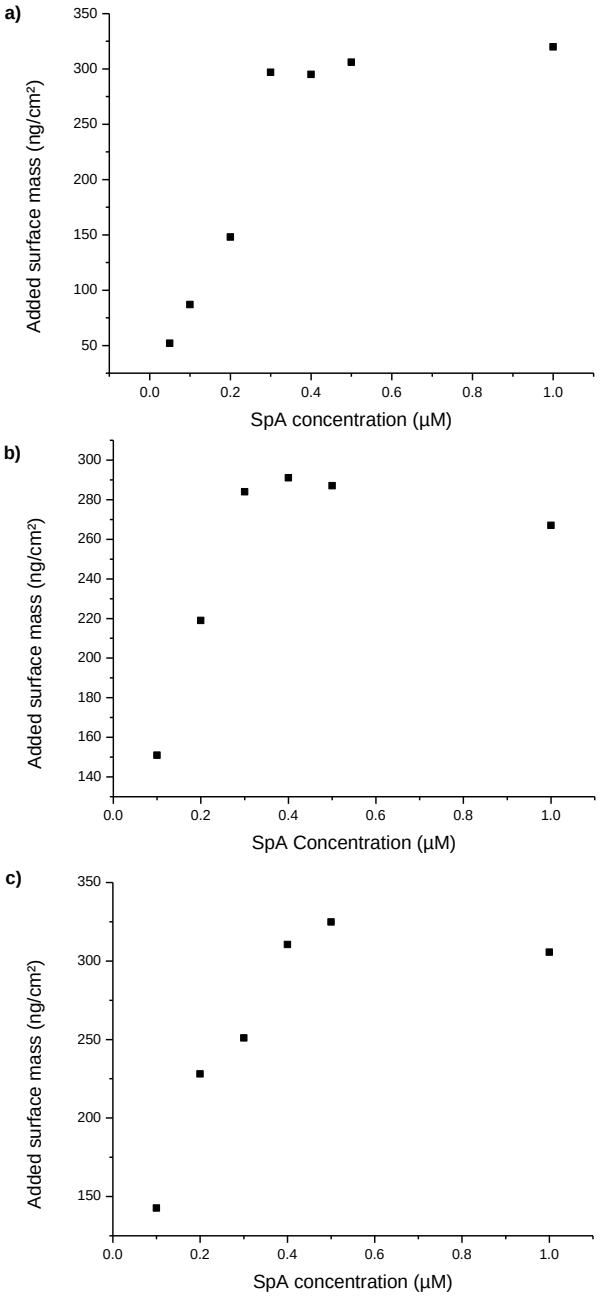

Figure 6: QCM-D results for a) **P1**, b) **P2** and c) **P3** for different SpA concentrations.

From the overview of the QCM-D results at different concentrations, it is clear that for all polymers the surface was saturated when SpA concentrations of 0.4 µM or higher were used. For polymers **P1** and **P2**, a SpA concentration of 0.3 µM was sufficient. The maximal added surface mass was approximately 320 ng/cm² and this value was obtained for polymers **P1** and **P3**. **P2** showed a slightly lower maximal added mass (approx. 290 ng/cm²). It is noteworthy to see that saturation of the surface occurs quite fast (within 20 minutes), while click immobilization is expected to take more time (since the proteins have to rotate into the correct position for click immobilization to occur). Possibly, aspecific adsorption of SpA onto the polymer films might be occurring. This presumption was analyzed by a control experiment for all three polymer films, in which all reaction conditions were kept constant but no copper was added to the reaction mixture, impeding the click reaction (Figure 7). The same frequency decrease due to mass accumulation on the sensor surface could be observed for all polymers, indicating strong aspecific interactions between the protein and the surface. Furthermore, the protein could not be removed by rinsing with PBS, as can be seen in Figure 5. Moreover, even onto the bare gold-coated quartz crystal, strong aspecific adsorption is occurring (Figure 7d). This makes randomly alkynylated SpA an unsuitable candidate for monitoring of the click reaction onto PPE thin films.

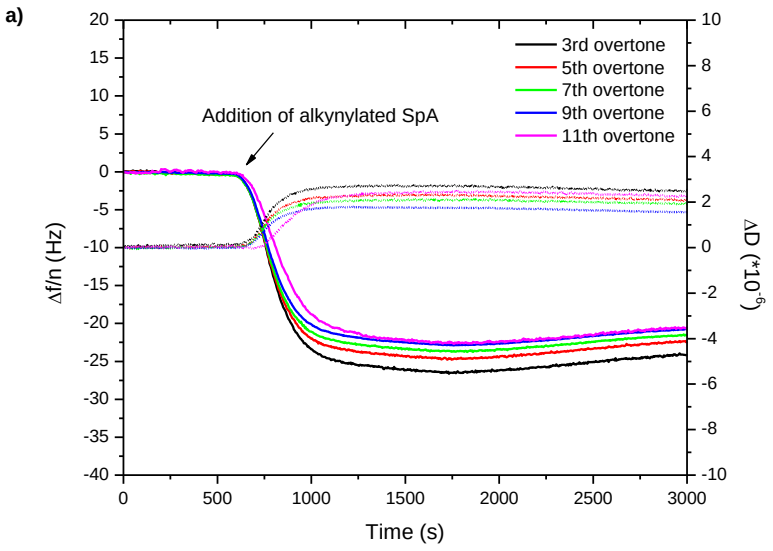

b)

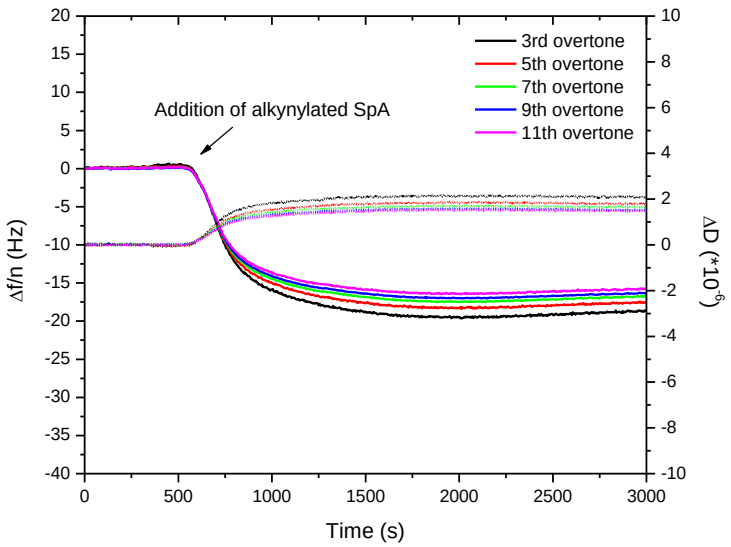
3rd overtone
5th overtone
7th overtone
9th overtone
11th overtone
Addition of alkynylated SpA
Δf/n (Hz)
ΔD (*10⁻⁶)
Time (s)

c)

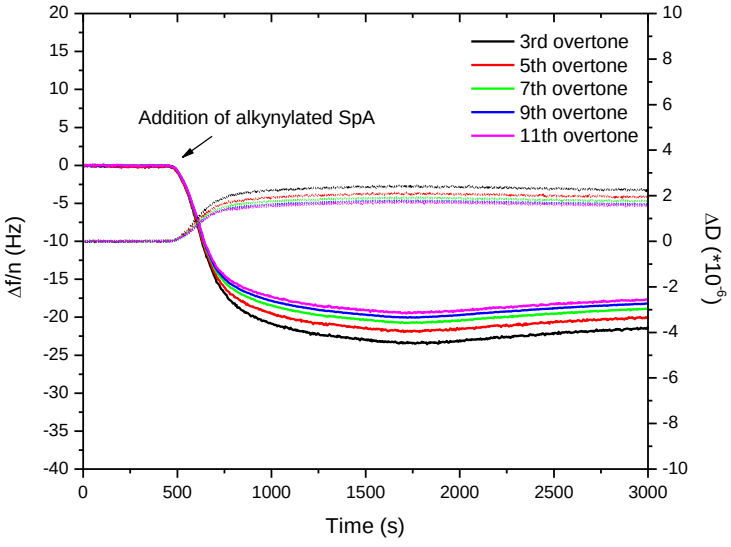
3rd overtone
5th overtone
7th overtone
9th overtone
11th overtone
Addition of alkynylated SpA
Δf/n (Hz)
ΔD (*10⁻⁶)
Time (s)

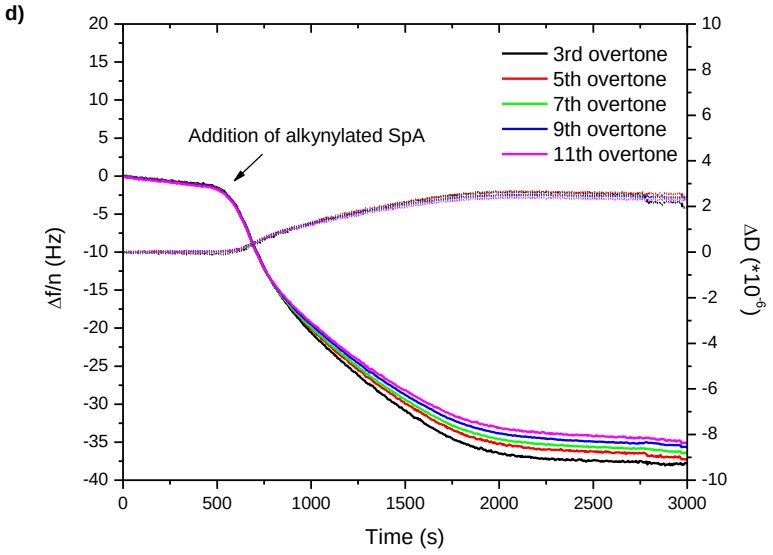

Figure 7: Time evolution of Δ*f*/n and Δ*D* during QCM-D experiments with randomly alkynylated SpA (0.5 µM) in the absence of copper towards surface functionalization of a) **P1**, b) **P2**, c) **P3** and d) a Au-coated quartz crystal.

To prevent aspecific interactions between the 'click molecule' and the polymer film, alkynylated poly(ethylene glycol)$_{300}$-acid (Alkyne-PEG$_{300}$-COOH, with an average molar mass of 300, Figure 8) was selected. The click reaction conditions used for randomly alkynylated SpA were maintained and click immobilization was examined on a **P1** film (Figure 9).

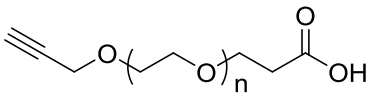

Alkyne-PEG$_{300}$-COOH
Alkyne-PEG$_{2000}$-COOH

Figure 8: Chemical structures of Alkyne-PEG$_{300}$-COOH and Alkyne-PEG$_{2000}$-COOH.

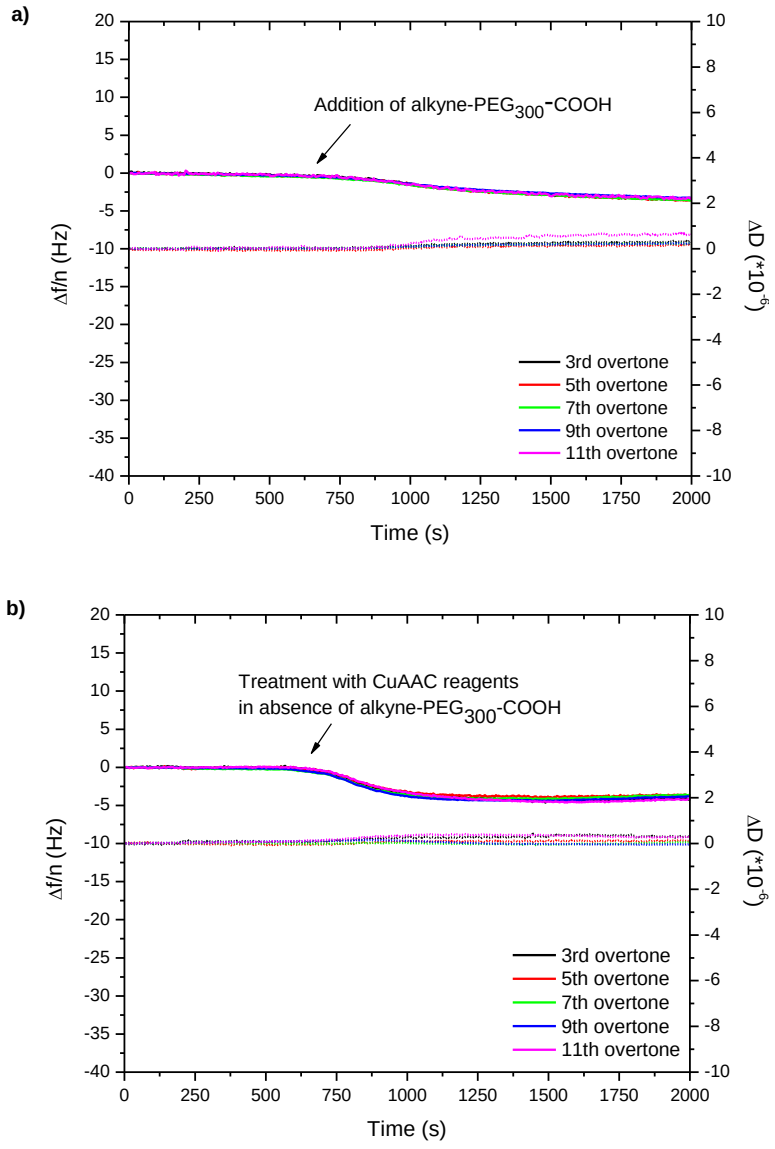

Figure 9: Time evolution of Δ*f*/n and Δ*D* during a QCM-D experiment of the surface treatment of a) **P1** with alkyne-PEG_{300}-COOH (0.5 μM) under CuAAC conditions and b) **P1** under CuAAC conditions in the absence of alkyne-PEG_{300}-COOH.

A small decrease in sensor frequency could be observed after the injection of the reaction mixture (Figure 9a), but the control experiment in the absence of

alkyne-PEG_{300}-COOH shows the same frequency drop (Figure 9b). Since copper is added in a large excess, this frequency change can possibly be ascribed to copper complexes that are formed on the polymer film surface. However, since the molar mass of the alkyne-PEG_{300}-COOH chains is rather small, only small perturbations in the frequency curve are expected after click reaction. To increase the signal-to-noise ratio, an alkynylated PEG chain with a higher average mass (Alkyne-PEG_{2000}-COOH) was employed for click immobilization on **P1**.

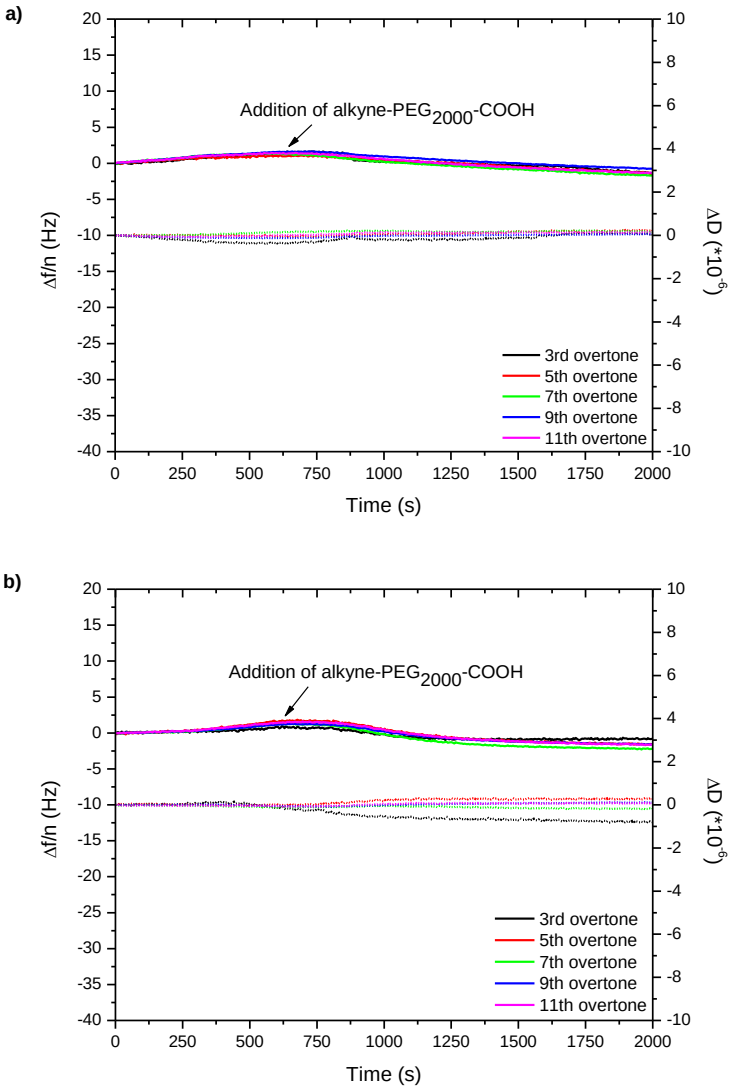

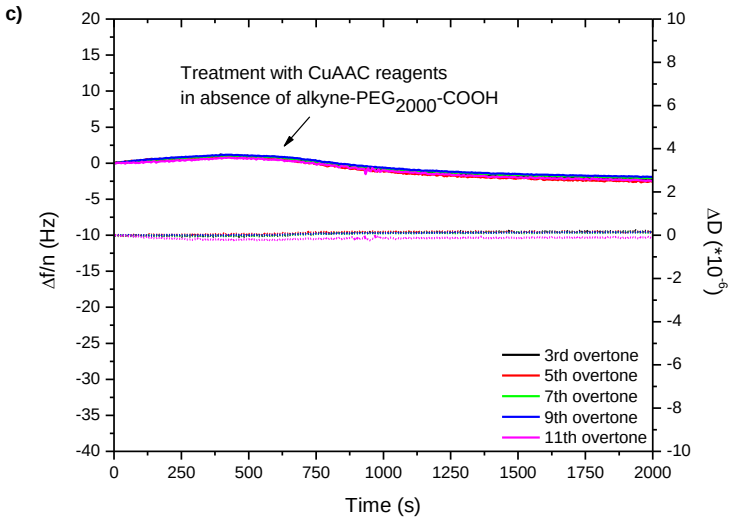

Figure 10: Time evolution of Δ*f*/n (solid lines) and Δ*D* (dashed lines) during a QCM-D experiment of the surface treatment of a) **P1** with alkyne-PEG_{2000}-COOH (0.5 µM) under CuAAC conditions, b) **P1** with alkyne-PEG_{2000}-COOH (50 µM) under CuAAC conditions and c) **P1** under CuAAC conditions in the absence of alkyne-PEG_{2000}-COOH.

Also in this case, only a small decrease in frequency could be observed (Figure 10a), which was also seen in the control experiment without alkyne-PEG_{2000}-COOH (Figure 10c). To push the reaction, a 100-fold larger concentration of the alkynylated PEG_{2000}-COOH was added to the reaction mixture, but also here no larger frequency drop could be observed (Figure 10b).

Finally, the click immobilization of randomly alkynylated NbBCII10, a β-lactamase recognising nanobody, was investigated on a **P1** film. Once more, the reaction conditions developed for randomly alkynylated SpA immobilization were extended to those experiments. Unfortunately, the observed frequency drop (Figure 11a) was comparable to the one observed for the control experiment (Figure 11b), indicating that no click immobilization was occurring.

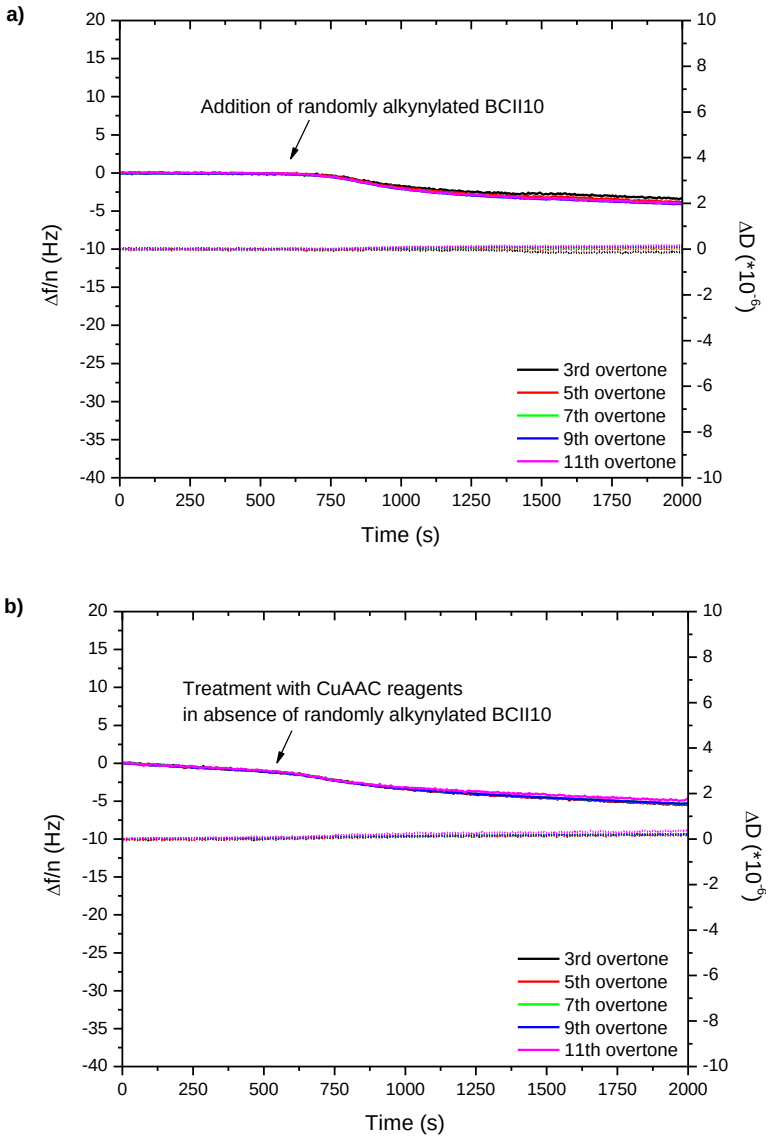

Figure 11: Time evolution of Δ*f*/n and Δ*D* during a QCM-D experiment of the surface treatment of a) **P1** with randomly alkynylated NbBCII10 (0.5 µM) under CuAAC conditions and b) **P1** under CuAAC conditions in the absence of randomly alkynylated NbBCII10.

6.3 CONCLUSIONS

Since specificity is of main importance for biosensing, the immobilization of particular receptors onto thin polymer films is of great interest. Most often, small molecular recognition groups are introduced via reactions forming stable and strong amide bonds. When small molecules or functional groups are used as recognition sites, this offers no difficulties. However, since biomolecules are receptors designed by nature to bind specific targets, the use of those large bioreceptors might increase the selectivity of sensors, hence making them more interesting than small molecule counterparts. For the formation of amide bonds between the polymer and the receptor, carboxylic acid or amine groups are needed. However, this leads to immobilization in random directions, possibly with unwanted amino acids, leading to denaturation or activity loss of the natural receptors. Furthermore, the recognition sites of the receptors might be turned away from the medium, leading to lower sensitivities.

To improve on this, CuAAC chemistry was proposed, because both alkyne and azide groups are bio-orthogonal and the reaction can be conducted under mild reaction conditions in aqueous media. Thin films were prepared from three different PPE polymers, each consisting of the same backbone structure but with different side chains to vary the hydrophilicity of the polymer film. SpA was randomly alkynylated and click immobilization onto the three polymer films was monitored by QCM-D. For all films, saturation of the surface occurred within 20 minutes after the addition of the reaction mixture. The saturation density and speed was equal for all different polymer layers. A control experiment showed, however, that the same trend could be observed in the absence of copper, indicating that aspecific adsorption on the surface occurred.

Alkynylated PEG-COOH with two different molar masses was tested under the same reaction conditions as SpA, trying to circumvent the aspecific interactions, but no click immobilization was observed, even not after a 100-fold concentration increase. As a last resort, the randomly alkynylated NbBCII10 was assessed, but also in this case, no immobilization on the surface could be observed. Those failed experiments indicate that click immobilization on those PPE surfaces is troublesome, at least using the experimental set-up elaborated herein.

6.4 EXPERIMENTAL SECTION

6.4.1 Materials and instruments

NMR chemical shifts (δ, in ppm) were determined relative to the residual $CHCl_3$ (7.26 ppm) absorption or the ^{13}C resonance shift of $CDCl_3$ (77.16 ppm). UV-Vis measurements were performed on a VARIAN Cary 5000 UV-Vis-NIR spectrophotometer at a scan rate of 600 nm/min. The films for the UV-Vis measurements were prepared by drop casting a solution of the polymer in chloroform on a quartz substrate. The solid-state UV-Vis spectra were used to estimate the optical bandgaps (from the wavelength at the intersection of the tangent line drawn at the low energy side of the absorption spectrum with the baseline: E_g (eV) = 1240/(wavelength in nm)). Lamp corrected steady-state emission spectra were recorded on a fluorimeter using a band pass of 1 nm for the excitation monochromator and a scanning speed of 1 nm/s. Spectra were collected at room temperature at an excitation wavelength of 446 (**P1**), 428 (**P2**) and 432 nm (**P3**) in $CHCl_3$ solution and 488 (**P1**), 484 (**P2**) and 444 nm (**P3**) for the thin films (without deoxygenation). Analysis of the molar masses and molar mass distributions of the polymers was performed on a Tosoh EcoSEC System, comprising of an autosampler, a PSS guard column SDV (50 x 7.5 mm), followed by three PSS SDV analytical linear XL columns (5 µm, 300 x 7.5 mm) and a UV-detector using THF as the eluent at 40 °C with a flow rate of 1.0 mL/min. The SEC system was calibrated using linear narrow polystyrene standards ranging from 474 to 7.5 x 10^6 g/mol (K = 14.1 x 10^{-5} dL/g and α = 0.70). Electrochemical measurements (cyclic voltammetry) were performed with an Eco Chemie Autolab PGSTAT 30 potentiostat/galvanostat using a three-electrode microcell with a platinum working electrode, a platinum counter electrode and a $Ag/AgNO_3$ reference electrode (silver wire dipped in a solution of 0.01 M $AgNO_3$ and 0.1 M NBu_4PF_6 in anhydrous acetonitrile). The reference electrode was calibrated against ferrocene/ferrocenium as an external standard. Samples were prepared by dip coating the platinum working electrode in the respective polymer solutions (also used for the solid-state UV-Vis measurements). The CV measurements were done on the resulting films with 0.1 M NBu_4PF_6 in anhydrous acetonitrile as electrolyte solution. To prevent air from entering the system, the experiments were carried out under a curtain of

argon. Cyclic voltammograms were recorded at a scan rate of 100 mV s^{-1}. For the conversion of V to eV, the onset potentials of the first oxidation/reduction peaks were used and referenced to ferrocene/ferrocenium, which has an ionization potential of −4.98 eV *vs.* vacuum. This correction factor is based on a value of 0.31 eV for Fc/Fc^+ *vs.* SCE[27a] and a value of 4.68 eV for SCE *vs.* vacuum[27b]: $E_{HOMO/LUMO}$ (eV) = −4.98 − $E_{onset\ ox/red}^{Ag/AgNO3}$ (V) + $E_{onset\ Fc/Fc+}^{Ag/AgNO3}$ (V). SpA (Cowan strain, recombinant, *Staphylococcus aureus subsp. aureus* strain NCTC 8325, expressed in *E. coli*) and human IgG were obtained from Thermo Scientific. NbBCII10 was kindly provided by prof. S. Muyldermans (VUB). Contact angle measurements were performed with a dataphysics OCA 15+ goniometer (Filderstadt, Germany). Contour ellipse fitting of the water droplets was done by the SCA 1.0 software. The droplet size was 1 L dispensed at 0.1 L/s. Alkyne-PEG_{300}-COOH and alkyne-PEG_{2000}-COOH were purchased from nanocs.

6.4.2 Synthesis

All known monomers (**1**, **2**, **4** and **5**, Scheme 2) were synthesized according to literature procedures.[19,21-25]

1,4-bis(2-(2-(2-methoxyethoxy)ethoxy)ethoxy)benzene (3). Modified procedure:[24] Hydroquinone (1.43 g, 13.0 mmol) and K_2CO_3 (14.25 g, 105 mmol) were dissolved in dry DMF (15 mL). After heating the solution to 100 °C, 1-chloro-2-(2-(2-methoxyethoxy)ethoxy)ethane (5.00 g, 27.4 mmol) was added dropwise. After stirring for 20 h, the reaction mixture was cooled down to room temperature. The precipitate was filtered off and rinsed with diethyl ether. Water was added to the filtrate and the mixture was acidified with HCl (1M). The water layer was extracted with diethyl ether (3x), after which the organic layer was washed with NaOH solution (2.5 M), water (2x) and brine (1x) and dried over $MgSO_4$. After filtration and removal of the solvent, the excess side chains were removed by kugelrohr distillation (T = 95 °C, p = $2*10^{-2}$ mbar) and the pure product was obtained as a colourless oil (1.63 g, 31%). ^1H NMR (400 MHz, $CDCl_3$): δ (ppm) 6.82 (s, 4H), 4.07−4.04 (m, 4H), 3.82−3.80 (m, 4H), 3.73−3.70 (m, 4H), 3.68−3.63 (m, 8H), 3.54−3.52 (m, 4H), 3.36 (s, 6H).

P1 (SEC (THF): M_n 20.8 kg/mol, $Đ$ 2.7)[25] and **P3** (SEC (THF): M_n 6.4 kg/mol, $Đ$ 2.1)[19] were prepared according to reported procedures.

P2. A mixture of dry toluene (3.2 mL) and diisopropylamine (1.3 mL) was degassed for 5 min. 1,4-Bis(8-azidooctyloxy)-2,5-diethynylbenzene (0.051 g, 0.111 mmol), 1,4-diiodo-2,5-bis(2-(2-(2-methoxyethoxy)ethoxy)ethoxy)-benzene (0.070 g, 0.108 mmol), CuI (1.0 mg, 5 mol%) and $Pd(PPh_3)_4$ (3.8 mg, 5 mol%) were added and the mixture was stirred for 3 h at 70 °C. The polymer was end-capped by adding an excess of iodobenzene (2 drops), after which it was stirred for 30 min at 70 °C. Then, an excess of phenylacetylene (2 drops) was added and the mixture was stirred again for 15 min at 70 °C. After cooling down to room temperature, the resulting polymer was precipitated in hexane at 0 °C and filtered off, yielding a sticky orange solid (55.4 mg, 59%). SEC (THF): M_n 11.2 kg/mol, $Đ$ 1.8; ^{1}H NMR (400 MHz, $CDCl_3$), δ (ppm): 7.05–6.92 (m, 4H), 4.29–4.16 (m, 4H), 4.09–3.97 (m, 4H), 3.94–3.87 (m, 4H), 3.78–3.74 (m, 4H), 3.60–3.57 (m, 8H), 3.54–3.46 (m, 4H), 3.36–3.32 (m, 6H), 3.27–3.17 (m, 4H), 1.88–1.82 (m, 4H), 1.55–1.45 (m, 4H), 1.40–1.27 (m, 12H). IR (NaCl), ν_{max} (cm^{-1}): 2967, 2925, 2182.

Randomly alkynylated SpA and NbBCII10 were prepared according to reported procedures.[20]

6.4.3 QCM-D

QCM-D is an acoustic surface-sensitive technique based on the inverse piezoelectric effect. An AC voltage is applied over the sensor electrodes, which causes an oscillation of the piezoelectric quartz crystal at its acoustic resonance frequency. This results in a transverse acoustic wave that propagates across the crystal, reflecting back into the crystal at the surface. After turning off the AC voltage, the oscillation amplitude decays exponentially. This decay is recorded and the frequency (f) and the energy dissipation factor (D) of different overtones are extracted.[28] The dissipation is the ratio between the dissipated energy during one vibration cycle and the total kinetic and potential energy of the crystal at that moment. A Q-sense E4 instrument (Gothenborg, Sweden) monitoring the frequency shift (Δf) and the dissipation change (ΔD) was used

with AT-cut quartz crystals with Au coating (diameter 14 mm, thickness 0.3 mm, surface roughness 3 nm and resonant frequency 4.95 MHz). The QCM crystals were first cleaned with chloroform, then with a 5:1:1 mixture of Milli-Q water, ammonia and hydrogen peroxide and afterwards with acetone. The sensors were UV-ozone treated with a Digital PSD series UV-ozone system from Novascan for 15 min. The changes in Δf and ΔD were monitored at five different overtones (from the 3rd to the 11^{th} overtone, the fundamental frequency is rather unstable since it may be disturbed by the O-ring). The experiments were carried out at 25 °C. The measurements were done in flow mode with a flow rate of 30 µL/min.

6.5 REFERENCES

[1] (a) C. E. Halkyard, M. E. Rampey, L. Kloppenburg, S. L. Studer-Martinez and U. H. F. Bunz, *Macromolecules*, 1998, **31**, 8655. (b) T. Miteva, L. Palmer, L. Kloppenburg, D. Neher and U. H. F. Bunz, *Macromolecules*, 2000, **33**, 652. (c) J. J. Lavigne, D. L. Broughton, J. N. Wilson, B. Erdogan and U. H. F. Bunz, *Macromolecules*, 2000, **36**, 7409. (d) J. N. Wilson, Y. Q. Wang, J. J. Lavigne and U. H. F. Bunz, *Chem. Commun.*, 2003, 1626.

[2] U. H. F. Bunz, Poly(arylene ethynylene)s: From synthesis to application, 2005, Springer.

[3] (a) D. T. McQuade, A. E. Pullen and T. M. Swager, *Chem. Rev.*, 2000, **100**, 2537. (b) S. W. Thomas, G. D. Joly and T. M. Swager, *Chem. Rev.*, 2007, **107**, 1339. (c) H. Dong, X. Cao and C. M. Li, *ACS Appl. Mater. Interfaces*, 2009, **1**, 1599. (d) S. Rochat and T. M. Swager, *ACS Appl. Mater. Interfaces*, 2013, **5**, 4488. (e) U. H. F. Bunz, K. Seehafer, M. Bender and M. Porz, *Chem. Soc. Rev.*, 2015, **44**, 4322.

[4] E. Steen Redeker, D. T. Ta, D. Cortens, B. Billen, W. Guedens and P. Adriaensens, *Bioconjugate Chem.*, 2013, **24**, 1761.

[5] J. Chung, E. T. Hwang, H. Gang and M. B. Gu , *React. Funct. Polym.*, 2013, **73**, 39.

[6] E. K. U. Larsen, M. B. L. Mikkelsen and N. B. Larsen, *Biomacromolecules*, 2014, **15**, 894.

[7] C. A. DeForest and K. S. Anseth, *Angew. Chem*., 2012, **124**, 1852.

[8] P. Kumar, S. K. Agarwal and K. C. Gupta, *Bioconjugate Chem.*, 2004, **15**, 7.

[9] J. Park, S. Kurosawa, M. Takai and K. Ishihara, *Colloids Surf., B.*, 2007, **55**, 164.

[10] D. Sung, D. H. Shin and S. Jon, *Biosens. Bioelectron.*, 2011, **26**, 3967.

[11] F. Lin, J. Zheng, J. Yu, J. Zhou and M. L. Becker, *Biomacromolecules*, 2013, **14**, 2857.

[12] G. Bayramoglu, O. Celikbicak, M. Y. Arica and B. Salih, *Ind. Eng. Chem. Res.*, 2014, **53**, 4554.

[13] S. Averick, E. Paredes, W. Li, K. Matyjaszewski and S. R. Das, *Bioconjugate Chem.*, 2011, **22**, 2030.

[14] P. Cooreman, R. Thoelen, J. Manca, M. vandeVen, V. Vermeeren, L. Michiels, M. Ameloot and P. Wagner, *Biosens. Bioelectron.*, 2005, **20**, 2151.

[15] (a) R. Janmanee, S. Chuekachang, S. Sriwichai, A. Baba and S. Phanichphant, *J. Nanotechnol.*, 2012, **1**, 1. (b) F. Ekiz, F. Oguzkaya, M. Akin, S. Timur, C. Tanyeli and L. Toppare, *J. Mater. Chem.*, 2011, **21**, 12337. (c) J. H. Wosnick, C. M. Mello and T. M. Swager, *J. Am. Chem. Soc.*, 2005, **127**, 3400. (d) W. Tang, M. L. Becker, *Chem. Soc. Rev.*, 2014, **43**, 7013.

[16] H. Dong, X. Cao and C. M. Li, *ACS Appl. Mater. Interfaces*, 2009, **1**, 1599.

[17] J. K. Lee, S. Ko and Z. Bao, *Macromol. Rapid Commun.*, 2012, **33**, 938.

[18] (a) V. D. Bock, H. Hiemstra and J. H. van Maarseveen, *Eur. J. Org. Chem.*, 2006, **1**, 51. (b) C. Barner-Kollowik, F. E. Du Prez, P. Espeel, C. J. Hawker, T. Junkers, H. Schlaad and W. Van Camp, *Angew. Chem. Int. Ed.*, 2011, **50**, 60. (c) L. Liang and D. Astruc, *Coord. Chem. Rev.*, 2011, **255**, 2933.

[19] L. D'olieslaeger, Y. Braeken, S. Cheruku, J. Smits, M. Ameloot, D. Vanderzande, W. Maes and A. Ethirajan, *J. Colloid Interface Sci.*, 2017, **504**, 527.

[20] T. Vranken, E. Steen Redeker, A. Miszta, B. Billen, W. Hermens, B. de Laat, P. Adriaensens, W. Guedens and T. J. Cleij, *Sens. Actuator B-Chem.*, 2017, **238**, 992.

[21] H. Liu, Z.-B. Gao, Z. Yao, S. Zheng, Y. Li, W. Zhu, X. Tan, X. Luo, J. Shen, K. Chen, G.-Y. Hu and H. Jiang, *J. Med. Chem.*, 2007, **50**, 83.

[22] M. Asakawa, P. R. Ashton, S. E. Boyd, C. L. Brown, R. E. Gillard, O. Kocian, F. M. Raymo, J. F. Stoddart, M. S. Tolley, A. J. P. White and D. J. Williams, *J. Org. Chem.*, 1997, **62**, 26.

[23] P. I. Abronina, A. I. Zinin, A. V. Orlova, S. L. Sedinkin and L. O. Kononov, *Tetrahedron Lett.*, 2013, **54**, 4533.

[24] A. R. G. Srinivas, T. E. Kerr-Phillips, H. Peng, D. Barker and J. Travas-Sejdic, *Polym. Chem.*, 2013, **4**, 2506.

[25] Y. Braeken, P. Verstappen, L. Lutsen, D. Vanderzande and W. Maes, *Polym. Chem.*, 2015, **6**, 6720.

[26] (a) G. Sauerbrey, *Z. Phys.*, 1959, **155**, 206. (b) D. Buttry, Electroanalytical chemistry, Volume 17 - Applications of the QCM to electrochemistry, CRC Press, 1991.

[27] (a) J. Bard and L. R. Faulkner, Electrochemical methods: fundamentals and applications, Wiley, 2001. (b) S. Trasatti, *Pure Appl. Chem.*, 1986, **58**, 955.

[28] C. A. Keller and B. Kasemo, *Biophys. J.*, 1998, **75**, 1397.

6.6 SUPPORTING INFORMATION

^{1}H NMR spectrum of P2

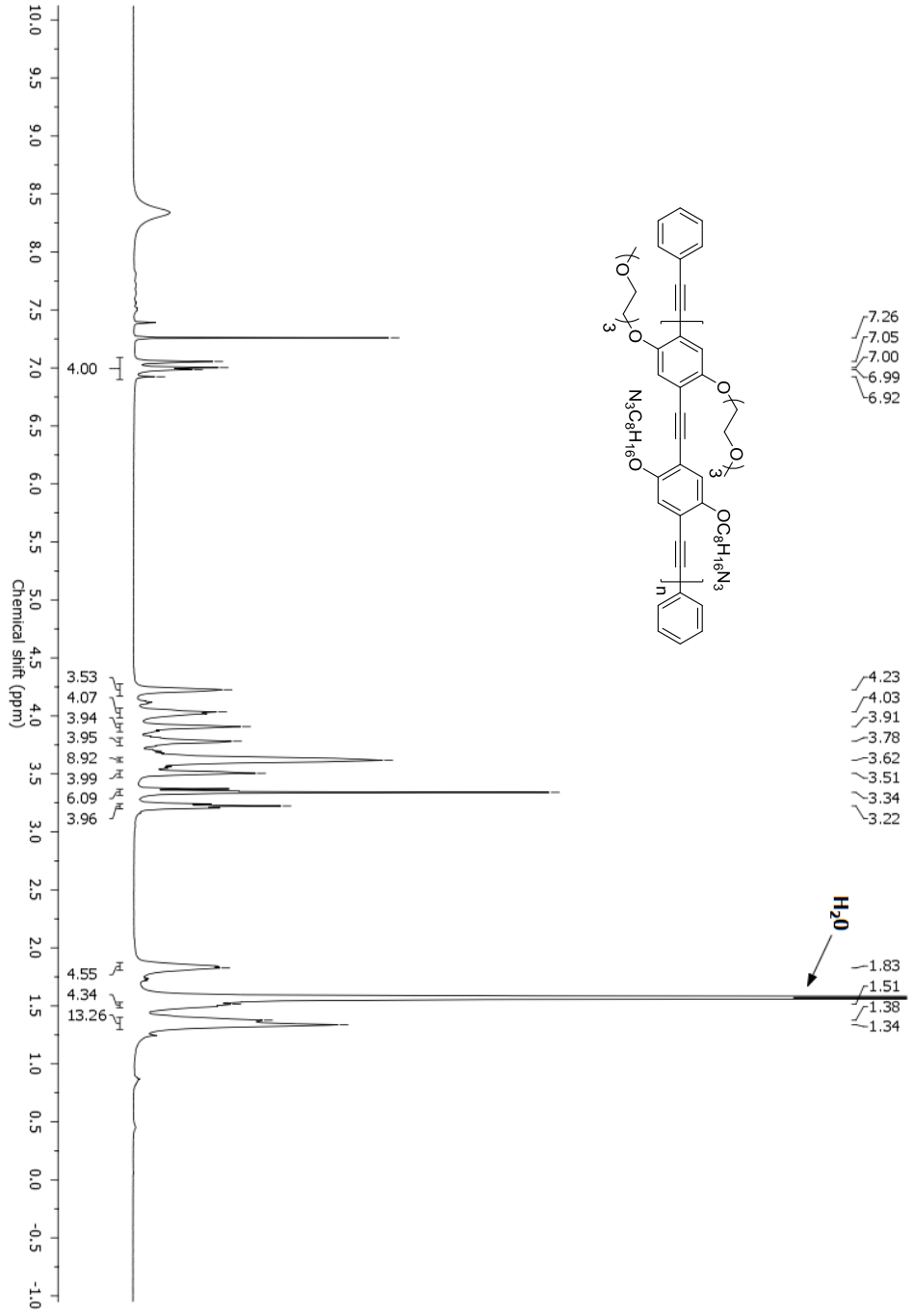

Chapter 7

Summary and Outlook

7.1 SUMMARY

In the medical sector, imaging of fractures, tumors, vains etc. is of high importance to make correct diagnoses and to propose treatments. However, most of the imaging techniques used nowadays are expensive and they are damaging to tissue. Conjugated polymers are of interest to this field because they exhibit excellent optical properties, and they are generally non-cytotoxic. Research into the use of those materials as fluorescent probes for optical imaging is ongoing. For applications in biological media, water solubility is key. Therefore, different techniques to make these conjugated polymers soluble in aqeous environment have been developed. By the introduction of charges on the polymer side chains or backbones, hydrophilicity is increased, leading to a better solubility. However, the most frequently employed technique is the formation of conjugated polymer dispersions in water, by which nanoscale conjugated polymer particles are formed. Unfortunately, the dense packing of the emissive polymer chains in a particle induces fluorescence quenching. In this PhD thesis, an overview was given of the different strategies to improve particle emission (Chapter 2), going from the introduction of bulky side chains and matrix materials to playing around with monomer ratios and polymer freezing in the relaxed state. Furthermore, particle functionalization is important for specific labelling of cells or organelles. A wide variety of functional groups to achieve (bio)conjugation have been studied. The most employed functional moieties are carboxylic acids and *N*-hydroxy succinimides, which lead to stable amide bonds. Possible alternatives are phenylboronic acid groups, β-cyclodextrins and click

functionalities (alkynes, azides, maleimides, ...). When the particles are able to target specific cells, they can act as theranostics, meaning that they can also act as a therapeutic agent by the release of encapsulated drug molecules or by triggering the formation of reactive oxygen species.

Poly(*p*-phenylene ethynylene)s (PPEs) are interesting materials to be used in biosensors as well as imaging probes due to their simple but rigid backbone structure. Moreover, their bandgap is easily adjustable to the application by the introduction of acceptor moieties into the backbone, while the side chains open a lot of opportunities for the introduction of functional groups for the immobilization of (bio)conjugates. The investigation of different synthetic routes towards azide-functionalized PPEs is described in Chapter 3 of this thesis. The azide functionalities are interesting handles for post-polymerization functionalization via copper catalysed alkyne-azide click (CuAAC) chemistry. The azide groups are introduced on the polymer octyloxy side chains, and this in a pre- or post-polymerization functionalization approach. For all of the obtained copolymers, dispersities were comparable ($Đ$ = 2.1−2.4), but some variations in the molar masses of the PPEs synthesized via the different routes were observed. The introduction of azide functionalities on the diiodo-substituted monomers before polymerization leads to the best results (M_n = 28.6 kg/mol). Since alkyne end groups have an influence on gelation of the polymers during reaction (work-up) or processing of the polymers at elevated temperature, end-capping of all copolymers was done. Furthermore, as a proof-of-principle, a first click reaction onto the azidified polymer with phenylacetylene was successfully performed (in solution).

The polymer developed in Chapter 3 was formulated into nanoparticles and its properties were compared to those of a more hydrophobic PPE without azide functionalities and a more hydrophilic polymer where the azide functionalities were introduced onto tetraethylene glycol (TEG) side chains (Chapter 4). The influence of the functionalization pattern on the size and the optical properties of the resulting PPE nanoparticles was studied using transmission electron microscopy, dynamic light scattering, UV-Vis absorption and fluorescence spectroscopy. The polymer containing azide functionalized TEG chains afforded larger particles (188 nm compared to 78 nm for non-azidified polymer and 87 nm for the azidified hydrophobic polymer), which can be attributed to hydration

of the outer layer and the interior of the more hydrophilic polymer particles. However, this did not impact the fluorescence quantum yield of the nanoparticles. The two azide functionalized PPE particles exhibited the highest quantum yields (13%). As a proof-of-principle, a fluorescent dye was also clicked onto the CPNPs after particle formation.

In this thesis, we also introduced a new methodology to improve the photoluminescence quantum yield (PLQY) of conjugated polymer nanoparticles (CPNPs). The synthesis of PPE networks, which are formed by the inclusion of 2D (1,3,5-tribromobenzene) or 3D (2,2',7,7'-tetrabromo-9,9'-spirobifluorene) crosslinkers, is described in Chapter 5. The crosslinkers bridge the different polymer chains and thereby prevent tight stacking in the nanoparticles. Amounts of 3 and 5 mol% of the linkers were introduced during the Sonogashira polymerization reaction and CPNPs were synthesized of all samples. The PLQY of the nanoparticles doubled (from 5% for the linear polymer to 11%) when 5 mol% of 1,3,5-tribromobenzene was introduced and also the fluorescence brightness doubled for each of the crosslinkers when added in 5 mol%. Crosslinker incorporation also seemed to have no influence on the facile particle internalization in cells.

Since polymer functionalization is of huge importance to obtain high selectivity for sensing applications, CuAAC functionalization of a randomly alkynylated biological probe (protein A (SpA)) on PPE films was monitored via quartz-crystal microbalance with dissipation monitoring (QCM-D) in the final Chapter 6. Furthermore, click immobilization is also of interest for (bio)molecule immobilization on CPNPs. A comparison between three different PPE films was made. The first PPE polymer had octyloxy side chains of which 50% were azide terminated. In the second PPE, the non-azide terminated side chains were replaced by TEG side chains while in the third PPE, 50% of azide-terminated TEG side chains were introduced (while the non-functionalized octyloxy side chains are maintained). The variation in side chains caused changes in hydrophilicity of the PPE films. Unfortunately, aspecific interactions between SpA and any of the surfaces made the interpretation of the results troublesome. To circumvent adsorption to the surface, alkynylated oligoethylene glycols were exposed to the surfaces under the same reaction conditions, but here no response could be observed by QCM-D, not even when the concentration was increased 100-fold.

As a last option, the films were exposed to randomly alkynylated NbBCII10, but also in this case, no response was detected.

7.2 OUTLOOK

In this thesis, azide functionalities were successfully introduced onto the side chains of PPEs. CPNPs were prepared of those polymers and their properties were compared to PPE CPNPs without these functionalities. Polymers containing azide terminated side chains have higher PLQYs than CPNPs synthesized from standard PPEs. These functionalities are not only of interest for an increase in emission, they are also important for click immobilization of (bio)molecules that are usefull for specific targeting. Unfortunately, standard PPE CPNPs have emission maxima at approximately 530 nm. Strongly electron accepting moieties could be introduced into the PPE backbone to lower the bandgap and red-shift the emission to the near infrared (NIR) region. This is beneficial for bio-imaging purposes because the background emission is low in this wavelength range. Furthermore, those long wavelengths are not damaging to tissue and ensure deep tissue penetration. Typical acceptor monomers employed to lower conjugated polymer bandgaps for organic photovoltaics are thieno[3,4-*c*]pyrrole-4,6-dione (TPD), diketopyrrolopyrrole (DPP) and benzothiadiazole (BT).[1]

Also in this thesis, a new strategy to improve the PLQY of CPNPs has been disclosed. By introducing 1,3,5-tribromobenzene, a 2D-crosslinker, to the Sonogashira polymerization reaction, PPE networks were formed. Those networks were formulated into CPNPs and the quantum yield of those particles doubled compared to the CPNPs synthesized from the linear PPE. The same trend could be observed for the fluorescence brightness of the particles. However, the maximal PLQY obtained with the PPE-NPs was only 13%. It would be interesting to test this strategy on linear CPs with higher emission efficiencies. Typical examples described in literature are variations of poly(fluorene-*alt*-benzothiadiazole) (PFBT), which can reach PLQYs over 50% when formulated into NPs.[2,3] In a later step, it would be interesting to introduce azide functionalities on those polymers as well, to enable specific targeting.

Click immobilization of randomly alkynylated protein A (SpA), NbBCII10 and alkynylated oligoethylene glycols onto PPE films was troublesome. Aspecific interactions between the films and SpA made analysis via QCM-D difficult. Furthermore, no response in the frequency and dissipation signals could be observed after exposing the films to randomly alkynylated NbBCII10 and alkynylated oligoethylene glycols. It might be interesting to introduce alkyne functionalities onto the PPEs and azide functionalities onto the biomolecules to improve the availability of the functional groups (i.e. switch the functionalities between the two coupling partners).

7.3 REFERENCES

[1] L. Lu, T. Zheng, Q. Wu, A. M. Schneider, D. Zhao and L. Yu, *Chem. Rev.*, 2015, **115**, 12666.

[2] A. L. Koner, D. Krndija, Q. Hou, D. J. Sherratt and M. Howarth, *ACS Nano*, 2013, **7**, 1137.

[3] J. M. Behrendt, J. A. Esquivel Guzman, L. Purdie, H. Willcock, J. J. Morrison, A. B. Foster, R. K. O'Reilly, M. C. McCairn and M. L. Turner, *React. Funct. Polym.*, 2016, **107**, 69.

7.4 NEDERLANDSE SAMENVATTING

Medische beeldvorming is van groot belang voor het stellen van correcte diagnoses en om goede behandelingen te kunnen voorstellen. Jammer genoeg zijn de meeste beeldvormingstechnieken schadelijk voor bepaalde weefsels en bovendien zijn ze erg duur. Tegenwoordig wordt er veel onderzoek verricht naar het gebruik van geconjugeerde polymeren als beeldvormingssondes aangezien ze zeer goede optische eigenschappen hebben en over het algemeen niet toxisch zijn voor cellen. Het grootste nadeel verbonden aan het gebruik van deze geconjugeerde polymeren is dat ze meestal niet oplosbaar zijn in water. Voor het gebruik in biologisch milieu is dit echter een noodzakelijke voorwaarde en daarom werden er verscheidene technieken ontwikkeld om hun gebruik in waterige omgevingen te vereenvoudigen. Een voor de hand liggende oplossing is de introductie van ladingen op de polymeerketen zelf of op de zijketens. Aangezien dit synthetisch gecompliceerd is, is een makkelijkere en meer gebruikte techniek de vorming van geconjugeerde nanopartikels. Hierbij wordt er een dispersie van het opgeloste polymeer in water gemaakt. Aangezien de verschillende polymeerketens op deze manier dicht bij elkaar gepakt worden in de deeltjes, zijn onderlinge interacties mogelijk en deze leiden meestal tot een demping van de fluorescentie. In deze thesis wordt eerst een overzicht gegeven van de technieken die in de literatuur beschreven staan om de emissie-efficiëntie van nanopartikels op basis van geconjugeerde polymeren te verhogen. De meest gebruikte strategie is het introduceren van omvangrijke zijketens en/of het gebruik van matrices. Verder kunnen variatie in de monomeerverhoudingen en het bevriezen van polymeren in hun gerelaxeerde toestand de efficiëntie ook verhogen. Niet enkel een hoge zichtbaarheid van de sondes is noodzakelijk, het is ook van belang dat de nanodeeltjes specifieke cellen of organellen kunnen opsporen en binden. Dit kan gereguleerd worden door bepaalde functionele groepen te introduceren op de polymeerketens, waardoor immobilisatie van eender welk (bio)molecule mogelijk wordt. Verschillende functionele groepen zijn reeds bestudeerd. De belangrijkste zijn de carbonzuren en *N*-hydroxy succinimiden, die stevige amidebindingen kunnen vormen. Mogelijke alternatieven zijn fenylboorzuren, β-cyclodextrines en click-functionaliteiten (alkynen, azides, maleïmides, ...). Wanneer de partikels de

specifieke cellen kunnen detecteren, bestaat de mogelijkheid om ze eveneens te laten optreden als therapeutische agentia. Hierbij kan het polymeer bijvoorbeeld zo ontwikkeld worden dat het de productie van reactieve zuurstofverbindingen kan aanwakkeren en op deze manier celsterfte kan veroorzaken.

Poly(*p*-fenyleenethynyleen) (PPE) verbindingen zijn ideale materialen voor het gebruik in beeldvormingstechnieken. Ze hebben een simpele maar stevige structuur die makkelijk synthetisch aanpasbaar is aan de toepassing die men voor ogen heeft. De *bandgap* kan bijvoorbeeld aangepast worden door andere monomeren in de polymeerketen te introduceren en de zijketens geven heel wat mogelijkheden naar functionalisatie toe. In dit werk wordt de synthese van een azide-gefunctionaliseerd PPE bestudeerd. De azidegroepen zijn interessant voor de clic-immobilisatie van bio(moleculen) via koper-gekatalyseerde azide-alkyn (CuAAC) chemie. Deze functionele groepen zijn geïntroduceerd op het uiteinde van de octyloxy-zijketens van het PPE, en dit zowel in een pre- als post-polymerisatie aanpak. Al de gesynthetiseerde copolymeren hebben vergelijkbare polydispersiteiten ($Đ$ = 2.1−2.4), maar er kon wel een onderscheid gemaakt worden in de moleculaire gewichten van de verschillende materialen. Wanneer de azidefunctionaliteiten geïntroduceerd worden op het dijood-gesubstitueerd monomeer vóór polymerisatie, worden de beste resultaten bekomen (M_n = 28.6 kg/mol). Omdat alkyn-eindgroepen kunnen leiden tot gelatie van het polymeer tijdens de opwerking en de bewaring, worden alle polymeren eind-gefunctionaliseerd. Verder is er een eerste stap gezet richting de functionalisatie van de polymeren door middel van CuAAC-chemie. Fenylacetyleen is succesvol geïmmobiliseerd in oplossing.

Het azide-gefunctionaliseerd polymeer werd daarna geformuleerd in nanopartikels, waarna de eigenschappen vergeleken werden met partikels gevormd uit een meer hydrofoob en een meer hydrofiel polymeer. Het hydrofobe polymeer heeft geen azide-functionaliteiten terwijl er bij het hydrofiel polymeer tetraethyleenglycol (TEG) zijketens zijn geïntroduceerd. Het effect van het functionalisatiepatroon op de grootte van de PPE deeltjes en op de optische eigenschappen werd bestudeerd aan de hand van transmissie elektron microscopie (TEM), dynamische lichtverstrooiing (DLS), UV-Vis absorptiespectroscopie en fluorescentiespectroscopie. De partikels gevormd uit het hydrofiele polymeer met de TEG-ketens (188 nm) zijn groter dan de andere

deeltjes. Dit effect kan verklaard worden door de hydratatie van zowel de periferie als de kern van de partikels. De deeltjes geformuleerd uit de polymeren met azidefunctionaliteiten hebben een hogere fluorescentie-quantumopbrengst (13%) dan de partikels zonder azides. Om aan te tonen dat de azidegroepen bruikbaar zijn voor de immobilisatie van (bio)moleculen, werd er een fluorescente kleurstof aan de nanodeeltjes gehecht als eerste test.

Verder wordt er in deze thesis een nieuwe methode voorgesteld om de quantumopbrengst van geconjugeerde nanodeeltjes te vergroten. De synthese van niet-gefunctionaliseerde PPE-netwerken, welke gevormd zijn door de incorporatie van 2D (1,3,5-tribroombenzene) en 3D (2,2',7,7'-tetrabroom-9,9'-spirobifluoreen) crosslinkers wordt beschreven in hoofdstuk 5 van dit werk. De crosslinkers vormen bruggen tussen de verschillende polymeerketens waardoor ze stapeling van de ketens in de nanodeeltjes voorkomen. Beide crosslinkers werden zowel in 3 als 5 mol% toegevoegd tijdens de Sonogashira polymerisatiereacties. Nanodeeltjes van alle stalen werden geformuleerd en gekarakteriseerd. De fluorescentie quantumopbrengst van de deeltjes verdubbelt (van 5 tot 11%) na het toevoegen van 5% 1,3,5-tribroombenzeen en bovendien is er ook een opmerkelijke verbetering merkbaar in de helderheid van de deeltjes. Verder heeft crosslinking geen invloed op de makkelijke opname van de deeltjes in cellen.

Omdat de functionalisatie van polymeren van groot belang is voor de ontwikkeling van selectieve sensoren, werd de CuAAC-immobilisatie van een *random* gealkyneerde biologische probe (proteine A (SpA)) op PPE films bestudeerd aan de hand van QCM-D. Een vergelijking tussen drie verschillende PPE-films werd gemaakt. De eerste film bestaat uit het azide-gefunctionaliseerd PPE waarvan de synthese beschreven werd in hoofdstuk 3. Het polymeer werd vergeleken met twee meer hydrofiele polymeren. Bij het eerste polymeer zijn de niet-gefunctionaliseerde octyloxy-zijketens vervangen door TEG-ketens, terwijl bij het tweede polymeer de niet-gefunctionaliseerde octyloxy-zijketens behouden werden en het azide geïntroduceerd werd op het uiteinde van de TEG-zijketens. Jammer genoeg treden er aspecifieke interacties op tussen de polymeerfilms en het SpA, waardoor de interpretatie van de resultaten lastig is. Om adsorptie te vermijden werd in een tweede poging gekozen voor oligoethyleenglycolen met verschillende moleculaire massa's en in verschillende

concentraties, maar hier werd geen signaal gedetecteerd na blootstelling van de PPE-films. In een laatste poging werden de films blootgesteld aan reactiemengsels met *random* gealkyneerd NbBCII10, maar ook hier werd geen respons waargenomen.

List of Publications

Y. Braeken, P. Verstappen, L. Lutsen, D. Vanderzande and W. Maes, Synthesis of a multifunctional poly(p-phenylene ethynylene) scaffold with clickable azide-containing side chains for (bio)sensor applications, *Polym. Chem.*, 2015, **6**, 6720.

- Article writing
- All polymer synthesis, characterization and data analysis

L. D'olieslaeger*, Y. Braeken*, S. Cheruku, J. Smits, M. Ameloot, D. Vanderzande, W. Maes and A. Ethirajan, Tuning the optical properties of poly(p-phenylene ethynylene) nanoparticles as bio-imaging probes by side chain functionalization, *J. Colloid Interface Sci.*, 2017, **504**, 527.
(*Shared first authorship)

- Article writing
- All polymer synthesis, characterization and data analysis

Y. Braeken, S. Cheruku, A. Ethirajan and W. Maes, Conjugated polymer nanoparticles for bio-imaging, *manuscript submitted.*

- Article writing
- Complete literature search

Y. Braeken, S. Cheruku, S. Seneca, L. Berden, L. Kruyfhooft, L. Lutsen, D. Vanderzande, A. Ethirajan and W. Maes, The influence of crosslinking on the optical properties of poly(p-phenylene ethynylene) nanoparticles for bio-imaging, *manuscript submitted*.

- Article writing
- All polymer synthesis, characterization and data analysis
- Fluorescence studies of all particles dispersed in water

Dankwoord

Tot slot zou ik graag nog een aantal personen bedanken voor alle tijd en moeite die ze in mijn PhD gestoken hebben.

Op de eerste plaats zou ik graag mijn promotor, Prof. dr. Wouter Maes, bedanken om mij de kans te geven om een doctoraat te beginnen aan de UHasselt. Aangezien het onderwerp van mijn doctoraat afweek van het grootste deel van de onderzoeksgroep, was het soms moeilijk om de juiste weg te vinden, maar uiteindelijk is het ons toch gelukt. Bedankt om richting te geven aan het project en bedankt voor al het verbeterwerk!

Verder verdient natuurlijk ook mijn copromoter, Prof. dr. Dirk Vanderzande, een woordje van dank. Bedankt om de interesse in organische chemie aan te wakkeren en bedankt voor het nalezen van de papers en de thesis.

Furthermore, I would like the thank my other copromotor, dr. Laurence Lutsen. Thank you for managing the lab and for pushing us to organize lab cleans, since this was definitely necessary from time to time.

Furthermore, I would like to thank all the members of the jury for taking the time to evaluate my work and the IWT for financial support.

Anitha, thank you for taking the time to discuss and criticise my work. Without you, my thesis would have looked very different, that's for sure!

Furthermore, I would like to thank Lien, Joeri, Srujan and Senne for the NP synthesis and characterization they did. I enjoyed working with all of you!

Brecht and Tien, thank you for helping me with the random alkynylations of the biomolecules. Nothing was too much for you, but unfortunately, our hard work didn't pay off. Anyway, I learnt a lot from you!

Daarnaast heb ik de voorbije jaren erg veel plezier en steun gehad aan heel wat collega's. Sanne, bedankt om de voorbije 4 jaren naar heel wat geklaag en gezaag te luisteren, en bedankt om alle mooie en jammer genoeg ook minder mooie momenten met mij te delen in de vroege 'bijpraat meetings' die we elke ochtend hadden. Het was een plezier om jou langs me te hebben op de bureau.

Verder zou ik ook Mathias en Jeroen willen bedanken voor de vele keren dat we samen gelachen hebben, en Mathias uiteraard ook voor de chocomousse-taart die de ene keer al eens beter lukte dan de andere keer.

Pieter en Jurgen, bedankt om mij wegwijs te maken in het reilen en zeilen van de UHasselt en om altijd klaar te staan met advies en raad als ik even niet wist hoe het verder moest.
Bovendien zou ik ook alle andere collega's willen bedanken die er in de voorbije jaren voor gezorgd hebben dat de sfeer optimaal was, dat de teambuildings dagen waren om nooit te vergeten en dat de lunchpauze altijd een moment was om naar uit te kijken. Bedankt Evelien, Joris, Geert, Veronique, Ruben, Jorne, Dries, Sam, Frederik, Tom, Nok, Luk, Neomy, Stephan, Joke, Joachim, Martijn, Erika, Gijs, Svitlana, Kirsten, Maarten, Jeroen D.N, Lowie, Jeroen V., Roald, Wouter V.G. en Rebekka.
Natuurlijk mag ik ook het vast personeel niet vergeten. Zij zorgen er immers voor dat wij uberhaupt kunnen werken. Bedankt Huguette voor de vele lastige PLQY metingen en bedankt om die kennis aan mij door te geven zodat ik het nu ook zelf kan ☺. Gunter en Peter, bedankt voor de vele NMR spectra die jullie voor mij opnamen. Vervolgens wil ik prof. dr. Bruno Van Mele en Maxime van de Vrije Universiteit Brussel bedanken voor de thermische analyses.
Verder heb ik ook het geluk gehad om enkele bachelor- en masterstudenten te mogen begeleiden tijdens hun stages. Ik hoop vooral dat jullie iets opgestoken hebben van deze periode. Er zijn in elke geval enkele mooie resultaten uit voortgevloeid, waarvoor mijn dank. Bedankt Tom, Annelore, Marlies, Louis and Laurens.
Verder zou ik graag mijn ouders, zus en schoonfamilie willen bedanken om geïnteresseerd te zijn in wat ik doe. Jullie hebben gezorgd voor heel wat hoognodige ontspanning en afleiding.
En last but not least, in tegendeel zelfs, zou ik Thomas willen bedanken. Bedankt om alle moeilijke momenten net iets makkelijker te maken. Bedankt om te doen alsof je alles wat ik over het werk vertel begrijpt en beter nog, dat het interessant is ☺. Bedankt om me de voorbije 4 jaar door te sleuren en steeds opnieuw te motiveren. Bedankt om er voor me te zijn en me te steunen in alles wat ik doe. Ik hou van je!

BEDANKT ALLEMAAL!